eman ta zabal zazu

Universidad del País Vasco

Euskal Herriko Unibertsitatea

Role of Oncostatin M signalling axis in breast cancer progression: Implications in the tumour microenvironment.

Angela Sofia Monteiro Araujo

PhD directors:

Dr. Charles Lawrie
Dr. Maria Muñoz Caffarel

2021

"In the world there is a multitude of causes and we need to make one as ours" –
Dominique Lapierre, City of Joy, 1985.

To all animals used in the name of science, you are my truly heroes! My personal cause will always be to fight unnecessary human and animal suffering in this world.

Acknowledgments

I would like to thank my PhD supervisors **Dr. Charles Lawrie** and **Dr**. **Maria Caffarel** for giving me the opportunity to develop this project and for all support and intellectual guidance along these years. Without them this would not be possible!

Maria Caffarel, you have thought me so much in all aspects of life that I cannot thank you enough for this opportunity and the beautiful friendship we have built along these years. I truly admire you as a scientist, mentor and as a person. I am truly blessed to have such role model. Thank you with all my heart!

I am grateful to the **Gobierno Vasco** for the financial support, to **Biodonostia** for accommodating me, to the **UPV** for accepting me in their PhD program, to my tutor **Dr. Gorka Larriñaga** and to **Dr. Begoña Ruiz Larrea** for helping me with administration tasks. Sometimes it is easy to forget what a privileged place we live in.

With a big smile on my face, I am now thanking the most amazing lab mates in the world. **Andrea**, you have been my partner in crime, I am very proud of what a great scientist you have become. We have learnt a lot together and I cannot thank you enough for all your help and partnership along these years! You are the moon, always there even if it likes to be invisible sometimes. **Joanna**, you have thought me so much about resilience in life, and my days have become immensely better after you arrived. You are my sunshine. **Peio,** you are a start in the making, within such a short time you have thought me what passion for science really means, I admire all your focus in life. **Iñaki** and all master students that have come and gone, it has been a real pleasure working with you all. I am incredibly happy to see this lab grow and what it has become. I will surely miss you all very much!

Thank you **Dr. Ander Urruticoechea** and **Dr. Isabel Alvarez** for all your feedback and clinical perspective during the lab meetings, I really appreciate all the basic-clinical discussions we had.

Erika, Giovanni, Lorea, Marta, Maria Arestin, Carla, Maria Armesto and all Charles Lawrie group present and former members, thank you for your help during these years.

I would like to thank **Prof. Clare Isacke** and **all her lab members** for welcoming me into their lab at the ICR for my PhD internship. We have met in a beautiful island in Greece during a party and suddenly I discovered the tumour microenvironment! I am so proud of everything I have learnt and all the work we have done together! Another great mentor I was lucky to come across in my life.

Dr. Maria Oliveira and TMI group, thank you for the unique opportunity to work with you at i3S in Porto. I enjoyed every single moment and really appreciate your welcoming environment. I have to say I felt at home twice!

I want to especially thank **Carmen** at the genomic platform, I cannot stress enough how much I appreciate all the technical work you have done for us. You were many times my saviour during these years!

Thank you to all people at the institute platforms that have given me immense technical help and advice, **Ana Gorostidi, Ana Anastui, David Otaegui, Carlos, Eli, Iñaki, Mariasun.**

I would like to thank all lab members from other groups, especially the ones we shared our space, which names are too many to write down. Most of you really made the difference in my days and actively helped me in many ways!

Thank you **Laurinha** for this beautiful friendship we have built and for the fun moments in the corridor. **Mikel,** thank you for all your patience in teaching me Spanish and for the fun moments along these years. **Haizea, Estefania, Haizpea, Julia, Nanda, Leire Moreno, Olatz, Paula, Sandra, Pedro,** some of you have come and gone and I will not forget all your help, happy memories together and friendship.

I want to thank my dearest friend **Taty** for starting this adventure of science with me, for being a constant in my life and all the memories we treasure so much.

Thank you to my amazing present and former **housemates (Rocio, Marie, David, Iñigo, Javi)** and all my **friends** in Spain, UK, and Portugal (too many to mention) that made my life enjoyable outside the lab. A special hug to my old friends from home "**Os bravos**" whom I adore immensely and that never fail to show me their love. **Alex, Melisa, Mohab, Nerea, Rizó, Leo**, **David**, you have given me so much during this time. I treasure you all very much!

Javi, I cannot thank you enough for all your help and patience during this time in every aspect of my life. Behind every PhD student there is a victim listening to all frustrations. You were the one. Diglet forever!

A special thank you to my **maninha, mom, dad, and bó,** my beautiful **FAMILY.** You are a constant support in every aspect of my life, there is no place like home and a tight hug from the ones we love the most.

Finally, I want to dedicate this last paragraph to the memory of my best friend **Paula.** There was not a single day that I did not think of you. You have always inspired me to be the best version of myself, and I do not know how you still manage to do this from wherever you are. I will miss your hug today and every day, but I just want you to know that I will love you forever.

List of publications

Associated with the work presented in this thesis:

- **Angela M Araujo**, Andrea Abaurrea, Peio Azcoaga, Joanna I. López-Velazco, Ricardo Rezola, Iñaki Osorio-Querejeta, Fátima Valdés-Mora, Juana M. Flores, Liam Jenkins, Patricia Fernández-Nogueira, Nicola Ferrari, Natalia Martín-Martín, Alexandar Tzankov, Serenella Eppenberger-Castori, Isabel Alvarez-Lopez, Ander Urruticoechea, Paloma Bragado, Nicholas Coleman, Arkaitz Carracedo, David Gallego-Ortega, Fernando Calvo, Clare M. Isacke, Maria M. Caffarel, Charles H. Lawrie. 2021. Stromal Oncostatin M axis promotes breast cancer progression. *Submitted. https://www.biorxiv.org/content/10.1101/2020.10.30.356774v2*

- Andrea Abaurrea**, Angela M Araujo** and Maria Caffarel. Role of the IL-6 cytokine family in regulating Epithelial to Mesenchymal Plasticity in cancer progression. *Submitted.*

- Justyna A Kucia-Tran, Valtteri Tulkki, Cinzia G Scarpini, Stephen Smith, Maja Wallberg, Marta Paez-Ribes, **Angela M Araujo**, Jan Botthoff, Maria Feeney, Katherine Hughes, Maria M Caffarel, Nicholas Coleman. Anti-oncostatin M antibody inhibits the pro-malignant effects of oncostatin M receptor overexpression in squamous cell carcinoma. *Journal of Pathology*. **244**, 283-295. (2018).

- Justyna A Kucia-Tran, Valtteri Tulkki, Stephen Smith, Cinzia G Scarpini, Katherine Hughes, **Angela M Araujo**, Ka Yin Matthew Yan, Jan Botthof, Eduardo Pérez-Gómez, Miguel Quintanilla, Kate Cuschieri, Maria M Caffarel & Nicholas Coleman. Overexpression of the oncostatin-M receptor in cervical squamous celll carcinoma is associated with epithelial-mesenchymal transition and increased metastasis. *British Journal of Cancer*. **115**, 212-222 (2016)

Previous work:

- Caffarel MM, Chattopadhyay A, **Araujo AM**, Bauer J, Scarpini CG, Coleman N. Tissue Transglutaminase mediates the pro-malignant effects of oncostatin M receptor overexpression in squamous cell carcinoma. The Journal of Pathology. **231**, 168-247. ISSN 1096-9896 (2013).

Table of contents

Acknowledgments ... *3*

List of publications ... *5*

Table of contents ... *7*

Abbreviations: ... *11*

Abstract ... *17*

Resumen ... *19*

Chapter 1: Introduction ... 21

1.1 Breast cancer ... *23*
1.1.1 Breast cancer statistics ... 23
1.1.2 Breast cancer subtypes ... 24
1.1.2.1 Classical immunohistochemical molecular classification ... 25
1.1.2.2 Gene expression profiling classification (Intrinsic subtypes) ... 26
1.1.3 Breast cancer therapies ... 28
1.1.3.1 Early-stage breast cancer ... 29
1.1.3.2 Advanced breast cancer ... 31

1.2 Tumour microenvironment and inflammation in cancer ... *33*
1.2.1 The tumour microenvironment ... 33
1.2.1.1 Cancer associated fibroblasts ... 34
1.2.1.2 Myeloid cells ... 35
1.2.2 Inflammation in cancer ... 36
1.2.2.1 Inflammation ... 37
1.2.2.2 Pro-tumoral inflammation ... 38
1.2.2.3 Anti-tumour immunity and tumour-induced immunosuppression ... 39
1.2.3 Inflammation in breast cancer ... 41
1.2.4 Targeting cytokines in cancer ... 41

1.3 IL-6 family and inflammation in cancer ... *42*
1.3.1 IL-6 family ... 42
1.3.2 OSM:OSMR ... 44
1.3.3 OSM:OSMR in cancer ... 46
1.3.4 OSM:OSMR in breast cancer ... 49
1.3.5 Breast tumour microenvironment and OSM:OSMR signalling ... 50

Hypothesis and aims of this PhD project ... 53

Hypothesis ... *53*

Objectives ... *53*

Chapter 2: Materials and methods ... 55

2.1 Clinical samples and datasets ... *57*
2.1.1 Tissue microarrays ... 57
2.1.2 Bioinformatic analysis of publicly available datasets ... 57

2.2 Cell culture ... *59*
2.2.1 Cell thawing ... 61
2.2.2 Cell maintenance and subculture ... 61
2.2.3 Cell freezing ... 62
2.2.4 Cell seeding for experiments ... 62
2.2.5 OSM treatment ... 63

2.2.6 Cell transfections 63
2.2.6.1 siRNA 63
2.2.6.2 shRNA 64
2.2.6.3 Lentiviral production 65
2.2.6.4 Cell line infection and selection 65
2.2.6.5 Cell transfection with over expressing plasmids 66
2.2.7 HL-60 differentiation 66
2.2.8 Isolation and culture of primary monocytes 67
2.2.9 Conditioned media used in myeloid cells experiments 67
2.2.10 3D fibroblast spheres 68
2.2.11 Collagen cell contraction assays 68

2.3 Cell and animal tissue processing for DNA, RNA and protein analysis 68

2.4 DNA analysis 69
2.4.1 DNA extraction 69
2.4.2 gDNA samples analysis 69

2.5 RNA analysis 70
2.5.1 RNA extraction from animal tissue and cell lines 70
2.5.2 Reverse transcription: RNA to cDNA conversion 71
2.5.3 Real-time quantitative PCR analysis 71
2.5.5 Microarray analysis of gene expression 73
2.5.6 Single cell RNA sequencing 73

2.6 Protein analysis 74
2.6.1 Protein extraction from animal tissue and cell lines 74
2.6.2 Protein quantification 74
2.6.3 Protein sample preparation for Western blot analysis 74
2.6.4 Western blotting 75
2.6.5 Cytokine and chemokine quantification 77
2.6.6 Histopathology and immunohistochemistry analysis of murine samples 77

2.7 Flow cytometry and FACS sorting 79

2.8 Animal studies 82
2.8.1 Mouse models 82
2.8.1.1 Orthotopic xenografts in nude mice 82
2.8.1.2 TS1 orthotopic injections in OSMR KO and control mice 83
2.8.1.3 MMTV-PyMT model 84
2.8.2 Animal tissue collection at culling points 84
2.8.3 Mouse colonies maintenance 85

2.9 Statistical analyses 87

Chapter 3: Results 89

3.1 Role of OSM:OSMR signalling in breast cancer progression. 91
3.1.1 Summary 91
3.1.2 OSM and OSMR are associated with decreased overall survival in breast cancer, especially in the ER- subtype. 91
3.1.3 OSM and OSMR are associated with decreased overall survival in multiple types of cancer. 93
3.1.4 OSM and OSMR are not frequently mutated in breast cancer. 95
3.1.5 OSMR pathway activation is increased in ER- breast cancer cells 96
3.1.6 Exogenous OSM treatment activates the OSMR pathway and induces pro-malignant factors in the MDA-MB-231 breast cancer cell line. 98
3.1.7 OSM treatment of breast cancer cell lines induces pro-malignant factors through the OSMR receptor. 100
3.1.8 OSMR overexpression promotes a pro-malignant phenotype in the SK-BR-3 cell line. 101
3.1.9 MDA-MB-231 cells constitutively expressing OSM are a reliable model of constant OSMR pathway activation. 103

3.1.10 OSM signalling induces tumorigenesis and metastasis in mice xenografts in nude mice. 104
3.1.11 Depletion of OSMR in the MMTV-PyMT breast cancer mouse model halts tumour progression. 107

3.2 OSM:OSMR signalling in the tumour microenvironment. 112
3.2.1 Summary 112
3.2.2 OSM:OSMR signalling is increased in human tumour stroma. 112
3.2.3 Single cell RNA-seq reveals that OSM:OSMR signalling is paracrine within the tumour and its pattern of expression differs from IL-6 family. 113
3.2.4 OSM is mostly expressed by myeloid cells while OSMR is present in tumour cells and fibroblasts. 116
3.2.5 OSMR expression correlates with fibroblast content while OSM expression associates with myeloid cell infiltration in human breast cancer samples. 118
3.2.6 Human breast cancer cells, fibroblasts and myeloid-derived cell lines maintain the expression pattern of the OSM:OSMR pathway observed in tumours. 119
3.2.7 OSM:OSMR signalling in the tumour microenvironment contributes to tumour progression. 121
3.2.8 Exogenous OSM activates OSMR pathway in fibroblasts. 124
3.2.9 Exogenous OSM induces proliferation and contractility in CAFs but it does not affect normal fibroblasts. 125
3.2.10 Exogenous OSM induces activation markers in CAFs. 126
3.2.11 Exogenous OSM induces a pro-tumoral signature in CAFs. 129
3.2.12 Depletion of OSMR in CAFs delays tumour onset. 130
3.2.13 Activation of CAFs by OSM induces tumour progression and metastasis. 132

3.3 Modulation of the immune system by OSM:OSMR signalling. 135
3.3.1 Summary 135
3.3.2 OSM induces an inflammatory signature and secretion of chemoattractants in CAFs and cancer cells. 135
3.3.3 OSMR depletion in MMTV-PyMT reduces myeloid infiltration within the primary tumour. 138
3.3.4 Conditioned media from macrophages induces OSMR in cancer cells and conditioned media from OSM-treated cancer cells induces OSM expression in macrophages, suggesting the existence of feedforward loops. 141
3.3.5 Conditioned media from cancer cells prevents monocyte differentiation while conditioned media from CAFs induces M2 phenotype in primary monocytes, independently of OSM. 142

Chapter 4: Discussion 145

4.1 OSM and OSMR associate with decreased survival in breast cancer and OSMR signalling is increased in ER negative breast cancer. 148

4.2 OSM signalling promotes breast cancer progression in multiple pre-clinical models. 150

4.3 OSM:OSMR signalling in the tumour microenvironment promotes breast cancer progression. 153

4.4 OSM:OSMR axis shapes the immune system in the tumour microenvironment. 158

4.5 Summary and future perspectives 162

Chapter 5: Conclusions 167

References 171

Supplementary information 189

Abbreviations:

AIDS: Acquired immunodeficiency syndrome

AKT: Protein Kinase B

Alu: *Arthrobacter luteus*

ATCC: American type culture collection

BC: Breast cancer

BCA: Pierce bicinchoninic acid

BSA: Bovine serum albumin

CAF: Cancer associated fibroblast

CCL (number): C-C Motif chemokine ligand (number) eg: CCL2

CCl4: carbon tetrachloride.

CCR2: C-C chemokine receptor type 2

CDK (number): Cyclin dependent kinase (number) eg: CDK4

cDNA: complementary DNA

CLC: cardiotrophin-like cytokine

CM: Conditioned media

CMP: Common myeloid progenitor

CNTF: Ciliary neurotrophic factor

CO_2: Carbon dioxide

COVID-19: Coronavirus disease 2019

CRUK: Cancer Research United Kingdom

CT: Cycle threshold

CT-1: Cardiotrophin 1

CTC: Circulating tumour cell

CTLA-4: Cytotoxic T-lymphocyte-associated protein 4

CXCL (number): C-X-C motif chemokine ligand (number) eg: CXCL16

DAB: 3,3'-Diaminobenzidine.

DAPI: 4’,6-diamidino-2-phenylindole

DFS: Disease free survival

DMEM: Dulbecco’s modified eagle’s medium

DMFS: Distant metastasis free survival

DMSO: Dimethyl sulfoxide

DNA: Deoxyribonucleic acid

DNase: Deoxyribonuclease

dNTP: Deoxyribonucleotide triphosphate

ECL: Enhanced chemiluminescence

ECM: Extracellular matrix

EDTA: Ethylenediaminetetraacetic acid

EGF: Epidermal growth factor

EGFR: Epidermal growth facor receptor

ELISA: Enzyme-linked immunosorbent assay

EMT: Epitelhium mesenchymal transition

ER: Oestrogen receptor

EU: European Union

FACS: Fluorescence-activated cell sorting

FBS: Fetal bovine serum

FDA: Food and drug administration

FDR: False discovery rate

FFPE: Formalin fixed paraffin-embedded blocks

FMO: Fluorescence minus one

gDNA: genomic DNA

GEP: Gene expression profiling

GFP: Green fluorescent protein

GM-CSF: Granulocyte-macrophage colony-stimulating factor

GO: Gene ontology

gp130: Glycoprotein 130

GSEA: Gene set enrichment analysis

HCl: Hydrochloric acid

HEK: Human embryonic kidney cells

HER2: Human epidermal growth factor receptor 2

HET: Heterozygous

HK: Housekeeping genes

HMGA2: High-mobility group AT-hook 2

HMGB1: High mobility group box 1

hOSM: Human OSM

ICR: Institute of cancer research

IFN: Interferon

IHC Immunohistochemistry

IL-(number): Interleukin (number), eg; Interleukin- 6, IL-1α

IMEM: Improved minimum essential medium

ISH: *In situ* hybridization

JAK (number): Janus kinase (number), eg: JAK2

KO: Knockout or Knockdown

KM: Kaplan-Meier

LIF: Leukaemia inhibitory factor

LIFR: Leukaemia inhibitory factor receptor

MAPK: Mitogen-activated protein kinase

M-CSF: macrophage colony-stimulating factor

MDSC: Myeloid derived suppressor cell

MEM: Minimum Essential Medium

MHC: Major histocompatibility complex

miRNA: micro-RNA

MMP (number): Metalloproteinase (number), eg: MMP-2

MMTV-PyMT: Mouse mammary tumour virus-polyoma middle tumour-antigen

MSC: Mesenchymal stem cells

mTOR: Mammalian target of rapamycin

NaOH: Sodium hydroxide

NF-KB: Nuclear factor kappa-light-chain-enhancer of activated B cells.

OS: Overall survival

OSM: Onconstatin M

OSMR: Onconstatin M receptor

OSMRs: Onconstatin M receptor short-form

PARP: Poly ADP-ribose ppolymerases

PBS: phosphate buffered saline

PCR: Polymerase chain reaction

PD-1: Programmed cell death protein 1

PDGF: Platelet-derived growth factor

PDL-1: Programmed death-ligand 1

PF-4: Platelet factor 4

PI3K: Phosphoinositide 3-kinase

PMN-MDSCs: Polymorphonuclear myeloid-derived suppressor cells

PR: Progesterone receptor

qPCR: Real-time quantitative polymerase chain reaction

RIN: RNA quality number

RNA: Ribonucleic acid

rpm: Revolutions per minute

RPMI: Roswell Park Memorial Institute

RT-qPCR: Reverse transcription real-time quantitative polymerase chain reaction

SCCs: Squamous cell carcinomas

scRNA-seq: Single cell RNA sequencing

SD: Standard deviation

SEM: Standard error

shRNA: Short hairpin RNA

siRNA: Small interfering RNA

SOCS (number): Suppressor of cytokine signalling (number), eg: SOCS3

sOSMR: Soluble OSMR

STAT (number): Signal transducer and activator of transcription (number), eg: STAT3

STR: Short tandem repeats

TAC: Transcriptome analysis console

TAM: Tumour associated macrophage

TAN: Tumour associated neutrophil

TBS: Tris buffered saline

TBS-T: Tris buffered saline with Tween

T-DM1: Trastuzumab emtansine

TGF-β (number): Transforming growth factor beta (number), eg: TGF- β1

TGM2: Tissue transglutaminase 2

TIL: Tumour infiltrating lymphocyte

TIM: Tumour infiltrating myeloid

TMA: Tissue microarray

TME: Tumour microenvironment

TNBC: Triple negative breast cancer

TNF- α: Tumour necrosis factor

TPA: 12-*O*-tetradecanoylphorbol-13-acetate

Treg: Regulatory T cell

UMAP: Uniform manifold approximation and projection

VEGF: Vascular endothelial growth factor

WT: Wild type

ZEB1: Zinc Finger E-Box Binding Homeobox 1

Abstract

The tumour microenvironment (TME) is composed of different cell types such as fibroblasts, adipocytes, endothelial and infiltrating immune cells, that harbour complex cell interactions that are often manipulated and hijacked by tumour cells in every step of cancer progression. It is clear now that understanding the interactions between tumour cells and the surrounding microenvironment is fundamental to design more effective therapeutic strategies to treat cancer. Inflammation in the TME is highly associated with tumour initiation, tumour growth, angiogenesis, and metastasis. Cytokines are important modulators of inflammatory processes and are often found dysregulated in cancer. Oncostatin M (OSM) is a cytokine belonging to the interleukin 6 family (IL-6), and it has been shown to play important roles in physiologic and pathological conditions including inflammation, angiogenesis, bone remodelling and tumour progression. This work sought to determine the role of OSM:Oncostatin M receptor (OSMR) axis in breast cancer progression and to investigate its importance in modulating the tumour microenvironment. To address this, a wide range of tools including clinical data, *in vivo* models, single cell RNA-sequencing (scRNA-seq), fluorescence activated cell sorting (FACS) and cell cultures of breast cancer cell lines, cancer-associated fibroblasts (CAFs) and macrophages have been used in this study.

OSM and OSMR were found to be associated with worse survival in breast cancer clinical data. Furthermore, OSM signalling induced tumour onset and progression in mice xenografts. On the contrary, OSMR depletion delayed tumour onset, decreased tumour growth and generation of lung metastasis in MMTV-PyMT mice model. OSM and OSMR were found to be induced in the tumour microenvironment of human cancer samples. Orthotopic injections of murine TS1 cells in OSMR deficient mice resulted in a decrease in tumour growth compared to control mice, suggesting that OSMR signalling is important in the tumour microenvironment. scRNAseq and FACS sorting analyses of murine tumours and bioinformatic analysis of human clinical data revealed that cancer cells and fibroblasts express the receptor OSMR while the ligand OSM was found to be mainly secreted by myeloid cells suggesting the existence of a paracrine signalling between the tumour microenvironment and cancer cells. Co-injections of human immortalised CAFs with breast cancer cells demonstrate that activation of OSMR in fibroblasts leads to a more aggressive

phenotype which supports that OSMR signalling is important not only for cancer cells but also for fibroblasts in tumour progression. Furthermore, OSM:OSMR signalling on cancer cells and CAFs creates an important feedback loop stimulating the release of chemoattractants responsible for increased infiltration of myeloid cells in the TME. On the other hand, OSM-activated cancer cells induce the expression of OSM on myeloid cells ensuring a constant production of the cytokine and consequent tumour progression.

The results of this thesis support that OSM:OSMR pathway acts as a central regulator of the communication between the immune compartment, CAFs, and cancer cells. This crosstalk has important consequences on tumour initiation, progression, and in modulating the tumour microenvironment. OSMR could be blocked by antibody-based inhibition, strategy that has had a major impact on breast cancer, which makes it a promising candidate for therapeutic targeting.

Resumen

El microambiente tumoral (TME) está compuesto por diferentes tipos celulares, entre los que se incluyen los fibroblastos, adipocitos, células endoteliales e inmunes, que interaccionan entre ellas de forma compleja y que, a menudo, son manipuladas por las células del cáncer en cada paso de la progresión tumoral. Comprender las interacciones entre las células cancerígenas y el microambiente circundante es fundamental para diseñar nuevas estrategias terapéuticas para tratar el cáncer. La inflamación en el TME está altamente asociada con la tumorigénesis, la angiogénesis y la metástasis. Las citoquinas son moduladoras importantes de los procesos inflamatorios y a menudo se encuentran desreguladas en enfermedades como el cáncer. La citoquina oncostatina M (OSM) pertenece a la familia de la interleuquina 6 (IL-6) y se ha demostrado que desempeña un papel relevante en procesos fisiológicos y patológicos como la inflamación, angiogénesis, remodelación ósea y en la progresión tumoral. Este proyecto de Tesis tiene como objetivo determinar el papel del eje de señalización del OSM y su receptor (OSMR) en la progresión del cáncer de mama e investigar su importancia en la modulación del microambiente tumoral.

Para abordar este objetivo se ha utilizado una amplia gama de herramientas que incluyen datos clínicos, modelos animales, secuenciación de ARN de célula única (scRNA-seq), citometría de flujo (FACS) y cultivos celulares de líneas de cáncer de mama, fibroblastos asociados al cáncer (CAF) y macrófagos.

Nuestros resultados han demostrado que OSM y OSMR se asocian con una peor supervivencia en pacientes de cáncer de mama. Además, la señalización de OSM induce la aparición y progresión del tumor en experimentos de xenoinjertos en ratones. Por el contrario, el silenciamiento de OSMR retrasa la aparición del tumor, disminuye el crecimiento tumoral y la generación de metástasis pulmonares en el modelo genético murino de cáncer de mama MMTV-PyMT. Análisis de muestras de tumores humanos demostraron que OSM y OSMR se encuentran sobre-expresados en el microambiente tumoral. Inyecciones ortotópicas de células murinas (TS1) en ratones deficientes en el gen OSMR revelaron una disminución en el crecimiento tumoral en comparación con los animales control, lo que sugiere que la señalización de OSMR es importante en el estroma tumoral. Los análisis de scRNAseq y FACS de tumores murinos y el análisis bioinformático

de muestras clínicas humanas revelaron que las células tumorales y los fibroblastos expresan el receptor OSMR mientras que el ligando OSM se expresa principalmente en el sistema inmune, principalmente en el linaje mieloide presente en el microambiente tumoral, lo que sugiere la existencia de una señalización paracrina entre el microambiente tumoral y las células cancerígenas. Las co-inyecciones de CAFs con líneas celulares de cáncer de mama en ratones inmunodeficientes demostraron que la activación de OSMR en los fibroblastos conduce a un fenotipo más agresivo. Esto respalda la idea de que la señalización por OSMR en el contexto de la progresión tumoral no solo es importante en las células cancerígenas, sino también en los fibroblastos. Además, la señalización por OSM:OSMR en células tumorales y en los CAFs crea un circuito importante de retroalimentación positiva que estimula la liberación de quimioatrayentes responsables de una mayor infiltración de células mieloides en el TME. Por otro lado, las células tumorales activadas por OSM inducen la expresión de OSM en las células mieloides asegurando una producción constante de la citoquina y favoreciendo la progresión tumoral.

Los resultados de esta Tesis Doctoral apoyan que la vía de OSM:OSMR actúa como un regulador central de la comunicación entre el compartimento inmunológico, los CAFs y las células tumorales. Esta interacción tiene consecuencias importantes en la iniciación y progresión del tumor y en la modulación del microambiente tumoral. OSMR podría bloquearse mediante la inhibición basada en anticuerpos, estrategia que ha tenido un gran impacto en el cáncer de mama, convirtiéndolo en una diana prometedora para el desarrollo de nuevas estrategias terapéuticas.

Chapter 1: Introduction

1.1 Breast cancer

1.1.1 Breast cancer statistics

Breast cancer (BC) is the most common cancer found in women worldwide with 2,088,849 diagnoses in 2018 alone[1]. In Spain, there were 32,825 new cases recorded in the same year, accounting for 28.7% of all cancers diagnosed in women[1]. Although BC can also be diagnosed in men, the incidence in this group is comparatively low representing only 1% of all BC cases[2]. Despite a significant decline in breast cancer mortality rates in recent years (16.4% in the EU, in women aged 50-69 years), largely due to the implementation of screening programs[3], the total number of deaths worldwide has remained more or less unchanged[4]. This apparent contradiction can be explained by an increasing incidence in breast cancer due to implementations of screening programs along with aging populations in developed countries, and a worldwide population increase[4]. Survival rates for breast cancer vary greatly worldwide, ranging from 80% in North America down to 40% in low-income countries[5]. This variation is a consequence of the less developed early detection programs and lack of access to healthcare assistance in poorer countries. It is estimated that around 30% of patients present local advanced disease and 5-8% with incurable metastatic disease at the moment of diagnosis[6]. BC incidence also varies significantly amongst age groups. According to Cancer Research UK (CRUK) statistics[7], the rate of diagnosis increases with age, with the 85 to 89 age group representing the highest rate of incidence. Nevertheless, women aged 65-70 constitute the highest number of new diagnoses every year[7] (Fig. 1.1).

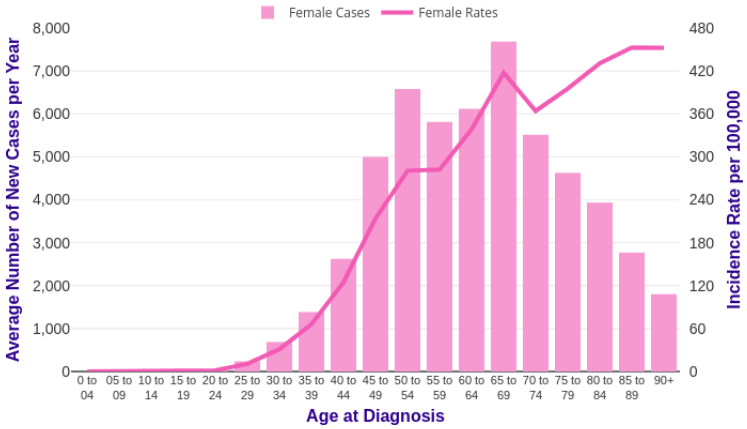

Fig. 1.1: Breast cancer average number of new cases per year, age-specific incidence, and rates per 100,000 females in the UK, 2015-2017. Reproduced from: CRUK[7].

In addition to the clinical symptoms associated with breast cancer, patients frequently develop post-traumatic stress symptoms, that often persist at least for a year and can result in cognitive dysfunction[8]. In addition to the social cost, there is a clear economic burden associated with this disease. In the Basque Country, for example, the initial costs for breast cancer treatment are estimated to range from 9,838 to 28,776 € depending on the initial stage of the disease, with an annual follow up cost of 172€ for stage 0 to 17,879€ for stage IV disease[9].

Considering all factors mentioned above, it is indisputable that breast cancer remains a serious global health problem with an urgent need for novel and more effective therapeutic options.

1.1.2 Breast cancer subtypes

Breast cancer is a highly heterogeneous disease consisting of distinct phenotypes that vary greatly in molecular pathogenesis and prognostic outcome. Consequently, defining a single treatment approach to such a complex disease is nearly impossible, and therefore, the most useful way is to divide breast cancer into subgroups that share similar characteristics with higher probability to respond to specific treatments. Breast cancer can be classified by histological analysis as ductal or lobular carcinomas (Fig. 1.2). **Ductal carcinomas** are the most common type comprising around 80% of all diagnoses[10]. Ductal carcinomas affect the line of cells surrounding the milk ducts. *In situ* ductal carcinoma evolve to invasive carcinoma once the tumour cells disrupt the duct anatomy and start to invade surrounding

tissues. **Lobular carcinomas** only account for 10-20 % of breast cancer diagnostics, they originate in lobules and are considered invasive when the tumour spreads to neighbouring tissues[10] (Fig. 1.2).

All breast cancer tumours can be stratified into three clinical grades associated with distinct predictive prognostic values. The grading system in BC considers factors such as differentiation state, tubule formation, nuclear grade, and mitotic rate[11]. Each parameter is given a score, and at the end, the sum of all parameters is ranked into Grade I (well differentiated), Grade II (moderately differentiated) and Grade III (poorly differentiated), where the higher the grade the lesser resemblance to the counterpart normal cells and worse prognosis for the patient[11].

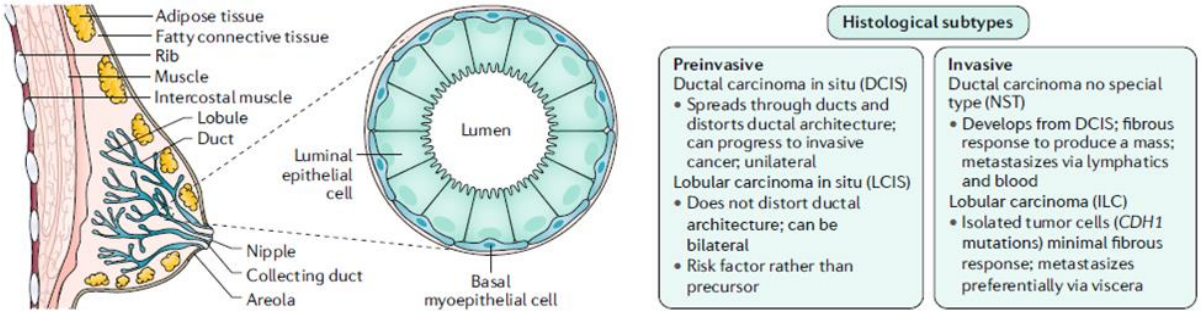

Fig. 1.2: Breast structures that give rise to different types of breast cancer. Reproduced from: Harbeck *et al* (2019)[12].

Apart from the histology and tumour grade, tumours can be further subdivided according to their molecular characteristics. The distinct subtypes have substantially different prognosis, natural histories, metastatic patterns, gene expression profiles as well as sensitivity to therapies[13].

1.1.2.1 Classical immunohistochemical molecular classification

Historically, tumours have been defined in the clinic according to the expression of three molecular markers. Immunohistochemical (IHC) staining of oestrogen receptor (ER), progesterone receptor (PR) and induction of human epidermal growth factor receptor 2 (HER2) is used to classify tumours into hormone-dependent tumours or ER positive (ER+), HER2 positive (HER2+) and triple negative (TNBC).

ER+ tumours, also sometimes referred to as luminal tumours, account for 70-80% of all invasive ductal carcinomas[14]. These tumours are characterised by positive ER and PR hormone receptors expression. Tumours are considered ER and/or PR positive when more than 1% of the tumour cells express one or both receptors[15]. Most PR+ tumours are also ER+, as progesterone is mainly induced in response to oestrogen receptor mediated transcriptional events[15]. Ki67, a proliferation marker, can be used to further subclassify ER+ tumours into Luminal A-like and Luminal B-like[16], in an attempt to derive surrogate intrinsic subtypes from the classical IHC classification (Fig. 1.3 and section 1.1.2.2)

Luminal A-like tumours are typically characterised by low proliferative index and present low levels of Ki67 staining and high ER and PR staining. These tumours are usually low grade and patients have a good prognostic outcome[16].

Luminal B-like tumours are characterised by high levels of Ki67 staining and worse prognosis than luminal A tumours[17]. These cases can also be further subclassified into **Luminal B-like HER2+** or **Luminal B-like HER2-** depending on the HER2 expression status. This classification facilitates the prediction of response to targeted therapies (See section 1.1.3).

ER- tumours represent approximately 20% of all invasive ductal carcinoma diagnostics[14] and are characterised by the lack of ER and PR markers. ER- tumours with the same stage exhibit worse prognosis than ER+ breast cancers in 5-year survival studies[18]. These types of tumours can be further subclassified into two distinct subtypes, HER2+ and triple negative breast cancer (TNBC).

HER2+ tumours are characterised by the expression of HER2 and they are generally high grade and highly proliferative. These tumours have an intermediate prognosis, but they usually respond to targeted anti-HER2 therapies.

Triple negative tumours are characterised by the absence of ER, PR and HER2 expression[19], and they are three times more common in pre-menopausal women[20]. They usually present high degree of proliferation and possess the worst prognosis of all subtypes[21].

1.1.2.2 Gene expression profiling classification (Intrinsic subtypes)

The traditional immunohistochemical classification of breast cancer has its limitations and not all tumours perfectly fit in the established group divisions. Microarray-based gene

expression profiling (GEP) allows a more comprehensive analysis of the genes involved in distinct breast cancer subtypes and it can help to identify more homogeneous subgroups than those defined by IHC. For example, GEP confirmed that, in general, ER negative tumours differ from ER positive tumours at the level of gene expression[22]. GEP allowed the further subclassification of tumours into intrinsic subtypes with distinct clinical outcomes (Luminal A, Luminal B, HER2 enriched, basal like, normal-like and later, claudin-low)[23–25] (Fig. 1.3).

Luminal A tumours are characterised by strong expression of oestrogen receptor and ER regulated genes such as GATA binding protein 3, X-box binding protein 1, trefoil factor 3, hepatocyte nuclear factor 3α, and oestrogen-regulated *LIV*-1, and are associated with good prognosis[23,26].

Luminal B subgroup generally has a higher expression of genes involved in mitosis and cell proliferation. This subgroup presents higher proliferation and poorer prognosis than luminal A tumours[27,28].

HER2 enriched tumours are characterised by high expression of several genes in the amplicon 17q22.24 including *ERBB2* and *GRB* genes and they tend to respond to targeted therapies focused on inhibiting HER2 signalling[23].

Basal like tumours are defined by a robust cluster of genes expressed by epithelial cells in the basal layer of the mammary gland. This subtype is particularly aggressive and a major clinical challenge as they often present insensitivity to hormone therapy and they are more prevalent in younger women, often relapsing rapidly[29]. There have been attempts to identify these tumours by immunohistochemistry using cytokeratin 5/6 and/or EGFR markers[30]. Nowadays there is still no consensus on the criteria used to define cancers as basal like in formalin-fixed paraffin-embedded tissues (FFPE). Tumours that lack ER, PR and HER2 expression are usually classified as triple negative in the clinic[31].

Normal-like tumours exhibit a gene expression profile that most closely resembles normal breast tissue[23,24]. In contrast, **Claudin-low** tumours are characterised by having low/absent expression of luminal differentiation markers, high enrichment of epithelial to mesenchymal transition (EMT) markers and cancer stem cell-like features[32]. Claudin-low is not simply a subtype analogous to any intrinsic subtype, but rather a complex additional phenotype which may contain tumours of various intrinsic subtypes[33].

The continuous attempts to subdivide groups of tumours with more homogeneous characteristics and relevant biomarkers are a fundamental step in the development of personalised medicine. Despite all the advantages of gene expression analysis and even added prognostic value compared to IHC classification[33], the majority of breast cancer classification in the clinic is still carried out by immunohistochemistry analysis, largely due to cost reasons and/or the need for specialised instrumentation to perform gene expression analysis, all of which is beyond the reach of the majority of healthcare institutions.

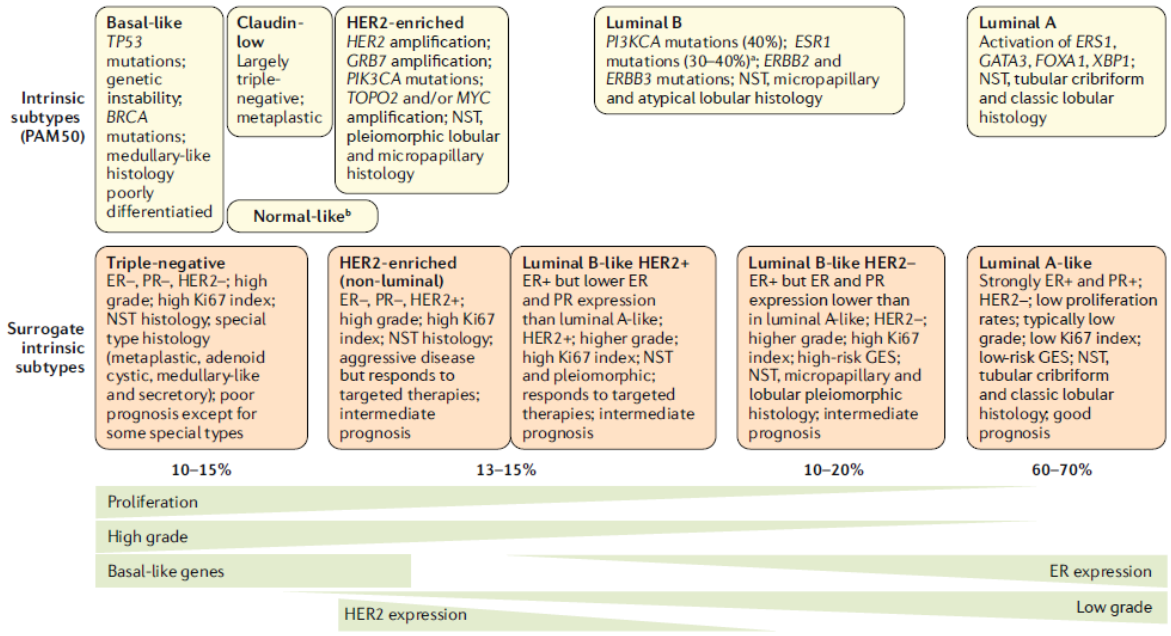

Fig. 1.3: Subtypes of breast cancer defined by gene expression profiling (intrinsic subtypes) and classical IHC molecular classification (surrogate intrinsic subtypes). Reproduced from: Harbeck *et al* (2019)[12].

1.1.3 Breast cancer therapies

The therapeutic decision process in breast cancer is driven by multiple clinical factors such as tumour stage, tumour subtype, patient's age, and general patient's health. The main therapies applied to breast cancer are surgery, radiotherapy, and systemic therapy, being the last one further subdivided in chemotherapy, or targeted therapy.

In early-stage breast cancer, defined as cancers localised within the breast, or those that have only spread to the axillary lymph nodes, treatment is applied with a curative intention. Advanced breast cancer (metastatic) is not considered curable and the main therapeutic goal is to prolong survival, to control symptoms and to maintain or improve quality of life[12,34].

1.1.3.1 Early-stage breast cancer

For early-stage breast cancer, tumour size and subtype are the main factors considered when deciding the therapeutic course for a patient[34]. Surgery is still the most common treatment choice to achieve a cure for BC patients. Most patients undergo surgery to remove local tumour, and post-surgery radiotherapy and/or systemic therapy (adjuvant therapy) is given depending on the tumour burden and molecular characteristics[12]. For patients with large tumour burden pre-surgery systemic therapy (neoadjuvant therapy) can also be given to decrease tumour size[12]. Radiation therapy is usually applied after surgery and independently of tumour subtype. It helps increase disease-free survival (DFS) and overall survival (OS) by elimination of residual tumour cells[35].

Depending on the tumour subtype, different treatment strategies are adopted in neoadjuvant and adjuvant settings (Fig. 1.4). All luminal tumours receive endocrine therapy, aimed at blocking ER signalling, after surgery, and if the patient is at risk of relapse (determined by high-risk gene expression signatures and affected lymph nodes), it can be complemented with chemotherapy. In TNBC and HER2+ breast cancer, subtype specific systemic neoadjuvant therapy is recommended (chemotherapy and/or anti-HER2 drugs) followed by further systemic therapy depending on the tumour response at the moment of surgery[12].

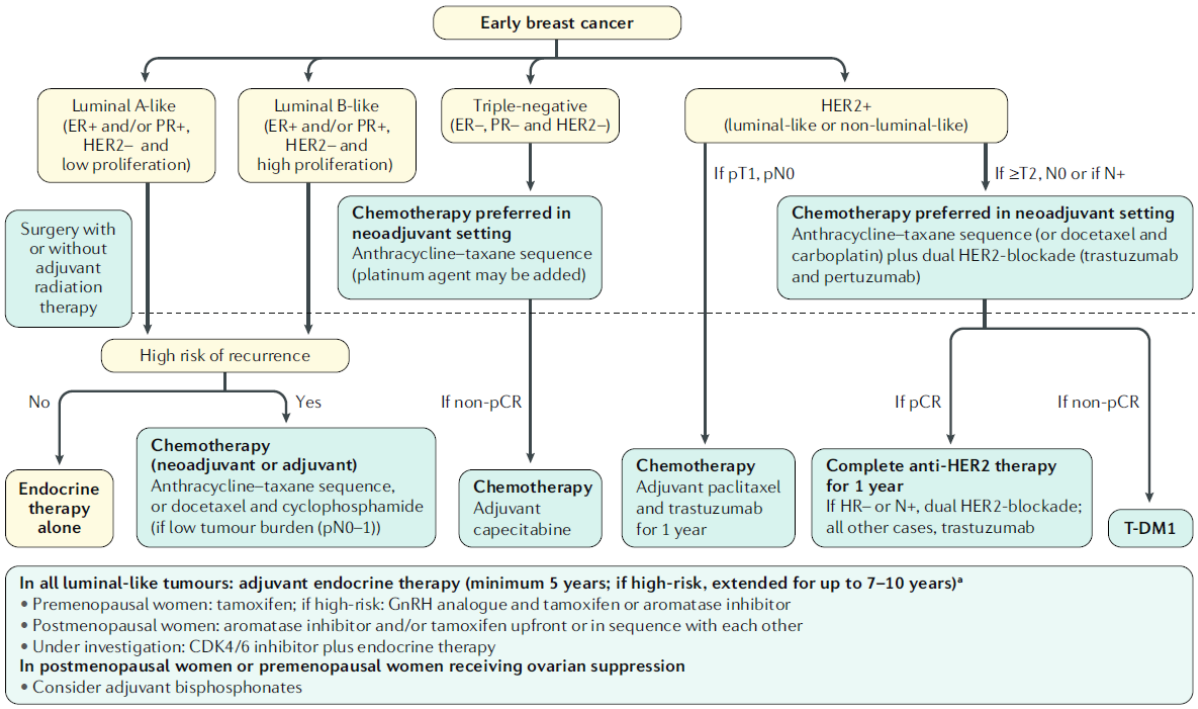

Fig. 1.4: Early-stage breast cancer treatment scheme based on molecular subtypes. Reproduced from: Harbeck *et al* (2019)[12].

Luminal tumours are usually treated with hormonal or endocrine therapy to disrupt the ER pathway[36]. Standard hormonal therapies include tamoxifen or fulvestrant, that target the oestrogen receptor, or aromatase inhibitors (anastrozole, exemestane and letrozole) that interfere with the conversion of androgens to oestrogen in post-menopausal women, reducing the amount of oestrogen available capable of binding to the ER receptor[37].

HER2+ tumours were historically treated with surgery and chemotherapy but have drastically improved their clinical prognosis with the introduction of anti-HER2 antibodies such as trastuzumab and pertuzumab[38–40].

Triple negative tumours lack the expression of ER and HER2 markers, making them unresponsive to hormonal therapy and trastuzumab. The standard treatment for TNBC, in general, remains systemic chemotherapy, mainly anthracyclines and taxanes[12].

Tumour relapse and consequent acquired resistance to conventional therapies is one of the most important challenges in breast cancer management. An estimated 10-20% of patients relapse within 10 years[41] of conventional treatment in early stages of BC with ER- tumours relapsing approximately three times more often and earlier than ER+ tumours[17]. Understanding the mechanisms of relapse in early breast cancer could allow the design of

more effective therapies and prevent or delay disease progression to more advanced stages.

1.1.3.2 Advanced breast cancer

Advanced breast cancer is characterised by inoperable local breast tumour or metastatic disease when the tumour has spread to distant organs. The most common metastatic sites for breast tumours are bone, lungs and liver[36]. The bone is the most common metastatic site for all subtypes of BC except for basal or TNBC which present the highest incidence of brain and lung metastasis. In comparison with luminal tumours, HER2 tumours also present a higher rate of brain, liver and lung metastasis[42].

Surgery, radiotherapy and systemic therapy are still applied on an individual basis as palliative treatment that aims to alleviate symptoms, pain and to extend survival and quality of life. Systemic therapy is also applied based on the molecular characteristics of the lesions. For all luminal and HER2+ cancer, all possible lines of endocrine therapy and HER2 targeted therapy are recommended until no further response is obtained[12].

In **luminal tumours** the PI3K/Akt/mTOR pathway has been linked with resistance to hormonal therapy[43]. A phase III trial (BOLERO-2) has demonstrated that the addition of mTOR inhibitors to hormonal therapy improved disease free survival which result in the approval of Everolimus (mTOR inhibitor) for the treatment of advanced BC with ER+ and HER2- tumours[44]. Cyclin dependent kinase 4/6 (CDK4/6) has also been implicated in the development of breast cancer. Palbociclib and ribociclib (CDK4/6 inhibitors) in combination with hormonal therapy have been recently FDA approved for the treatment of hormone receptor-positive, HER2-negative advanced-stage or metastatic breast cancer, although intrinsically endocrine resistant patients are less likely to benefit from this treatment[45].

In **HER2+** tumours, resistance to targeted therapies can arise from multiple factors, such as obstacles preventing trastuzumab binding to HER2, upregulation of HER2 downstream signalling pathways, signalling through alternate pathways and/or failure to trigger an immune-mediated mechanism to destroy tumour cells[45]. In an attempt to overpower some mechanisms of resistance, trastuzumab emtansine (T-DM1) (antibody–cytotoxic drug conjugate) was developed for HER2+ tumours and it significantly improved both DFS and OS when compared to patients treated with conventional HER2 therapies[46].

A significant percentage of **TNBC** bears *BRCA* mutations (10 to 40%). *BRCA1/2* genes are involved in DNA repair and it was hypothesised that the inhibition of further DNA repair enzymes, like Poly ADP-ribose polymerases (PARP), would lead to cell death[47]. The use of PARP inhibitors in patients bearing *BRCA* mutations has shown clinical benefit[48], being very recently approved for germline *BRCA* mutated metastatic breast cancer[49]. A summary of breast cancer targeted therapies for early and advanced BC can be found in Fig. 1.5.

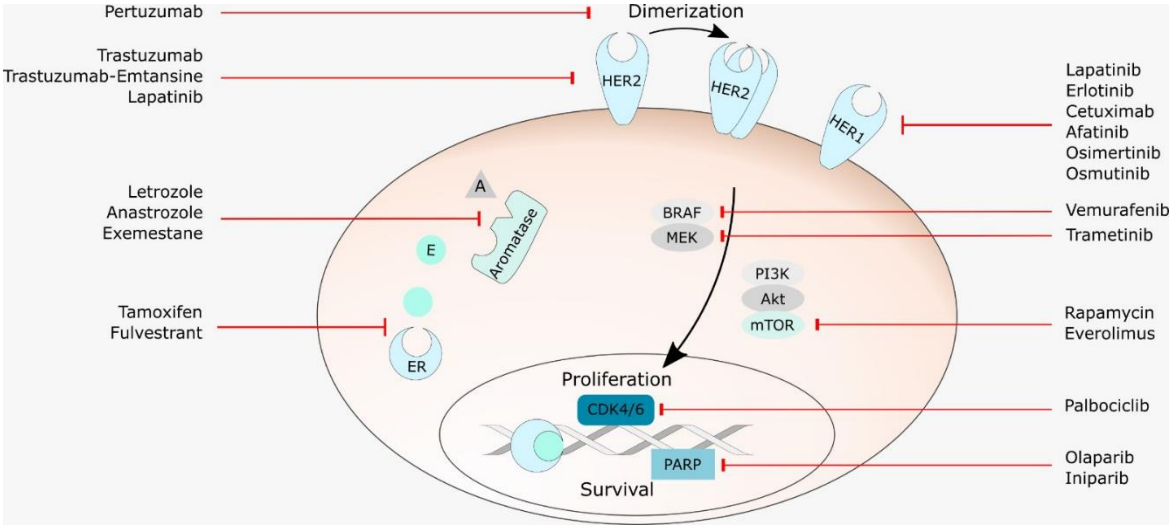

Fig. 1.5: Targeted therapies currently approved for early and advanced breast cancer. Image provided by Andrea Abaurrea.

Despite improvements to overcome drug resistance, in the advanced setting it is estimated that that 50% of patients with metastatic disease will not respond to endocrine therapy[50] and that around 50% of the patients treated with anti-HER2 therapies will progress within one year[51]. TNBC are the group with worse prognosis when it comes to metastatic disease with a mean overall survival of only 18.5 months[52].

The high incidence of tumour relapse and consequent progression to advanced stages underlines the need to better understand the mechanisms of resistance and to identify alternative therapies less prone to generate resistance.

A growing amount of evidence links the tumour microenvironment with response or resistance to treatments[53,54]. In fact, the interplay between cancer cells with the

surrounding tumour microenvironment has been linked with all stages of cancer progression, including primary and acquired resistance[55]. Targeting tumour microenvironment interactions has been on the spotlight to discover new therapeutic targets in cancer. In the following sections, a few concepts pertinent to the tumour microenvironment and inflammation will be introduced to contextualise the work presented in this thesis.

1.2 Tumour microenvironment and inflammation in cancer

1.2.1 The tumour microenvironment

Tumours are defined as a mass of heterogeneous cancer cells co-existing with a variety of non-malignant host cells, secreted factors and an extracellular matrix that together constitute the tumour microenvironment (TME)[56,57]. The seed and soil metaphor has been used many times to describe tumour and its microenvironment. It resembles the extreme importance of the soil (microenvironment) in providing hosting, nutrients, and support for the seed (tumour) to grow. The TME profoundly influences tumour cells and ultimately determines the fate of the tumour by actively influencing all stages of tumour progression from intravasation into the blood circulation to metastasis formation (Fig. 1.6). Consequently, the TME represents an appealing target for cancer therapy[54,58,59].

Constituents of the TME include cells of the immune system, blood cells, endothelial cells, fat cells (particularly important in the breast microenvironment), and the stroma, that is, in turn, classified as cellular and non-cellular connective tissue that supports functional tissue. The stroma is composed of specialized connective-tissue cells, including fibroblasts, mesenchymal stromal cells, osteoblasts, and chondrocytes, and the extracellular matrix (ECM)[56]. There is still some controversy in defining tumour stroma as some researchers in the TME field occasionally include other specialized cell types, such as endothelial cells, pericytes, adipocytes, and immune cells, as members of the stromal compartment[57,59,60].

In the next sections, a small introduction to fibroblasts and myeloid cells will be presented as they are the most relevant TME populations for this work.

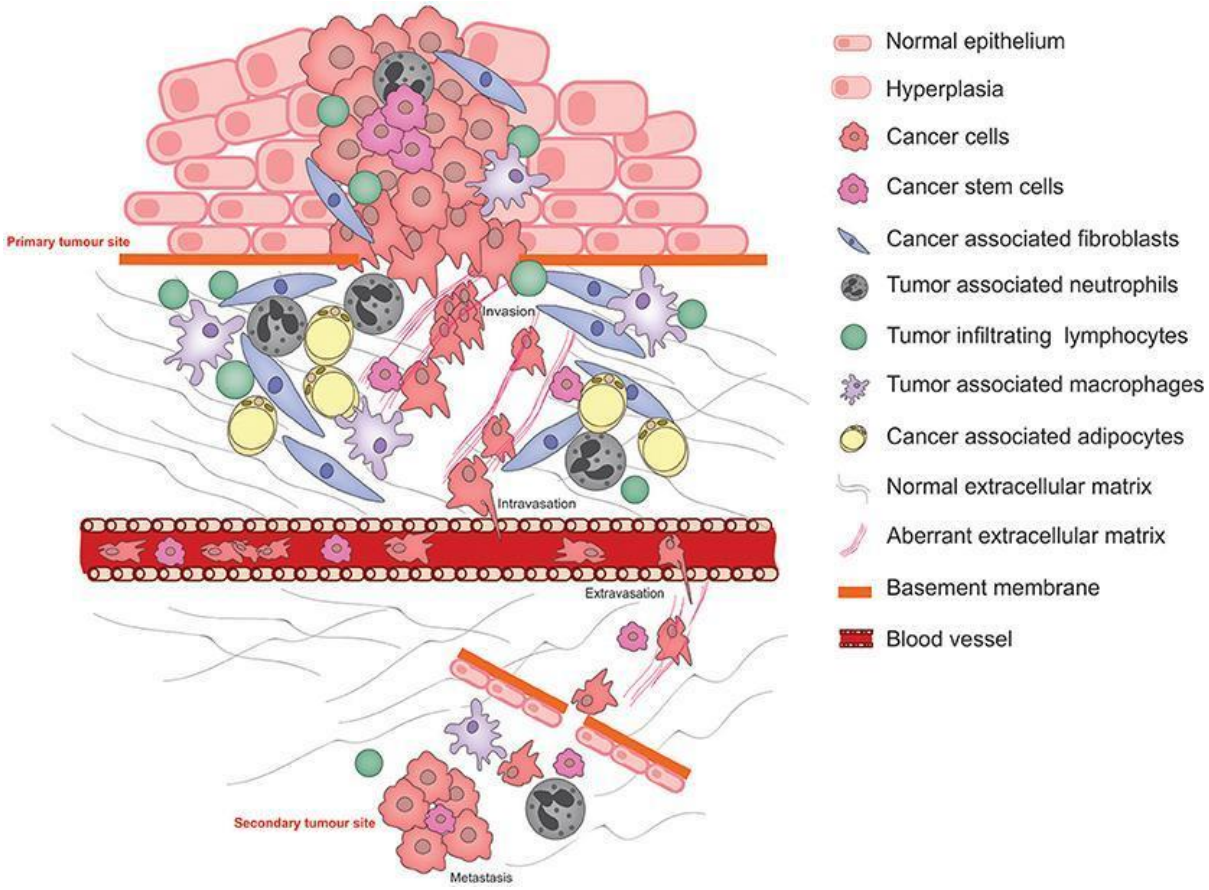

Fig. 1.6: Tumour microenvironment components and different stages of cancer progression (invasion, intravasation, extravasation and metastasis). Reproduced from: Poltavets *et al* (2018)[61].

1.2.1.1 Cancer associated fibroblasts

Under physiological conditions, fibroblasts play an important role in maintaining the architecture and structural framework of tissues and in wound healing[62]. Upon tissue injury, they have the capacity to differentiate to myofibroblasts, synthesise and remodel extracellular matrix, and communicate with the innate immune system[63]. In the TME, these physiological functions are many times hijacked by tumour cells and used to their advantage.

Cancer associated fibroblasts (CAFs) are highly heterogeneous and they are defined as cells with no expression of epithelial, endothelial and leukocyte markers, with an elongated morphology and lacking the mutations found within cancer cells[64]. Some studies have attempted to identify the origin of CAFs, associating it with reprogrammed resident tissue fibroblasts[65], bone marrow-derived mesenchymal cells (MSCs)[66], adipocytes[67], and

endothelial cells[68]. Due to the lack of specific markers, there is still some uncertainty regarding the origin of CAFs[64].

In most solid tumours, such as breast and pancreatic carcinomas, CAFs are the most prominent cell type within the TME[69]. They become activated by several mechanisms such as changes in mechanical cues, metabolic stress, DNA damage and inflammatory signals[64] (Fig. 1.7). The presence of activated CAFs in the TME is associated with worse prognosis in several types of cancer[70]. They have been shown to enhance tumour progression by remodelling the ECM, inducing angiogenesis and secreting growth factors that stimulate tumour proliferation[71–73]. They have also been implicated in mediating the recruitment and activation of immune cells[74], and recent studies suggest that these tumour promoting activities are mediated by distinct subpopulations of CAFs[64,66,74,75].

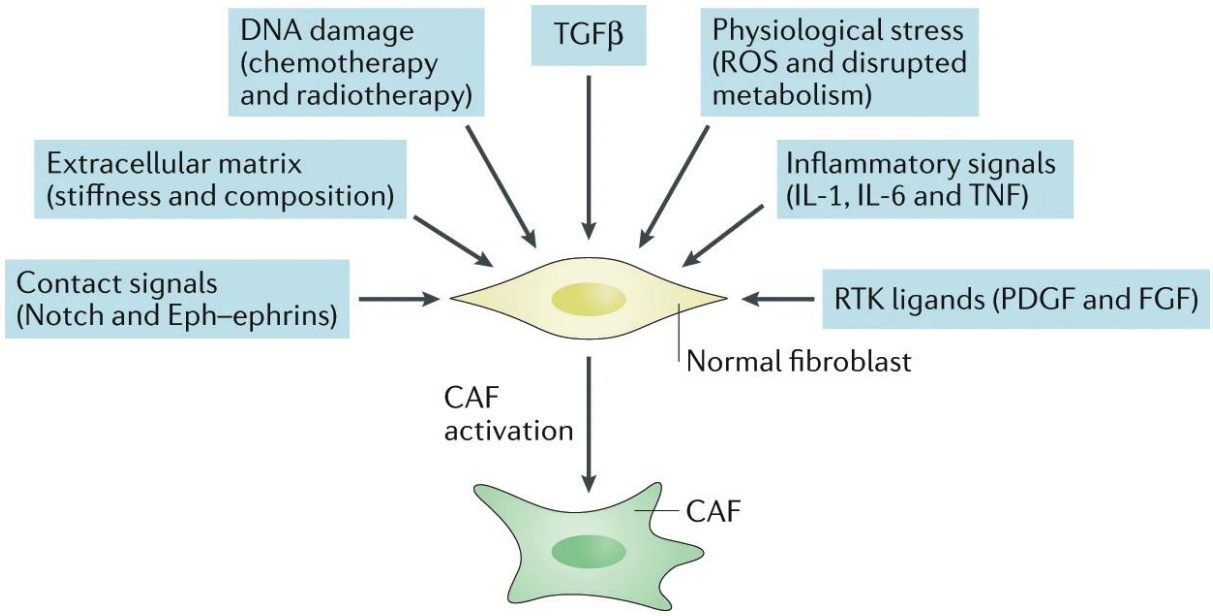

Fig. 1.7: Mechanisms of activation of cancer associated fibroblasts. Reproduced from: Sahai *et al* (2020)[64].

1.2.1.2 Myeloid cells

Myeloid cells belong to the innate immune system and they form a diverse group of cells with highly adaptive phenotypes depending on their tissue of residence[76].

They all arise from a common myeloid progenitor (CMP), found in the bone marrow, that can further differentiate into subtypes including neutrophils, monocytes, dendritic cells and macrophages[77] (Fig. 1.8). Although it is believed that most cells enter blood circulation

and infiltrate distant tissues, some of them, such as macrophages, can also arise from embryonic precursors and develop into tissue-resident macrophages[78].

Myeloid cells exist in different states and possess very distinct functions being the predominant leukocyte population within the TME[79]. Their number and function can be shaped by tumour cells and the natural evolution of the tumour microenvironment[79]. Macrophages and myeloid derived suppressor cells (MDSCs) have received a lot of interest in the last decades as they have been associated with a strong immune suppressive capacity that facilitates tumour progression[80]. Their pro-tumoral functions will be discussed further in the following sections.

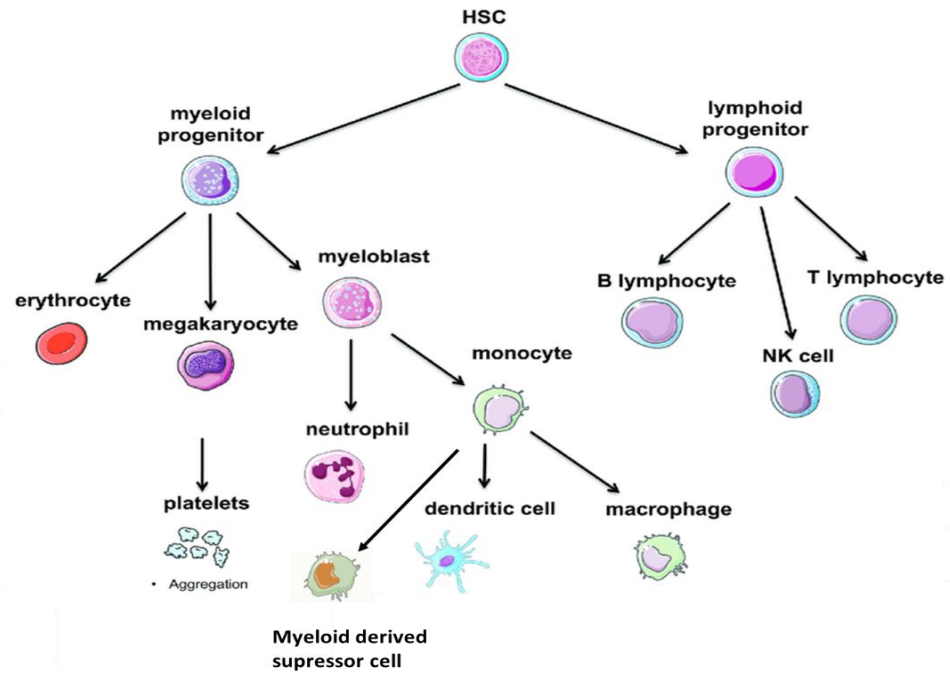

Fig. 1.8: Myeloid and lymphoid blood cell lineage. Reproduced and adapted from: Axelrod *et al* (2014)[77].

1.2.2 Inflammation in cancer

Inflammation is defined as a biological response triggered by the body's immune system to fight harmful insults to tissues. Inflammatory responses in the tumour microenvironment have been long described to contribute to cancer progression[81]. The role of inflammation in cancer progression was first postulated by Rudolph Virchow in 1858[82]. A century later, Dvorak described cancer as "a wound that does not heal"[83] and in

2011, Hanahan and Weinberg stated in their renowned review that inflammation was an underlying event essential to foster many hallmarks of cancer[84]. It is now well known that inflammation plays a key role in all stages of cancer progression, and during the last couple of decades, inflammation has generated a great deal of interest in cancer research[81,85,86]. Taking the seed and soil metaphor to represent the complex interactions between tumour cells and their microenvironment, inflammation is seen as the rain in this metaphor. Rain (inflammation) is the fuel that allows the seed to grow in the soil. To comprehend the importance of inflammation in cancer, first, it is important to understand its physiological role, described in section 1.2.2.1.

1.2.2.1 Inflammation

The major regulators of inflammation are cytokines, which are small-secreted molecules that function in cell-to-cell communication. Chemokines are a subfamily of cytokines involved in chemotactic activation of leukocytes. When tissue injury happens, a complex network of events is triggered to ensure wound healing and host defence against possible pathogens. In initial stages, leukocytes such as neutrophils, monocytes and eosinophils are recruited to the injury site. This migration of cells is mainly led by chemotactic factors such as TGF-β, PF-4, PDGF, chemokines (CCL2,3,4, 7 & 8) and cytokines IL-1β and TNF-α[81]. Once at the tissue site, monocytes get activated and convert to mature macrophages or immature dendritic cells[87], the main source of growth factors and cytokines that modulate tissue repair. This activity has a profound impact in endothelial, epithelial, mesenchymal and neuroendocrine cells. Apart from this, macrophages can also modulate angiogenesis, clear apoptotic cells, regulate local tissue remodelling and inducing ECM deposition[81,88]. TGF-β1, -β2 and -β3, PDGF, IL-1α, -1β and -4, and mast cell tryptase induce fibroblasts to deposit collagen, a substance necessary for consequent re-epithelialization of the injury site, the last step of wound healing[81].

All these processes are tightly regulated by extensive negative feedback mechanisms designed to stop inflammation once injury is resolved. A clear example of this mechanism is the action of TGF- β, a pro-inflammatory cytokine that regulates leukocyte recruitment, adhesion and regulation of secretion and activation of metalloproteinases (MMPs). As inflammatory cells get activated, their TGF-β receptors change resulting in sensitivity to TGF-β mediated suppression, a critical event to resolve inflammation[89].

Acute inflammation is, therefore, regulated by pro- and anti-inflammatory components that ensure injury repair and end of inflammatory responses upon restoration of normal tissue function.

1.2.2.2 Pro-tumoral inflammation

Chronic inflammation has been linked to neoplastic processes in patients with chronic inflammatory conditions such as bronchitis, gastritis, inflammatory bowel disease, Crohn's disease, chronic ulcerative colitis, skin inflammation, hepatitis, AIDS, amongst others[81,90]. Sustained chronic inflammation induces DNA damage in proliferating cells as a result of reactive oxygen and nitrogen species production by leukocytes, a natural response to fight infection[91]. If the initial tissue disturbance is accompanied by an oncogenic event, inflammation may not remove the cause of the perturbance but rather, sometimes, provide a nourishing microenvironment that feeds the tumour with enhanced inflammatory responses and cytokines that favour tumour growth and progression[92], as illustrated in Fig. 1.9. Nevertheless, a vast number of tumours do not arise from pre-established long-term chronic inflammation[85], but they have the capacity to activate the expression of different chemokines and cytokines capable of inflammatory cells recruitment and establishment of long-term inflammation[93]. According to Mantovani *et al* (2008), most solid tumours, including breast cancer, trigger an inflammatory response that builds up a pro-tumorigenic microenvironment[92].

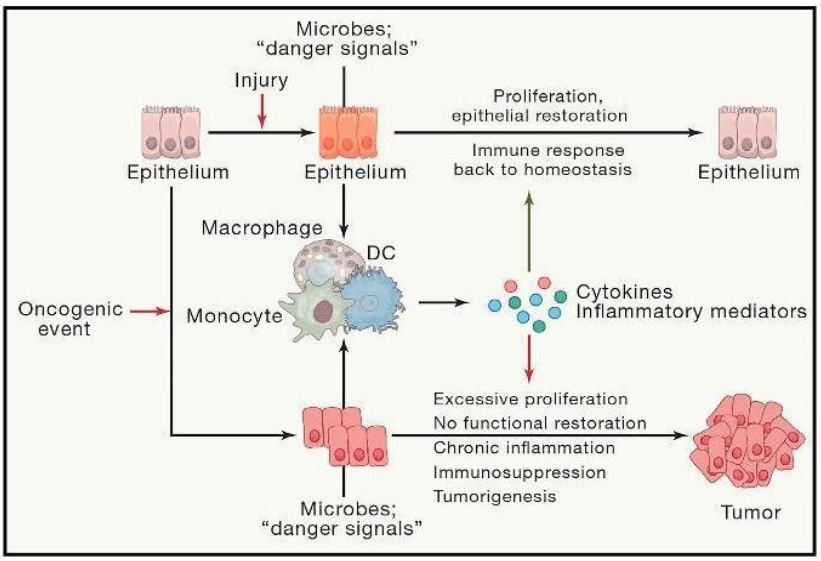

Fig. 1.9: Functional differences and similarities between inflammation in cancer and inflammation during infection and tissue regeneration. Reproduced from: Greten *et al* (2019)[85].

Activation of oncogenes is often mechanistically associated with the production of cytokines and chemokines and consequent recruitment of myeloid cells that generate a supportive TME. For example, K-RAS activation is associated with induction of CXCL3 cytokine, a potent myeloid modulator in colorectal cancer[94]. In mutated cells, cytokine receptor signalling might promote the induction of pro-survival signals particularly mediated by NF-kB, STAT3, and other types of signalling, increasing the survival probability of mutated clones[95–97]. Solid tumours at some point develop a hypoxic core due to the lack of sufficient blood supply. This consequently results in cell death and release of pro-inflammatory cytokines such as IL-1 and HMGB1 that triggers an inflammatory response that promotes neo-angiogenesis and provides additional growth factors[98].

1.2.2.3 Anti-tumour immunity and tumour-induced immunosuppression

Almost paradoxically, despite benefiting from some degree of inflammation within the TME that feeds the tumour with growth factors and survival signals, tumours also face constant immune system surveillance[99]. Altered cancer cells often produce neoantigens and generate an immunogenic context that is susceptible to T cells targeted elimination. The ratio of T cells is crucial to determine the successful elimination of tumour cells[100]. As a response, the tumour develops mechanisms to suppress the immune response to be able to survive[101]. CD8+ and CD4+ T cells recognise antigens presented by the MHC class I and

II complex, respectively. Some of the most well described mechanisms by which tumours cells manage to escape T cells surveillance is by downregulating the expression of MHC molecules on the cell surface[102], by expressing high levels of the immune checkpoint inhibitors (CTLA-4 and PDL-1), by modulating regulatory T cells (Treg) function, and by recruiting and shaping immune myeloid suppressive cells such as tumour associated macrophages (TAMs), MDSCs, and tumour associated neutrophils (TANs)[101]. TAMs, TANs and MDSCs are considered the most relevant immune cell types for cancer progression as they are the main tumour infiltrating myeloid (TIMs) subsets found within most established cancers[103]. The tumour promoting functions of TIMs are typically activated by cytokines and growth factors such as IFN-γ, IL-4, IL-6, IL-10, IL-13, and TGF-β that upregulate various transcription factors including the master regulator STAT3 in most myeloid cell subsets[104,105].

In summary, the tumour microenvironment contains anti- and pro-inflammatory components with high degree of plasticity, and sometimes even ambiguous roles, which evolve with tumour progression. When cancer succeeds in tipping the balance to a more pro-tumoral microenvironment is when the tumour is able to survive and progress, as summarised in Fig. 1.10.

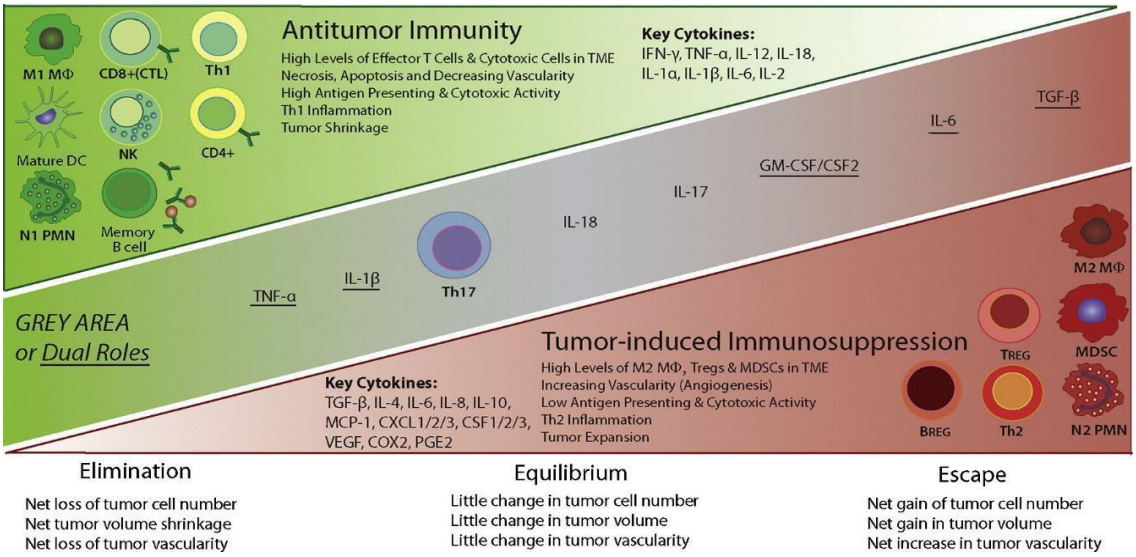

*MΦ: macrophage; Th1/2: T helper cells; DC: dendritic cells; PMN: polymorphonuclear leukocyte; NK: Natural Killer; Treg: Regulatory T cells; MDSC: Myeloid derived suppressor cells; Breg: regulatory B cells.

Fig. 1.10: Anti- and pro-tumoral cells in the immune TME component and associated factors. Reproduced from: Burkholder *et al* (2014)[106].

1.2.3 Inflammation in breast cancer

Historically, breast tumours have been described to have low mutation burden and to present a low degree of immune infiltration, therefore being regarded as "cold tumours"[107,108]. It has been demonstrated that even the cancers not directly associated with persistent infections or chronic inflammation, such as breast cancer, can exhibit tumour-associated inflammation, which has important consequences in tumour promotion, progression and metastasis[109,110].

Despite the lack of extensive infiltration, the composition of the infiltrates themselves can give important information regarding the state of the tumour microenvironment and even correlate with prognosis in some breast cancer subtypes. For example, TNBC and HER2+ breast tumours with higher degree of tumour infiltrating lymphocytes (TILs) tend to respond better to therapy than those with lower degree of TILs infiltration and they even present a higher likelihood of a complete pathological response after neoadjuvant chemotherapy[108,111–113]. On the contrary, presence of tumour infiltrating myeloid cells, especially MDSCs and the non-myeloid Treg cells, have been associated with an immune suppressive TME that aids tumour cells to escape immune surveillance by inducing T cell suppression[103,114,115].

1.2.4 Targeting cytokines in cancer

Cytokines have been linked to all stages of breast cancer progression from tumour initiation, tumour growth, angiogenesis to metastasis[116–119]. In a study conducted on 185 patients with breast cancer and 54 volunteers, Kawaguchi *et al* (2019)[120] found that BC patients were distinguishable from healthy volunteers based on the cytokine composition present in the blood serum. Furthermore, they identified the cytokines that could form a metastasis signature[120], suggesting that cytokines could potentially be used as biomarkers and therapeutic targets to modulate immune responses within the tumour.

The idea of targeting and manipulating cytokines in cancer treatment is not new. Preclinical experiments with interferon alpha (IFNα), granulocyte-macrophage colony-stimulating factor (GM-CSF), interleukin IL-2, IL-12, IL-15, and IL-21 have shown efficacy in multiple murine cancer models, but, nevertheless, cytokines have not fulfilled the initial high expectations of a possible monotherapy to treat breast cancer[120]. This might be due to the

fact that inflammation is a very tightly regulated process and manipulating a single cytokine can trigger feedback loops that neutralise the treatment and even produce associated toxicity[120]. Cytokine targeting has also been exploited for some time as a possible strategy to reprogram/reduce TIMs and shape the microenvironment tipping the balance to a more anti-tumoral TME. For example, Bin-Zhi Qian *et al* (2011)[121] demonstrated that the inhibition of CCL2-CCR2 signalling blocks the recruitment of inflammatory monocytes, inhibits metastasis in vivo and prolongs the survival of tumour-bearing mice. Dominguez *et al* (2007) have described that neutralising IL-8 with a monoclonal antibody (HuMax-IL8) in TNBC significantly decreases the recruitment of polymorphonuclear myeloid-derived suppressor cells (PMN-MDSCs) at the tumour site, an effect substantiated when used in combination with docetaxel[122]. All these studies suggest that targeting cytokines could be a good strategy to reshape the influence of TIMs in the tumour microenvironment. Some clinical investigations combine cytokines with anti-cancer vaccines, checkpoint inhibitor antibodies (anti-CTLA-4 or anti-PD-1/PD-L1), and the injection of cytokines with cancer-directed monoclonal antibodies in order to increase the antibody-dependent cellular cytotoxicity of these antibodies, thereby augmenting their anti-tumour efficacy[123].

Despite initial great promise as a potential new therapeutic approach for the treatment of cancer progression, no therapies targeting cytokines have successfully reached the clinic yet. Designing a cytokine-based drug is a big challenge that requires deep knowledge of cytokine biology to be able to exploit their anti-tumour activity while keeping toxicity to a minimum[123].

1.3 IL-6 family and inflammation in cancer

1.3.1 IL-6 family

Interleukin 6 (IL-6) is a multifunctional cytokine with a wide range of biologic activities consisting of 184 amino acids and a molecular weight of 26 kilodaltons (kDa)[124,125]. IL-6 family plays an important role in inflammation, immune responses, and haematopoiesis[126]. Deregulation of IL-6 signalling has been associated with chronic inflammation, autoimmunity, infectious disease and cancer, where it often acts as a diagnostic or prognostic indicator of disease and response to therapy[85,127,128]. More recently, IL-6 has

also been proposed as a target to treat macrophage activation syndrome-like disease in COVID-19, making it an appealing target for clinical intervention in several contexts[129].

The interleukin 6 family is composed of IL-6, IL-11, IL-27,IL-30 (also called IL-27P28), IL-31 ciliary neurotrophic factor (CNTF), leukaemia inhibitory factor (LIF), cardiotrophin 1 (CT-1), cardiotrophin-like cytokine (CLC), and Oncostatin M (OSM), all sharing the common receptor signalling subunit gp130 (gp130)[127,130] (Fig. 1.11). Cytokine specificity is dependent on the unique cell surface receptor which dimerises with gp130, present in all body cells, while specific receptors show a more restricted expression pattern depending on cell type. This restricted pattern is what makes some cells more responsive to certain cytokines than others[127]. Activation of the dimer (cytokine specific subunit + gp130) triggers the activation of the Janus kinase (JAK)-STAT pathway and the mitogen-activated protein kinase (MAPK) pathway. Cytokine receptors do not possess intrinsic kinase activity. The binding of extracellular ligands induces conformational changes in the receptors that facilitate interactions with the intracellular JAKs and consequent mutual phosphorylation. Trans-phosphorylated JAKs then phosphorylate downstream substrates such as the signal transducers and activators of transcription (STATs) which act as transcription factors. Activated STATs enter the nucleus and activate context dependent genes[131].

STATs also induce suppressors of cytokine signalling (SOCS)[132,133] which bind to tyrosine-phosphorylated JAK and gp130[134] to stop IL-6 related cytokine signalling by means of a negative feedback loop[127].

In breast cancer, IL-6 signalling has been associated with a multitude of cancer hallmarks and malignant processes. It has been associated with tumour growth[135], invasiveness and angiogenesis[136], metastasis[137], stem cell maintenance[138], EMT[139], disease stage[140], and it has also been linked to modulation and immune suppression in the tumour microenvironment[141]. Whether all these roles in cancer are exclusive of IL-6 or interchangeable amongst members of the same family is still not entirely clear. The IL-6 family has been described to have a great deal of promiscuity, with some members binding different receptors and inducing different physiological outcome[127]. Discovering exclusive/redundant roles for IL-6 and other members of the family could be an important milestone to design effective targeted therapies for breast cancer patients.

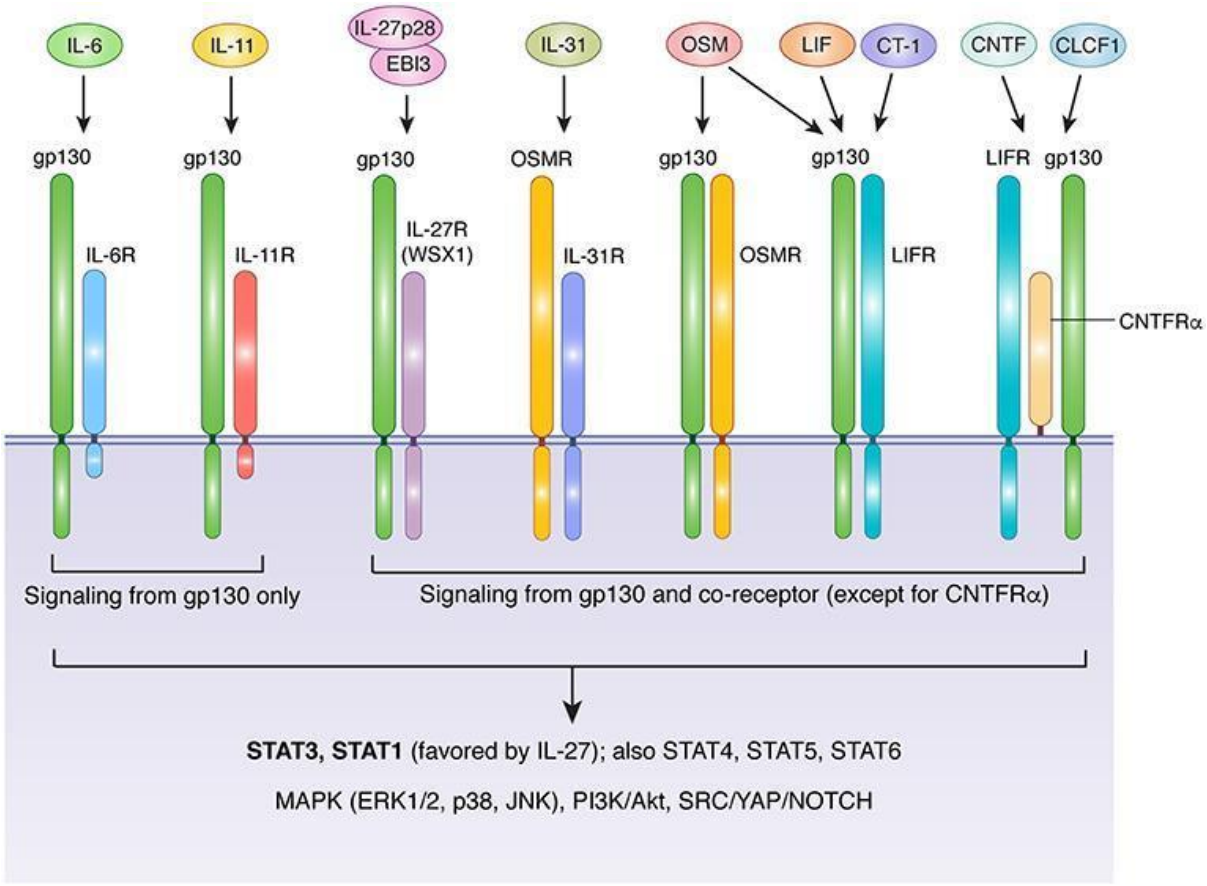

Fig. 1.11: IL-6 cytokine family. Reproduced from: West *et al* (2019)[130].

1.3.2 OSM:OSMR

OSM is a pleiotropic cytokine that is composed of 196 amino acids in its active form[142,143]. It belongs to the IL-6 family and it is probably one of the most controversial cytokines due to the reported contradictory functions[144]. It was first identified in 1986 when it was characterised by its antiproliferative effect on A375 melanoma cells, a function that gave origin to its name "*Onco Statin*"[145]. OSM signals mainly through the cell receptor Oncostatin M receptor (OSMR), but also through the leukaemia inhibitory factor receptor (LIFR), and both form heterodimers with the subunit gp130[143,146] (Fig. 1.11 and Fig. 1.12). OSM shares similar structural and functional features with LIF, that can also bind LIFR. Nevertheless, OSM distinct functions can be explained by its unique ability to interact with OSMR[146].

Most of the cancer associated studies report critical roles for OSM:OSMR axis but very little is associated with its activity through LIFR[147] mainly due to the fact that LIFR is expressed at low levels in epithelial, haematopoietic and mesenchymal cells while OSMR is found

highly expressed in epithelial cells and various non haematopoietic mesenchymal cells, including fibroblasts, endothelial cells, smooth muscle cells, osteoblasts and adipocytes, as well as hepatocytes, mesothelial cells, glial cells and epithelial cells from several organs[144,147–149].

Like other members of the IL-6 family, OSM signals through JAK/STAT pathway (Fig. 1.12). Unlike IL-6 that relies solely on JAK1 activation, OSM can send downstream signals through JAK1 and JAK2, which makes the nature of OSM signalling context dependent and provides OSM with unique biological activities[143,150]. OSMR can bind gp130 to form a high affinity receptor for OSM but it can also bind IL31RA to act as a receptor for IL-31 cytokine[149,151]. OSM signalling itself promotes OSMR expression creating a positive feedback loop[152].

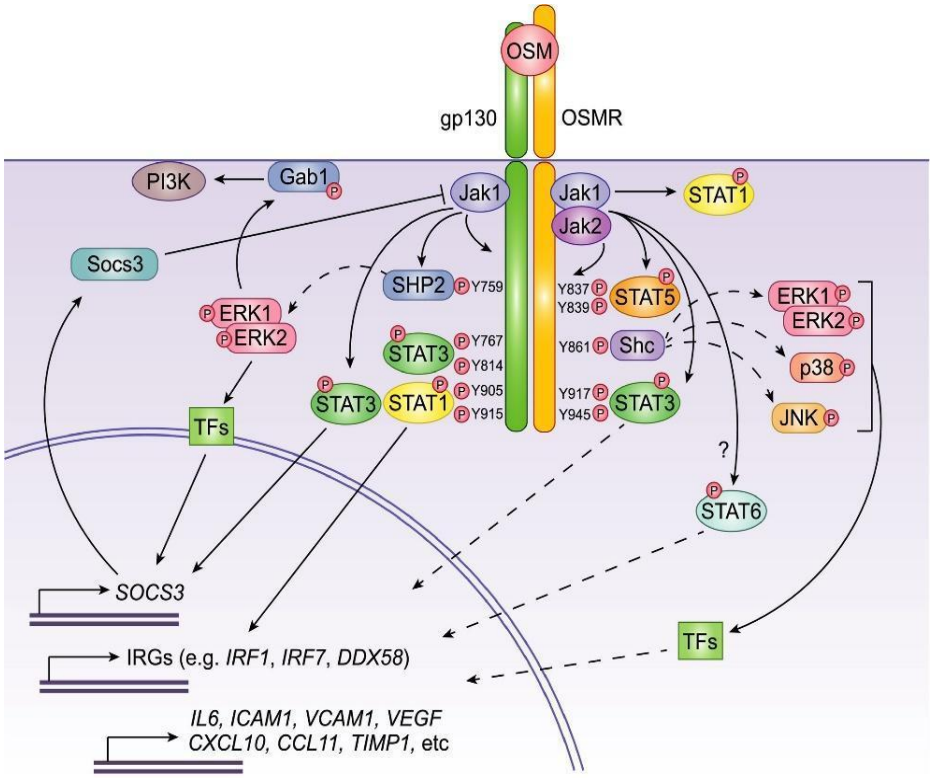

Fig. 1.12: OSM:OSMR signalling. Reproduced from: West *et al* (2018)[147].

OSM has been described to play important roles in homeostatic and pathological processes. Together with other members of the IL-6 family it has been associated with cell proliferation control, apoptosis, differentiation, survival and it has been described as a strong contributor of inflammatory, haematopoietic and immune responses[144,147,149,153]. $OSM^{-/-}$ and $OSMR^{-/-}$ mice and rat models are important tools that allowed the dissection of relevant physiological functions of OSM:OSMR signalling. In more detail, OSM was

described to play a role in liver homeostasis after OSMR$^{-/-}$ mice showed impaired liver regeneration after carbon tetrachloride (CCl4) exposure[154]. Lower numbers of peripheral erythrocytes and platelets were also observed in OSMR$^{-/-}$ compared to wild-type mice, being demonstrated that OSM regulates hematopoiesis *in vivo* through stimulation of megakaryocytic and erythrocytic progenitors[155]. OSM was demonstrated to confer neuroprotection after ischemic stroke when OSMR$^{-/-}$ rats exhibited a larger infarct size than their OSMR$^{+/+}$ littermates, after being exposed to the same brain lesion[156]. Some of the most important described functions of OSM signalling are summarised in Fig. 1.13. Despite numerous studies that elucidated the role of OSM in specific tissue and organs, its function in other contexts remains uncertain and not so well understood as IL-6.

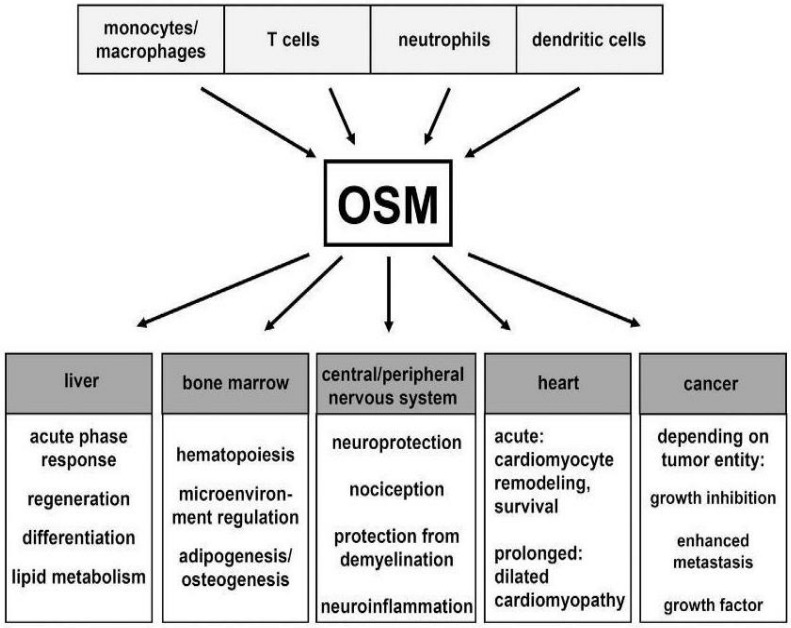

Fig. 1.13: Summary of target tissues and activities of OSM in physiological and pathophysiological functions. Reproduced from: Hermanns (2015)[149].

1.3.3 OSM:OSMR in cancer

As a member of the IL-6 family, it is unsurprising that OSM:OSMR axis has been linked with cancer. OSM was first described to have anti-proliferative effects in melanoma cells[145]. Later, it was also linked to decreased proliferation in MDA-MB-231 and MCF7 breast cancer cells *in vitro*[157], and glioblastoma cells *in vivo*[158]. In hepatocellular carcinoma it was shown

to induce differentiation and apoptosis and reduced cell viability of SMMC-7721 cells[159]. OSMR methylation was shown to correlate with resistance of colorectal cancer cells to anti-proliferative features of OSM[160]. Pan *et al* (2014), described that OSM repressed metastasis of lung adenocarcinoma cells by enhancing the suppressive effect of the STAT1 signalling and inhibiting the stimulatory effect of the STAT3 signalling pathway[161]. OSM was reported to reduce tumour proliferation and increased apoptosis in chondrosarcoma through JAK3/STAT1 axis[162]. These studies suggest that the inhibitory effect of OSM could be associated with STAT1 activation rather than STAT3, but further studies are needed to further understand the mechanisms of anti-tumoral effects of OSM signalling.

In general OSM is considered to have anti-proliferative functions, with few exceptions such as in Kaposi's sarcoma cells[163], ovarian cancer[164], Ewing sarcoma[165] and prostate cancer cell lines[166], but one the other hand, OSM:OSMR axis has been linked with several hallmarks of cancer described below.

OSM has been shown to enhance malignant progression of prostatic intraepithelial neoplasia *in vivo*[167]. Metastatic melanoma cell lines were shown to be insensitive to inhibitor effect of OSM and this was correlated to the loss of the specific OSMR chain[168]. Other studies have also linked OSM with an invasive and pro-metastatic capacity. Fossey *et al* (2011) described that OSM induced MMP-2 and VEGF expression in human osteosarcoma cells *in vitro* and an increase in invasiveness through matrigel[169]. In gastric cancer OSMR was shown to promote cancer growth and metastasis upon treatment with OSM[170]. Besides promoting metastasis, OSM:OSMR was also associated with EMT, a developmental process strongly associated with invasion, resistance to apoptosis and dissemination[171]. OSM was described to induce EMT in lung and pancreatic cancer cell lines *in vitro*[172], and in glioma cells through STAT3 signalling[173].

In glioblastoma it was described to associate with EGFRvIII and act as a co-receptor for EGF and OSM capable of inducing STAT3 phosphorylation[174]. OSMR knockdown strongly reduced cell proliferation and tumour growth of mouse glioblastoma cells and human brain tumour stem cells xenografts in mice[173].

Mechanisms of OSM signalling regulation have been associated with the ability of cells to contour OSM inhibitory effect. Truncated forms of OSMR have been reported such as soluble OSMR (sOSMR) or OSMR short-form (OSMRs) in lung adenocarcinomas[175], glioblastoma and melanoma[176], oesophageal squamous cells carcinoma[177] and they are

believed to act as decoy receptors[175]. Methylation of OSMR resulting in OSMR downregulation has also been associated with decreased sensitivity to OSM and a possible mechanism of escaping OSM anti-proliferative effect[160,178]. The reported mixed observations between *in vitro* and *in vivo* settings and between different disease models suggest that OSM can be extremely context dependent.

The work performed in Prof. Coleman's laboratory in Cambridge (UK), has demonstrated that, in cervical squamous cell carcinoma, OSMR is copy number gained and overexpressed which led to the hypothesis that OSM:OSMR axis promoted a pro-tumoral effect in cervical cancer[179]. Our previous work suggested that OSMR could be a new therapeutic target in cervical cancer[180] after linking OSMR with a pro-angiogenic phenotype, increased cell motility and invasiveness[181] and described that OSMR was exerting its malignant effects through OSMR/TGM2/integrin-α5β1/fibronectin pathway[182]. Later, we also described that OSM induces EMT in cervical cancer and it is associated with poor survival[183] (Fig. 1.14).

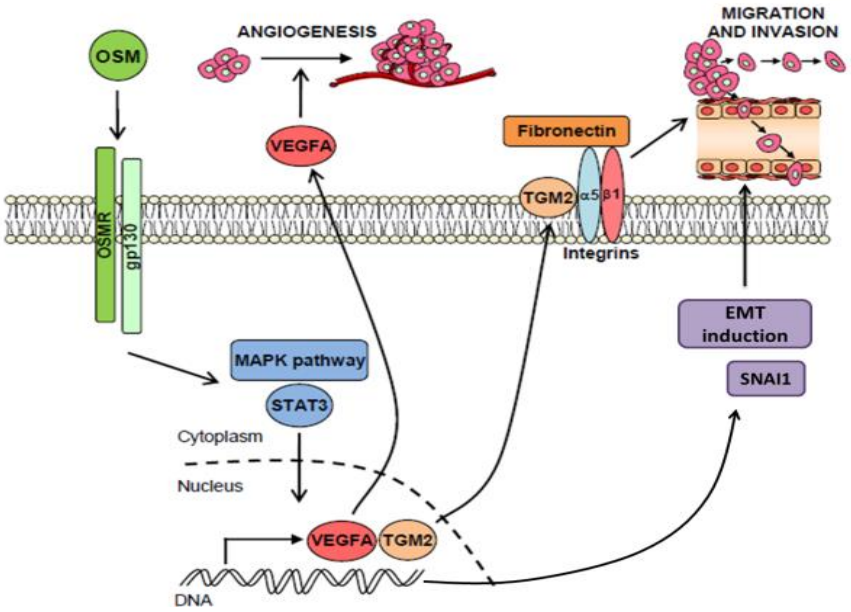

Fig. 1.14: Described pro-malignant effects of OSMR in cervical cancer and associated downstream signalling pathways. Reproduced from: Caffarel & Coleman (2013)[182].

This work suggested that OSMR was contributing to cervical cancer malignancy, that it could be a candidate for targeted therapy, and that it could potentially be extrapolated to other squamous cell carcinomas (SCCs) of different origin such as head and neck SCCs[183,184]. Malignant effects of OSMR signalling in cervical cancer were reverted using an antibody

against OSM *in vivo* strongly supporting the idea that blocking OSMR signalling is a potential targeted therapy to be tested in clinical trials[184].

In summary, OSM:OSMR axis in cancer has been described to play important roles in survival, proliferation, angiogenesis, invasiveness, and metastasis. The above described pro- and anti-tumoral roles of OSM highlight the need to understand the biology of OSM signalling in each specific context to allow the development of more efficient targeted therapies. Some of the unpublished data from our work performed on cervical cancer suggested that OSM:OSMR signalling could be involved in shaping the tumour microenvironment after seeing a lower CD4/CD8, Th17/Treg ratio and neutrophil count in orthotopic tumours generated in OSMR KO mice (unpublished data).

Despite recent improvements in 3D *in vitro* cultures with increasing complexity and resemblance with the *in vivo* tumour architecture and composition[185], *in vitro* models to study tumour microenvironment interactions are still limited as they lack many components and mechanical forces present in the *in vivo* models. As this signalling pathway can be extremely context dependent, and most likely dependent on tumour microenvironment interactions, it was necessary to study the role of OSM:OSMR in relevant animal models with a fully competent TME.

At the beginning of this project, the group had preliminary data suggesting that OSM:OSMR expression could be associated with decreased survival in breast cancer after performing survival analysis in the METABRIC dataset. BC is a widely studied disease and a variety of physiologically relevant breast cancer genetic and orthotopic models have been developed. Moreover, some focus has been put on developing models with engineered TME as tumour-microenvironment interactions have been increasingly recognised to contribute to breast cancer progression[109,186,187]. Therefore, breast cancer was found to be the perfect setting to study the effect of OSM:OSMR signalling in shaping the tumour microenvironment and this project aimed to study the role of OSM:OSMR in breast cancer progression, with particular emphasis in the TME, using relevant *in vitro* and *in vivo* models, and clinical data.

1.3.4 OSM:OSMR in breast cancer

Several lines of evidence suggest that OSM is important in breast cancer progression. Despite being reported as anti-proliferative and to induce differentiation of breast cancer

cells[188], OSM has been associated with a migratory and invasive phenotype in breast cancer cells[189,190]. C-myc induction is thought to reduce OSM anti-proliferative effects by cooperating with OSM to increase anchorage independent growth, a process associated with metastasis[191]. OSM and OSMR have been reported to be elevated in *in situ* carcinoma compared to benign lesions suggesting an association between OSM:OSMR expression and increased malignancy[192]. High levels of OSMR have been associated with shorter recurrence free and overall survival in BC and OSMR has been shown to supress ER receptor expression[193]. West *et al* (2014), linked OSM signalling with the induction of EMT and stem-like differentiation in breast cancer through PI3K signalling[194]. Guo *et al* (2013), described that STAT3 signalling was responsible for initiating and sustaining EMT in breast cancer. This process was dependent on Lin-28–let-7–HMGA2 and miR-200–ZEB1 circuits and knockdown of HMGA2 significantly impaired OSM driven EMT[195]. Tawara *et al* (2018), reported that OSM promoted breast cancer metastasis to the lungs by potentiating pre-intravasation events and increase of circulating tumour cells (CTC) counts[196].

All these studies strongly suggest that OSM:OSMR signalling in breast cancer could be contributing to cancer progression and pointed to the need of validating OSM:OSMR as a new therapeutic target for breast cancer. As mentioned previously, this work aims to understand not only how OSM:OSMR signalling axis influences tumour cells but also how it affects and shapes the tumour microenvironment.

1.3.5 Breast tumour microenvironment and OSM:OSMR signalling

Growing evidence suggests that the innate immune cells (macrophages, neutrophils, dendritic cells, innate lymphoid cells, myeloid-derived suppressor cells, and natural killer cells) as well as adaptive immune cells (T cells and B cells) in certain contexts can contribute to tumour progression[197]. In 2005, epigenetic modifications in the non-neoplastic stromal cells during breast cancer progression were described for the first time[198]. Finak *et al* (2008) described that stromal gene expression predicted clinical outcome in breast cancer[199]. Kramer *et al* (2009) reported that a stroma-related gene signature predicted resistance to neoadjuvant chemotherapy in breast cancer[200]. Low tumour-stroma ratio has also been linked with poor prognosis in breast cancer, especially in TNBC[201].

It is clear now that cancer cells take advantage of their surroundings and that they are in constant communication with the TME hijacking many physiological mechanisms and

converting them into essential factors for cancer progression. Therefore, targeting the tumour microenvironment's pro-tumoral factors and blocking those cancer-stroma interactions has been of great interest in recent years not only in cancer but also in breast cancer in particular[59,202,203].

OSM:OSMR axis has been mentioned by West *et al* (2018) to be a promising target candidate to target stroma alterations in many disease contexts including inflammatory diseases[147]. The rationale behind it is that OSM plays important physiological roles in haematopoiesis, bone turnover, and wound repair and that the molecular mechanisms involved in those processes confer the ability to modulate cellular differentiation and reparative immune responses, particularly when acting through stromal cells[147]. Those mechanisms are widely known to be used by cancer cells in tumour progression, making OSM:OSMR a possible candidate for stromal modulation in cancer.

Despite being extensively linked to cancer, including breast cancer, and associated with stromal alterations in inflammatory diseases through mechanisms that could also be used by cancer, very little is known about the OSM:OSMR role in the tumour microenvironment and its impact in tumour progression. Tripathi *et al* (2014) demonstrated that OSM and Eotaxin convert recruited macrophages into a pro-angiogenic M2-polarized phenotype demonstrating that OSM was possibly contributing to the TME modulation[204].

Hypothesis and aims of this PhD project

Hypothesis

OSM:OSMR signalling contributes to breast cancer progression by modulating responses in the tumour microenvironment.

Objectives

The overall aims of this project are to determine the contribution of OSM:OSMR signalling to breast cancer progression, to dissect its molecular mechanisms and to study its role in the tumour microenvironment. The final purpose of this study is to determine the relevance of OSM:OSMR as a new potential therapeutic target for breast cancer treatment.

This investigation was divided into 4 main objectives aimed to:

- **Investigate OSM and OSMR expression in human breast cancer samples and its association with prognosis and other clinical parameters.**
- **Determine the contribution of OSM:OSMR signalling to breast cancer development and progression.**
- **Investigate the expression and the role of OSM:OSMR signalling axis in the tumour microenvironment.**
- **Explore the effects of OSM:OSMR signalling in modulating the immune system in the tumour microenvironment.**

Chapter 2: Materials and methods

2.1 Clinical samples and datasets

All clinical samples were used with the approval of the corresponding ethical committees. BC clinical samples from the University Hospital Basel and publicly available datasets were used to study the association of OSM:OSMR pathway with the different clinical features of breast cancer patients.

2.1.1 Tissue microarrays

Formalin-fixed and paraffin-embedded (FFPE) samples of 141 breast cancer tumours surgically resected from patients attending the University Hospital Basel between 1991 and 2013 were included in tissue microarrays (TMA). Complete histopathological information, date, and cause of death, as well as date of local and/or distant relapse were available for all the patients. All patients have given informed consent for their archival tissue to be used for scientific research, and the TMA construction was authorized by the Hospital Ethic Committee. The TMAs were generated by punching 1 mm spot of each sample.

Tissue sections were subjected to a heat-induced antigen retrieval step prior to exposure to primary OSM antibody (1:50, HPA029814, Sigma-Aldrich). Immunodetection was performed using the Roche Ventana BenchMark ULTRA IHC/ISH staining system, with DAB as the chromogen. Cases were reviewed by two independent pathologists and OSM staining was evaluated by the semiquantitative method of H-score (or "histo" score), adapted from quantification of ER staining[205] and used to assess the extent of immunoreactivity in tumour samples. Inflammation was assessed by a pathologist as high or low tumour infiltration of immune cells according to their morphology.

2.1.2 Bioinformatic analysis of publicly available datasets

Publicly available datasets where raw data were extracted and used for bioinformatic analysis are described in Table 2.1.

Table 2.1: Publicly available datasets used for bioinformatic analysis.

Dataset	Tissue	Reference	Analysis performed	Webtool for the analysis
METABRIC	Breast cancer	Curtis *et al* (2012)[206]	Survival	Cancertool[207]
Wang	Breast cancer	Wang *et al* (2005)[208]	Survival	Cancertool[207]
Datasets included in the KM plotter	Multiple cancer types	N/A	Survival	KM plotter[209]
Finak GSE9014	Breast cancer stroma	Finak *et al* (2008) [199]	Analysis of gene expression	Custom analysis of gene expression
Casey GSE10797	Breast cancer	Casey *et al* (2009)[210]	Analysis of gene expression	Custom analysis of gene expression
Yeung GSE40595	Ovarian cancer	Yeung *et al* (2013)[211]	Analysis of gene expression	Custom analysis of gene expression
Nishida GSE35602	Colon cancer	Nishida *et al* (2012)[212]	Analysis of gene expression	Custom analysis of gene expression
Human protein Atlas	Human cell lines	Uhlén *et al* (2015)[213]	Analysis of gene expression	Custom analysis of gene expression
TCGA	Breast cancer	Koboldt *et al* (2012)[214]	Correlations of OSM/OSMR with microenvironment cell populations and purity	TIMER[215]
Datasets included in the KM plotter	Breast cancer	N/A	Correlations of OSM/OSMR with microenvironment cell populations and purity	xCell[216]
Datasets included in cBioPortal	Breast and cervical Cancer	N/A	Mutational analysis	cBioPortal[217]

* N/A: Not available. Different datasets combined. See webtool reference.

For gene expression analysis, mRNA raw data were downloaded and transformed into Z-score with the formula shown in Fig. 2.1. Z-scores were then used for the statistical analysis performed with GraphPad Prism software.

$$z = \frac{x - \mu}{\sigma}$$

Fig. 2.1: Formula used to calculate Z score, where **x** corresponds to the raw mRNA value, **μ** to the mean and **σ** to standard deviation.

Survival analysis was performed using the Log-rank (Mantel-Cox) with best threshold cut-offs selected automatically by the program (KM plotter) or comparing the top Q1 samples versus the rest (Cancertool). OSM and OSMR correlations with microenvironment cell populations were calculated with the Spearman's rank correlation coefficient.

2.2 Cell culture

The cell lines and primary cells used in this study are listed in Table 2.2. The list includes breast cancer cell lines, human immortalised fibroblasts, HEK-293 cells used for transfection, human promyelocytic leukaemia cells and primary culture of monocytes extracted from blood from healthy donors.

Cells were cultured in their respective culture media (RPMI, DMEM, Ham´s F 12 or IMEM, Gibco) as indicated by ATCC, 10% Fetal Bovine Serum (FBS, Gibco), 1% L-glutamine (Thermo Fisher Scientific) and 100 U/mL of penicillin and 100 µg/mL of streptomycin (Thermo Fisher Scientific). Additional specific reagents for each cell line are indicated in Table 2.2. Breast cancer cell lines were authenticated by short tandem repeat profiling (STR profiling) in the genomics core facility at "Alberto Sols" biomedical research institute, Madrid, Spain. All cell lines were periodically tested for mycoplasma infection (Minerva Biolabs).

Table 2.2: Cell lines and primary cells used in the study.

Human breast cancer cell lines						
Cell line	**Gene cluster**[218]	**(ER**	**PR**	**HER2)**[218]	**Cell culturing medium**	**Obtained from**
BT-549	Basal B	neg	neg	neg	RPMI	ATCC
HCC38	Basal B	neg	neg	neg	RPMI	ATCC
MDA-MB-157	Basal B	neg	neg	neg	DMEM	ATCC
MDA-MB-231	Basal B	neg	neg	neg	DMEM	ATCC
HCC1806	Basal A	neg	neg	neg	RPMI	ATCC
HCC70	Basal A	neg	neg	neg	RPMI	ATCC
MDA-MB-468	Basal A	neg	neg	neg	DMEM	ATCC
HCC1569	Basal A	neg	neg	pos	DMEM	ATCC
HCC1954	Basal A	neg	neg	pos	DMEM	ATCC
SK-BR-3	Luminal	neg	neg	pos	DMEM	ATCC

MDA-MB-453	Luminal	neg	neg	neg	DMEM	ATCC
CAMA-1	Luminal	pos	neg	neg	DMEM	ATCC
ZR-75-1	Luminal	pos	neg	neg	RPMI	ATCC
T-47D	Luminal	pos	pos	neg	RPMI	ATCC
MCF7	Luminal	pos	pos	neg	RPMI	ATCC
BT-474	Luminal	pos	pos	pos	DMEM	ATCC
SUM149PT	Basal B	neg	neg	neg	Ham's F12 + 5% FBS + 20 ng/mL EGF + 10 ug/mL Insulin + 500 ng/mL hydrocortisone	ATCC
Murine breast cancer cell lines						
Cell line	**Origin**				**Cell culturing medium**	**Obtained from**
TS1	MMTV-PYMT mammary tumours[219]				DMEM	Fernando Calvo (IBBTER, Santander)
4T1	Mammary gland of BALB/C mice				DMEM	ATCC
Human immortalised breast fibroblasts						
	Origin[220]	**ER PR HER2**[220]			**Cell culturing medium**	**Obtained from**
CAF-173	Breast tumour	neg	neg	1+	DMEM	Bagrado (UCM, Madrid)
CAF-200	Breast tumour	70%	70%	2+	DMEM	Bagrado (UCM, Madrid)
CAF-220	Breast tumour	80%	20%	2+	DMEM	Bagrado (UCM, Madrid)
CAF-318	Breast tumour	neg	neg	neg	DMEM	Bagrado (UCM, Madrid)
RMF-31	Normal breast (Reduction mammoplasty)	-	-	-	DMEM	Bagrado (UCM, Madrid)
RMF-39	Normal breast (Reduction mammoplasty)	-	-	-	DMEM	Bagrado (UCM, Madrid)
Monocytes and primary cultures						
	Origin	**Cell type**			**Cell culturing medium**	**Obtained from**
HL-60	Acute promyelocytic leukemia	Promyeloblastic cell line			IMEM + 20% FBS	ATCC

Primary monocytes	Human Blood	Monocytes	RPMI + M-CSF 50 ng/mL	Healthy donors
Other cell lines				
	Origin		**Cell culturing medium**	**Obtained from**
HEK-293	Embryonic kidney cells		DMEM	ATCC

2.2.1 Cell thawing

Cell vials, stored in liquid nitrogen, were quickly defrosted in pre-warmed water bath at 37ºC. Once completely defrosted, cells were transferred to a T25 flask with 5 mL of pre-warmed media and kept in the incubator overnight at 37ºC and 5% CO_2. Media was changed 12 hours after to remove residual DMSO and non-adherent cells present in the media. For cell suspension cultures such as HL-60 cell line, cells were defrosted as mentioned above, transferred to a 15 mL falcon with 9 mL of warm media and centrifuged for 5 min at 1200 rpm. Supernatant media was aspirated, cell pellet resuspended in 5 mL of media and transferred to a T25 flask and kept in the vertical position overnight.

2.2.2 Cell maintenance and subculture

Adherent cells were maintained until they reached approximately 80% confluency in T25 or T75 flasks before doing a cell subculture. All reagents were warmed to 37ºC before cell passaging. Medium was aspirated, cells washed twice with sterile Dulbecco's phosphate buffered saline (PBS, Gibco) between aspirations, and 1 or 3 mL of 0.5% Trypsin-Ethylenediaminetetraacetic acid (Trypsin-EDTA, Gibco) were added to cells in T25 and T75 flasks, respectively. Cells were kept in the incubator at 37ºC from 2-6 min (depending on the cell line) until they completely detached from the culture surface. Trypsin was neutralized with at least twice the volume of their respective complete growth media mentioned in Table 2.2. (4 mL for T25 and 7 mL for T75 flasks). Cells were resuspended to achieve a homogeneous suspension, and following ATCC subculture recommendations for each cell line, 1-3 mL of cells suspension was transferred to a new flask containing 4 or 10 mL of pre-warmed complete growth medium.

Collagen pre-coated flasks were used for fibroblasts maintenance and subculture. Collagen (Corning) was diluted in PBS to achieve a concentration of 50 mg/L and 5 mL of the solution was added to T75 flasks. Culture flasks were then left for 3 hours in the incubator to allow

collagen adherence to the cell surface. Medium was aspirated before flask usage, and for short-term storage of pre-coated flasks, 10 mL of PBS was added to the flasks and they were kept in the incubator up to 5 days.

HL-60 cells were cultured in cell suspension, every 2-3 days cells were counted, and cell concentration was calculated and readjusted to optimal conditions indicated by the ATCC (100.000-300.000 cells per mL).

Cell counting was performed by mixing 10 µL of cell suspension with 10 µl of 0.4% Trypan Blue (Gibco) in a 1:1 volumetric ratio. A volume of 10 µL of the cell mixture was transferred to the counting chamber of the haemocytometer and cell concentration was calculated based on the formula C (cells/mL) = (nº of cells in each square/nº of squares counted) x dilution factor (2) x 10 000. All dead cells determined by the infiltration of the blue colour in the cytoplasm were excluded from the counting. The calculated volume of cell suspension was transferred to a new flask containing pre-warmed complete growth medium.

All cells were kept in the incubator at 37ºC and 5% CO2 and were used until passage 25 when they were discarded.

2.2.3 Cell freezing

Cells were trypsinised, transferred to 15 mL falcons and counted as described in the cell maintenance and subculture section (2.2.2) to determine the number of cells in suspension. Falcons were centrifuged at 300 *g* for 5 min and pellet resuspended in the calculated volume of complete growth media + 5% of sterile DMSO (Sigma) to achieve a final concentration of $2x10^6$ cells/mL. 1 mL of the mixture was transferred to cryovials which were then kept for 24 h in the Mr Frosty™ freezing containers at -80ºC to achieve a gradual cooling. Vials were transferred to liquid nitrogen for long-term storage.

2.2.4 Cell seeding for experiments

Cells were grown between 60-80% confluency and microscopically checked every time to ensure standard shape and appearance before being seeded for experiments.

Cells were seeded at concentrations mentioned in Table 2.3 in different size culturing plates depending on the technique performed. All optimal concentrations were based on literature research or optimization performed in the laboratory.

Table 2.3: Cell seeding concentrations used for the different cell lines.

Cell line	Seeding concentration
MDA-MB-231	7000-10.000 cells/cm^2
HCC1569	15.000 cells/cm^2
SK-BR-3	15.000 cells/cm^2
RMF-31	8000 cells/ per well*
CAF-173	8000 cells/ per well*
CAF-318	8000 cells/ per well*
CAF-200	8000 cells/ per well*
HEK-293	73.000 cells/cm^2
TS1	5000 cells/cm^2

* In 96 ultra-low attachment well plates (Costar).

2.2.5 OSM treatment

Recombinant human or mouse OSM (R&D systems) resuspended in PBS was added to monolayer cultures at 10 ng/mL concentration, while for 3D fibroblasts spheres treatment, human OSM was added at 30 ng/mL. The same volume of PBS was used as control condition in all OSM treatments. Length of the treatment varied between experiments ranging from 1 hour up to 4 days.

2.2.6 Cell transfections

2.2.6.1 siRNA

OSMR was silenced with gene specific siRNA (Dharmacon, GE Healthcare) using Lipofectamine RNAiMax (Invitrogen). Non-targeting siRNA and cyclophilin B siRNA (Dharmacon) were used as negative and positive controls, respectively. A pool of four siRNA (Table 2.4) was used at 40 nM and 100 nM to determine best transfection conditions. Briefly, cell lines were seeded in 6 well plates at densities mentioned in Table 2.3 in their respective 800 µL medium without antibiotics. 24h later, 2.4 µL of lipofectamine was added to 100 µL of Opti-MEM media (Gibco) (without FBS and antibiotics) without touching the eppendorf tube walls and incubated for 5 min at room temperature. Separately, 2.4 µL of either 40 nM or 100 nM siRNA conditions (previously prepared stock solutions at different concentrations in PBS) were added to 100 µL of Opti-MEM media and incubated for 5 min

at room temperature. siRNA mixture was added into the lipofectamine tube, mixed gently, and left for 20 min at room temperature before the final 205 µL were added dropwise to the cells. Transfection solution was left in contact with the cells for 6 hours at 37ºC and the mixture was then replaced by fresh media without antibiotics. OSM treatment was added 24 h later, and media was left in contact with cells for 3 and 5 days.

Table 2.4: siRNA sequences.

Gene	**ON-TARGETplus SMART pool (Dharmacon)**	**Sequences**
OSMR	008050-00-0005	AGUCUUGGCUGAACGUUUA
		UUUGAGAACUUGACCUAUA
		CCUCGAUUGCUGAUUCAUAU
		AAUCUGAGCUCCCUUUGGA
Cyclophilin B (positive control)	D-001820-10-20	ACAGCAAAUUCCAUCGUGU
		GAAAGAGCAUCUACGGUGA
		GAAAGGAUUUGGCUACAAA
		GGAAAGACUGUUCCAAAAA
Non-targeting (negative control)	D-001810-10-20	UGGUUUACAUGUCGACUAA
		UGGUUUACAUGUUGUGUGA
		UGGUUUACAUGUUUUCUGA
		UGGUUUACAUGUUUUCCUA

2.2.6.2 shRNA

Human breast cells were infected with lentiviruses carrying pLKO-Tet-On shOSMR plasmids (Sigma) to produce a stable knockdown for OSMR or pLKO-Tet-On shRNA-Control (with scramble shRNA, Addgene), plasmid kindly provided by Dr. Arkaitz Carracedo. pLKO-Tet-ON plasmids contain GFP for visual inspection of effective transduction and Puromycin resistance cassette for effective selection of transduced cells. pLKO-Tet-On shOSMR plasmids presented in Table 2.5 were tested by Andrea Abaurrea in the laboratory, and the more efficient plasmid (TRCN0000289933) was selected for further experiments.

Table 2.5: shOSMR plasmid sequences.

Plasmid clone ID	Target sequence
TRCN0000058683	GCACTCCATAAGGAATAATTT
TRCN0000289933	CGAGTTGACTAAGCCTAACTA
TRCN0000296351	AGGAGAACCCTCACCTAATAA
TRCN0000310280	TAACCTGACTCATCGAGTTTA

2.2.6.3 Lentiviral production

HEK-293 cells were seeded in p100 plates at the cell density mentioned in Table 2.3 in complete growth media. The next day, cells were transfected with the packaging plasmids pMDLg-pRRE, pRSV-REV, pMD2.G (Addgene) and the corresponding pLKO-Tet-On vector using Turbofect™ transfection reagent (Thermo Fisher). Briefly, packaging plasmids and vectors were defrosted on ice. The cocktail (previously optimised in the lab) was prepared in a 1.5 mL eppendorf tube with serum-free DMEM and Turbofect™ was added after the DNA (Table 2.6). The solution was gently mixed, incubated at room temperature for 20 min and added drop wise to the HEK-293 cells. Media was changed 6 hours later, and 7.5 mL of fresh complete media added to the plate. Viral particles were produced during 48 h before being collected for breast cancer cell line infection.

Table 2.6: Transfection cocktail used for lentiviral production.

Reagent	Quantity used for transfection of a p100 plate
pMDLg-pRRE	2.6 µg
pRSV-REV	1 µg
pMD2.G	1.4 µg
pLKO-Tet-On shRNA/ GFP vector	4 µg
Serum free media	Up to 1 mL
Turbofect™	19.2 µL

2.2.6.4 Cell line infection and selection

Viral particles containing the pLKO-Tet-On vector produced by HEK-293 cells were added to human breast cancer cell lines. Briefly, MDA-MB-231 and HCC1569 cell lines were

seeded at the concentration mentioned in Table 2.3 in p100 plates in their respective complete growth media. The following day, media containing the viral particles from HEK-293 cells was filtered with 0.2 µm filters (Sigma-Aldrich), polybrene was added at 5 µg/mL and mixture transferred to human breast cell lines. Infection process was repeated in two consecutive days transferring media from HEK-293 to breast cancer cell lines. On day 4, media containing the viral particles was removed from human breast cancer cell lines. GFP transfection was microscopically checked to ensure successful technique and fresh complete growth media was added containing 2 µg/mL of puromycin selection agent (Thermo Fisher Scientific) maintained for subsequent cultures.

2.2.6.5 Cell transfection with over expressing plasmids

MDA-MB-231 cells were transfected with p-UNO Control or p-UNO1-hOSM (containing Blasticidine resistance, InvivoGen), and SK-BR-3 cells with pcDNA3.1 zeo Control or pcDNA3.1 zeo-OSMR (Containing Zeocin resistance, Addgene). Both plasmids were kindly donated by Prof. Nicholas Coleman to produce a cell line with stable expression of human OSM or OSMR. Cells were seeded at the concentration mentioned in Table 2.3. The following day, the transfection cocktail mix was prepared adding 5 µg of the plasmid into 960 µL of serum-free media followed by addition of 19.2 µL of Turbofect^{TM} . Solution was incubated from 20 min at room, added drop wise to the cells and left in contact for 6 hours before transfection media was swapped to fresh complete growth media. 48 h after, Blasticidine (Sigma-Aldrich) or Zeocin (Invitrogen) selection agents were added to the cells at previously optimized concentrations: 10 µg/mL of Blasticidine for MDA-MB-231 and 300 µg/mL Zeocin for SK-BR-3. Both selection agents were maintained in subsequent cultures.

2.2.7 HL-60 differentiation

HL-60 cell differentiation to macrophages was achieved using a concentration of $1.5x10^6$ cells per p100 plates and adding 1 nM of 12-O-tetradecanoylphorbol-13-acetate (TPA) for 24 hours[221]. Prior to conditioned media experiments, remaining non differentiated cells were removed from the plate by aspiration and fresh complete growth media added.

2.2.8 Isolation and culture of primary monocytes

Primary human monocytes were obtained from blood extracted from healthy subjects. All donors have given informed consent for their blood to be used in research. The whole protocol was carried at room temperature. Briefly, approximately 12 mL of blood was transferred to a 50 mL falcon, the sample was spun at 1200 *g* for 30 min to separate the blood phases, the white buffy coat was collected with a pasteur pipette and transferred to a 15 mL tube. Volumes were recorded for each buffy coat collected and PBS was added in equal volumes to produce a ½ dilution. Rosettesep™ human monocyte enrichment cocktail (Stemcell) was added at the mixture (67 µL for each mL of buffy coat), and sample was incubated for 20 min at room temperature on the roller with slow rotation. Meanwhile, high density media Histopaque R-1077 (Sigma) was added to fresh tubes with the same previously recorded volumes for each buffy coat collected and falcons briefly spun down to avoid drops on the walls. Carefully, the sample was added to the high-density media by dropping the sample on the wall of the tube in a 45-degree angle to avoid mixing of the sample with the media. Samples were centrifuged at 1200 *g* for 30 min, and tubes were handled carefully once centrifugation was completed. The ring of enriched cells sitting on the plasma interface was collected trying to avoid as much red blood cells as possible and the sample was transferred to a new 15 mL tube. Cells were washed 2 times with PBS + 2% FBS and spun at 1200 rpm for 6 min. Cell pellet was resuspended in 10-20 mL of RPMI and cells counted. Macrophages were seeded at 1.2 million cells per well in 6 well plates coated with glass coverslip in a total volume of 1.2 mL of complete media + 50 ng/ mL M-CSF (Immunotools). Media was changed to fresh complete media (without M-CSF) 7 days after. For conditioned media experiments (CM), media was changed on day 10 and left in contact with cells for 2 days.

2.2.9 Conditioned media used in myeloid cells experiments

MDA-MB-231 and CAFs conditioned media was generated by culturing cells in monolayer for 48-72 h in DMEM with 2% FBS +/- OSM 10 ng/µL. Media was filtered with a 0.22 µm filter (Sigma-Aldrich), transferred to the differentiated HL-60 or primary monocyte cells, and left in contact for 48-72 hours. Cells were washed twice with cold PBS and pellets collected for RNA extraction or flow-cytometry analysis.

2.2.10 3D fibroblast spheres

All fibroblast assays were performed at the Institute of Cancer Research (ICR) in London under the supervision of Prof. Clare Isacke and Dr. Liam Jerkins during the PhD placement. Fibroblast spheres were formed seeding 8000 cells/well in a 96 ultra-low attachment Corning plate (Costar). Cells were treated with 30 ng/µL of OSM for 4 days. Pictures were taken using EVOS FL Cell Imaging System and area of spheres in pixels was analysed using Fiji-Image J software.

2.2.11 Collagen cell contraction assays

To assess the collagen remodelling capacity, fibroblasts were treated for 4 days with PBS/OSM at 10 ng/µL. On day 4 cells were trypsinised and 150.000-250.000 cells per well of RMF-31, RMF-39, HS27, CAF-200, CAF-220, CAF-318 and CAF-173 were embedded in a mixture of 1x DMEM (Gibco), 20% 5x DMEM (Gibco), 10% FBS (Gibco), and collagen (Corning) at a final concentration of 2 mg/mL in a total volume of 500 µL per well in 6 well plates. After polymerisation at 37ºC for 45 min, gels were detached from the walls and 1 mL of DMEM was added with PBS/OSM at 10 ng/mL. Pictures were taken 48 hours later and area of the collagen disks (in pixels) was calculated using Fiji-Image J software.

2.3 Cell and animal tissue processing for DNA, RNA and protein analysis

Cell pellets from 80% confluent plates and animal tissue (e.g. tumours, lungs, etc) were collected, processed, and stored at -80ºC for further DNA, RNA and protein analysis. For adherent cells seeded in monolayer, media was aspirated, and cells washed twice with cold PBS. 1 or 0.5 mL of cold PBS was added to p100 or p6 plates respectively, and cells were scraped gently using sterile cell scrapers. The detached cells were transferred to a 1.5 mL eppendorf tube and spun for 5 min at 300 *g* and 4ºC. The supernatant was aspirated, and cell pellet was snapped frozen in liquid nitrogen or dry ice and kept at -80ºC until further analysis. Cells cultured in suspension, such as HL-60 cell line or fibroblasts spheres, were collected with the media and transferred to a 15 mL falcon. The cell suspension was

centrifuged for 5 min at 300 *g* and 4ºC and supernatant aspirated. Cell pellet was washed with 10 mL of cold PBS and remaining pellets were snap frozen and stored as mentioned above. Animal tissue was snap frozen in liquid nitrogen immediately after animal culling. Tissue was cut into small pieces and disaggregated using a mortar and pestle until it was converted into powder. The disaggregation of the tissue was performed on dry ice and liquid nitrogen was frequently added to the mortar to avoid tissue to defrost. Homogeneous powder was then separated into several cold eppendorf tubes and kept at -80ºC until further analysis.

2.4 DNA analysis

2.4.1 DNA extraction

Genomic DNA (gDNA) was extracted from mice lungs frozen powder using the QIAmp DNA mini kit (Qiagen) and following the manufacturer's instructions. In summary, 180 µL of buffer ATL was added to the lung frozen powder followed by addition of 20 µL of proteinase K and a 1-2 hour incubation at 56ºC. After complete tissue dissociation, 200 µL of buffer AL was added to sample where it was further incubated for 10 min at 70ºC. Once cell lysis was achieved, 200 µL of 100% ethanol was added to the sample and vortexed for 15 sec. The sample was passed through the QIAamp Mini spin column and centrifuged for 2 min at 8000 rpm followed by a series of washes with buffers AW1 and AW2. The column was centrifuged for 3 min at maximum speed to dry the membrane followed by the addition of 200 µL of pure water (Gibco) to elute the DNA. Concentration of DNA in the elution was determined by measuring absorbance at 260 nm with the Nanodrop ND-1000 spectrophotometer (Isogen Life Sciences). Samples were then frozen and kept at-20ºC until further analysis.

2.4.2 gDNA samples analysis

Real-time quantitative PCR was used to detect human Alu sequences in the mice lungs that could indicate the presence of micrometastases. Details of PCR reaction are explained in section 2.5.3. Primers used for qPCR analysis of genomic samples can be found in Table 2.7.

Table 2.7: Primers used for qPCR analysis of human Alu DNA in murine lungs.

Gene	Forward	Reverse	Origin
18 S	CGCGGTTCTATTTTGTTGGT	CGGTCCAAGAATTTCACCTC	Primer bank
Alu 1	ACGCCTGTAATCCCAGCACTT	TCGCCCAGGCTGGAGTGCA	Zijlstra *et al* (2002)[222]
Alu 2	CACCTGTAATCCCAGCACTTT	CCCAGGCTGGAGTGCAGT	Schneider *et al* (2002)[223]

2.5 RNA analysis

2.5.1 RNA extraction from animal tissue and cell lines

RNA was extracted from cell pellets and from frozen animal tissue powder. The nucleic acid extraction was performed using TRIzol™ Reagent (Invitrogen) and following the manufacturer instructions. Briefly, 1 mL of trizol was added to the eppendorf tubes containing frozen pellets or tissue powder, sample was pipetted up and down several times and left at room temperature (RT) for 5 min. After the incubation time, 200 µL of chloroform (Sigma) was added to the tube, sample vortexed for 10 seconds and left at RT for 10 min before being centrifuged at 12000 *g* for 10 min at 4ºC. The aqueous phase containing the RNA was transferred to a fresh 1.5 mL tube, 0.5 mL of isopropanol (Sigma) and 1 µL of glycogen (Ambion) was added to the sample. The tube was mixed by inversion and kept at -20ºC overnight. On the following day, the sample was centrifuged for 10 minutes, supernatant discarded, and RNA pellet washed with 1 mL of 75% ethanol. The sample was then centrifuged for 5 min at 12000 *g* and 4ºC, supernatant discarded, and pellet was left air drying for 5-10 min before being resuspended in 30-50 µL of ultra-pure water (Invitrogen). Sample concentration was determined using the nanodrop by measuring absorbance at 260nm and the ratios A260nm/A280nm and A260nm/A230nm were calculated to assess RNA purity. Samples were then used for cDNA conversion or stored at -80ºC.

2.5.2 Reverse transcription: RNA to cDNA conversion

Complementary DNA (cDNA) was obtained from RNA using the Maxima first strand cDNA synthesis kit with DNase incorporated (Thermo Scientific). In the first step of the protocol, DNase treatment was performed by mixing in RNase free PCR tubes 1 µL of dsDNase buffer, 1 µL of dsDNase and 1 µg of RNA + ultra-pure water in a volume up to 10 µL. Sample was incubated for 2 min at 37ºC in the Thermal cycler C1000 (BIO-RAD) to allow genomic DNA degradation. A mastermix was prepared with 4 µL of 5x reaction mix, 2 µL of maxima enzyme mix, 4 µL of ultra-pure water and added to the sample. For cDNA conversion the sample was subjected to the following cycling conditions: 10 min at 25ºC, 15 min at 50ºC, 5 min at 85ºC and cooling down at 4ºC. cDNA was then used for PCR analysis or stored at -20ºC.

2.5.3 Real-time quantitative PCR analysis

Real-time quantitative PCR analysis (qPCR) was used to analyse genomic (gDNA) and cDNA samples. When analysing cDNA samples, qPCR can also be referred as reverse transcription qPCR (RT-qPCR) as it assumes the cDNA conversion of RNA samples. In summary, for gDNA and cDNA analysis, PCR reaction was performed in a total volume of 10 µL per reaction using 2ng of gDNA or cDNA diluted in pure water in a volume of 4 µL (0.5ng/ µl), 5 µl of SYBR Green PCR Master Mix (Applied Biosystems) and 1 µL of Forward and Reverse primer mixture with 1 nM concentration for each primer. Primers used for qPCR analysis of gDNA and cDNA are listed in Tables 2.7 and 2.8, respectively. All conditions were tested in triplicates and for multiple gene analysis 384 or 96 well plates were run on the CFX384 Real-Time System (BIO-RAD) or on the Light Cycler 96 Thermocycler (Roche), respectively, with the following the cycling conditions: (1) Preincubation: 50°C for 120 seconds and 95°C for 600 sec; (2) Amplification: 45 cycles for 15 sec at 95°C and for 60 sec at 60°C, 1 cycle for 15 sec at 95°C and for 15 sec at 60°C; (3) Melting curve: 95°C for 10 sec, 65°C for 60 sec and 97°C for one sec. Primer efficiencies were calculated based on the slope of the standard curve generated using 5-point serial of dilutions of control gDNA/cDNA. Melting curves were analysed every single run to ensure single PCR product amplification. Genomic analysis was performed using 18S gene as housekeeping (primers capable of targeting human and mouse 18S gene) and cDNA analysis was performed using 3 housekeeping

genes (HK) previously optimized for each condition being tested. qPCR analysis was done using the comparative threshold cycle (CT) method described by Pfaffl *et al* (2001)[224] (Fig. 2.2).

$$\text{Ratio} = \frac{(E_{target})^{\Delta CT_{target}^{(control-sample)}}}{(E_{ref})^{\Delta CT_{ref}^{(control-sample)}}}$$

Fig. 2.2: Formula used to calculate the comparative threshold cycle described by Pfaffl *et al* (2001)[224]. **E** stands for primer efficiency and **ΔCT** represents the difference between cycle threshold of control and sample.

Table 2.8: Primers used for RT-qPCR analysis.

Gene	Species	Forward	Reverse
OSM	mouse	ATGCAGACACGGCTTCTAAGA	TTGGAGCAGCCACGATTGG
OSMR	mouse	CATCCCGAAGCGAAGTCTTGG	GGCTGGGACAGTCCATTCTAAA
STAT3	mouse	CACCTTGGATTGAGAGTCAAGAC	AGGAATCGGCTATATTGCTGGT
VEGF	mouse	TTACTGCTGTACCTCCACC	ACAGGACGGCTTGAAGATG
IL-6	mouse	TAGTCCTTCCTACCCCAATTTCC	TTGGTCCTTAGCCACTCCTTC
18S	human/ mouse (HK)	CGCGGTTCTATTTTGTTGGT	CGGTCCAAGAATTTCACCTC
HPRT	human/ mouse (HK)	TGACACTGGCAAAACAATGCA	GGTCCTTTTCACCAGCAAGCT
GFP	N/A	CTAGGCCACAGAATTGAAAGATCT	GTAGGTGGAAATTCTAGCATCATCC
OSM	human	CTCGAAAGAGTACCGCGTG	TCAGTTTAGGAACATCCAGGC
OSMR	human	AATGTCAGTGAAGGCATGAAAGG	GAAGGTTGTTTAGACCACCCC
SOCS3	human	AGACTTCGATTCGGGACCA	AACTTGCTGTGGGTGACCA
STAT3	human	CAGCAGCTTGACACACGGTA	AAACACCAAAGTGGCATGTGA
IL-6	human	CCAGGAGCCCAGCTATGAAC	CCCAGGGAGAAGGCAACTG
LIF	human	CCAACGTGACGGACTTCCC	TACACGACTATGCGGTACAGC
LIFR	human	TGGAACGACAGGGGTTCAGT	GAGTTGTGTTGTGGGTCACTAA
GP130	human	AGGACCAAAGATGCCTCAAC	GAATGAAGATCGGGTGGATG
POSTN	human	CTCATAGTCGTATCAGGGGTCG	ACACAGTCGTTTTCTGTCCAC
FAP	human	CAAAGGCTGGAGCTAAGAATCC	ACTGCAAACATACTCGTTCATCA
ACTA2	human	CTATGAGGGCTATGCCTTGCC	GCTCAGCAGTAGTAACGAAGGA
CCL2	human	CAGCCAGATGCAATCAATGCC	TGGAATCCTGAACCCACTTCT
CXCL12	human	GCCCTTCAGATTGTAGCCCG	GCGTCTGACCCTCTCACATC
CXCL7	human	CTGGCTTCCTCCACCAAAGG	GACTTGGTTGCAATGGGTTCC
CCL20	human	CTGGCTGCTTTGATGTCAGT	CGTGTGAAGCCCACAATAAA
HMBS	human (HK)	GGCAATGCGGCTGCAA	GGGTACCCACGCGAATCAC
YWHAZ	human (HK)	ACTTTTGGTACATTGTGGCTTCAA	CCGCCAGGACAAACCAGTAT

2.5.5 Microarray analysis of gene expression

Microarray analysis from animal tumours and cell lines were performed by the genomic platform at Biodonostia Health Research Institute. Data processing and analysis was done together with Andrea Abaurrea in the laboratory.

RNA extraction was performed using the Recover all Total Nucleic Acid Isolation kit (Invitrogen, ref AM975). RNA quality was checked measuring the RNA quality number (RIN) with the Bioanalyzer (Agilent) and only samples with RIN >7 were used for microarray analysis. Microarrays were performed using Clariom S human or mouse assays (Thermo Fisher). Data were analysed using the Transcriptome Analysis Console 4.0 (TAC). Genes with FDR<0.1 and fold change $\geq|2|$ were considered significantly modulated. Gene ontology (GO) analysis was performed using Panther (http://pantherdb.org/). Gene set enrichment analysis (GSEA) was performed as described in Subramanian *et al* (2005)[225]. FDR < 0.25 or 0.05 was regarded as statistically significant, depending on the type of permutations performed. The GSEA signatures used in results sections 3.2 and 3.3 were extracted from the Molecular Signatures Database (MsigDB) by the Broad Institute or they were manually curated from the literature.

2.5.6 Single cell RNA sequencing

Single cell RNA sequencing analysis (scRNA-seq) was performed in collaboration with Dr. David-Gallego Ortega laboratory (Garvan Institute of Medical Research, Sydney). Our collaborators performed RNA sequencing and its subsequent bioinformatic analysis following our project needs and requests. Drop-seq[226] dataset raw data for MMTV-PyMT tumours was obtained from Valdes-Mora *et al* (2020)[227]. This subset was subsequently analysed using Seurat[228] (v Seurat 3.2). Briefly, a total of 9,636 sequenced cells from 8 MMTV-PyMT tumours pass the QC filter, with <5% mitochondrial to nuclear gene content[226], and <8,000 molecules/cell as they potentially represented cell doublets. Downstream analysis was performed according to Butler *et al* (2018)[228], using 30 principal components to build a Shared Nearest Neighbour (SNN) graph calculating k-nearest neighbour (Jaccard Index) for each cell, subsequent cluster calling and UMAP dimensional reduction projection[229].

2.6 Protein analysis

2.6.1 Protein extraction from animal tissue and cell lines

Protein was extracted from cell pellets and frozen animal tissue powder. A master mix for cell lysis was prepared with 1 mL of RIPA lysis buffer 10x (Thermo Fisher), 9 mL of ultra-pure water, 1 tablet of easy pack protease inhibitor cocktail (Roche) and 1 tablet of PhosSTOP (Roche). The mixture was agitated gently until tablets completely dissolved and 100-150 µl of the solution was added to frozen cell pellets or tissue powder. The eppendorf tube was vortexed for 5 sec every 5 min and left on ice for 30 min for complete cell lysis and protein recovery. Sample was centrifuged at 14000 *g* for 10 min at 4ºC and supernatant transferred to a new 1.5 mL tube and immediately proceeded with protein quantification.

2.6.2 Protein quantification

Protein quantification was assessed by the Pierce bicinchoninic acid (BCA) protein assay kit (Thermo Fisher Scientific). Bovine serum albumin (BSA) was used to generate a standard curve with different protein concentrations: 2, 1.5, 1, 0.5, 0.25 mg/mL. Briefly, 5 µL of the protein standard, 5 µL of negative control containing only lysis buffer and 1 µL of the protein sample were added to the bottom of the 96 well plate in triplicates. A master mix was done mixing 50 parts of reagent A and 1 part of reagent B and immediately 95 µL (standard) or 99 µL (sample) of the master mix added to the wells. The plate was incubated at 37ºC for approximately 15 min and sample absorbance was measured at 570 nm using the Halo LED 96 plate reader (Dynamica).

2.6.3 Protein sample preparation for Western blot analysis

For Western blot analysis, the same amount of protein for all samples was loaded in the gel. Considering the protein concentration calculated by the BCA method as described above, samples were prepared as follows: 20-30 µg of protein (unless otherwise stated), ultrapure water and 3 µL of sample loading buffer 5X, containing beta-mercaptoethanol and bromophenol blue, in a total volume of 15 µL. Sample was then denatured at 95ºC for 5 min and immediately used in Western blot analysis or stored at -20ºC.

2.6.4 Western blotting

Western blot was performed using the BIO-RAD equipment and following standard protocols. In the first stage of electrophoresis, gradient pre-cast gels 4-15% (BIO-RAD) were inserted into the gel cassette, the whole tank was assembled, and the electrode chamber filled with buffer electrophoresis 1X (Table 2.9). Gel wells were loaded with 10 µL of kaleidoscope pre-stained protein ladder (BIO-RAD) or 15 µL of sample, and electrophoresis was run for 120 V for approximately 1:30 h. In the second stage, a transfer sandwich was prepared containing the following material in their following order oriented towards the cathode pole of the gel holder cassette: Sponge, Whatman paper, gel, gel sized cut membrane (nitrocellulose blotting membrane 0.2 µm, Amersham, GE Health Care), Whatman paper and sponge. Transfer buffer 1X including 20% methanol (Table 2.9) was added to the tank until the top line mark and transfer was left running for 2 hours at 220 mA under cold conditions to avoid heating up of the material. Once the transfer was finished, the nitrocellulose membrane was stained with Ponceau-S Staining Solution (Sigma-Aldrich) for 5 min on the shaker to assess the transfer and the quality of the protein. The membrane was washed with TBS with 0.5% Tween 20 (TBS-T) for 5 min and incubated with blocking buffer (5% skimmed milk, or BSA in TBS-T) for 1 hour at room temperature. Overnight incubation with primary antibody (diluted in blocking buffer, Table 2.10) was done in the cold room at 4ºC and the following morning the membrane was washed 3 times with TBS-T for 10 min each washing. The membrane was incubated with the secondary antibody diluted in blocking buffer for 1 hour at room temperature and a series of washes was performed before membrane development (3 washes with TBS-T for 10 min). Chemiluminescence images were acquired using ECL prime Western blotting detection reagents (Invitrogen) mixing 1 part of reagent A and 1 part of reagent B and left in contact with the membrane for 1 min. Images were acquired using the iBright FL1000 imaging system (Thermo Fisher Scientific) with several exposure times. Densitometric analysis of the images was performed using the Fiji-Image J software and normalizing samples to β Actin loading control.

Table 2.9: Buffers used for Western blot.

Buffer electrophoresis (10x)		
Reagents	**Quantity**	
Tris	30.3 g	Bring up to 1 L with distilled water
Glycine	144 g	
SDS	15 g	
Transfer buffer (5x)		
Reagents	**Quantity**	
Tris	30.3 g	Bring up to 1 L with distilled water
Glycine	144 g	
SDS (Stock 25%)	2 mL	
TRIS 1 M pH=8		
Reagents	**Quantity**	
Tris	242.2 g	Add 1700 mL water, measure pH and bring volume to 2L
TBS (10 X)		
Reagent	**Quantity**	
Tris 1M pH=8	100 mL	Bring up to 1 L with distilled water
NaCl	90 g	
TBS-T 0.1 %		
Reagent	**Quantity**	
Distilled water	900 mL	Agitate to homogenise mixture
TBS 10X	100 mL	
Tween	1 mL	

Table 2.10: Antibodies used in Western blot analysis.

Antibody	Company	Reference	Dilution
OSMR (mouse)	R&D Systems	AF662	1/500
P-STAT3 (mouse and human)	Cell Signaling	9145	1/2000
STAT3 (mouse and human)	Cell Signaling	9139	1/1000
beta-actin (mouse and human)	Sigma	A5441	1/2000
FN (mouse and human)	Abcam	AB2413	1/1000
OSMR (human)	Santa Cruz	30010	1/500

2.6.5 Cytokine and chemokine quantification

Human Oncostatin M (OSM) DuoSet ELISA DY295 (R&D) assay was used to measure OSM concentration in conditioned media of several cell lines. Cells were cultured until they reached 80% confluence or pre-established endpoints. Conditioned media was collected and frozen at -80º C until further analysis. Plate preparation and assay procedure were performed following the manufacturer's protocol. Optical density of each well was measured at 450 nm with a wavelength correction at 570 nm using the HaloLED 96 microplate detector (Dynamica). Cytokine and chemokine arrays were performed by Dr. Iñaki Osorio and Peio Azcoaga in the laboratory. Briefly, cytokine and chemokine levels were analysed in conditioned media from CAF-173 treated with OSM (30 ng/mL) or vehicle for 72 hours, and from MDA-MB-231-hOSM and corresponding control cells. A panel of 31 human chemokines was analysed by Human Chemokine Array Kit (Proteome Profiler Array, R&D Systems), and VEGF levels were quantified by Human VEGF Quantikine ELISA Kit (R&D Systems) following the manufacturer's instructions. Mouse VEGF, CXCL1 and CXCL16 levels on plasma from 14-week-old MMTV-PyMT: OSMR KO, HET and WT mice were analysed by mouse Premixed Multi-Analyte Kit (Magnetic Luminex Assay, R&D Systems) following the manufacturer's instructions. Detection was carried out with the MAGPIX® detector and data analysis was performed using the xPOTENT® software, both from R&D Systems.

2.6.6 Histopathology and immunohistochemistry analysis of murine samples

All histological and immunohistochemistry processing of murine samples was done by the histopathology service of Dr. Juana Maria Flores at UCM (Madrid) and data analysis was

performed together with Joanna Lopez in the laboratory. For histological analysis, mouse tumours and lungs were extracted, fixed in formalin for 72 hours and embedded in paraffin blocks where serial sections were cut and stained with haematoxylin-eosin. Immunohistochemical staining was performed on FFPE sections using the streptavidin–biotin–peroxidase complex method. Tissue sections were processed with 10 mM citrate buffer (pH 6.0) in a microwave (100º C, 15 min). Endogenous peroxidase activity was inactivated by incubation with 3% hydrogen peroxide in methanol (15 min, room temperature). Tissue sections were incubated in a humidified chamber (overnight, 4 ºC) using the antibodies described in Table 2.11 diluted in Tris-buffered saline (TBS). For negative controls, primary antibodies were replaced by non-immune serum. After three rinses in TBS (5 min each), samples were incubated with the secondary antibody (Table 2.11). After 30 min incubation, tissue sections were washed in TBS (5 min, 3 times) and immediately incubated for 30 min with streptavidin–peroxidase complex diluted 1:400 in TBS (Zymed Laboratories, Invitrogen, CA, USA). The chromogen was 3-30-diaminobenzidine (DAB peroxidase substrate kit, Vector Laboratories). Nuclei were counterstained with Harris haematoxylin for 1 min. Pictures were taken using the Nikon eclipse 8i microscope acquiring 8 representative pictures per tumour section with the NIS element software. Analysis of the images was performed using Image J program and counting the number of positive cells per area (F4/80 and LY6G) or the percentage of positive tumour cells per area (Ki67 and Caspase 3) in 5-10 different areas of samples from 5 mice per experimental group.

Table 2.11: Antibodies used in immunohistochemistry.

Antibody	**Company**	**Reference**	**Dilution**
F4/80	Bio Rad	MCA497GA	1/10
LY6G	BD Pharmigen	551459	1/70
Ki67	Novocastra	ACK02	1/800
Caspase 3	R&D	AF835	1/1000
Secondary antibodies	Vector Laboratories Burlingame CA		1/400

2.7 Flow cytometry and FACS sorting

Flow cytometry was performed on primary human monocytes obtained during the PhD placement in the i3S research institute in Porto. All experiments were conducted in Porto under the supervision of Dr. Maria Oliveira and her team members.

Conditioned media from macrophages was collected and stored at -20ºC or aspirated and discarded. Cells were washed with warmed PBS and 300 µL of accutase (eBioscience) was added to each well and samples were left in the incubator for 30 min at 37ºC. Cells were gently detached from the surface with a cell scraper and the suspension was transferred to a 15 mL falcon. 1 mL of cold PBS was added to the well to wash the remaining cells and the sample was transferred to the falcon. Cells were centrifuged at 1500 rpm for 5 min at 4ºC. The supernatant was discarded, and cells resuspended in 300-400 µL of FACS buffer (PBS + 2% FBS). For flow cytometry analysis, cells were stained with a cocktail of antibodies (Table 2.12). Single antibody staining, isotype control IgGs and unstained cells were used as controls. For each staining, 150 µL of samples (cells + FACS buffer) was added to a well in 96 well plate and samples were centrifuged at 1500 rpm for 5 min at 4ºC, and supernatant discarded. Antibody dilutions were made in the FACS buffer following the manufacturer instructions and added to the corresponding wells and incubated for 40 min at 4ºC in the dark. 150 µL FACS buffer was added and samples were centrifuged at 1500 rpm for 5 min at 4ºC. Two washes were performed by resuspending the cell pellet in 200 µL of FACS buffer and centrifuging in the same conditions mentioned previously. Cell pellet was finally resuspended in 1% PFA diluted in FACS buffer until flow cytometry analysis. Cells were filtered manually with a filtering net and transferred to FACS tubes. Flow cytometry was performed using the BD Bioscience FACSCanto™ II Cell Analyzer with FACS Diva software, and the gating strategy is represented in Fig. 3.3.5b. Data was analysed using FlowJo software version 10.

Table 2.12: Antibodies used in flow cytometry analysis.

Monocyte differentiation			
Antibody	**Dilution**	**Conjugated fluorochrome**	**Antibody reference**
CD14	1/25	APC	Immunotools Cat-No: 21620146
CD86	1/25	FITC	Immunotools Cat-No: 21480863
HLA-DR	1/25	FITC	Immunotools Cat-No: 21278993
CD163	1/10	PE	BD Pharmingen Ref: 556018
CD206	1/50	PE	BioLegend Cat. No. 321105
IgGs1	1/25	APC/ FITC and PE	Immunotools

FACS sorting was performed on mouse orthotopic tumours generated by injection of TS1 cells in FVB mice. All experiments were performed at the Institute of Cancer Research in London (ICR) and data analysed under the supervision of Prof. Clare Isacke and Dr. Liam Jerkins.

Tumours were surgically removed from animals after culling and converted into single-cell suspension using a tumour dissociation kit in combination with a gentleMACS Octo dissociator with heaters (Miltenyi Biotec, 130-096-427) according to the manufacturer's protocol. Specified volumes of supplied enzymes were added to tumour samples before running each sample on the Octo dissociator with the program 37C_m_TDK_2. Samples were subsequently applied to a 70 µm MACS SmartStrainer and washed in PBS. Erythrocytes were removed from tumour samples by suspension in a red blood cell lysis buffer (Sigma) for 5 minutes at room temperature. Samples were resuspended in FACS buffer (PBS with 1% FBS) for FACS staining. After tissue dissociation, cells were centrifuged for 5 min at 300 *g*, resuspended in 1 mL of blocking buffer diluted 1/100 in FACS buffer (Thermo Fisher Scientific) and left for 10 min at room temperature. 1/20 of the suspension was transferred to a new falcon with 1 mL of FACS buffer to use for live/dead staining with

fixable violet dead stain kit (Invitrogen). All cells were centrifuged, resuspended with antibody solution in FACS buffer (Table 2.13) and left for 30 min at 4ºC. During the incubation time, the following controls were prepared: compensation beads (eBiosciences) with each individual antibody staining, cell suspension with live/dead staining and negative unstained suspension and FMO controls (Fluorescence minus one control). Cells and bids were spun down and washed with FACS buffer. After centrifugation cells were resuspended with 1 mL of DAPI staining (1/10000) (Thermo Fisher Scientific), centrifuged and resuspended in 2 mL of FACS buffer. Collection tubes were prepared with 2 mL of complete RPMI media and kept on ice. Cells were sorted using the FACSAria II cell sorter and gating strategy shown in Fig. 3.2.3b. Sorted cells were centrifuged for 5 min at 1500 rpm and immediately used for RNA extraction.

Table 2.13: Antibodies used for FACS sorting.

1st sorting			
Antibody	**Dilution**	**Conjugated fluorochrome**	**Antibody reference**
EPCAM	1/80	APC	Cat: 118214 LOT: B188951 BioLegend
CD31	1/10	FITC	LOT : 5180507080 MACS
CD45	1/80	PerCP/Cy5.5	Cat: 103131 BioLegend
2nd sorting			
Antibody	**Dilution**	**Conjugated fluorochrome**	**Antibody reference**
CD45	1/80	PerCP cy5.5	Cat:103131 Lot:B238619 BioLegend
CD3	1/40	PE	Ref: 12-0031-82 Lot: E00991-1636 eBioscience
CD11b	1/50	FITC	Cat: 561688 Lot: 6336928 BD Biosciences

2.8 Animal studies

All animal studies were conducted under the approval of the local ethical committee with the assigned project license codes: CEEA 15/016 and CEEA16/006.
Animals were kept in the institute animal facility and routinely maintained by the animal facility technicians. All procedures and animal culling were done under a personal animal license.

2.8.1 Mouse models

2.8.1.1 Orthotopic xenografts in nude mice

Athymic Nude-Foxn1 female mice (6-8 weeks old, Charles River) were used to induce orthotopic tumours by injecting human cells in the mammary fat pad of the 4th mammary gland. In summary, a small incision was performed next to the 4th right hand side nipple, the mammary gland exposed and 50 µL of cell suspension injected into the mammary gland. Animals not correctly injected due to leakage were excluded from the experiment. The incision was sutured with 2-3 stitches and animals monitored 3 times a week. Tumours were measured using a calliper and tumour volume was determined using the following formula[230]: $(4\pi/3) \times (\text{width}/2)^2 \times (\text{length}/2)$. Animals were culled when tumour volume in one of the experimental groups reached the maximum size allowed (1.5 cm diameter). All animal tissue samples were collected and stored as mentioned in section animal tissue collection at culling points.

The following xenograft experiments were performed:

1) **Injection of MDA-MB-231 hControl/ hOSM**.
   100.000 cells of MDA-MB-231 hControl or hOSM prepared in 50 µL DMEM (no FBS, no antibiotics) were injected.

2) **Co-injection of shOSMR CAF-173 and MDA-MB-231 hOSM.**
   CAF-173 were transfected with shRNA OSMR/Control. After selection cells were mixed with MDA-MB-231 hOSM at the following concentrations: 100.000 tumour

cells + 500.000 CAF-173 in 25 µL of DMEM (no FBS, no antibiotics). Cells were injected with matrigel in a 1:1 ratio (25 µL cell solution + 25 µL matrigel).

3) **Co-injection of OSM pre-treated CAF-173 and MDA-MB-231.**

CAF-173 were treated with 10ng/µL OSM for 4 days and mixed with MDA-MB-231 in a 1:1 ratio prior to injection (500.000 MDA-MB-231 + 500.000 CAF-173) in 25 µL of DMEM (no FBS, no antibiotics). Cells were injected with matrigel in a 1:1 ratio (25 µL cell solution + 25 µL matrigel).

2.8.1.2 TS1 orthotopic injections in OSMR KO and control mice

OSMR-/- mice (OSMR KO, B6.129S318 Osmr<tm1Mtan>, Riken BRC)[155] were initially generated on a C57BL/6J background. To transfer the OSMR KO line to the genetic background of the tumour-prone animals (FVB/NJ), the OSMR KO mice were previously backcrossed with FVB/NJ mice for 9 generations and kindly provided by Prof. Nicholas Coleman (Cambridge). Animals used for experiments were female littermates.

OSMR KO mice were used to generate orthotopic breast tumours to study tumour-stroma interactions in a fully competent immune system model. 6-8 weeks old OSMR KO females and their controls OSMR WT were used to induce orthotopic tumours by injecting MMTV-PYMT derived TS1 mouse cells[219]. Briefly, 300.000 cells were prepared in 25 µL of DMEM (no FBS, no antibiotics) and mixed with 25 µL of matrigel and injected into the 4th mammary gland. Animals were monitored 2-3 times a week and tumour volume (formula described in 2.8.1.1) recorded until it reached the maximum size allowed (1,5 cm diameter) in one of the experimental groups, when animals were culled. All animal tissue samples were collected and stored as mentioned in section 2.8.2.

TS1 orthotopic tumours in control FVB mice were generated for FACS sorting experiments. Briefly, 500.000 cells were prepared in 50 µL of PBS and injected into the 4th mammary gland of 6-8 weeks FBV females. Tumours were surgically excised 15 days later and immediately used for FACS sorting experiments (section 2.7).

2.8.1.3 MMTV-PyMT model

Transgenic FVB/NJ mice expressing the Polyoma Middle T antigen oncogene under the Mouse Mammary Tumour Virus promoter (MMTV-PyMT)[231] were kindly provided by Dr. Eva Suarez (CNIO, Madrid). MMTV-PyMT mice were crossed with OSMR KO mice and used to assess the role of OSMR in tumour development and disease progression. Cross breeding strategy is described in Fig. 2.3.

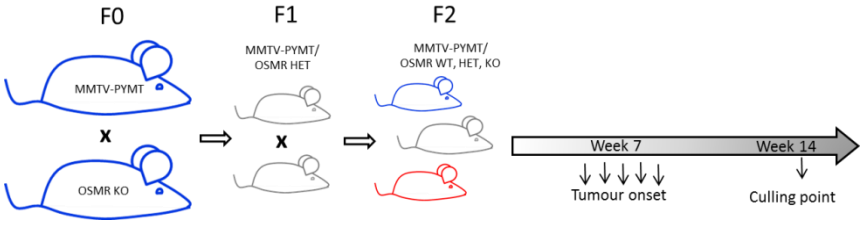

Fig. 2.3: MMTV-PyMT:OSMR crossing strategy.

Animals started to be monitored and palpated at week 5 to detect tumour onset and were checked weekly until they reach 14 weeks of age. All mammary tumours were measured with a calliper and tumour growth was calculated by adding individual tumour volumes. At culling point, all tumours were surgically removed and weighted together to determine final tumour burden. Animal samples were collected as described below.

2.8.2 Animal tissue collection at culling points

Blood, tumours, and viscera including lungs were collected from mice for further analysis. In summary, blood was collected from cardiac puncture and transferred to anticoagulant tubes (Sigma-Aldrich). Sample was centrifuged at 5000 rpm at 4ºC for 5 min and plasma transferred to a new tube and stored at -80ºC. Half of the tumour and a small lobe from the lungs were collected for protein and RNA analysis and snap frozen in liquid nitrogen. The other half of the tumour and whole-body organs were fixed in formalin for 48-72 h and stored in PBS at 4ºC until immunohistochemistry or histological analysis. For wholemount analysis of preneoplastic lesions, abdominal mammary glands from 9-week-old MMTV-PyMT:OSMR KO and control female mice were spread out on a glass slide, fixed overnight

in Carnoy's solution, stained with Carmine Alum, and cleared in ethanol and xylene. Pictures were taken with a Nikon D5000 at 60mm focal length.

2.8.3 Mouse colonies maintenance

OSMR KO and MMTV-PyMT mice colonies were maintained and bred in the animal facilities of Biodonostia Health Research Institute. 2-9 month-old mice were used as breeders. Most breeding cages were setup in trios (2 females and 1 male) and the male kept in the cage all the time to reduce stress levels. Pups were weaned at 3 weeks old, at 4-5 weeks animals were ear tagged and chipped with a unique identification number. Genotyping of the OSMR and PyMT genes was performed by laboratory members or by the in-house genomic platform service. Briefly, DNA was extracted from ear sample adding 75 µL of lysis buffer (NaOH at 25 mM and EDTA at 0.2 mM) and incubating the sample for 1 hour at 95ºC. After lysis, the sample was cooled down and 75 µL of neutralisation buffer (Tris-HCl 40 nM) was added. DNA was kept at 4ºC until PCR analysis was performed following conditions described in Tables 2.14-16. Platinum SuperFi PCR Master Mix qPCR kit (Invitrogen) and KAPA2G Fast HotStart PCR Kit (KAPABIOSYSTEMS) were used to genotype OSMR and MMTV-PyMT respectively. PCR product was run on a 2% agarose gel at 100-110 V for 1h and PCR band size was checked to identify individual genotype. Animal health monitoring was done by Dr. Carlos San José, veterinarian of the animal facility. When possible, female littermates were used for experiments.

Table 2.14: Genotyping primers for OSMR and MMTV-PyMT:

Primer name	Sequence	Amplicon size	Origin
OSMR-P1	GTAATCAGACCAATGGCTTTCTC		Riken
OSMR-P2	GATCCAACAGAGCAATCATGAAGC	P1 +P2 = 360bp for WT	
OSMR-P3	GCACATCTGAACTTCAGC	P1 +P3 = 750bp for KO	
PYMT-F	GGAAGCAAGTACTTCACAAGGG	556 bp	The Jackson laboratory
PYMT-R	GGAAAGTCACTAGGAGCAGGG		
PC-F (control)	CAAATGTTGCTTGTCTGGTG	206 bp	
PC-R (control)	GTCAGTCGAGTGCACAGTTT		

Table 2.15: OSMR genotyping conditions.

Master mix			**Cycling conditions**		
Component	**Volume (µL)**		**Temperature**	**Time**	
Master Mix Reagent	12,5		98 ºC	30 sec	
P1 (F) 10 µM	1,25		98 ºC	10 sec	40 cycles
P2 (R_{OSMR}) 10 µM	0,75		60 ºC	30 sec	40 cycles
P3 (R_{LACZ}) 10 µM	0,75		72 ºC	1 min	
DNA	1		72 ºC	5 min	
H_2O	8.75		4 ºC	hold	
Total volume	25				

Table 2.16: PyMT genotyping conditions.

Master mix			**Cycling conditions**			
Component	**Volume (µL)**		**Temperature**	**Time**		
5X Buffer M	2,4		94 ºC	2 min		
dNTP 10 mM	0,24		94 ºC	20 sec		10 cycles
$MgCl_2$ 25 mM	0,96		65 ºC	15 sec	-0,5 ºC per cycle	10 cycles
F_{PYMT} 10 µM	0,6		68 ºC	10 sec		28 cycles
R_{PYMT} 10 µM	0,6		94 ºC	15 sec		
F_{PC} 10 µM	0,6		60 ºC	15 sec		28 cycles
F_{PC} 10 µM	0,6		72 ºC	10 sec		
5 U Polymerase	0,025		72 ºC	2 min		
DNA	1		10 ºC	hold		
H_2O	4,975					
Total volume	12					

2.9 Statistical analyses

Statistical analyses were performed using GraphPad Prism or SPSS software. For Gaussians distributions, the student's t-test (paired or unpaired) was used to compare differences between two groups. Welch's correction was applied when variances were significantly different. One-way ANOVA was used to determine differences between more than two independent groups. For non-Gaussian distributions, Mann-Whitney's or Wilcoxon test were performed. Chi-square test was used to determine differences between expected frequencies. For Kaplan-Meier analysis the Log-rank (Mantel-Cox) test was used. P values inferior to 0.05 were considered statistically significant. Unless otherwise stated, results are expressed as mean values +/- standard errors (SEM).

Chapter 3: Results

3.1 Role of OSM:OSMR signalling in breast cancer progression.

3.1.1 Summary

Objectives 1 and 2 of this thesis were addressed in this section with the aim of investigating OSM and OSMR expression in human breast cancer samples and its association with prognosis, and unravelling the role of OSM:OSMR signalling in breast cancer development and progression.

Association of OSM:OSMR expression with clinical features in breast cancer was determined using multiple publicly available datasets of transcriptomic data and by analysing protein expression in samples from a cohort of breast cancer patients with associated clinical data. The role of OSM:OSMR signalling in breast cancer cells was evaluated in *in vitro* models using a panel of breast cancer cell lines, and its role in cancer progression was determined using human tumour xenografts and genetic mouse models of breast cancer.

3.1.2 OSM and OSMR are associated with decreased overall survival in breast cancer, especially in the ER- subtype.

The first step of this project was to determine the expression of OSM and OSMR in clinical samples of breast cancer. Analysis of a large publicly available dataset (METABRIC), with clinical data from approximately 2000 patients, showed that patients with tumours expressing high levels of OSM presented lower disease-free survival (DFS) (P = 0.004, Fig. 3.1.1a). In a smaller cohort published by Wang *et al*. (2005)[208] with 286 patients, a similar trend was observed associating higher expression of OSM with worse DFS (P = 0.075, Fig. 3.1.1b). To further validate these findings at protein level, the group used tissue microarrays (TMAs) that included 141 breast cancer samples from a cohort of patients with tumour biopsies at diagnosis and long-term follow-up clinical data provided by Prof. Tzankov, at the University Hospital of Basel. OSM immunohistochemistry staining of the TMAs revealed that, in accordance with the mRNA data, higher expression of OSM in the tumours correlated with worse overall survival (OS) (P = 0.029, Fig. 3.1.1c). Interestingly,

the association of OSM expression with decreased survival was only observed in the ER- cases (Fig. 3.1.1d) but not in the ER+ (data not shown). Data from Kaplan-Meier (KM) plotter were used to determine if OSM and OSMR mRNA levels were also associated with survival in a different cohort, and to explore the link with ER expression. The analysis revealed that OSM expression correlated with OS (P = 0.025), but that in this cohort, OSM was not associated with distant metastasis-free survival (DMFS) (P = 0.29). OSMR expression also correlated with worse OS (P = 0.041) and it showed a tendency for DMFS (P = 0.065, Fig. 3.1.1f). To further explore if OSM or OSMR were associated with a specific breast cancer subtype, the same KM plotter analysis was performed dividing data in ER+ and ER- tumours. OSM correlated with worse OS in ER- tumours (P = 0.008, Fig. 3.1.1g) while this trend was not significant for ER+ tumours (data not shown). On the other hand, OSMR expression correlated with worse DMFS in ER- tumours (P = 0.019, Fig. 3.1.1h) but no correlation was found in ER+ tumours (data not shown). These data suggested that, in general, both OSM and OSMR levels are associated with worse survival in breast cancer, and that this could be particularly relevant in ER negative tumours.

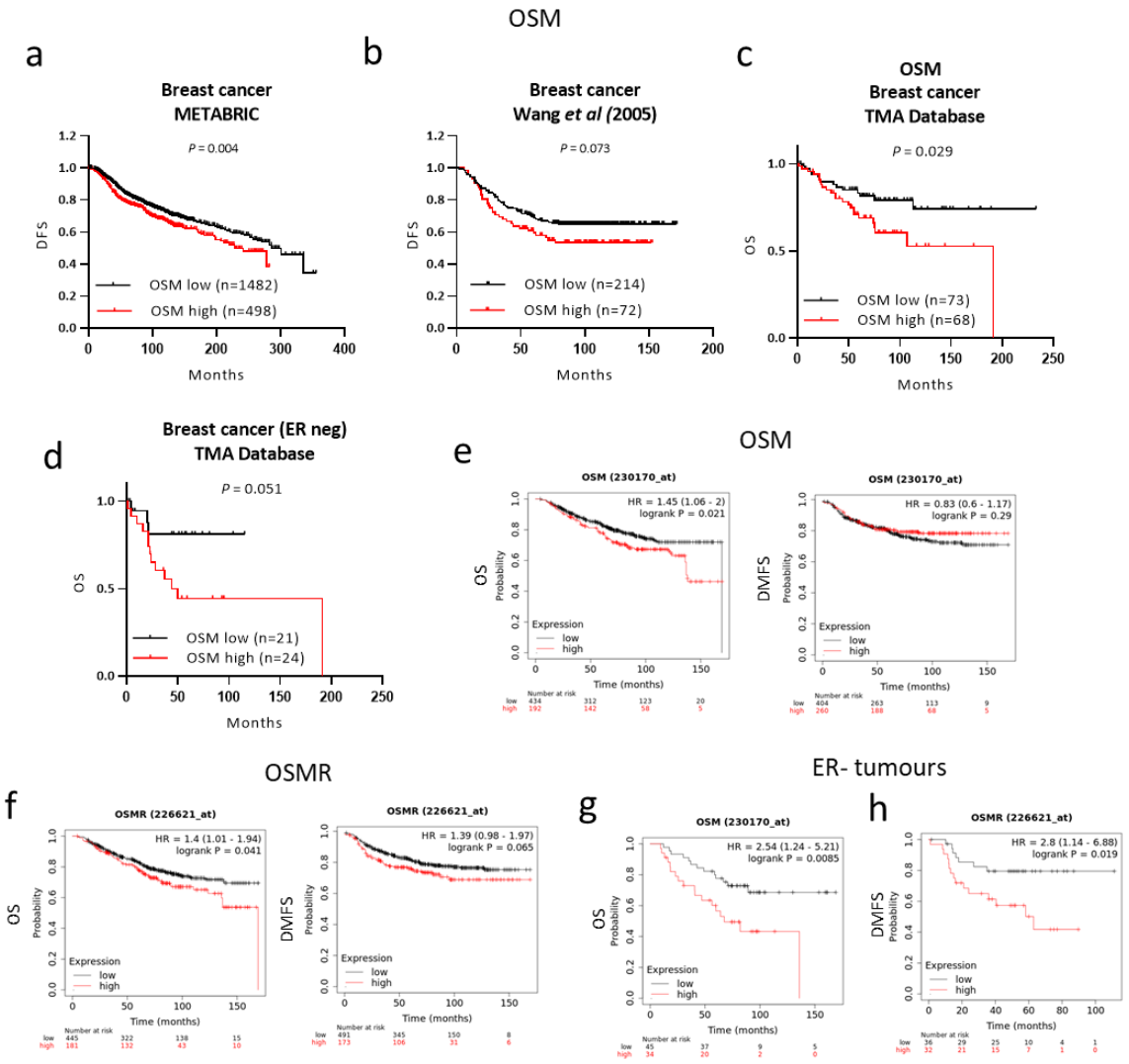

Fig. 3.1.1: OSM and OSMR are associated with poor overall survival in breast cancer, especially in the ER- tumours.
Kaplan-Meier curves from breast cancer clinical data showing: **a,b)** Disease free survival (DFS) for cancer patients with high versus low expression of OSM, included in the METABRIC **(a)** or Wang **(b)** datasets present in Cancertool. **c,d)** overall survival (OS) for cancer patients with high versus low levels of OSM for all subtypes of breast cancer **(c)** and for ER negative (ER-) breast cancer **(d),** whose samples were included in the tissue microarrays (TMAs) from the University Hospital Basel. **e,f)** OS and distant metastasis free survival (DMFS) for cancer patients with high versus low expression of OSM **(e)** and OSMR **(f)** included in KM Plotter using jet set probes and best cut-off. **g,h)** OS **(g)** and DMFS **(h)** for ER- breast cancer patients with high versus low expression of OSM and OSMR, respectively, included in KM Plotter. All P values were calculated using the Mantel-Cox test.

3.1.3 OSM and OSMR are associated with decreased overall survival in multiple types of cancer.

Our previous work has shown that overexpression of OSMR correlated with poor overall survival (OS) in cervical cancer[183]. To verify if OSM or OSMR expression was associated with

survival in other types of cancer, a pan-cancer analysis was done using KM plotter webtool. The results indicated that, in many cases, both the expression of the ligand and the receptor were significantly associated with decreased overall survival (cervical squamous cell carcinoma, kidney renal cell carcinoma, ovarian cancer, pancreatic ductal adenocarcinoma, stomach adenocarcinoma, thymoma) (P values shown in Fig 3.1.2 and 3.1.3). These results indicated that OSM:OSMR signalling could be an important player in cancer progression, not only in cervical and breast cancer, but also in other types of cancer.

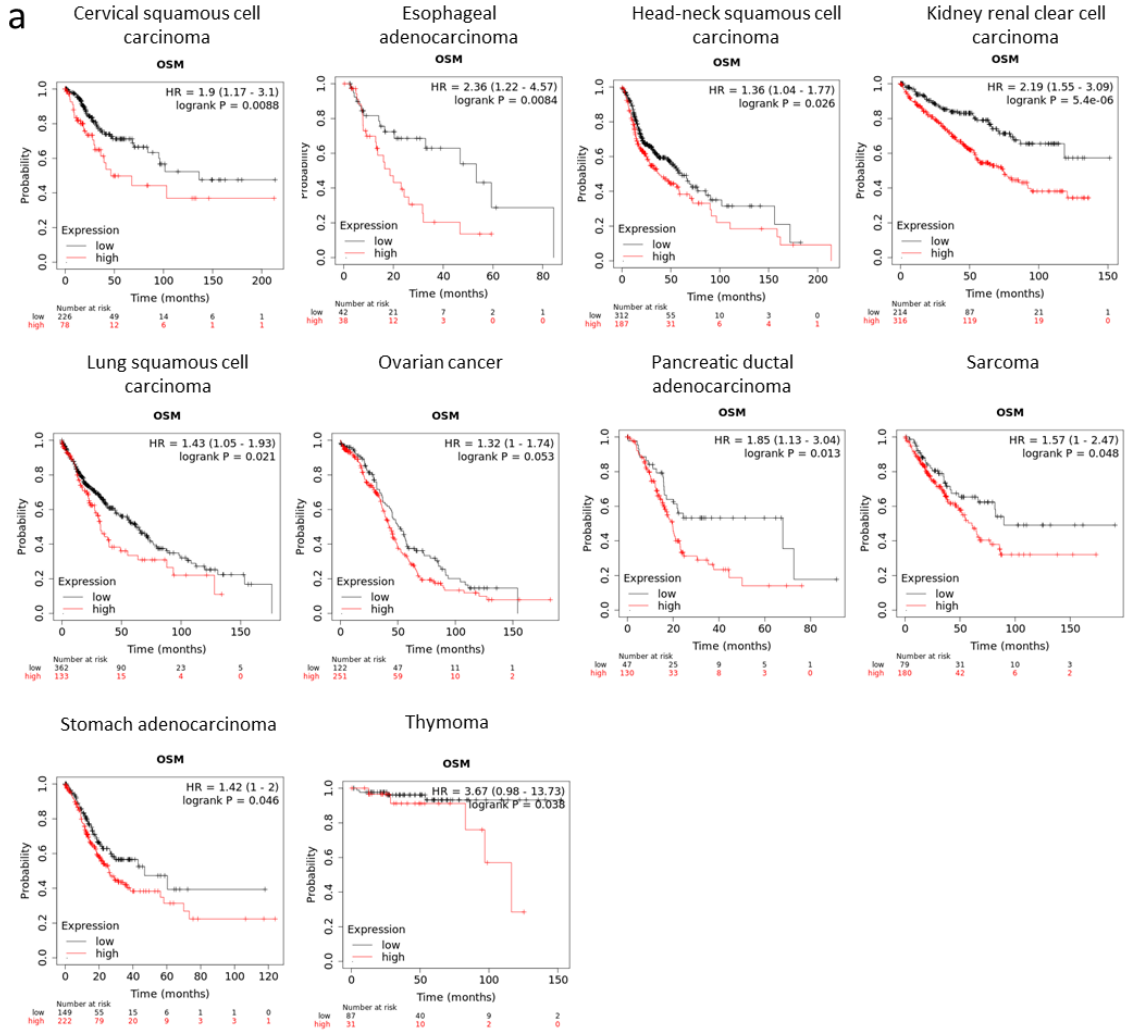

Fig. 3.1.2: OSM is associated with poor overall survival in multiple types of cancer.
a) Kaplan-Meier curves showing overall survival for cancer patients of the indicated subtypes with high versus low expression of OSM obtained from KM plotter using jet set probes and automatic best cut-off. P values were calculated using the Mantel-Cox test.

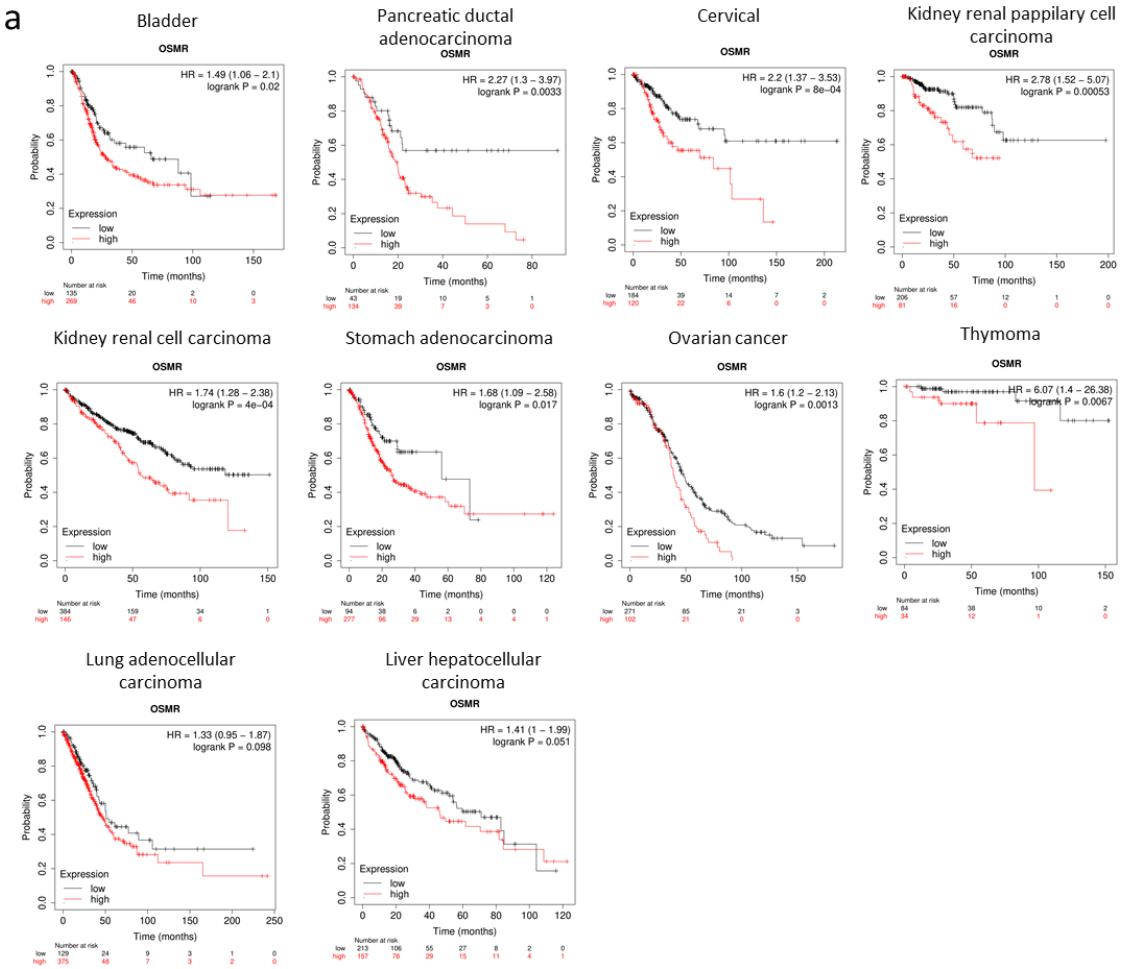

Fig. 3.1.3: OSMR is associated with poor overall survival in multiple types of cancer.
a) Kaplan-Meier curves showing overall survival for cancer patients of the indicated subtypes with high versus low expression of OSM obtained from KM plotter using jet set probes and automatic best cut-off. P values were calculated using the Mantel-Cox test.

3.1.4 OSM and OSMR are not frequently mutated in breast cancer.

Two previous works have shown that a subset of cervical squamous cell carcinoma samples show *OSMR* copy number gain and this is associated with gene and protein overexpression[179,181]. To verify if *OSM* or *OSMR* genes were frequently mutated or altered in breast cancer, genomic sequencing data available at cBioPortal from the METABRIC and TCGA datasets were used to look for frequency of mutations. Considering the results from both datasets, only 0.7-1% of the patients presented mutations in the *OSM* gene, being amplifications, the majority of the genetic alterations found. The data extracted from the METABRIC dataset showed that all *OSMR* mutations were amplifications (2.8%) while in TCGA dataset only 1% of patients showed gene amplification with a total 2.2% of patients

presenting *OSMR* mutations. In cervical cancer, around 6% of the patients presented amplifications in the *OSMR* gene and almost no mutations were found in *OSM* (Fig. 3.1.4a). These results revealed that *OSM* and *OSMR* genes are not frequently mutated in breast cancer and that upregulations of the pathway cannot be explained by genetic alterations.

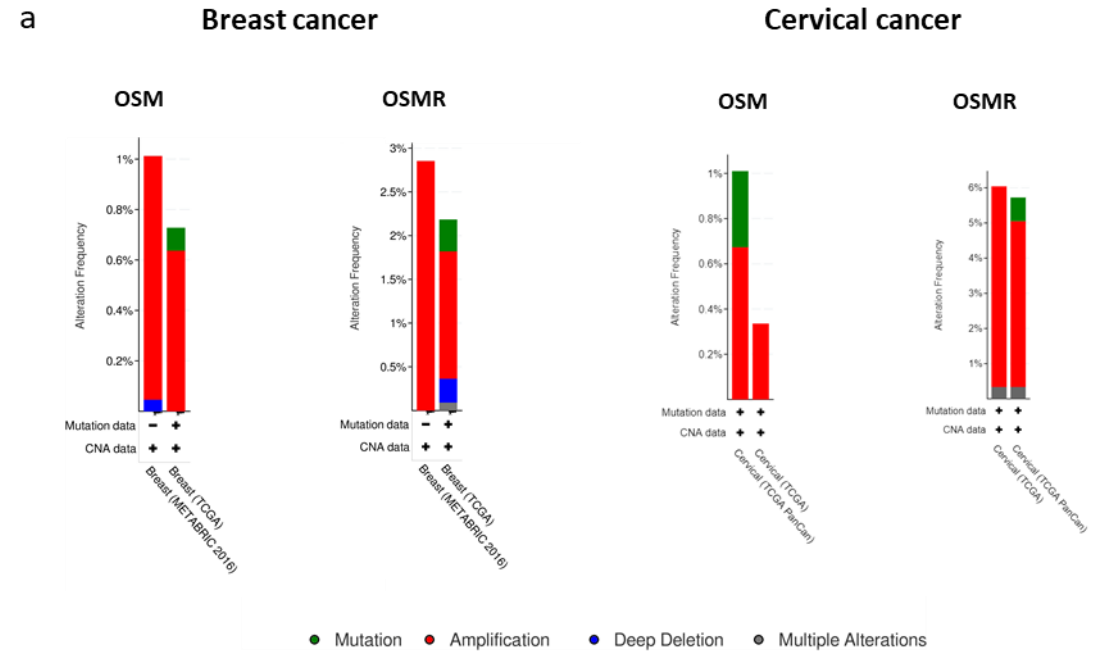

Fig. 3.1.4: OSM and OSMR are not frequently mutated in breast cancer.
a) *OSM* and *OSMR* mutation frequency in breast and cervical cancer, shown as reference. Graphs show frequency of mutations found in the indicated datasets. Data were obtained from cBioPortal.org.

3.1.5 OSMR pathway activation is increased in ER- breast cancer cells.

Considering that clinical data suggested that OSM and OSMR were linked to worse prognosis mainly in ER- breast cancer, next, OSM and OSMR expression was analysed in ER+ and ER- breast cancer cell lines. A panel of breast cancer cell lines (Table 2.2 in chapter 2) was used to assess the mRNA levels of OSM, OSMR and some of their downstream targets described in the literature. OSMR was found to be increased in ER- cell lines (P = 0.021) compared to the ER+ (Fig. 3.1.5a). The negative regulator of the JAK-STAT pathway, SOCS3[232], presented an inverse pattern of expression (P = 0.022), which further explains the OSMR induction in the ER- subset. STAT3, a well-known downstream target of OSMR[169], was not differentially expressed in ER- breast cell lines but, on the contrary, IL-6 expression,

a described target of OSMR-STAT3 activation[233], was increased in the ER- group (P = 0.043, Fig. 3.1.5a). Despite no changes in STAT3 mRNA levels between the two groups, phosphorylation of STAT3 (P-STAT3), analysed by Western blot, was increased in the ER- cell lines (data not shown).

Interestingly, in the breast cancer cell panel, OSM was detected at late qPCR cycles assessed by Ct values >30, and in some cases not detected at all, by qPCR analysis (Fig. 3.1.5b) and by ELISA assay (data not shown). This finding indicated that cancer cells do not express and secrete a relevant amount of OSM suggesting that they do not rely on an autocrine signalling to activate the OSMR pathway.

Publicly available mRNA data from breast cancer cell lines (GSE69017)[218] was used to further validate the observations obtained with the breast cancer cell line panel presented Fig 3.1.5a. In accordance with the results previously obtained, mRNA levels analysis revealed that OSMR was significantly increased in ER- cell lines (P = 0.01). Interestingly, there were no differences between the groups in OSM expression (Fig. 3.1.5c).

The clinical data and the *in vitro* characterisation of the breast cancer cell panel presented in this section strongly suggested that OSM:OSMR signalling could be particularly important in the ER- setting. Further experiments would need to be done to further confirm this observation. Due to the large nature of the project, another member of the lab (Andrea Abaurrea) is currently investigating the role of OSM:OSMR in the ER- context. This thesis project was set to study the contribution of OSM:OSMR signalling axis in breast cancer in general, therefore a variety of ER+ and ER- negative models were used in this study.

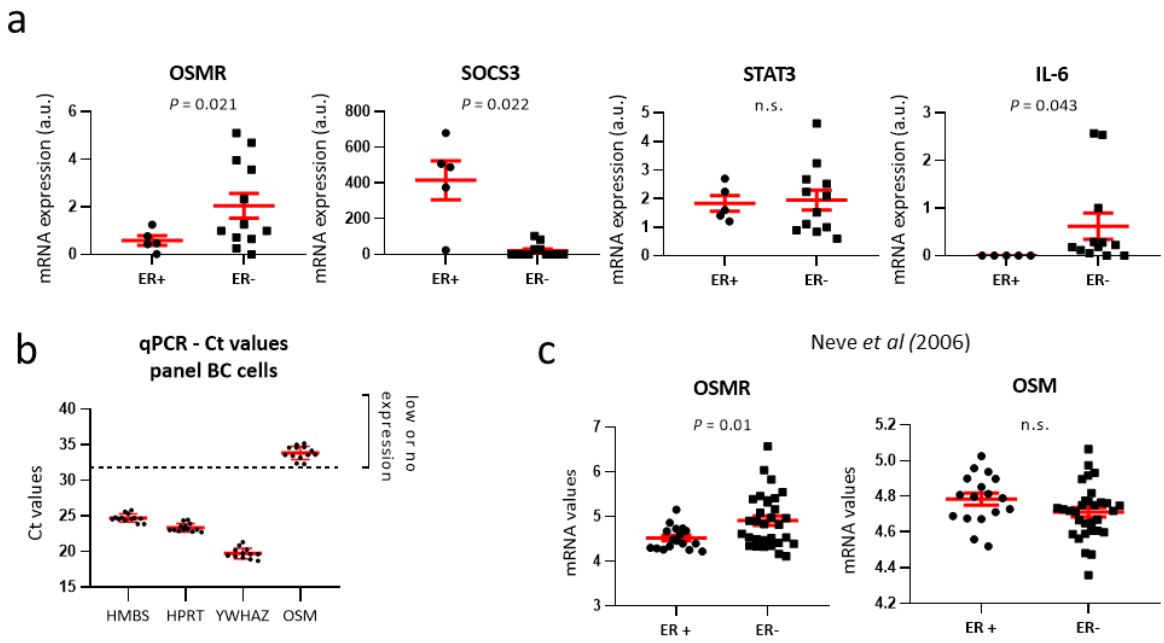

Fig. 3.1.5: OSMR pathway is increased in ER- breast cancer cells and cancer cells do not express biological significant levels of OSM.
a) mRNA expression of OSMR and its downstream targets in a panel of breast cancer cell lines with ER+ vs ER- expression. **b)** Ct values obtained from RT-qPCR analysis of different housekeeping genes (HMBS, HPRT, YWHAZ) and OSM in the breast cancer cell lines panel. **c)** OSMR and OSM mRNA levels in a panel of breast cancer cell lines from Neve *et al* (2006)[218] comparing ER+ vs ER- cell lines. Graphs represent mean ± SEM, and P values were obtained using the unpaired two-tailed t test.

3.1.6 Exogenous OSM treatment activates the OSMR pathway and induces pro-malignant factors in the MDA-MB-231 breast cancer cell line.

Fig. 3.1.5b shows that, in general, breast cancer cells do not express significant amounts of OSM to consider a relevant autocrine signalling. To verify if exogenous OSM could activate the OSMR pathway in breast cancer cell lines, recombinant OSM protein was added to the MDA-MB-231 cells. This cell line is one of the most widely used *in vitro* model of ER- breast cancer and it presents high levels of OSMR expression detected by qPCR and Western blot (Fig. 3.1.8a). MDA-MB-231 cells treated with OSM at 2 different concentrations (10 and 100 ng/mL) showed increased OSMR expression with the highest peak at 72h. Pro-malignant downstream targets of the pathway were also induced including IL-6, VEGF, SNAIL, and STAT3 (Fig. 3.1.6a). Although there was a small induction in STAT3 mRNA levels with OSM treatment, phosphorylation measured by Western blot with an antibody against P-STAT3 revealed that 10 ng/mL of OSM was enough to produce a strong phosphorylation

of STAT3 after 1 hour and that it was maintained at least up to 72 h (Fig. 3.1.6b,c). These data suggested that 10 ng/mL of OSM treatment is enough to activate the OSMR pathway in MDA-MB-231 breast cancer cell line and that this activation is maintained in time.

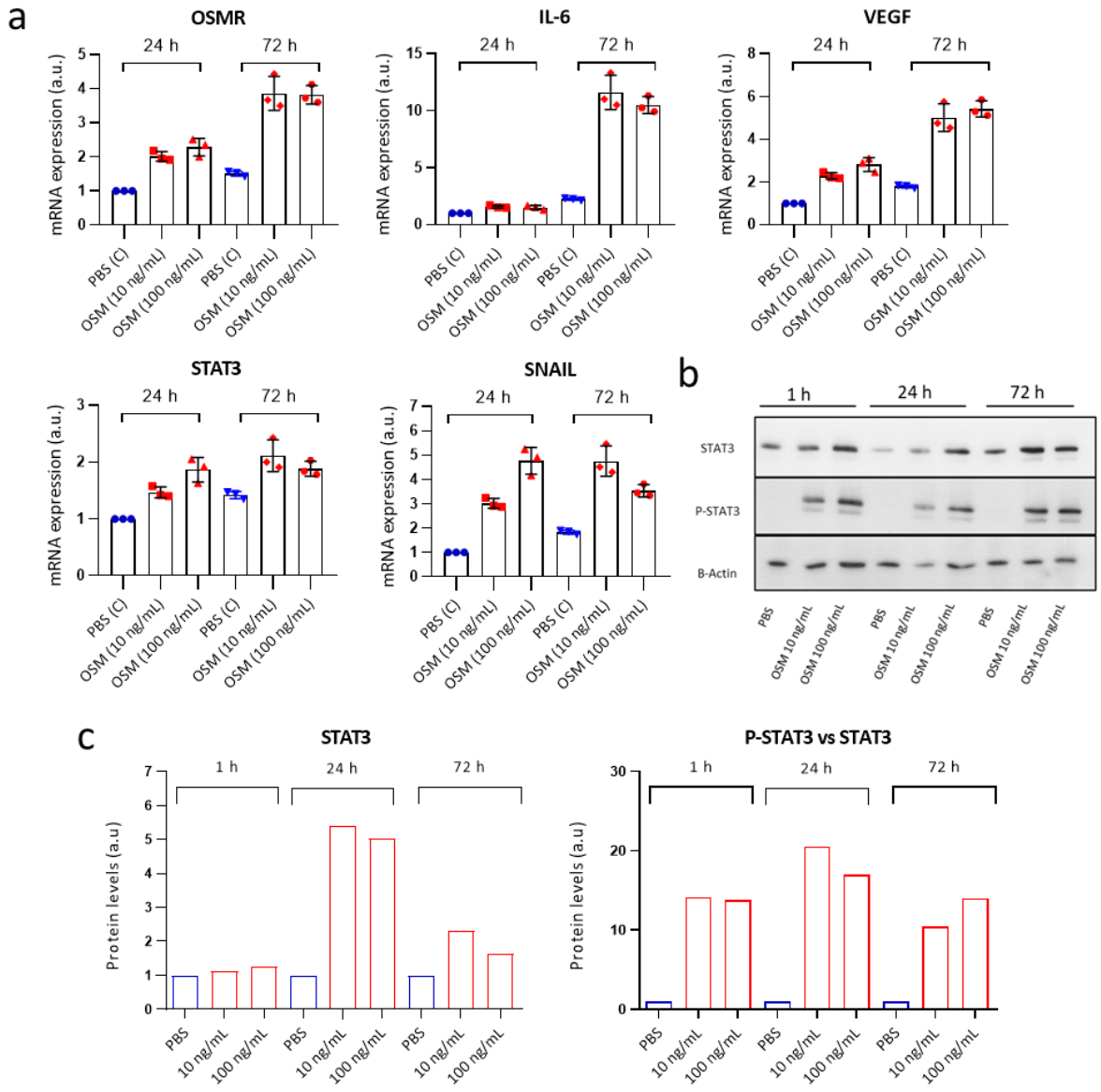

Fig. 3.1.6: OSM treatment of MDA-MB-231 cells activates the OSMR pathway and induces pro-malignant factors.
MDA-MB-231 cells were treated with recombinant OSM at different concentrations and time points. **a)** mRNA levels of OSMR and its downstream targets analysed by RT-qPCR. Graphs show mean ± SD of technical replicates. **b)** Protein levels of the indicated proteins assessed by Western blot and **c)** corresponding densitometric analysis.

3.1.7 OSM treatment of breast cancer cell lines induces pro-malignant factors through the OSMR receptor.

OSM, despite having a high affinity to OSMR, can also bind the LIF Receptor (LIFR)[192]. siRNA experiments to knockdown OSMR were performed in two ER- breast cancer cell lines (MDA-MB-231 and HCC1569) to determine if this receptor was responsible for activating the OSM mediated downstream signalling in breast cancer. Based on the manufacturer's recommendations, a minimum of 80% silencing was defined as necessary to be able to draw definite conclusions. Any silencing below that number was considered not to be sufficient to determine if OSM was signalling exclusively through OSMR. OSMR mRNA silencing was achieved at 84.2% for MDA-MB-231 and 68.8% for HCC1569 (Fig. 3.1.7a) after several optimisations (data not shown). Due to the low silencing achieved in HCC1569 further experiments were only performed with MDA-MB-231 cells. As seen in Fig. 3.1.7b, when OSMR receptor was knockdown in MDA-MB-231 cells, OSM was not capable of inducing downstream targets such as IL6, VEGF and SNAIL confirming this way that OSM activates these pro-malignant factors exclusively through OSMR in this context.

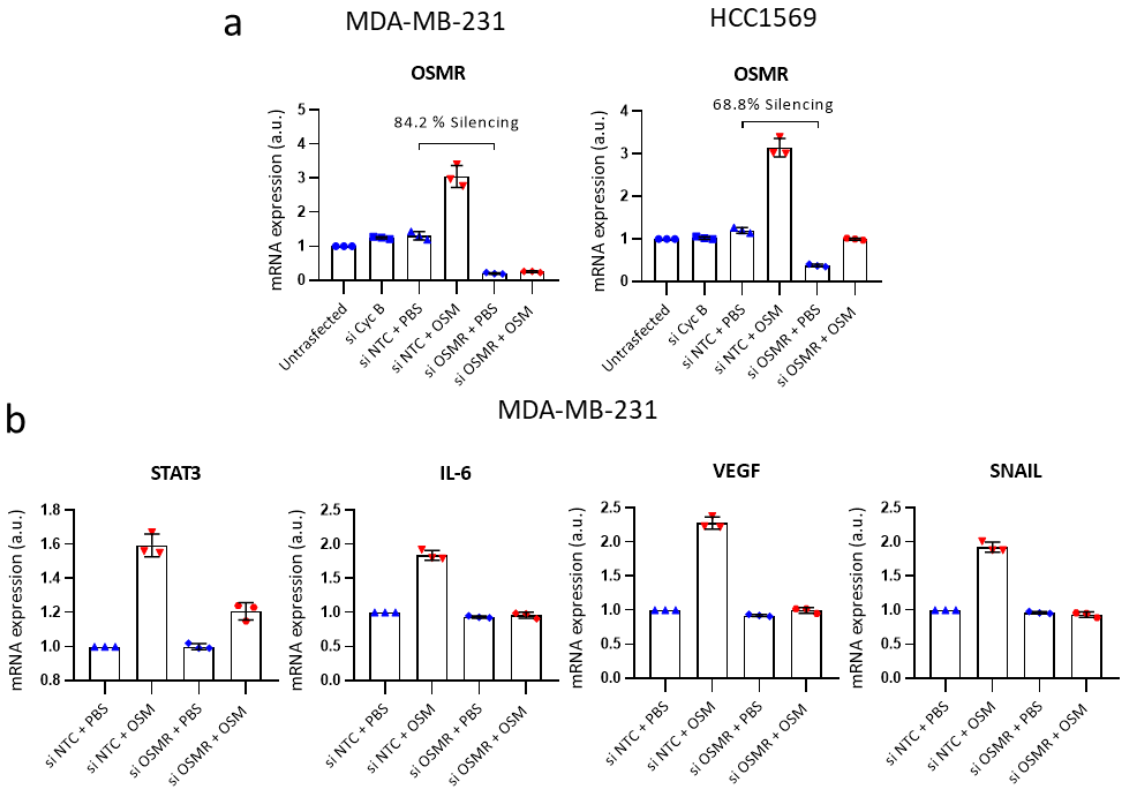

Fig. 3.1.7: OSM activates pro-malignant factors through OSMR.
a) MDA-MB-231 and HCC1569 cells were transfected with siRNA against Cyc B (positive control), non-targeting control (NTC) or OSMR and treated with PBS or 10 ng/mL OSM. Graphs represent

OSMR mRNA levels of technical replicates ± SD, and percentage of OSMR silencing calculated using si NTC PBS and si OSMR PBS values. **b)** mRNA levels of OSMR downstream targets after siRNA transfection and OSM treatment in MDA-MB-231 cells. Graphs represent mRNA levels of technical replicates ± SD of a representative experiment from 2 performed.

3.1.8 OSMR overexpression promotes a pro-malignant phenotype in the SK-BR-3 cell line.

Considering the clinical data that indicated that patients with OSMR overexpression had worse clinical outcome, and that activation of OSMR pathway with OSM induced pro-malignant factors in breast cancer cell lines, induction of OSMR expression in a breast cancer cell line with low basal levels of OSMR was hypothesised to promote a pro-malignant phenotype. SK-BR-3 cell line was selected to test this hypothesis as they possess low basal levels of OSMR (Fig 3.1.8a). Cells were transfected with a plasmid containing *OSMR* gene (hOSMR) that resulted in a 40-fold change in increased expression (Fig. 3.1.8b). Treating SK-BR-3 hOSMR with OSM promoted the induction of downstream targets such as IL-6 and fibronectin (FN) (Fig. 3.1.8b) previously described as an OSMR target in cancer cells[182]. Of interest, a phenotypic change was also observed in cells transfected with hOSMR plasmid and activated with OSM (hOSMR OSM). These cells presented a more elongated shape with lower adherence to the plate compared to the respective controls (hControl PBS/or OSM) (Fig. 3.1.8c,d). These phenotypic changes are usually associated with EMT[234], and are consistent with the induction of FN (Fig. 3.1.8b), a classical marker described to promote EMT transition in epithelial cells[235].

These results confirmed that induction of OSMR *in vitro* results in activation of pro-malignant downstream targets and induction of mesenchymal phenotype.

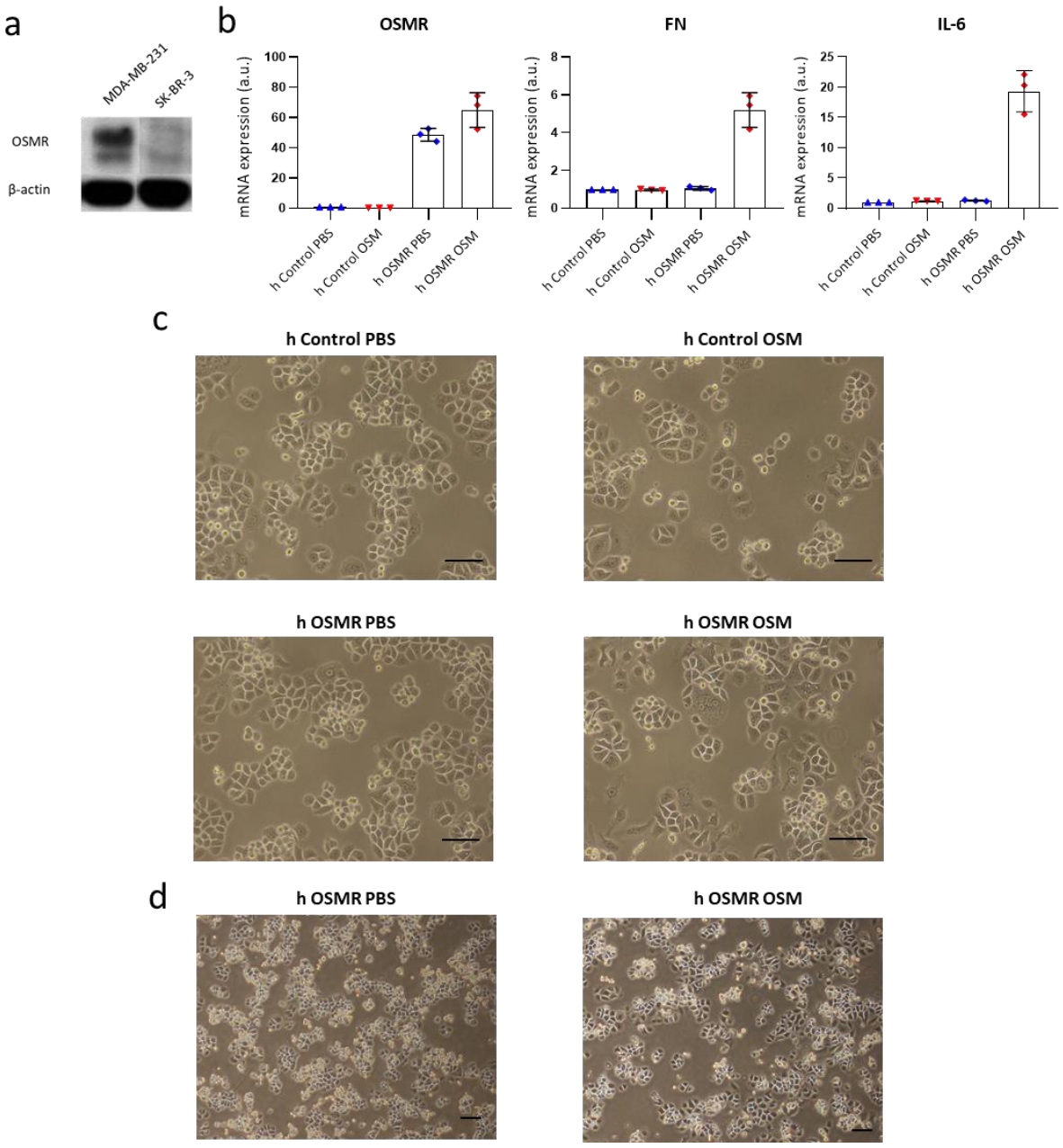

Fig. 3.1.8: OSMR expression in SK-BR-3 cells induces pro-malignant factors and a mesenchymal-like cell morphology.

a) Western blot showing OSMR levels in MDA-MB-231 and SK-BR-3 cell lines. **b)** SK-BR-3 cells were transfected with pcDNA3.1 zeo plasmid containg OSMR gene (hOSMR) or with control vector (h Control) and treated with PBS or OSM 10 ng/mL for 72h. Graphs represent mRNA levels of OSMR and downstream targets. Technical replicates ± SD of a representative experiment is shown. **c, d**) Representative pictures of the different conditions described in **(b)** showing cell morphology and adherence at higher **(c)** and lower **(d)** magnification.

3.1.9 MDA-MB-231 cells constitutively expressing OSM are a reliable model of constant OSMR pathway activation.

As described in Fig. 3.1.5b, cancer cells do not express significant levels of OSM, reducing the possibility of a sustained autocrine signalling. Furthermore, murine OSM is not capable of binding human OSMR[236]. To assess the role of OSMR signalling in breast cancer progression using xenografts of human cells it was necessary to create a system where human cancer cells were in contact with human OSM to induce OSMR pathway activation. Two possibilities were considered at this point to counter the issue of different cross-species reactivity: either periodical injections of human OSM into mice (intravenous or intraperitoneal injections), or the generation of a human breast cancer cell line with endogenous OSM production. Taking into consideration the downside and benefits of each system, the model of autocrine signalling in the MDA-MB-231 cells was chosen as it would ensure a constant liberation of OSM and it would save the animals the stress of periodical injections. To generate this model, MDA-MB-231 were transfected with p-UNO Control (hControl) or p-UNO1-hOSM (hOSM) plasmids containing the human *OSM* gene. As seen in Fig. 3.1.9a-b, both OSM mRNA and secreted protein levels, assessed by qPCR and ELISA, respectively, were shown to be greatly induced after plasmid transfection. OSM overexpression induced the expression of OSMR downstream targets (Fig. 3.1.9c) in a remarkably similar fashion observed in the MDA-MB-231 with OSM exogenous treatment (Fig. 3.1.6), demonstrating this way that OSM-induced autocrine signalling in MDA-MB-231 cells can activate the OSMR pathway.

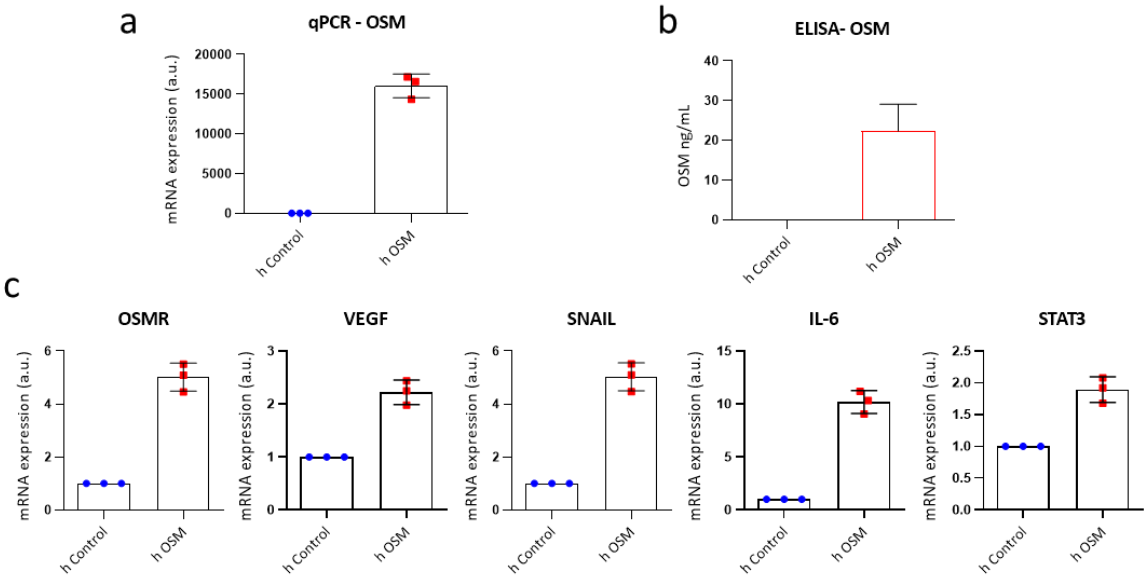

Fig. 3.1.9: MDA-MB-231 cells transfected with human OSM are a stable model for constant OSMR pathway activation.
MDA-MB-231 cells were transfected with a plasmid containing OSM gene (hOSM) or empty vector (hControl). **a)** OSM mRNA levels analysed by RT-qPCR. **b)** OSM protein levels secreted analysed by ELISA. **c)** mRNA levels of OSMR and downstream targets. Graphs represent mean ± SD of technical replicates of a representative experiment out of 2 performed.

3.1.10 OSM signalling induces tumorigenesis and metastasis in mice xenografts in nude mice.

Clinical data and *in vitro* experiments previously presented strongly suggested that OSMR signalling could be playing a role in breast cancer progression. Therefore, activation of the OSMR pathway in tumour cells was hypothesised to contribute to breast cancer progression *in vivo.* To assess the role of OSM:OSMR signalling *in vivo*, MDA-MB-231 hControl or hOSM (Fig. 3.1.9) were injected orthotopically in nude mice. Activation of OSMR pathway in MDA-MB-231 hOSM cells lead to an earlier tumour onset (P = 0.002, Fig. 3.1.10a) and increased tumour growth (Fig. 3.1.10b). Of the 6 mice injected with MDA-MB-231 hControl cells only 1 animal developed a tumour within the 45 days experimental window. On the contrary, 7 out of 7 animals injected with MDA-MB-231 h OSM developed tumours (Fig. 3.1.10a-c). Interestingly, the single tumour in hControl group appeared to have similar tumour volume to the hOSM tumours raising the question if OSM influences tumour growth or if it only delays tumour appearance.

MDA-MB-231 cells preferentially metastasise to the lungs in the *in vivo* models[237]. Disease progression was assessed by the presence of micrometastases in the lungs using qPCR to detect human Alu sequences in the mice lungs. This technique revealed that around 50% of the animals injected with MDA-MB-231 hOSM had detectable micrometastases in the lungs while none of the control animals tested positive for the presence of micrometastases ($P = 0.033$, Fig. 3.1.10d), suggesting that OSM signalling in cancer not only favours tumour onset but also the spread of the disease to distant organs.

mRNA levels in the tumours at the culling point were analysed by qPCR to confirm that the production of OSM was maintained in time. As seen in Fig. 3.1.10e, all mice tumours generated from MDA-MB-231 hOSM injection presented high levels of OSM expression compared to the single hControl tumour, except for 1 animal. This tumour seemed to have lost OSM expression with time, and, of note, it corresponded to the smallest tumour of the group, which suggests that OSM could also be influencing tumour growth, but further experiments would need to be performed to answer this question.

Analysis of the downstream targets in the different experimental groups showed that OSM overexpressing tumours presented higher levels of OSMR ($P < 0.001$), STAT3 ($P = 0.016$) and a trend to higher levels of VEGF and IL-6 (Fig. 3.1.10f), suggesting that OSM was activating OSMR pathway *in vivo* and promoting breast cancer progression in this xenograft mouse model.

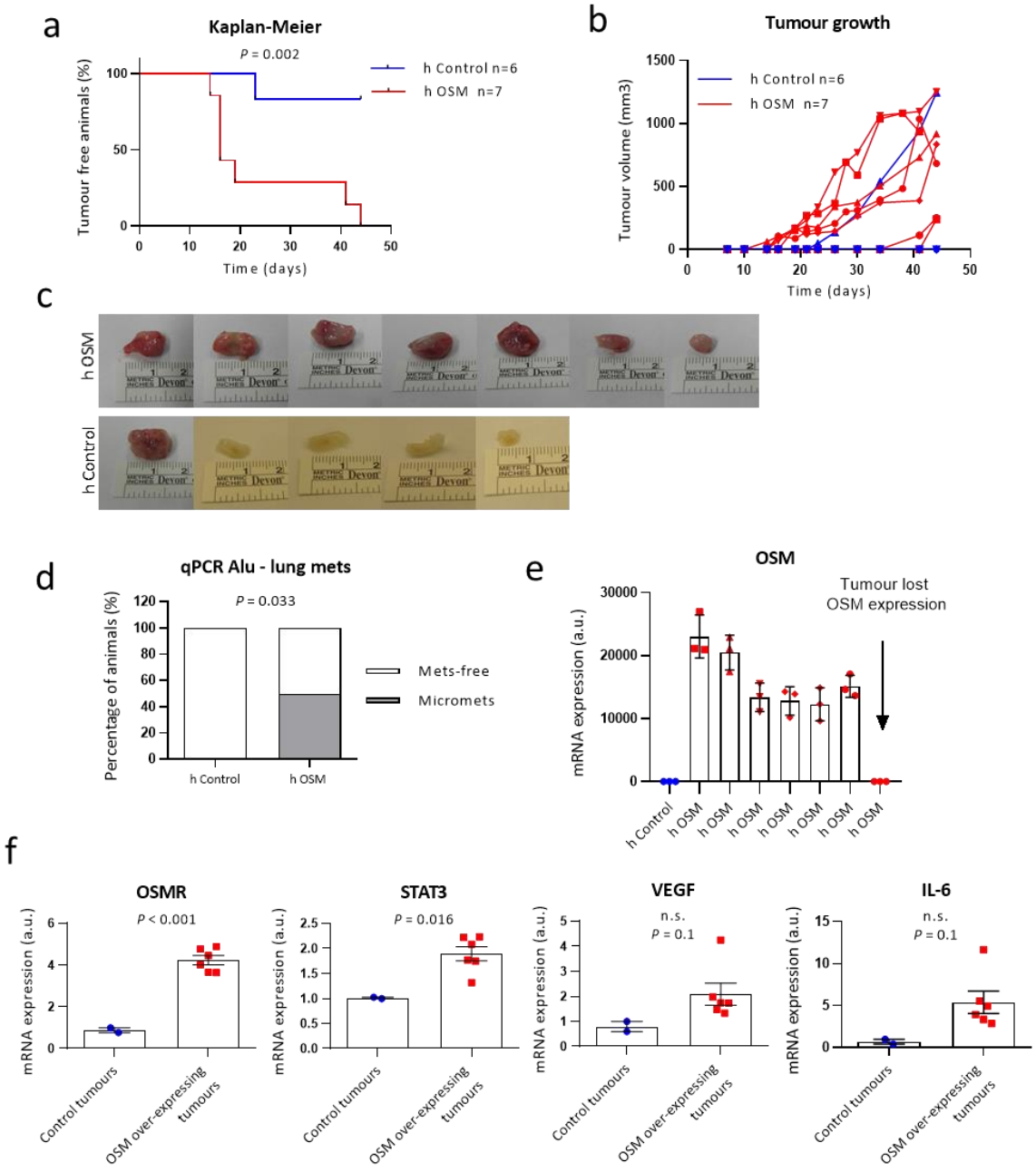

Fig. 3.1.10: OSM signalling promotes tumour progression in orthotopic xenografts in nude mice. MDA-MB-231 hControl and hOSM cells were injected in the 4th mammary gland of nude mice. **a)** Kaplan-Meier curve representing percentage of tumour free animals with time. P value was obtained using the Mantel-Cox test. **b)** Growth curve of individual tumours from the different experimental groups represented in different colours. **c)** Pictures of tumours and mammary glands of the different experimental groups after dissection at day 43. **d)** Percentage of animals with lung micrometastases assessed as presence of human DNA in murine lungs analysed by qPCR of human Alu sequences. P value was calculated using the chi-square test. **e)** OSM mRNA levels in tumours from the different experimental groups. Graph bars represent mean of technical replicates ± SD. **f)** mRNA levels of OSMR and its downstream targets in tumours with OSM overexpression and control tumours. Graphs represent mean ± SEM. n.s. non-significant. P values were obtained using the unpaired two-tailed t test.

3.1.11 Depletion of OSMR in the MMTV-PyMT breast cancer mouse model halts tumour progression.

Xenografts in nude mice are valuable models to study breast cancer progression, but an important handicap associated with those models is their immune system deficiency, an important factor in cancer progression. One of the aims of this thesis was to study the interaction of cancer cells with the tumour microenvironment, and the *in vitro* data suggested that tumour cells depend on paracrine signalling to activate the OSMR pathway. Therefore, it was important to study the role of OSM:OSMR signalling in a more physiological context where tumour cells could interact with an intact tumour microenvironment.

The MMTV-PyMT (mouse mammary tumour virus-polyoma middle tumour-antigen) mice express the Polyoma Virus middle T antigen under the direction of the mouse mammary tumour virus promoter/enhancer resulting in spontaneous generation of tumours in the female mammary glands starting at 7 weeks of age. By week 14, most mammary glands present fully developed carcinomas and approximately 50% of the animals have visible metastasis in the lungs. Tumours start as ER+ and with time they tend to lose ER expression becoming ER-[238]. This genetic mice model was first described by Guy et al (1992)[231] and it has been since then a widely used model of breast cancer development and metastasis[238]. MMTV-PyMT mice (provided by Dr. Eva Suarez, CNIO Madrid) were crossed with OSMR KO mice (provided by Prof. Nicholas Coleman, University of Cambridge, UK) in the animal facilities of Biodonostia Health Research Institute to check for the role of OSMR signalling in breast cancer progression, as described by the experimental scheme in Fig. 3.1.11a. As seen in Fig. 3.1.11b,c, depletion of OSMR in the MMTV-PyMT mice resulted in delayed tumour onset ($P < 0.001$). While most MMTV-PyMT:OSMR WT and HET animals presented palpable tumours by week 7, MMTV-PyMT:OSMR KO animals only started to have detectable tumours around week 9 of age ($P < 0.001$). OSMR deficient mice also generated smaller tumours, as seen by the reduced tumour growth (Fig. 3.1.11d), and tumour burden at the culling point ($P < 0.001$, Fig. 3.1.11e) compared to the control mice. OSMR depletion in the MMTV-PyMT:OSMR KO mice was confirmed by Western blot of tumour lysates ($P < 0.001$, Fig. 3.1.11f,g). Analysis of earlier time points revealed that by week 9, MMTV-

PyMT:OSMR KO animals had smaller lesions in the mammary gland compared to MMTV-PyMT:OSMR WT determined by wholemount staining of mammary glands (Fig. 3.1.11h).

This transgenic model progresses through four distinctly identifiable stages of tumour progression (from benign or *in situ* lesions to invasive carcinomas) and mimics well the progression of human breast cancer[238]. Histological analysis performed by Prof. Juana Flores in UCM Madrid, revealed that most of the animals in the WT group presented fully developed late stage carcinomas while only 50% of the tumours in the MMTV-PyMT:OSMR KO group presented this phenotype, with an important 40% of animals still presenting adenomas ($P = 0.007$, Fig. 3.1.12a,b). Immunohistochemical analysis of markers of proliferation and apoptosis (Ki67 and Caspase 3, respectively) showed that although MMTV-PyMT:OSMR KO tumours seemed to have slightly higher levels of proliferation (not statistically significant) compared to the WT control tumours, they also presented higher levels of apoptosis measured by active caspase 3 ($P = 0.01$, Fig. 3.1.12c). These results suggest that the increased cell death within those tumours could explain the smaller tumour volume present in this group (Fig. 3.1.11d). Protein analysis of tumours excised from animals at 14 weeks of age revealed that MMTV-PyMT:OSMR WT animals had higher levels of FN in the tumours, EMT[239], and fibroblast activation marker[240] ($P < 0.001$, Fig. 3.1.12d), suggesting that OSMR signalling could be contributing to EMT and also playing a role in shaping the tumour microenvironment.

MMTV-PyMT model is a very well characterised model of breast cancer progression and metastasis[238]. As previous data in breast cancer xenografts (Fig. 3.1.10d) suggested that OSM:OSMR signalling could contribute to metastasis, MMTV-PyMT:OSMR KO mice were hypothesised to have less metastasis in the lungs than the control mice. As seen in Fig. 3.1.13a, around 40% of MMTV-PyMT:OSMR WT animals presented visible lung metastases and around 40% more presented micrometastases detected by haematoxylin and eosin (H&E) staining (Fig. 3.1.13b). Strikingly, out of 15 animals in the OSMR KO group, none presented visible metastasis, and only around 20% of animals presented micrometastases detected by H&E analysis ($P < 0.001$), revealing a strong contribution of OSMR signalling for metastasis development in the MMTV-PyMT mouse model.

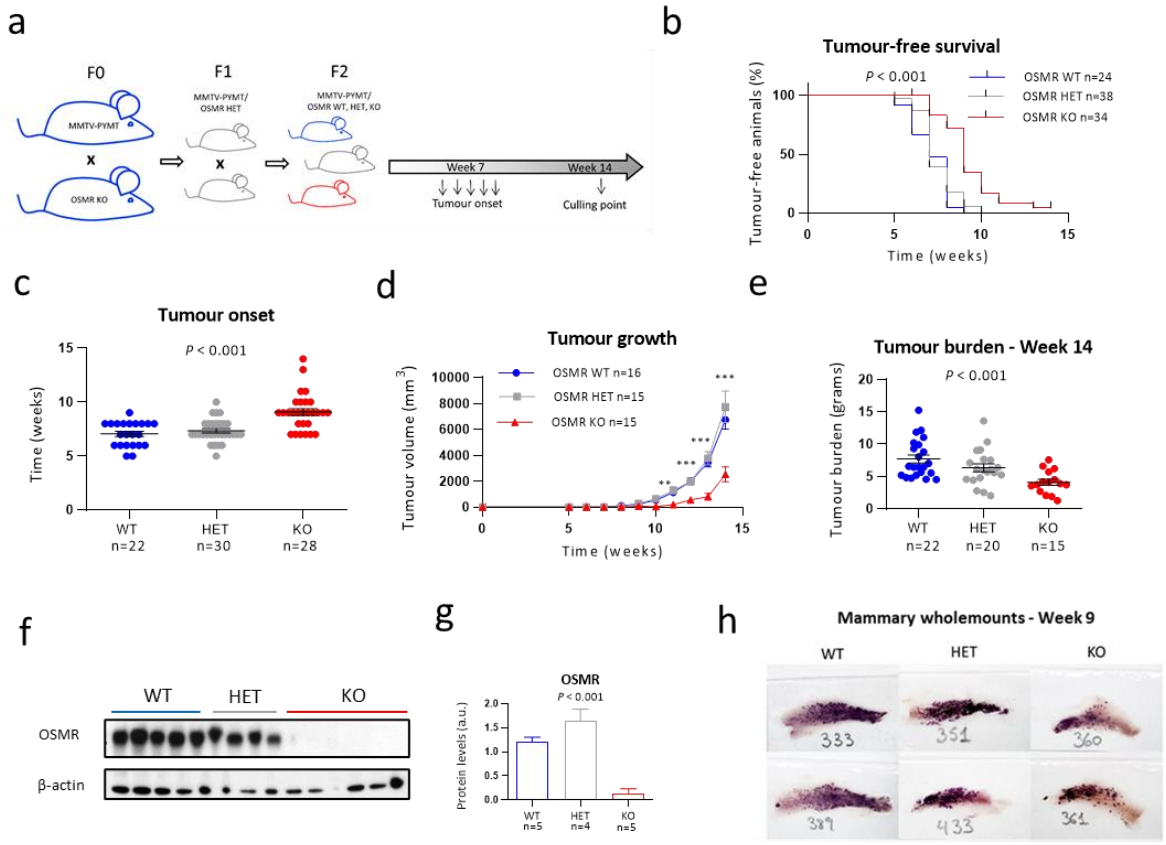

Fig. 3.1.11: Depletion of OSMR in the breast cancer mouse model MMTV-PyMT halts tumour progression.

a) Experimental setup of the *in vivo* experiment designed to assess the importance of OSMR signalling for disease progression in the MMTV-PyMT mouse model. **b-e)** Kaplan-Meier curves for tumour-free survival **(b)**, tumour onset **(c),** tumour growth **(d)** and final tumour burden **(e)** in MMTV-PyMT:OSMR wild-type (WT), MMTV-PyMT:OSMR heterozygous (HET), and MMTV-PyMT:OSMR knockout (KO) mice. **f-g)** Western blot **(f)** and densitometric analysis **(g)** of OSMR protein levels in tumours at culling point from the differential experimental groups. **h)** Representative pictures of whole mount staining of mammary glands at week 9. In **(b)** P values were calculated using the Mantel-Cox test; in **c,e,g)** P values were determined using one-way ANOVA test; in **(d)** P values were determined using unpaired two-tailed t test. Unless otherwise specified, graphs represent mean ± SEM, ** P < 0.01; *** P < 0.001.

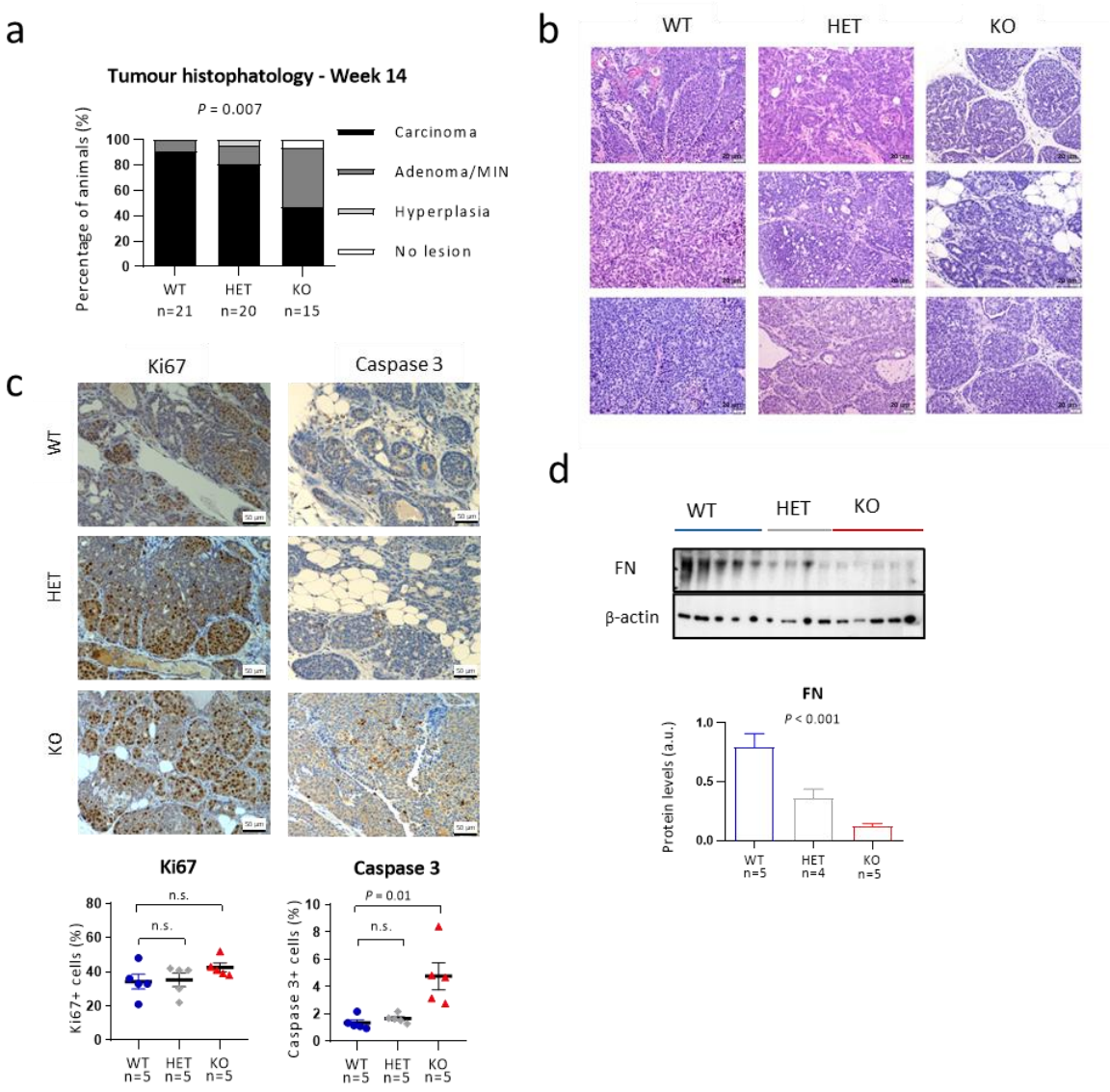

Fig. 3.1.12: Depletion of OSMR in the MMTV-PyMT mouse model changes primary tumour characteristics.

a) Histopathological analysis of tumours at culling point (week 14) from the different experimental groups of Fig. 3.1.11. Graph represents percentage of mice bearing carcinomas, adenomas, hyperplasia and no lesions in mammary glands. P value was determined comparing number of mice with malignant (carcinoma) vs non-malignant phenotypes (adenoma, hyperplasia) and no lesions using Chi-square test. **b-c)** representative pictures of histopathological analysis **(b)** and immunohistochemistry (IHC) staining (upper panels) and quantification (lower panels) of Ki67 and active caspase 3 (proliferation and apoptosis markers, respectively) **(c)** in tumours at culling point of the different experimental groups. Quantification was performed by manual counting of the percentage of positive cells per picture in a total of 8 pictures per tumour and 5 animals per group. P values between the different groups were calculated using unpaired two-tailed t test. **d)** Western blot (upper panel) and densitometry analysis (lower panel) of fibronectin protein levels in tumours at culling point from animals of the different genotypes. P value was determined by the one-way ANOVA test. Unless otherwise specified, graphs represent mean ± SEM. n.s. non-significant.

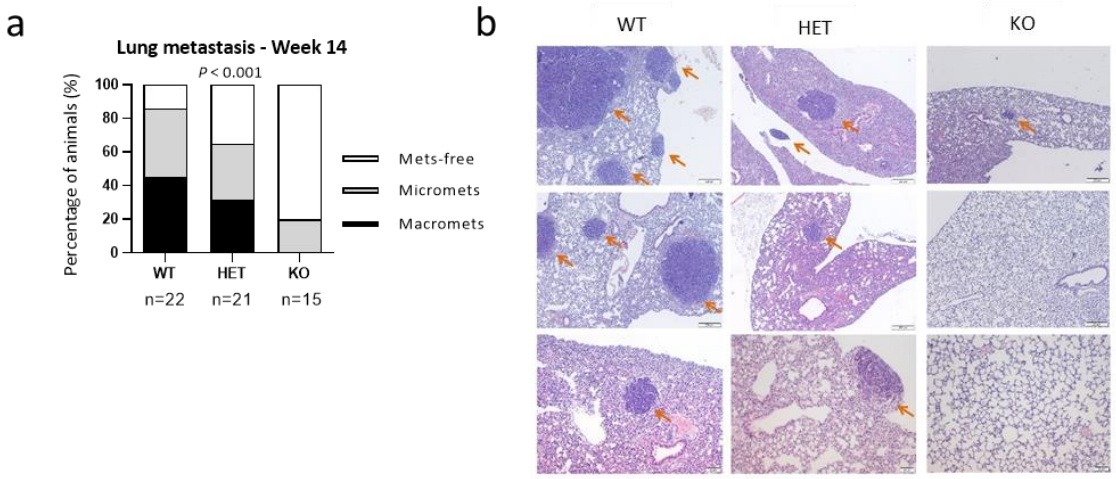

Fig. 3.1.13: Depletion of OSMR in the MMTV-PyMT mouse model decreases lung metastatic burden.

a) Percentage of animals with lung metastases at 14 weeks of age from the differential experimental groups of Fig. 3.1.11. Lung tumour masses were classified as macrometastases when they were visible by the naked eye at dissection and as micrometastases when they were only detectable by hematoxylin and eosin staining. P value was determined comparing number of animals with metastasis (macro and micro) vs number of animals without metastasis using Chi-square test. **b)** Representative pictures of lungs at week 14 in OSMR WT, HET and KO animals.

3.2 OSM:OSMR signalling in the tumour microenvironment.

3.2.1 Summary

In this section, objective 3 was addressed with the aim of investigating the expression and the role of OSM:OSMR in the tumour microenvironment.

OSM:OSMR expression in the tumour microenvironment was analysed in publicly available datasets of human breast, colon, ovarian cancer samples and in scRNA-seq data and RNA from FACS sorted populations of murine tumours. Murine orthotopic tumours in syngeneic mice were used to determine the role of microenvironment derived OSM:OSMR signalling in BC progression *in vivo*. *In vitro* cultures of fibroblasts, CAFs and myeloid cells were used to explore the effects of OSM:OSMR signalling in cells from the TME. The contribution of OSM activated CAFs to tumour progression was tested using xenografts.

3.2.2 OSM:OSMR signalling is increased in human tumour stroma.

NCBI Gene Expression Omnibus (GEO) dataset (GSE10797), that included mRNA expression data from laser captured cancer epithelial and cancer stroma, was used to understand the status of OSM:OSMR signalling in the tumour microenvironment and how it compared to the tumour cells. The analysis revealed that OSM and OSMR were elevated in the stroma compared to the tumour cell compartment in breast cancer ($P = 0.012$ and $P = 0.036$, respectively, Fig. 3.2.1a). Further analysis of GEO datasets, with matched samples of normal and cancer stroma taken from the same patient through tissue laser microdissection, revealed that OSM and OSMR levels were increased in cancer stroma compared to normal stroma in breast, colorectal and ovarian cancer (P values shown in Fig. 3.2.1b-d), suggesting that this signalling axis could have a relevant role in the tumour microenvironment.

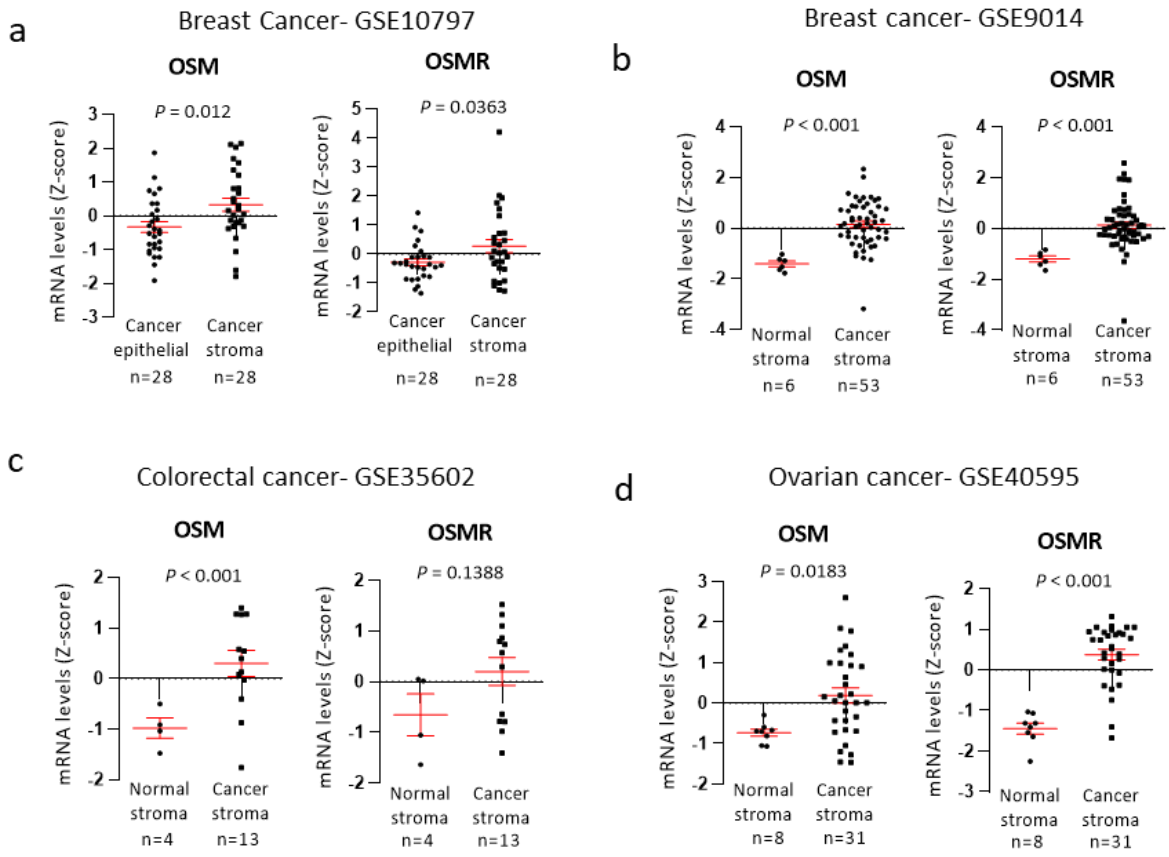

Fig. 3.2.1: OSM:OSMR signalling is increased in the tumour stroma (TME) of breast cancer and other tumour types.
a-d) OSM and OSMR mRNA expression in paired cancer epithelial vs. cancer stroma of breast cancer **(a)** and normal stroma vs. cancer stroma of breast **(b)**, colorectal **(c)** and ovarian cancer **(d)**. Data were downloaded from GEO datasets (GSE10797 and GSE9014, GSE35602, and GSE40595). P values were calculated using the unpaired two-tailed t test and graphs represent mean of mRNA Z-score ± SEM.

3.2.3 Single cell RNA-seq reveals that OSM:OSMR signalling is paracrine within the tumour and its pattern of expression differs from IL-6 family.

Data from section 3.1 indicated that cancer cells do not rely on OSM autocrine signalling. A collaboration with Dr. David Gallego Ortega (Garvan institute, Sydney) was established to characterise OSM and OSMR expression in the different cell tumour populations. His laboratory performed single cell RNA-seq (scRNA-seq) on MMTV-PyMT tumours (week 14) and the associated bioinformatic analysis presented in this thesis. Of 9,636 cells, 18 clusters were obtained and represented in Fig. 3.2.2a. Expression analysis of OSM and OSMR in the different cell subpopulations indicated that OSM was mainly expressed in clusters 7 and 15, defined by high expression of myeloid markers. On the other hand, OSMR was strongly

expressed in clusters 2, 3, 9 and 11, associated with cancer cells markers, and in clusters 5, 6 and 10, corresponding to classical markers of fibroblasts. These data together suggest that OSM is almost exclusively expressed by immune cells, mainly the myeloid subpopulation, and that OSMR is found in the majority of cancer cells and fibroblasts. (Fig. 3.2.2b,c). These results strongly support the existence of a paracrine signalling between immune system, cancer cells and fibroblasts. Strikingly, the pattern of expression of OSM and OSMR greatly differs from other members of the IL-6 family suggesting that OSM:OSMR could have unique functions independent from other members of the family. IL-6, as previously shown to be a downstream target of OSMR activation (Fig. 3.1.6a), was found mainly expressed in clusters 6 and 10 corresponding to fibroblasts (Fig. 3.2.2b,c), both with high expression of OSMR suggesting that maybe this pathway could be involved in inducing IL-6 levels in CAFs. Il6st (corresponding to the *GP130* human gene, coding for the common receptor subunit in the IL-6 family) was widely distributed while LIF, contrary to OSM, was mainly produced by cancer cells (clusters 2 and 3).

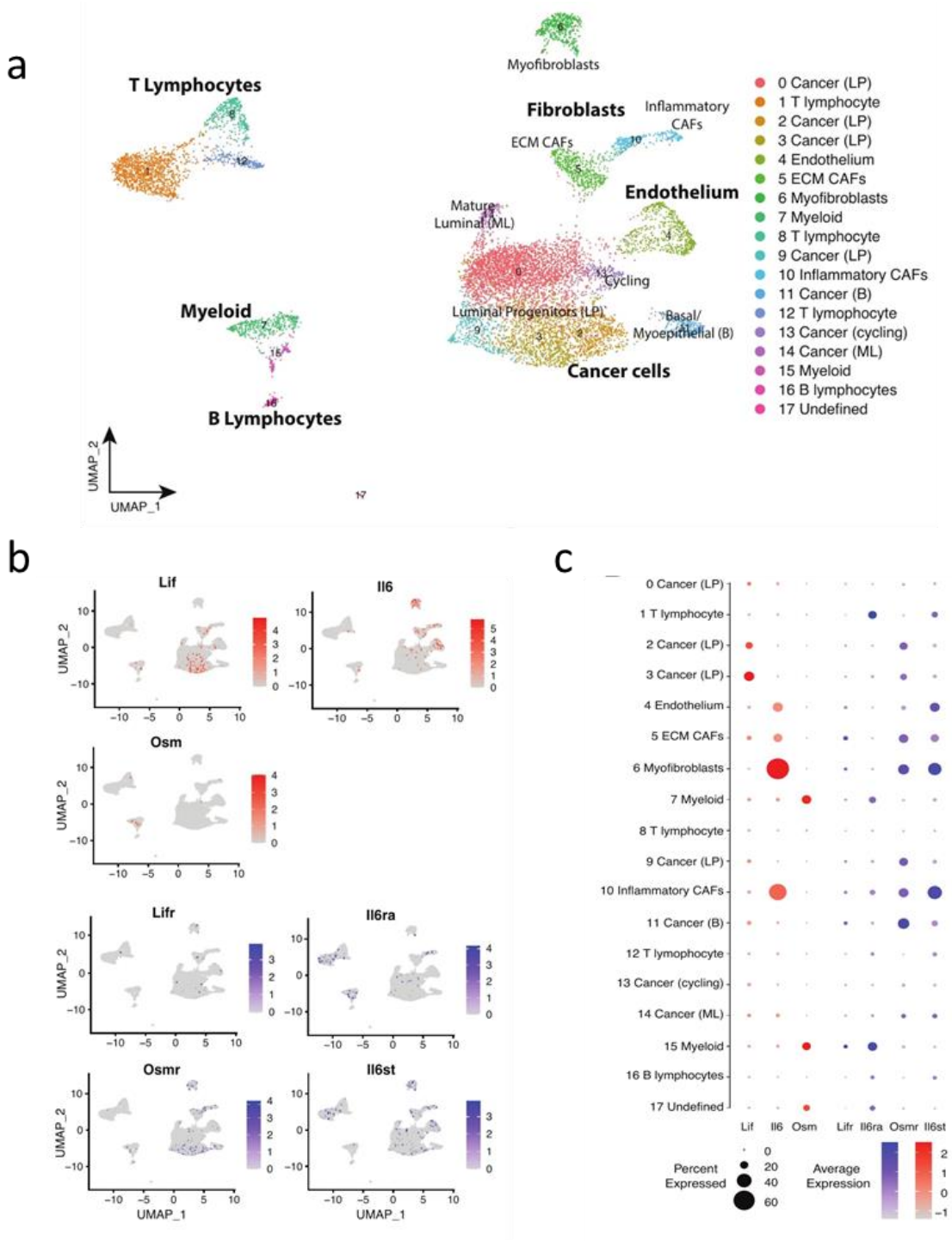

Fig. 3.2.2: The OSM:OSMR signalling module exhibits a distinct microenvironment-restricted expression.

a) Single cell RNA-seq (scRNA seq) Uniform Manifold Approximation and Projection (UMAP) plot showing cell clusters defined in each of the main cell lineages. Far right column depicts the main cell lineage of origin for each cluster, showing 7 clusters of epithelial origin, 6 immune and 4 stromal. LP: luminal progenitors, ECM: extracellular matrix, B: basal, ML: mature luminal. **b)** Feature UMAP plots showing the expression of the indicated genes in each of the main cell clusters. **c)** Dot plot representing the expression level (red or blue jet) and the number of expressing cells (dot size) of the indicated genes in each cluster.

3.2.4 OSM is mostly expressed by myeloid cells while OSMR is present in tumour cells and fibroblasts.

To validate the scRNA-seq data observations with other techniques, FACS sorting of tumours generated by orthotopic injections of TS1 cells in syngeneic mice[241], and consequent qPCR analysis of each individual sorted population were performed. TS1 tumours were initially separated into cancer (EPCAM+), endothelial (CD31+), immune (CD45+) cells and fibroblasts (negative selection), as described by the experiment scheme in Fig. 3.2.3a,b. In total accordance with scRNA-seq data, OSMR was mainly found expressed in fibroblasts, endothelial and cancer cells while OSM was exclusively present in the immune population. To further explore which immune population expressed higher levels of OSM, a second FACS sorting was performed separating the immune cells into myeloid (CD11b+), T (CD3+) cells and remaining immune population (Fig 3.2.3a). Again, OSM was confirmed to be expressed mainly by the myeloid population (Fig. 3.2.3c). This paracrine pattern was validated in FACS sorted tumours from the MMTV-PyMT mouse model using RNA kindly provided by Dr. Fernando Calvo[242]. Briefly, tumours were separated into cancer (EPCAM+), endothelial (CD31+), immune (CD45+) cells, fibroblasts (FAP+) and remaining populations (negative selection). Again, OSMR was mainly found in tumour cells and fibroblasts while OSM was detected in immune cells (Fig. 3.2.3d).

These data together strongly confirmed a unique microenvironment expression pattern for OSM and OSMR and pointed to the existence of OSM:OSMR paracrine signalling between myeloid cells, fibroblasts, and cancer cells.

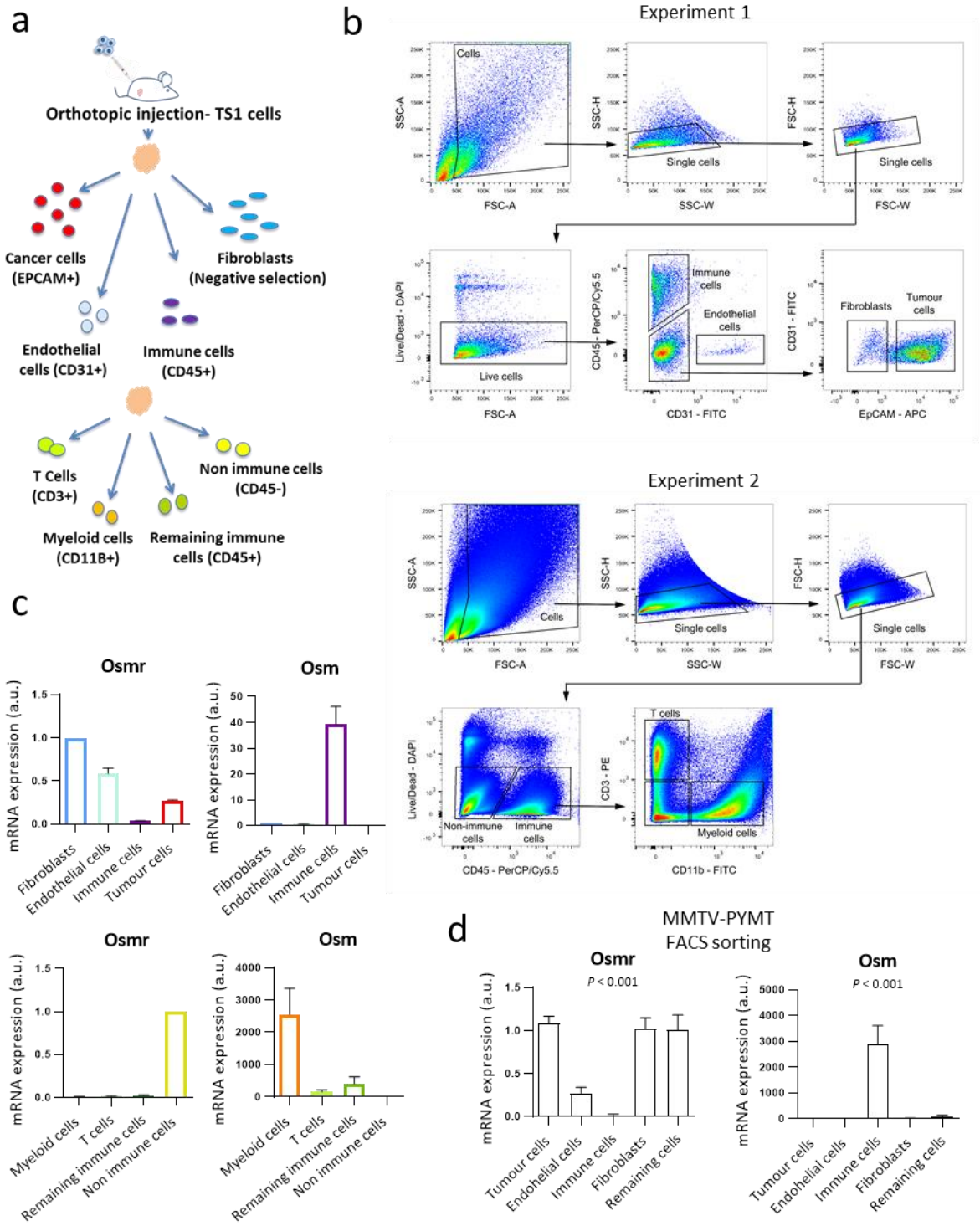

Fig. 3.2.3: OSM is mostly expressed by myeloid cells while OSMR is present in tumour cells and fibroblasts.

a-b) Schematic representation of FACS sorting **(a)** and gating strategy **(b)** of TS1 orthotopic tumours. The two different experiments were performed independently, each one using 4 tumours from individual animals. **c-d)** Osm and Osmr mRNA expression levels analysed by RT-qPCR of FACS sorted TS1 orthotopic **(c)** or MMTV-PyMT FACS sorted tumours as described in Ferrari *et al* (2019)[242] **(d)**. Graphs represent mean ± SEM of 3 technical replicates **(c)** or of 6 different tumours **(d)**. P values were determined using one-way ANOVA test.

3.2.5 OSMR expression correlates with fibroblast content while OSM expression associates with myeloid cell infiltration in human breast cancer samples.

Correlation of OSM and OSMR expression with tumour purity and TME content in clinical samples was explored using TIMER and xCell webtools, digital platforms designed to infer stromal cell type content based on gene signatures. Data analysis from TIMER[215] revealed that OSMR expression was strongly associated with the presence of cancer associated fibroblasts in the tumour while OSM was correlated with myeloid cell infiltration, mainly macrophages and neutrophils (correlation coefficients and P values shown in Fig. 3.2.4a). Both OSM and OSMR inversely correlated with tumour purity meaning that OSM and OSMR expression positively correlates with higher TME content of the tumour, supporting the hypothesis that OSM and OSMR are mainly stroma expressed molecules (Fig. 3.2.4a). Data obtained from xCell webtool[216] revealed that OSM was associated with enrichment of macrophages M2 and common myeloid progenitors, and that OSMR was associated with fibroblasts ($P < 0.001$ in all graphs, Fig. 3.2.4b), again suggesting a possible role of OSM:OSMR in shaping the TME in breast cancer.

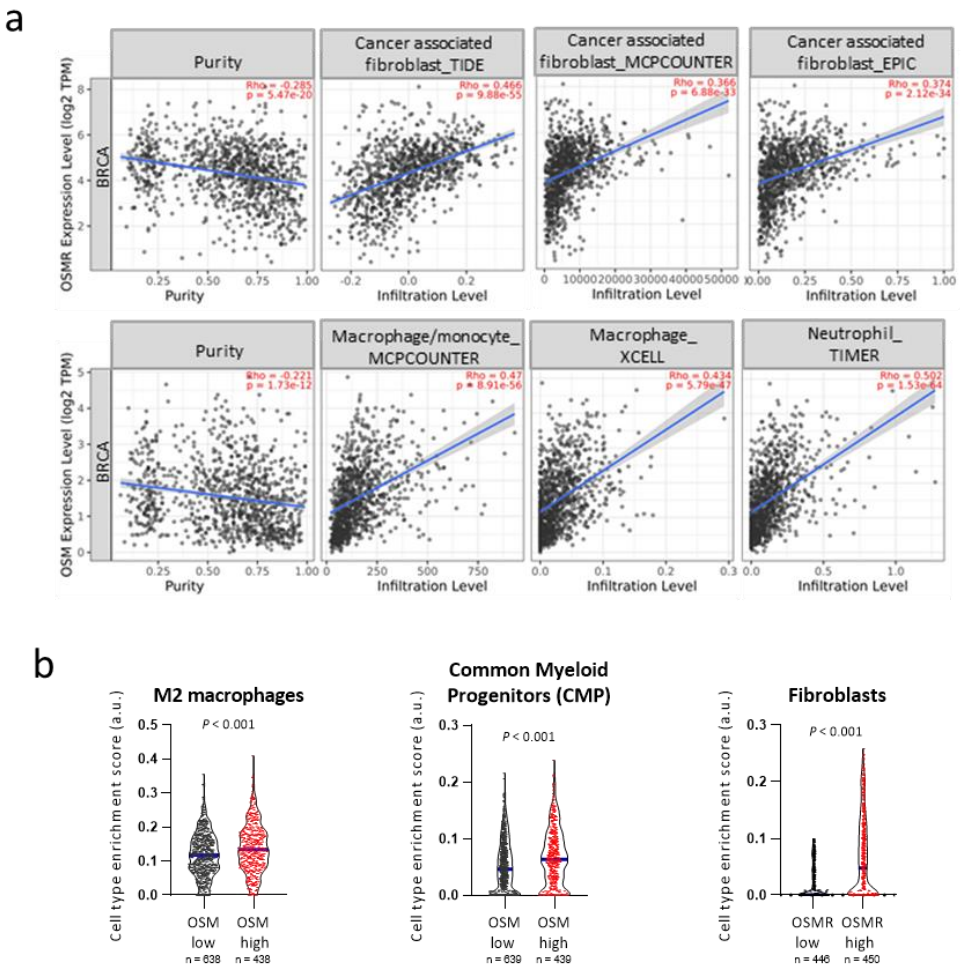

Fig. 3.2.4: OSMR expression is correlated with fibroblast content while OSM is associated with myeloid infiltration in breast cancer.
a) Correlation of OSMR (upper panels) and OSM (lower panels) expression with tumour purity and infiltration level of indicated cell types in breast cancer samples. Data were downloaded from TIMER web platform. Spearman correlation coefficients and P values are shown. **b)** Truncated violin plots showing cell type enrichment of the indicated populations in breast tumours according to high (top quartile) or low (lower quartile) OSM or OSMR expression. Data were obtained using xCell web resource on 1809 breast cancer samples from Kaplan-Meier Plotter website. P values were determined using Mann–Whitney's test.

3.2.6 Human breast cancer cells, fibroblasts and myeloid-derived cell lines maintain the expression pattern of the OSM:OSMR pathway observed in tumours.

scRNA-seq and FACS data revealed that fibroblasts and cancer cells express high levels of the receptor OSMR while the ligand OSM is mainly found in myeloid cells. Moreover, OSMR and OSM levels correlate with fibroblast and myeloid content, respectively, in the TME of clinical samples of breast cancer. Multiple human *in vitro* models were characterised to

further explore the OSM:OSMR expression in cancer cells, fibroblasts, and myeloid cells and to select relevant *in vitro* models to study the role of OSM:OSMR in modulating the communication between those cells. Gene expression was analysed in a breast cancer cell panel of 17 cell lines (Table 2.2, chapter 2). Human mammary fibroblasts, derived from reduction mammoplasty and breast cancer surgeries, were kindly provided by Dr. Paloma Bragado (UCM, Madrid), and used as *in vitro* models of normal and cancer associated fibroblasts (CAFs), respectively. The HL-60 cell line, a promyeloblastic cell line that can be differentiated to macrophages upon addition of TPA, was used as an *in vitro* model of human myeloid cells. RT-qPCR analysis of breast cancer cells and fibroblasts revealed that both cell types expressed OSMR, and that fibroblasts expressed higher levels of the receptor (P =0.001, Fig. 3.2.5a). OSM was detected at late cycles (32+) in both cell types and therefore considered not expressed (data not shown). Both OSM and OSMR had different pattern of expression from other cytokines/receptors of the IL-6 family as seen in Fig. 3.2.5a. IL-6 and LIF were expressed in fibroblasts and cancer cells (contrary to OSM), while IL6R seemed to be increased in breast cancer cells compared to fibroblasts (contrary to OSMR). In agreement with previous data, HL-60 cell line expressed high levels of OSM, both as undifferentiated monocytes or differentiated to macrophages (with TPA) and presented undetectable levels of OSMR using MDA-MB-231 cell line as positive control (P = 0.006 and P = 0.005, respectively, Fig. 3.2.5b). Both LIFR and IL-6 were not expressed in HL-60, and LIF was only found in TPA differentiated macrophages, but on the contrary, these cells expressed high levels of IL6R. Analysis of publicly available mRNA data from a variety of human cell lines of multiple origins (Human Protein Atlas)[213] further confirmed that OSMR was mainly found in cancer cell lines from multiple anatomical sites and fibroblasts, while OSM was exclusively present in cells from the immune system including myeloid and lymphoid cells (Fig. 3.2.5c). These data indicate that the *in vitro* models analysed conserve the OSM and OSMR expression pattern and that they are adequate models to further study OSM:OSMR interactions *in vitro* and *in vivo*.

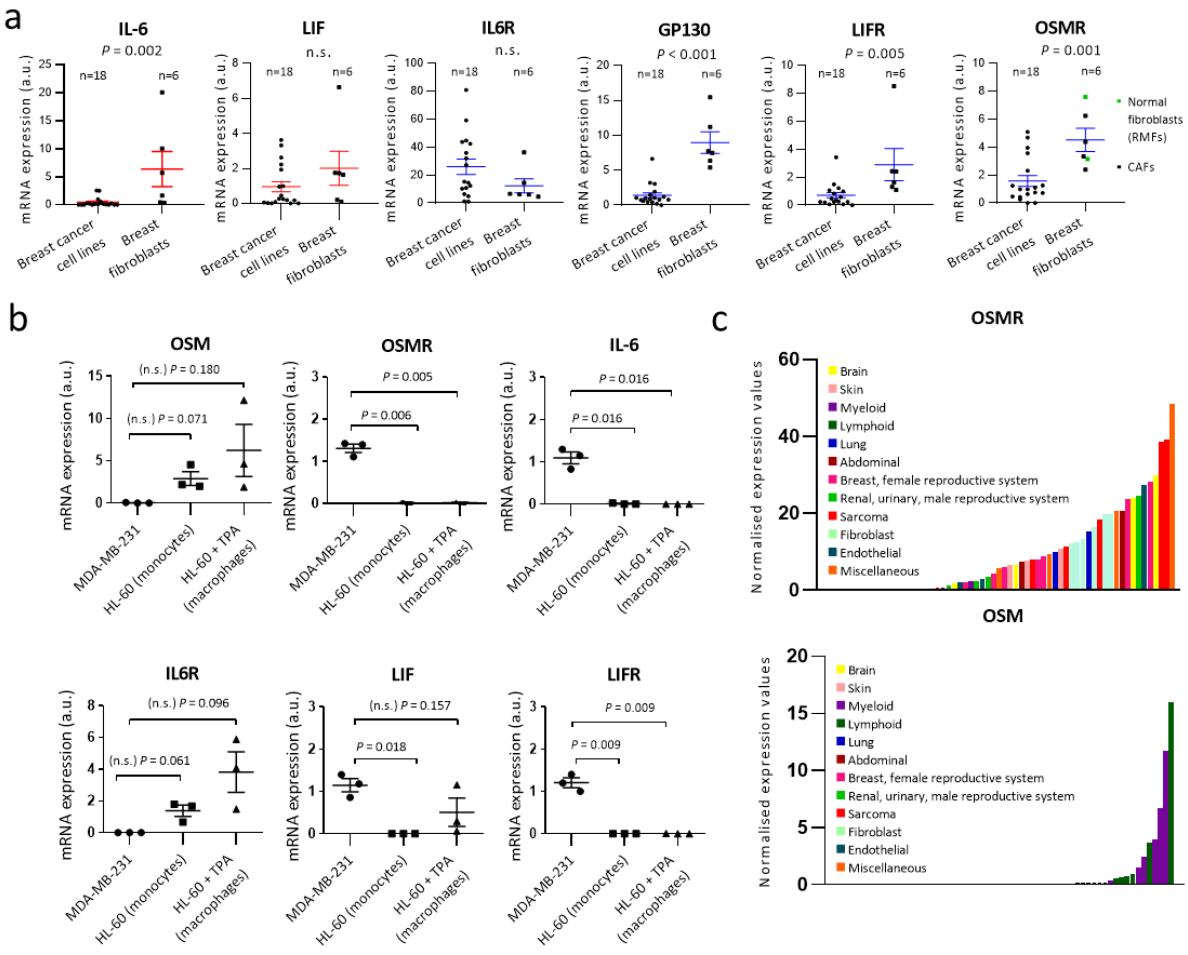

Fig. 3.2.5: Human breast cancer cells, fibroblasts and myeloid-derived cell lines are adequate models of OSM:OSMR signalling *in vitro* and maintain the expression pattern of the OSMR pathway observed in human and murine tumours.
a) mRNA expression levels of the indicated IL-6 family members and associated receptors analysed by RT-qPCR in a panel of breast cancer cell lines and immortalized fibroblasts. In the OSMR graph (right panel), green and black dots represent normal mammary fibroblasts and CAFs, respectively. **b)** mRNA expression levels of the indicated IL-6 family members and associated receptors analysed by RT-qPCR in MDA-MB-231 breast cancer cells and undifferentiated or TPA-differentiated HL-60 cells. **a,b)** Graphs represent mean ± SEM of 3 independent experiments. P values were calculated using the two-tailed unpaired t test. n.s. non-significant. **c)** OSM and OSMR mRNA relative values in a panel of human cell lines from multiple anatomical sites. Data were downloaded from Human Protein Atlas.

3.2.7 OSM:OSMR signalling in the tumour microenvironment contributes to tumour progression.

Clinical data revealed that OSM and OSMR were associated with poor prognosis and that both were elevated in cancer stroma suggesting a potential role of OSM:OSMR signalling in the TME and consequent contribution to cancer progression. To test this hypothesis, an

in vivo experimental setting was established to assess the exclusive contribution of OSM:OSMR signalling in the tumour microenvironment by injecting TS1 cells into syngeneic OSMR WT and KO mice. TS1 cells were treated with exogenous OSM to assess its capacity to respond to OSMR pathway activation. As seen in Fig. 3.2.6a, TS1 cells express OSMR, and upon exposure to exogenous OSM, an induction of OSMR protein levels and an increased phosphorylation of STAT3 were observed, indicating that these cells are susceptible to OSMR pathway activation by OSM. Syngeneic FVB OSMR WT or KO mice were used as recipients of TS1 orthotopic injections. This model provided an experimental setting where only the cells present in the tumour microenvironment lacked OSMR expression, while cancer cells expressed OSMR and, therefore, it was possible to assess if OSMR signalling in the TME was contributing to breast cancer progression (Fig. 3.2.6b). As demonstrated in Fig. 3.2.6c, the animals that lacked OSMR expression in the TME presented delayed tumour onset ($P = 0.002$). Tumour growth was significantly reduced (P values shown in Fig. 3.2.6d), and tumours exhibited a decreased weight ($P = 0.002$) and volume ($P = 0.022$) at the culling point, as seen in two independent experiments (Fig. 3.2.6e). Western blot analysis of the TS1 tumours showed reduced level of OSMR compared to WT controls due to the lack of the receptor in cells from the tumour microenvironment. This decrease was surprisingly high, which suggested that, in this context, OSMR is either highly expressed in the TME which could support the clinical data observations presented in Fig. 3.2.1, or that these tumours presented a high content of TME, or that the lack of OSMR in the TME somehow downregulated OSMR expression in cancer cells. Further analysis would need to be performed to answer this question.

These data together lead to the conclusion that lack of OSMR in the TME halts tumour progression, confirming its fundamental role in the breast TME.

One of the limitations associated with the OSMR KO mouse model is the fact that all cell types in the TME lack OSMR, being difficult to identify which specific populations of cells benefit from OSM:OSMR signalling in BC. The next step of this work aimed to identify which cells in the TME were contributing to the phenotype of the tumour model in OSMR KO mice and identify the mechanisms leading to cancer progression.

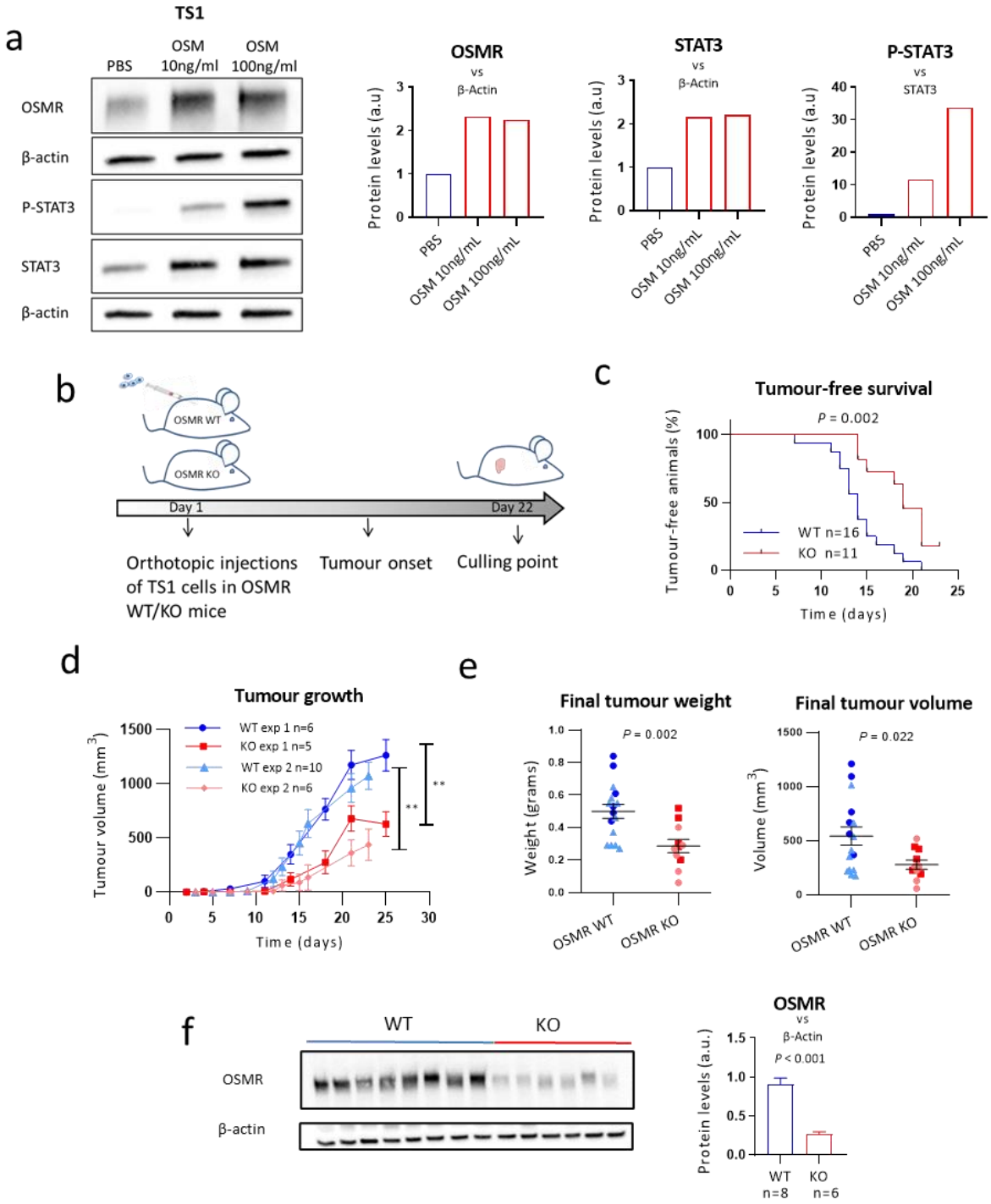

Fig. 3.2.6: OSM:OSMR signalling in the tumour microenvironment contributes to tumour progression.

a) Western blot (left panel) and densitometric analysis (right panels) of OSMR, P-STAT3 and STAT3 protein levels in TS1 cells treated with 10 and 100 ng/ml of recombinant OSM for 24h.

b) Experimental setup of the *in vivo* experiment designed to assess the importance of OSMR signalling in the tumour microenvironment, in which TS1 cells were orthotopically injected into the mammary gland of OSMR WT and KO mice. **c-e)** Kaplan-Meier curves for tumour-free survival **(c)**, tumour growth **(d)** and final tumour volume and weight after dissection **(e)** of orthotopic tumours described in **(b)**. Two independent experiments were performed, and the results were combined in **(c). f)** Western blot (left panel) and densitometric analysis (right panel) of OSMR protein levels in

tumours from OSMR WT or KO animals injected orthotopically with TS1 cells (exp 2 from **(d)**). **c)** P value was calculated using the Mantel-Cox test. **d,e,f)** P values were determined using the unpaired two-tailed t test. Unless otherwise specified graphs represent mean ± SEM. ** P < 0.01.

3.2.8 Exogenous OSM activates OSMR pathway in fibroblasts.

Fibroblasts are an important population in the tumour microenvironment and fibroblasts activation has been demonstrated to be intimately linked to cancer progression[64]. RT-qPCR analysis of FACS sorted tumours, breast cancer cell lines and mammary fibroblasts revealed that fibroblasts expressed higher levels of OSMR compared to cancer cells (Fig. 3.2.3c and 3.2.5a). Taking all of this into account, fibroblasts were hypothesised to be the main TME cell type transducing OSM:OSMR signalling and actively contributing to breast cancer progression. We previously showed that both normal and cancer associated fibroblasts express similar levels of OSMR (Fig. 3.2.5a). Exogenous treatment of OSM further increased OSMR receptor in all tested fibroblasts in 3 independent experiments analysed by RT-qPCR (P values shown in Fig. 3.2.7a) and Western blot analysis also revealed that OSM treatment induced STAT3 phosphorylation in CAF-173 (Fig. 3.2.7b), again, confirming that OSM was activating the OSMR pathway in fibroblasts.

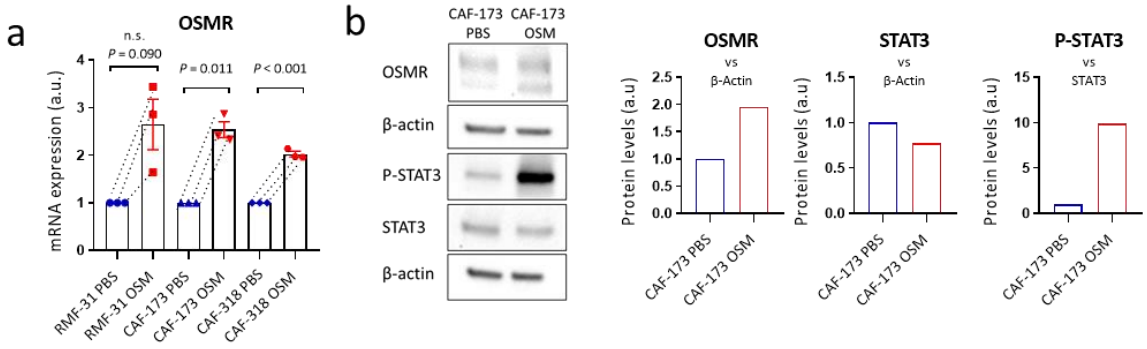

Fig. 3.2.7: Exogenous OSM activates OSMR pathway in fibroblasts.
a) OSMR mRNA expression levels analysed by RT-qPCR in 3D fibroblast spheres treated with OSM for 4 days. n=3 independent experiments. **b)** Western blot (left panel) and densitometric analysis (right panels) of OSMR, P-STAT3 and STAT3 protein levels in CAF-173 treated with OSM for 24 hours.

3.2.9 Exogenous OSM induces proliferation and contractility in CAFs but it does not affect normal fibroblasts.

Conversion of fibroblasts into an activated CAFs status is strongly associated with cancer progression[64]. When CAFs get activated they gain the ability to remodel the extracellular matrix, associated with the ability of cancer cells to escape the tumoral niche[243]. Collagen contraction assays are commonly used as a model to test the capacity of fibroblasts to contract the extracellular matrix, as collagen is the most abundant protein in the ECM[244,245]. This assay was used to test if OSMR pathway activation would convert fibroblasts into a more activated status. As seen in Fig. 3.2.8a, OSM did not affect contractility of normal skin and breast fibroblasts (HS27 and RMF-31, respectively) but, surprisingly, all tumour derived fibroblasts (CAF-200, CAF-173 and CAF-318) became more contractile upon addition of OSM, suggesting that OSMR activation was inducing an activated phenotype in CAFs (P values shown in Fig. 3.2.8a). Analysis of the area of fibroblast spheres growing in 3D in low-adherence plates showed that OSM induced sphere area (associated with cell proliferation) in all CAFs (P values shown in Fig. 3.2.8b). Again, surprisingly, OSM did not seem to affect fibroblast growth in normal breast fibroblasts (RMF-39 and RMF-31).

These data suggested that OSM has the capacity to reprogram CAFs into a more activated status while not affecting normal breast fibroblasts phenotypically.

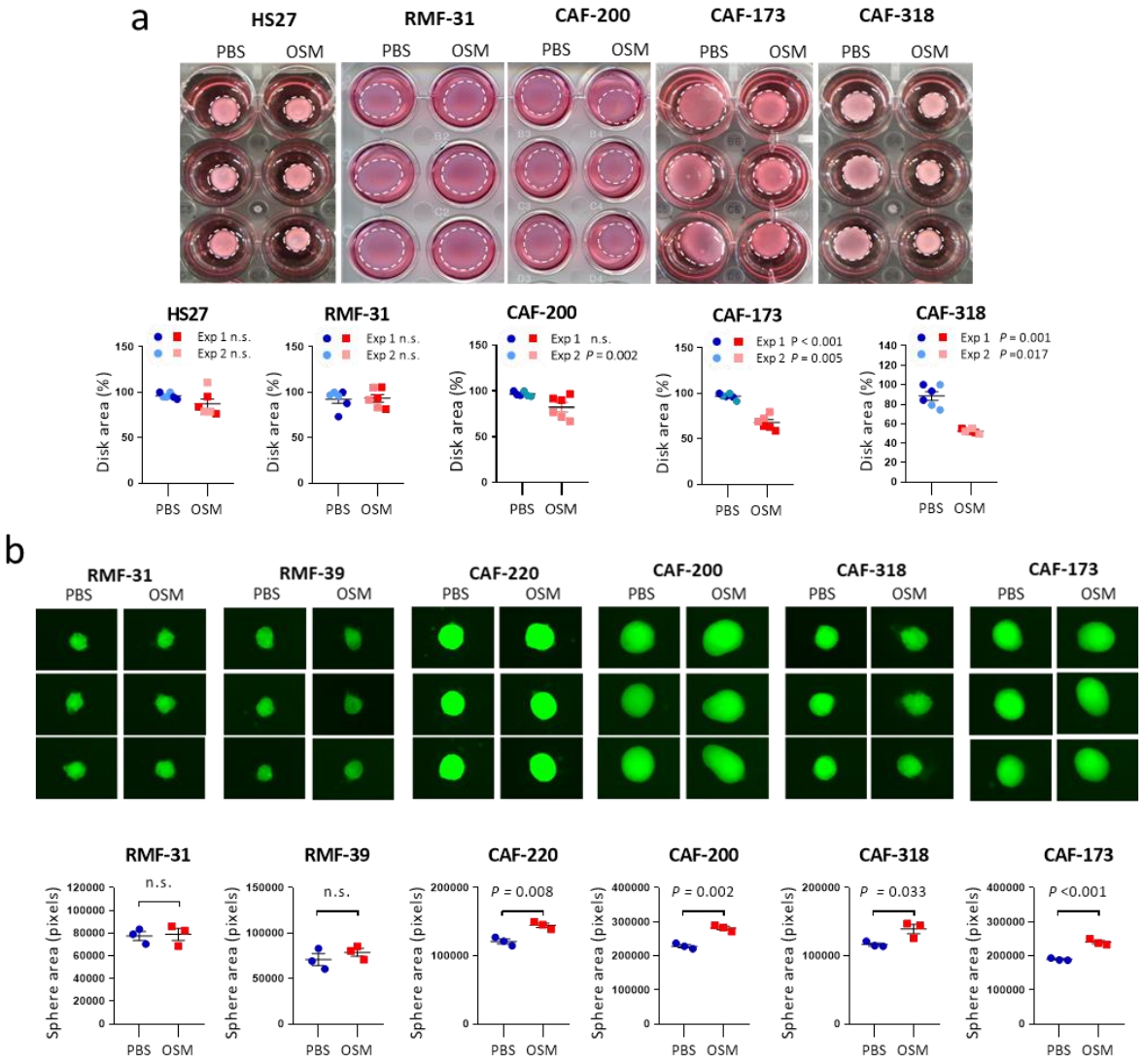

Fig. 3.2.8: Exogenous OSM induces contractility and proliferation in CAFs but it does not affect normal fibroblasts.

a) Representative pictures of collagen contraction assays (upper panels) and quantification of collagen disk areas (lower panels) of fibroblasts pre-treated in monolayer with PBS or OSM and seeded in collagen. Graphs represent mean ± SEM, and 2 independent experiments are plotted. **b)** Representative pictures (upper panels) and area quantification (lower panels) of 3D spheres proliferation assays of fibroblasts treated with PBS or OSM. Graphs represent mean ± SEM of a representative experiment out of 2 performed. P values were calculated using the unpaired two-tailed t test. n.s. non-significant.

3.2.10 Exogenous OSM induces activation markers in CAFs.

Fibroblasts are a very heterogeneous population within the tumour. One of the main challenges of studying CAFs is the lack of universal specific markers of fibroblast activation. Many studies have associated several markers with more activated status of fibroblasts

such as α-SMA, FAP, FN, PSTN, but different populations of CAFs present different markers[64]. Microarray analysis was performed on CAF-173 and CAF-318 treated with PBS or OSM to understand the gene expression changes caused by OSM treatment in CAFs. Using the list of CAF activation markers described in Sahai *et al* (2020)[64] (Supplementary Table 1), Andrea Abaurrea and Peio Azcoaga, members of the laboratory, performed gene set enrichment analysis (GSEA) to check if OSM was inducing this fibroblast activation markers signature in CAF-173 and CAF-318. As seen in Fig. 3.2.9a and b, OSM induced most of the CAF activation markers in both CAF-173 and CAF-318 ($P < 0.001$ in both CAFs). RT-qPCR analysis of some of the classical activation markers in both CAFs and normal fibroblasts (RMF-31) was performed to validate the microarray data. Again, in accordance with the phenotypic assays described in Fig. 3.2.8, OSM did not seem to induce any of the tested activation markers in normal fibroblasts. On the contrary, OSM induced PSTN, FAP, VEGF and IL-6 in CAF-173 (Fig. 3.2.9c). Despite showing enrichment of activated CAF's signature with OSM treatment by GSEA, CAF-318 did not show a significant mRNA increase of any the markers tested by qPCR analysis (Fig. 3.2.9c).

These data supported that OSM signalling was inducing CAF activation markers in both CAF-173 and CAF-318 but not in normal fibroblasts (RMF-31). It also suggested that CAF-173 and CAF-318 seemed to have a different expression profile and respond differently to OSM treatment.

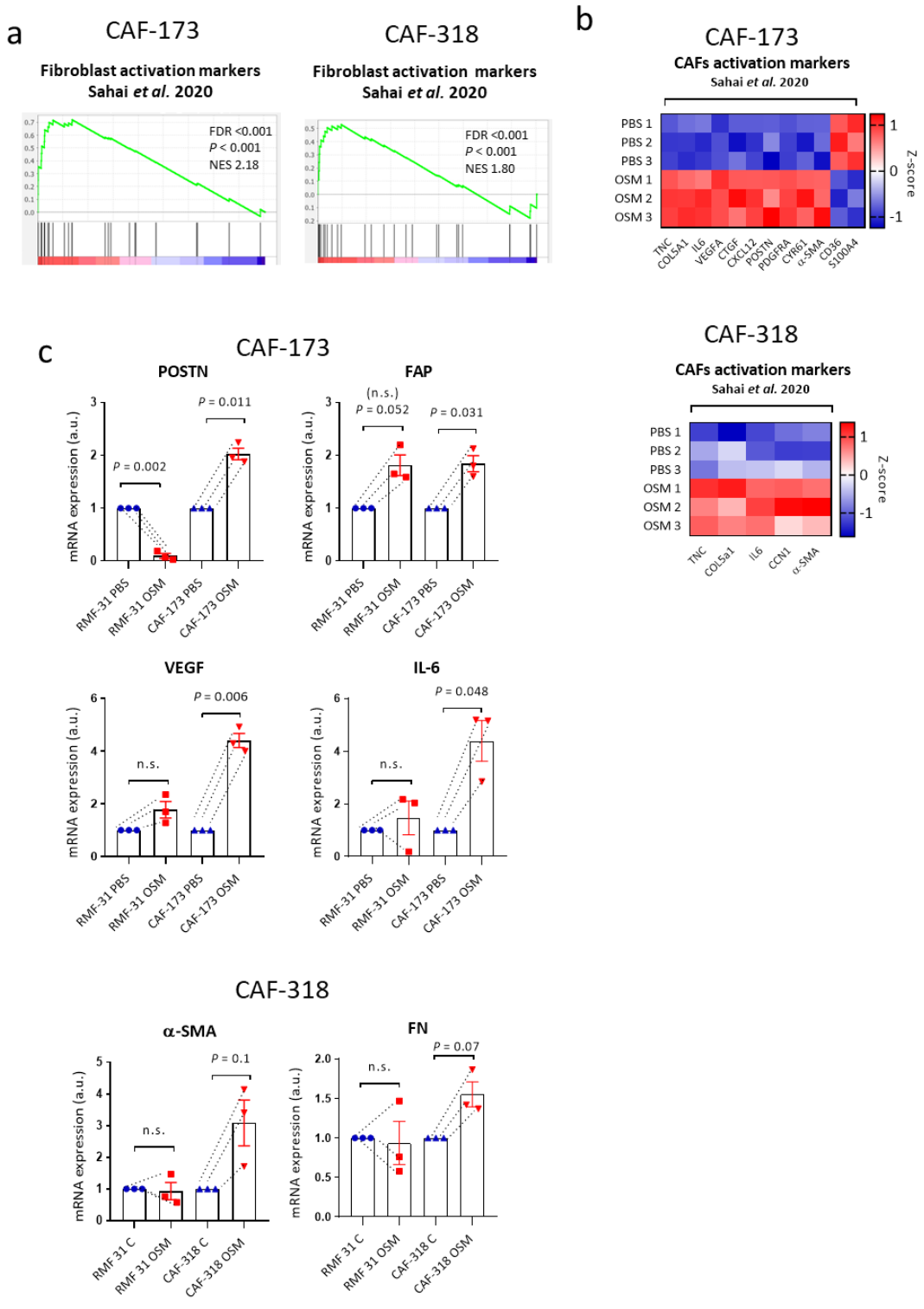

Fig. 3.2.9: Exogenous OSM induces activation markers in CAFs.
a) GSEA showing enrichment of fibroblast activation markers described in Sahai *et al* (2020)[64] in microarray data of CAFs treated with OSM. **b)** Heatmap showing normalized mRNA expression of fibroblasts activation markers induced by OSM and included in Sahai *et al* (2020)[64]. **c)** RT-qPCR analysis of mRNA levels of activation markers in normal (RMF-31) and cancer-associated fibroblasts (CAF-173 and CAF-318) cultured in 3D with PBS or OSM. Graphs represent mean ± SEM of 3 independent experiments. P values were determined using paired two-tailed t tests. n.s. non-significant.

3.2.11 Exogenous OSM induces a pro-tumoral signature in CAFs.

As seen in Fig. 3.2.10a, OSM induces a different gene signature in CAF-173 and CAF-318, supporting that both CAFs respond differently to OSM signalling. GSEA to identify enriched signatures in transcriptomic data of OSM-treated CAFs was performed to verify if OSM was inducing not only activation markers but also other genes associated with pro-malignant features. As seen in Fig. 3.2.10 b, GSEA revealed that OSM was inducing gene signatures associated with IL6-JAK-STAT3 signalling in CAF-173 fibroblasts ($P < 0.001$). In CAF-173 and CAF-318, OSM treatment induced genes included in the YAP conserved signature ($P = 0.012$ and $P = 0.001$, respectively), associated with an activated microenvironment[246], and in signatures of ECM modifying enzymes ($P = 0.002$ and $P = 0.003$), glycoproteins ($P = 0.006$ and $P = 0.008$) and collagen, important players in extracellular matrix remodelling during cancer progression[234] (Fig. 3.2.10b,c). Kaplan-Meier analysis of the top 4 induced genes by OSM in CAF-173 (*SERPINB4, THSB1, RARRES1* and *TNC*) revealed that high expression of these targets is associated with worse RFS in breast cancer patients ($P = 0.0017$, Fig. 3.2.10d). Of interest, OSMR expression correlated with the expression of RARRES1, THBS1 and TNC in breast cancer clinical samples (Fig. 3.2.10e). SERPINB4 was not expressed in this dataset (data not shown).

All these data together reinforce the idea that OSM is inducing a pro-malignant transcriptome in CAFs, which is clinically relevant.

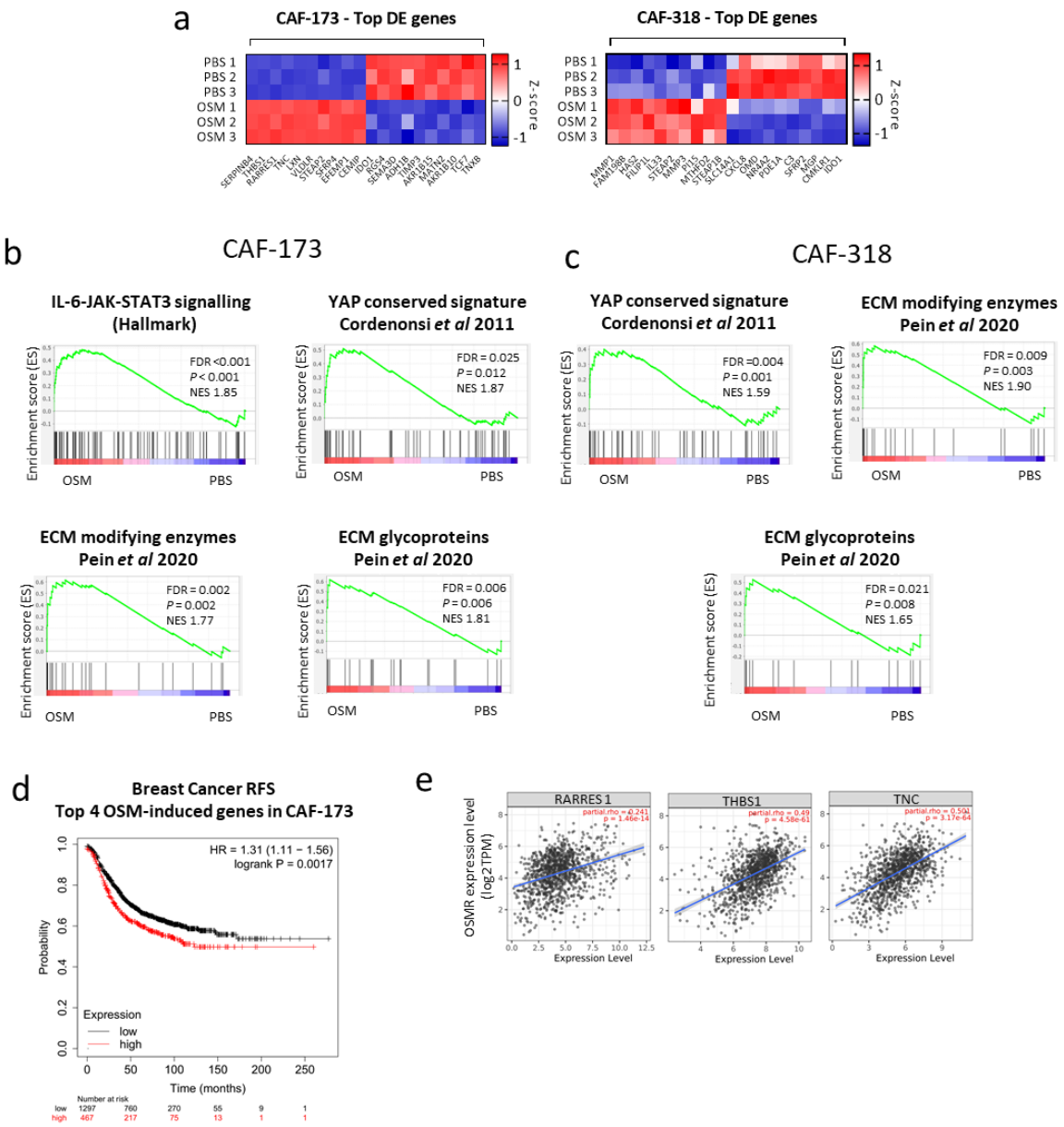

Fig. 3.2.10: Exogenous OSM induces a pro-tumoral signature in CAFs.
a) Top 10 up- and down-regulated genes in microarray data of CAF-173 and CAF-318 treated with PBS or OSM for 4 days. **b,c)** GSEA showing enrichment of the indicated signatures in microarray data of CAF-173 **(b)** and CAF-318 **(c)** treated with OSM. **d)** Kaplan-Meier curves showing relapse-free survival (RFS) for breast cancer patients according to the high or low expression in tumour samples of top 4 genes induced by OSM in CAF-173. Data were obtained using KM plotter website. **e)** Correlation of OSMR mRNA levels with RARRES1, THBS1 and TNC expression in breast cancer clinical samples. Data were downloaded from TIMER web platform, Spearman correlation coefficients and P values are shown.

3.2.12 Depletion of OSMR in CAFs delays tumour onset.

TS1 orthotopic tumours in syngeneic mice in Fig. 3.2.6 demonstrated that OSMR signalling in the tumour microenvironment was important for cancer progression. *In vitro* data

revealed that OSM signalling in CAFs induced fibroblast activation markers and a pro-malignant phenotype such as enhanced contractility and proliferation (Fig. 3.2.8). These observations reinforced the idea that fibroblasts could be the main cell type in the tumour microenvironment responsible for transducing OSM:OSMR signalling to promote cancer progression. To test this hypothesis *in vivo*, an experimental setup was designed where the OSMR receptor was knockdown by shRNA in CAF-173, and these cells were co-injected with MDA-MB-231 overexpressing OSM (MDA-MB-231 hOSM). This experiment allows the study of the effect of human OSM signalling in OSMR-deleted and control fibroblasts (Fig. 3.2.11a,b). It is important to mention again that human CAFs are not able to respond to the murine OSM present in the tumour microenvironment. As seen in Fig. 3.2.10c, animals injected with MDA-MB-231 hOSM + CAF-173 shOSMR showed a delay in tumour onset compared to the respective control injected with MDA-MB-231 hOSM + control CAF-173 ($P = 0.016$). As expected, co-injection of CAFs with tumour cells potentiated tumour development, as demonstrated in the same Fig. 3.2.10c, where it is possible to see that animals injected with MDA-MB-231 hOSM alone developed tumours later in time. Interestingly, in early stages of the experiment, CAF-173 shOSMR tumours seemed to have a smaller tumour growth compared to the control CAF-173, but with time, this difference became not significant (Fig. 3.2.11d). Technical concerns arouse at this point with this observation. It has been described that human fibroblasts injected in mouse tend to be replaced by mouse stroma[247] which generates a handicap in the experiment as replacement of human fibroblasts by mouse fibroblast could dilute the effect of OSMR silencing on tumour progression and interfere with the experimental conclusion. This technical issue did not allow a definite assessment of the OSMR signalling in CAFs and its contribution for breast cancer progression.

Despite no differences in tumour growth between control CAF-173 and CAF-173 shOSMR tumours in the last stages of the experimental window, tumours presented significantly lower expression of IL-6 ($P = 0.002$) and a tendency towards lower expression of OSMR and VEGF (Fig. 3.2.11e). It was also observed that GFP (tagging CAF-173 fibroblasts) levels were decreased in CAF-173 shOSMR tumours ($P = 0.023$, Fig. 3.2.11e). One possible explanation is that fibroblasts in this context show reduced proliferation or survival upon OSMR deletion. Further experiments would need to be done to evaluate this hypothesis.

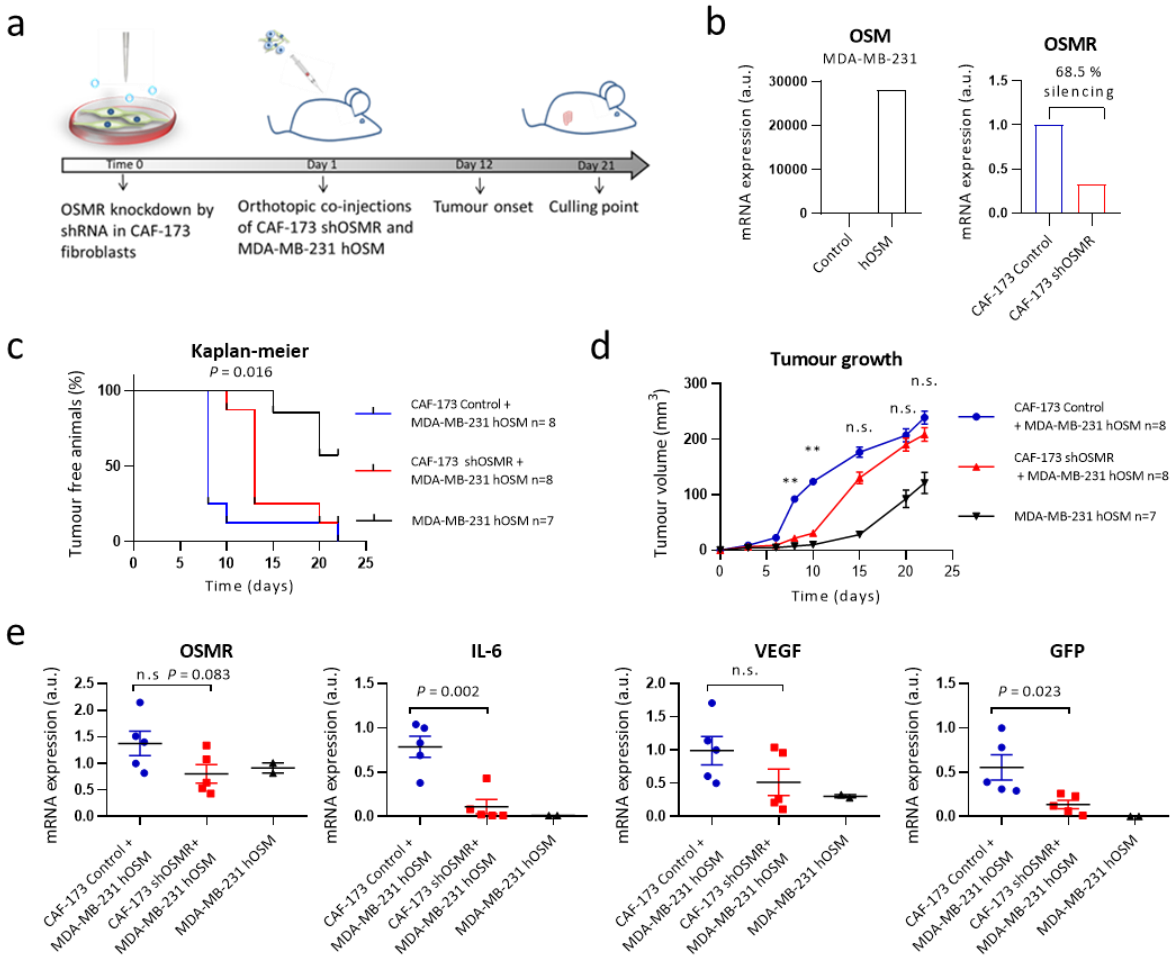

Fig. 3.2.11: Depletion of OSMR in CAFs delays tumour onset.
a) Experimental setup of the *in vivo* experiment designed to assess the contribution to breast cancer progression of OSMR knockdown in fibroblasts. Control and shOSMR CAF-173 were co-injected with MDA-MB-231-hOSM in the mammary gland of nude mice. **b)** OSM and OSMR mRNA expression levels analysed by RT-qPCR in MDA-MB-231 and CAF-173 after hOSM and shOSMR plasmid transfection, respectively. **c,d)** Kaplan-Meier curves for tumour-free survival **(c)** and tumour growth **(d)** of orthotopic tumours described in **a)**. **e)** OSMR, IL-6, VEGF, and GFP mRNA expression levels analysed by RT-qPCR in tumours of the different experimental groups, as described in **(a)**. Graphs represent mean ± SEM. P values were calculated using the Mantel-Cox test **(c)** or the unpaired two-tailed t test **(d, e)**. n.s. Non-significant. ** P < 0.01.

3.2.13 Activation of CAFs by OSM induces tumour progression and metastasis.

To further confirm that OSM signalling in CAFs was important for tumour progression, a complementary *in vivo* experiment was performed. Instead of knocking down the OSMR pathway in CAFs, OSM-activated CAFs were injected to check if this would result in a more

aggressive cancer phenotype in a shorter time frame to avoid extensive fibroblast replacement. Prior to injections, fibroblasts were pre-treated *in vitro* with OSM or PBS for 4 days to activate OSMR downstream targets and co-injected with MDA-MB-231 cell line (Fig. 3.2.12a). As seen in Fig. 3.2.12b and c, OSMR pathway activation in CAFs increased tumour growth and resulted in larger tumour weight and volume at the culling point (P = 0.002 and P = 0.001, respectively). qPCR of human ALU sequences in the lungs revealed that tumours generated with OSM-activated CAF-173 + MDA-MB-231 were more prone to colonise the lung (P=0.052, Fig. 3.2.12d), although, these results will need to be confirmed in further experiments. Puzzling, despite clear phenotypic differences, tumours did not present different molecular expressions of OSMR downstream targets or fibroblast activation markers (Fig. 3.2.12e). One possible explanation for this is that differences in fibroblasts activation markers get diluted in the bulk qPCR analysis of the tumours.

These data together strongly support that activation of the OSMR pathway in cancer associated fibroblasts contributes to breast cancer progression.

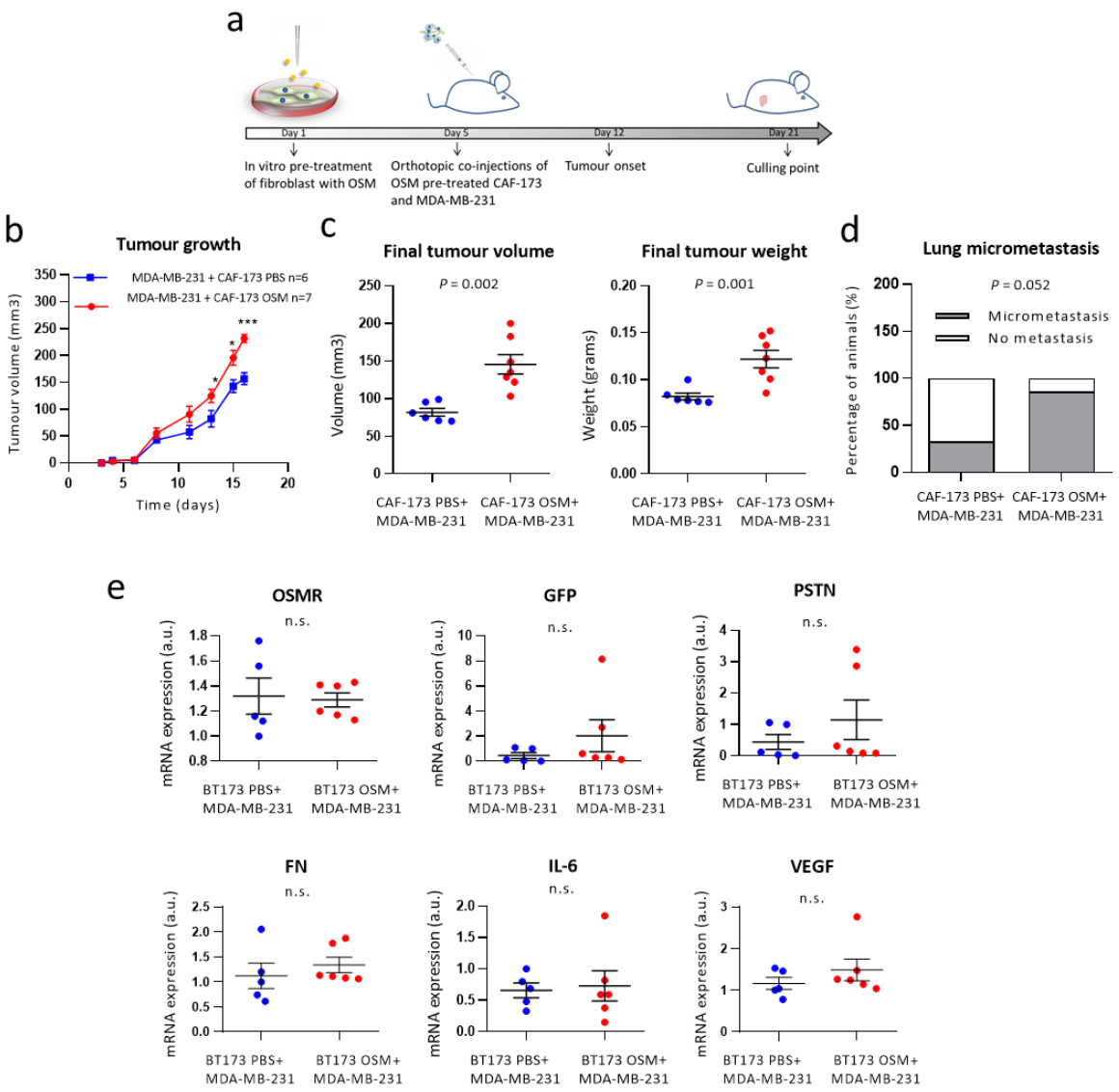

Fig. 3.2.12: Activation of CAFs by OSM induces tumour progression and metastasis.
a) Experimental setup of the *in vivo* experiment designed to assess the contribution of OSMR activation in fibroblasts to cancer progression. CAF-173 were pre-treated with OSM or PBS for 4 days prior to injection and were co-injected with MDA-MB-231 in the mammary gland of nude mice. **b,c)** Tumour growth **(b)** and final tumour volume and weight after dissection **(c)** of orthotopic tumours described in **a)**. **d)** Percentage of animals with lung micrometastases assessed using qPCR analysis of genomic human ALU sequences. Graph represents the percentage of animals with detectable qPCR signal and P value was calculated using the Chi-square test. **e)** mRNA expression levels of the indicated genes analysed by RT-qPCR in tumours described in **(a)**. **b,c,e)** Graphs represent mean ± SEM. P values were calculated using the unpaired two-tailed t test. n.s. non-significant. * $P < 0.05$; *** $P < 0.001$.

3.3 Modulation of the immune system by OSM:OSMR signalling.

3.3.1 Summary

Objective 4 of this thesis was addressed in this section with the aim of exploring the effects of OSM:OSMR signalling in modulating the immune system.

Microarray gene expression analysis was used to identify signatures and pathways activated by OSM in CAFs and tumour cells to look for cues on the immunomodulatory effect of OSM:OSMR signalling. Cultures of tumour cells, CAFs and primary human monocytes were used to study the interactions between different cell types in the OSM:OSMR signalling context. The role of OSM:OSMR in shaping the immune compartment of the TME *in vivo* was assessed using the genetic breast cancer model MMTV-PyMT used in previous sections of the chapter.

3.3.2 OSM induces an inflammatory signature and secretion of chemoattractants in CAFs and cancer cells.

Microarray gene expression analysis was performed on CAFs (CAF-173) and tumour cells (MDA-MB-231) treated with OSM to identify possible mechanisms linked with reprogramming of the tumour microenvironment and the immune system. Gene Ontology (GO) analysis of microarray data showed that leukocyte chemotaxis was one of the pathways significantly enhanced (P values shown in Fig. 3.3.1a). In addition, genes associated with neutrophil degranulation, a process intimately linked with cancer progression[248], were also induced in MDA-MB-231 upon OSM activation (P values shown in Fig. 3.3.1a). GSEA revealed that OSM induces an inflammatory signature in both cell types ($P = 0.006$ and $P < 0.001$ for CAF-173 and MDA-MB-231, respectively, Fig. 3.3.1b). RT-qPCR was performed to validate microarray data and the results confirmed that chemoattractant and inflammation-related factors such as VEGF, CCL2, IL-6 and CXCL12 in fibroblasts and VEGF, CCL2, CXCL7 and CCL20 in MDA-MB-231 cells were induced by OSM treatment in 3 independent experiments (P values shown in Fig. 3.3.1c).

Next, association between OSM levels and degree of inflammation in breast cancer clinical samples was tested using OSM IHC staining data obtained from the TMA. Inflammation was assessed by the pathologist as infiltration of inflammatory cells from all lymphoid and myeloid subtypes. Interestingly, OSM was mainly found expressed in myeloid-like cells, as determined by their larger size and more irregular shape (Fig. 3.3.1d). Lymphoid cells, characterized by being smaller and round and by having a round nucleus with little cytoplasm, showed very low or negative OSM expression. The results revealed that higher levels of OSM in the tumours also correlated with higher degrees of inflammation ($P = 0.011$, Fig. 3.3.1e) confirming that OSM was linked to inflammation in breast cancer.

Activated CAFs and cancer cells have been reported to produce chemoattractants responsible for inducing tumour promoting inflammation[69]. Considering the microarray data that suggested that inflammatory signatures were induced upon OSM treatment, activation of the OSMR pathway in cancer cells and CAFs was hypothesised to promote chemoattractant secretion, responsible for shaping the tumour immune landscape. As seen in Fig. 3.3.2a-b, OSM treatment led to the secretion of multiple leukocyte chemoattractants in CAF-173 and MDA-MB-231 cells (P values shown in Fig. 3.3.2). Interestingly, a significant part of the induced molecules were associated in the literature with myeloid chemoattraction, such as CXCL16[249], VEGF[250] and CCL2[251].

Analysis of data present in Cancertool[207], a platform designed to assess gene expression correlations in clinical data, revealed that OSM expression correlated with CCL2, CCL3, CCL4, CCL5, CXCL16 and IL-6 expression while OSMR mainly correlated with CXCL12, CXCL16 and RARRES2 in data from breast cancer patients (Fig. 3.3.2c), supporting the idea that OSM:OSMR signalling could be inducing the secretion of the aforementioned chemokines in the human cancer setting.

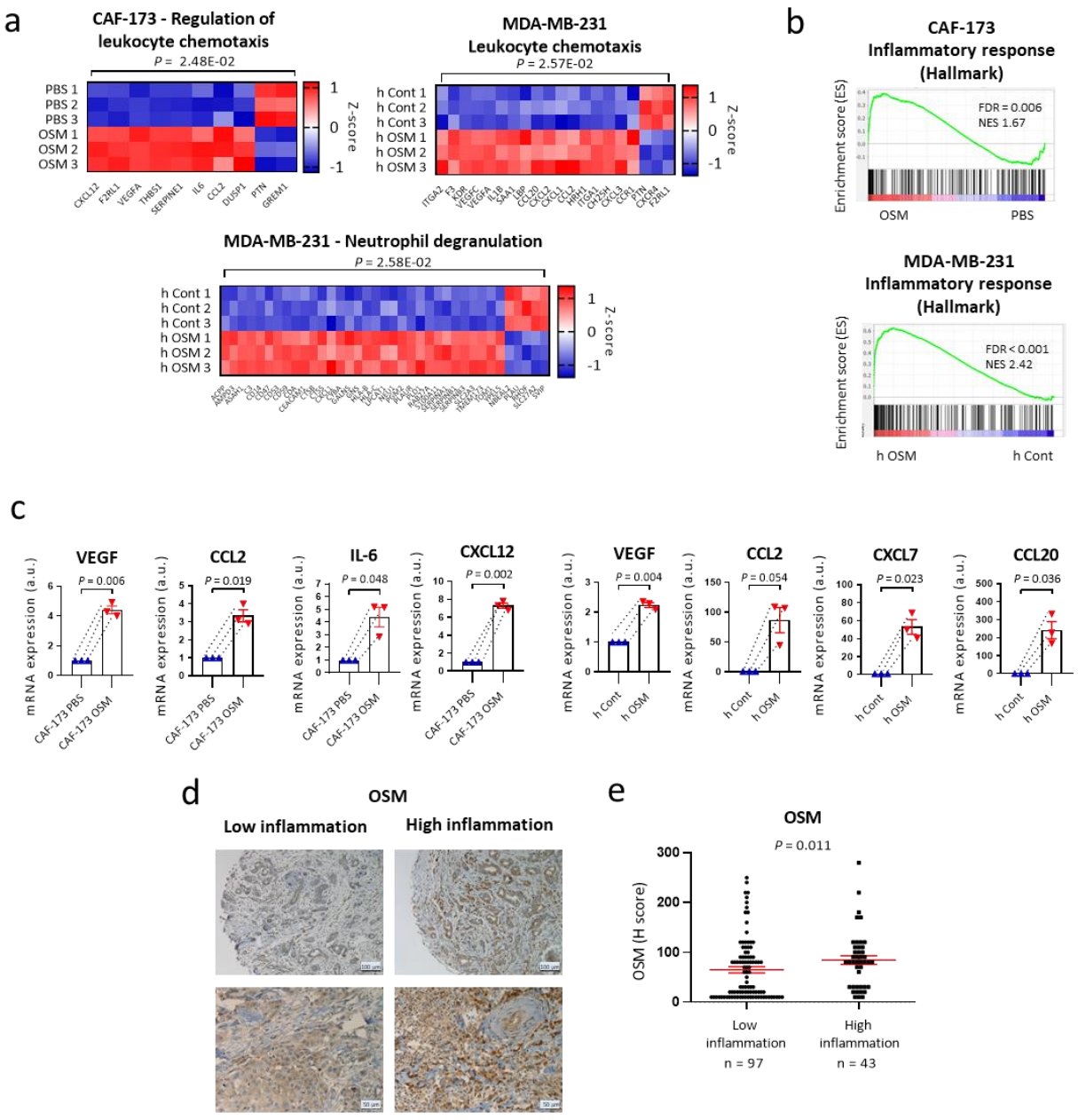

Fig. 3.3.1: OSM induces an inflammatory signature in CAFs and cancer cells.
a) Heatmap showing normalized mRNA expression of genes induced by OSM in CAF-173 and MDA-MB-231 cells and included in the indicated gene ontology (GO) pathways. **b)** GSEA showing enrichment of inflammatory hallmark signature in microarray expression data of CAF-173 spheres treated with PBS (Control) or OSM 30ng/ml for 4 days (upper panel) and MDA-MB-231 hControl or hOSM (lower panel). **c)** RT-qPCR analysis of the mRNA expression of the indicated genes in CAF-173 and MDA-MB-231 cells after OSM activation. Graphs represent mean ± SEM of 3 independent experiments. P values were determined using paired two-tailed t-test. **d, e)** Representative pictures **(d)** and quantification **(e)** of OSM staining in samples from breast cancer patients with low and high inflammation included in the TMA. Graph represents mean ± SEM. P value was determined using Mann–Whitney's test.

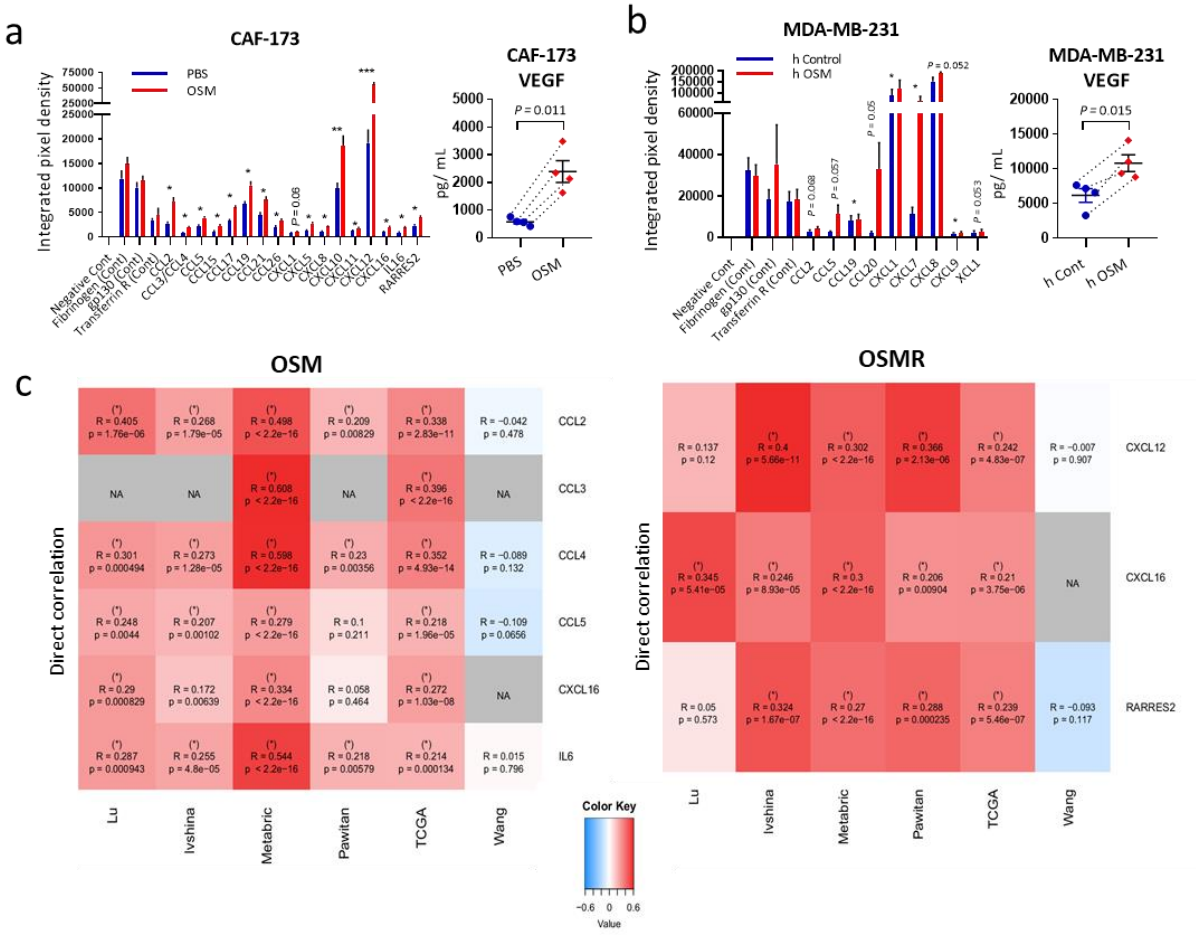

Fig. 3.3.2: OSM induces secretion of chemoattractants in CAFs and cancer cells.
a, b) Levels of indicated chemokines (analysed by chemokine array analysis or ELISA for VEGF levels) in conditioned media from CAF-173 treated with PBS (Control) or OSM 30ng/ml for 72 hours **(a)** or from MDA-MB-231-h OSM and control cells, 72h after seeding **(b)**. Graphs represent mean ± SEM (n=4 independent experiments, except for MDA-MB-231 chemokine array where n=3 independent experiments). P values were determined using the paired two-tailed t test. * P < 0.05; ** P < 0.01; *** P < 0.001. **c)** Heatmaps of correlations between OSM (left) and OSMR (right) levels and those of the indicated chemokines and cytokines in 6 datasets of breast cancer samples downloaded from Cancertool. R correlation coefficients and P values are shown.

3.3.3 OSMR depletion in MMTV-PyMT reduces myeloid infiltration within the primary tumour.

As OSM signalling was shown to induce myeloid chemoattractants in CAFs and tumour cells, MMTV-PyMT:OSMR WT, HET and KO mice were used to explore the effect of OSMR depletion in myeloid cell recruitment to the tumour niche.

Luminex assay analysis of blood plasma from the MMTV-PyMT different experimental groups confirmed that myeloid chemoattractant factors such as VEGF, CXCL16 and CXCL1

were reduced in the blood plasma of OSMR KO animals compared to control animals ($P < 0.001$, $P = 0.031$, $P = 0.024$, respectively, Fig. 3.3.3a). MMTV-PyMT:OSMR KO animals presented tumours with lower infiltration of macrophages ($P = 0.056$) and neutrophils ($P = 0.007$) in the TME, assessed by F4/80 and LY6G immunohistochemistry staining, respectively, compared to the control animals.

Of interest, OSM expression correlated with CXCL1 and CXCL16 levels while OSMR correlated with VEGF and CXCL16 in breast cancer samples analysed using TIMER webtool (P values show in Fig. 3.3.3c). Additionally, high levels of VEGF, CXCL16 and CXCL1 were associated with worse relapse-free survival in breast cancer patients ($P < 0.001$, Fig. 3.3.3d). These data strongly support that OSM:OSMR signalling contributes to the recruitment of myeloid cells to the tumour microenvironment.

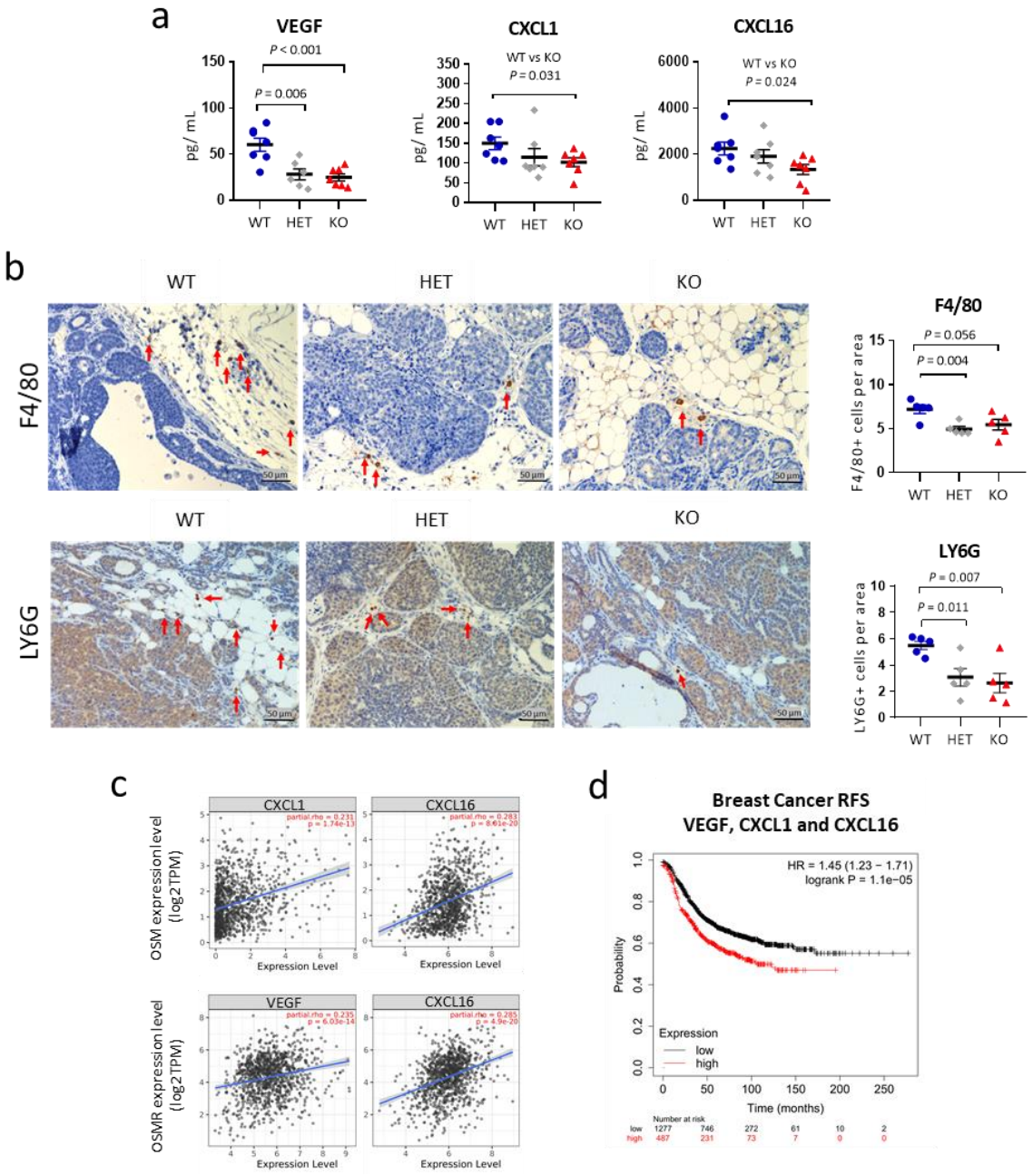

Fig. 3.3.3: OSMR depletion in the MMTV-PyMT mouse model reduces myeloid infiltration within the primary tumour.

a) VEGF, CXCL1 and CXCL16 levels in plasma from MMTV-PyMT:OSMR wild-type (WT), heterozygous (HET), and knockdown (KO) mice at 14 weeks of age analysed by Luminex assay. **b)** Representative pictures (left panels) and quantification (right panels) of F4/80 (upper panels) and LY6G (lower panels) immunohistochemistry staining in tumours from MMTV-PyMT:OSMR WT, HET and KO mice at 14 weeks of age. Quantification was performed by manual counting of positive cells per area in a total of 8 pictures per tumour and 5 tumours per group. **c)** Correlation of OSM (top) and OSMR levels (bottom panel) with VEGF, CXCL1 and CXCL16 expression in breast cancer samples. Data were downloaded from TIMER web platform. Spearman correlation coefficients and P values are shown. **d)** Kaplan-Meier curves showing relapse-free survival (RFS) for breast cancer patients according to the expression of VEGF, CXCL1 and CXCL16 in their tumour samples. Data

were downloaded from KM plotter. In **a, b)** graphs represent mean ± SEM. P values between the different groups were determined using unpaired two tailed t test.

3.3.4 Conditioned media from macrophages induces OSMR in cancer cells and conditioned media from OSM-treated cancer cells induces OSM expression in macrophages, suggesting the existence of feedforward loops.

As previously shown in Fig. 3.2.2, 3.2.3 and 3.2.5, myeloid cells produce OSM that presumably activates the OSMR pathway in CAFs and cancer cells. On the other hand, OSM-activated CAFs and cancer cells secrete chemoattractants responsible for myeloid infiltration, supporting the existence of a possible feedforward loop. HL-60 cell line was used as a model of human myeloid cells to test whether conditioned media (CM) from HL-60 cell line differentiated to macrophages (+TPA) could induce OSMR pathway in MDA-MB-231 cancer cells (Fig. 3.3.4a). As seen in Fig. 3.3.4b, conditioned media from macrophages was able to induce OSMR mRNA expression in 3 independent experiments (P = 0.023). The OSMR downstream target IL-6 showed a tendency for induction upon treatment with HL-60 CM, although, the variability of the experiments did not allow to draw definite conclusions. Next, the ability of cancer cells and/or fibroblasts to promote the expression of OSM in the myeloid cells was assessed. To test this hypothesis, an experiment setup was designed where MDA-MB-231 and CAF-173 cell lines were pre-treated with PBS or OSM for 4 days to allow pathway activation and corresponding conditioned media was transferred to TPA-differentiated HL-60 cells (macrophage-like cells) (Fig. 3.3.4c). As seen in Fig. 3.3.4d, conditioned media from fibroblasts treated with PBS or OSM did not change OSM mRNA levels in macrophages. On the contrary, conditioned media from cancer cells pre-treated with OSM promoted induction of OSM expression in macrophages (P = 0.031, Fig. 3.3.4d).

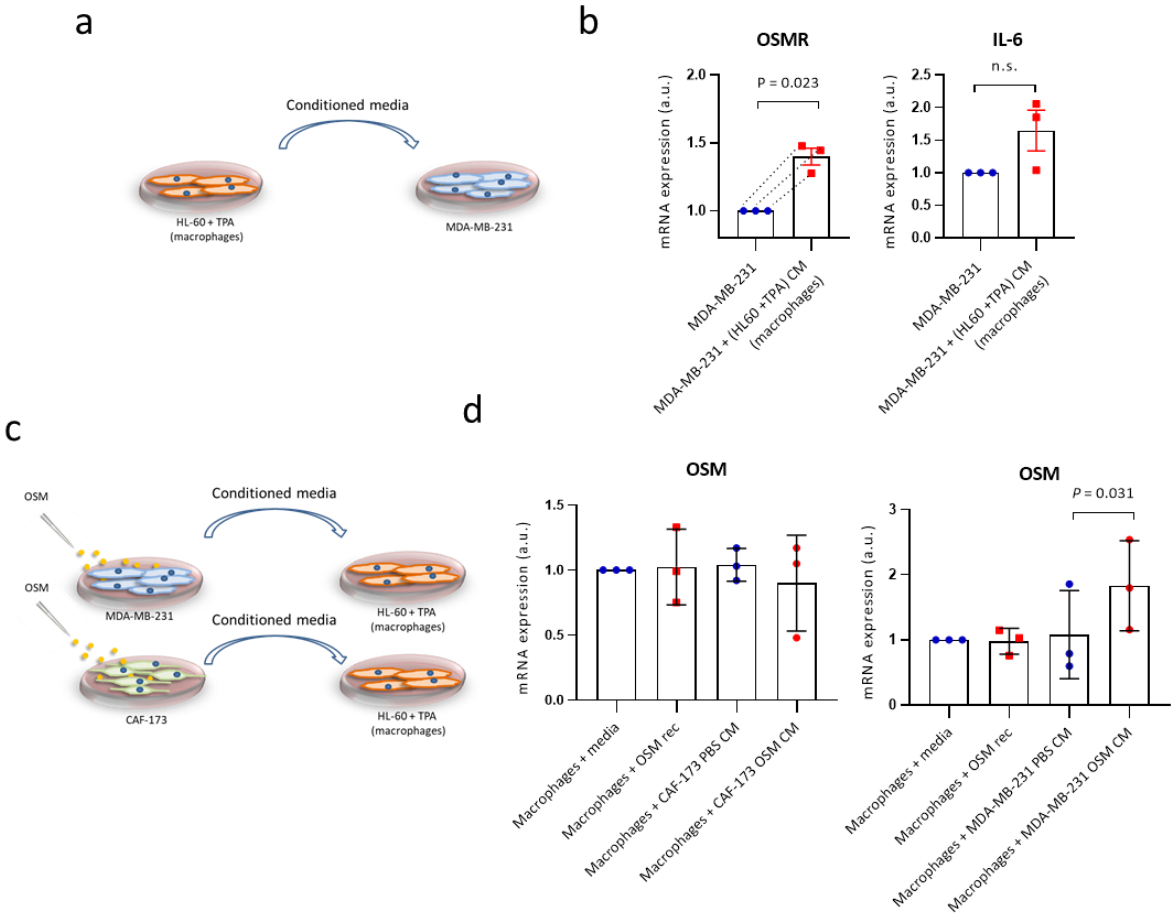

Fig. 3.3.4: Conditioned media (CM) from macrophages induces OSMR in cancer cells while CM from cancer cells induces OSM expression in HL-60 macrophages activating a feedforward loop. **a)** Experimental setup for results shown in **(b)**. HL-60 cells were differentiated to macrophages using TPA and CM was transferred to MDA-MB-231 cells and left in contact for 3 days. **b)** mRNA levels of OSMR and IL-6 in MDA-MB-231 cells treated with myeloid-differentiated HL-60 CM. **c)** Experimental setup for results shown in **(d)**. MDA-MB-231 cancer cells and CAF-173 fibroblasts were treated with OSM for 72h and media was transferred to macrophages and left in contact for 3 days before analysis. **d)** OSM mRNA levels in macrophages treated with CM from fibroblasts and cancer cells activated with OSM. Graphs represent mean ± SEM of three independent experiments. P value was calculated using the paired two-tailed t test.

3.3.5 Conditioned media from cancer cells prevents monocyte differentiation while conditioned media from CAFs induces M2 phenotype in primary monocytes, independently of OSM.

Data extracted from xCell webtool revealed that, in breast cancer patients OSM was associated with enrichment of M2 macrophages (Fig. 3.2.4). Tripathi *et al* (2014)[204] reported that OSM promotes M2 macrophages polarization in breast cancer. These data suggested that OSM could be involved in recruiting macrophages and shaping their

polarization status in the TME. To confirm if conditioned media from OSM-activated CAFs and cancer cells was capable of inducing M2 polarization, primary monocytes extracted from healthy donors were treated with CM from OSM-activated CAFs and tumour cells, and M1 and M2 polarization markers (CD86 and CD163) were analysed by flow cytometry (Fig. 3.3.5a,b). Intriguingly, OSM treated monocytes did not show any change in M1 or M2 markers, contradicting previous reports on the role of OSM in driving monocyte M2 polarization[204]. Of interest, monocytes treated with CM from MDA-MB-231 and CAF-173 cells significantly downregulated M1 marker CD86 ($P = 0.002$ and $P = 0.009$, respectively, Fig. 3.3.5c). Unexpectedly, CM from MDA-MB-231 cells downregulated M2 polarization marker ($P = 0.049$) while CM from CAFs greatly induced M2 marker in monocytes ($P = 0.002$), although all these effects seemed to be independent of OSM signalling (Fig. 3.3.5c). These data suggested that cancer cells were preventing M1 and M2 polarization of monocytes, keeping them into a more undifferentiated state, while CAF-173 CM was inducing M2 polarization. OSM was not found to induce direct M2 polarization or to contribute to CAFs/tumour cells mediated polarization on monocytes suggesting that the OSM signalling is not involved in shaping macrophage phenotype.

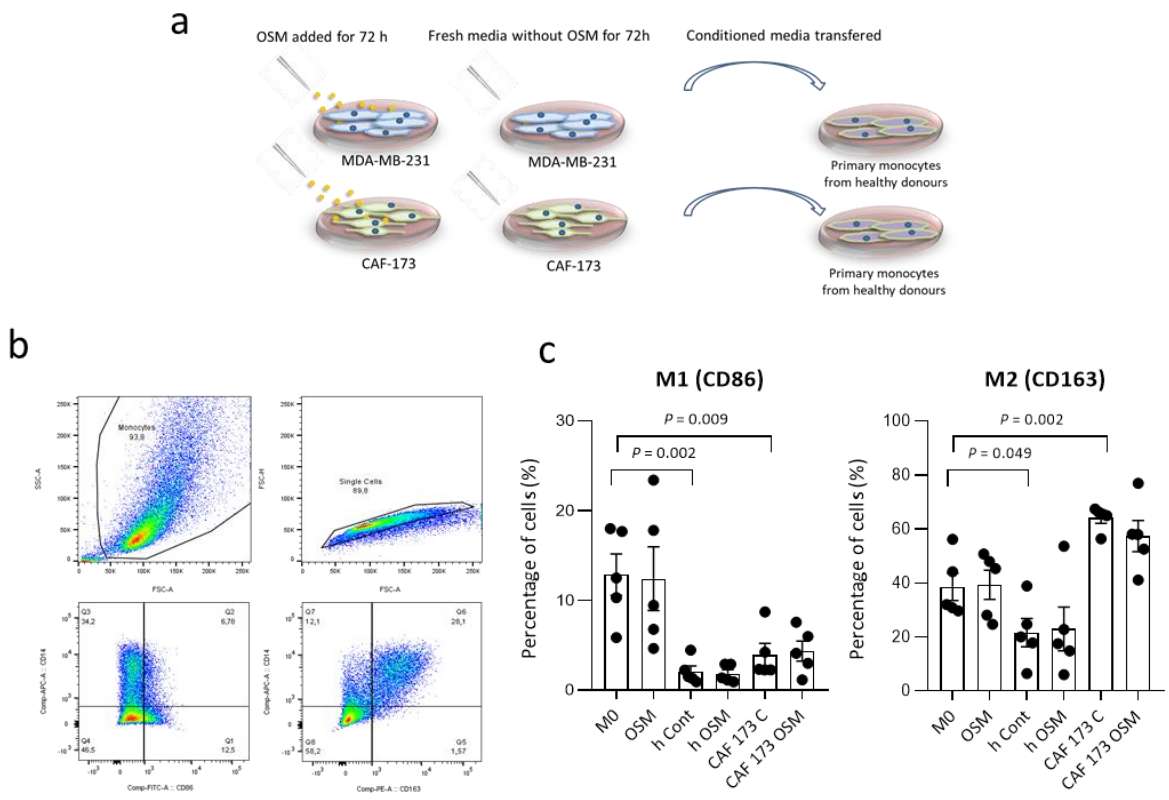

Fig. 3.3.5: Conditioned media from cancer cells prevents monocyte differentiation while CAFs induce M2 phenotype in primary monocytes, independently of OSM.
a) Experimental setup for results shown in **(b)** and **(c)**. **b)** Flow cytometry gating strategy to analyse CD14 (monocyte), CD86 (M1) and CD163 (M2) markers. **c)** Flow cytometry analysis showing percentage of monocytes expressing CD86 and CD163 markers after treatment with different conditioned media described in **(a)**. Graphs represent mean ± SEM of five independent experiments. P values were calculated using the paired two-tailed t test.

Chapter 4: Discussion

Breast cancer is a very heterogeneous disease that will affect 1 in 8 women during their lifetime[252]. Despite relevant improvement in therapeutic options in the last years, still an alarming 627,000 women die annually from the disease[253], highlighting the need of finding new therapeutic solutions to increase survival rates and improve patient's quality of life.

Extensive work has been done on the field to decipher the molecular mechanisms driving oncogenesis and metastasis in breast cancer and to develop targeted therapies. One example of how targeted therapies can change the course of the disease was the introduction of trastuzumab (a monoclonal antibody targeting HER2) to treat HER2-positive breast cancer, that has drastically improved the clinical prognosis of these patients[254]. Inevitably, primary or acquired resistance to conventional and targeted therapies affects a substantial number of patients leaving the clinicians with limited therapeutic options. This gap urges biological understanding of the advanced disease and development of new therapies.

Oncology research has suffered a change of paradigm in the last decades. Despite being fundamental to understand what happens within a malignant cell, a substantial amount of work has been focused on understanding the interactions of cancer cells with their tumour microenvironment. The tumour is no longer seen as an isolated group of cells but rather a dynamic process between tumour cells and all elements present in the tumour microenvironment[255]. It is not surprising that the role of the tumour microenvironment in disease progression and resistance to therapies has been intimately linked to all stages of cancer[56]. Understanding these complex interactions between tumour cells and the tumour microenvironment is fundamental to design more effective therapies.

As summarised in the introduction of this thesis, inflammation in the tumour microenvironment has been described to play a key role in cancer progression. Inflammatory cells, within the tumour, acquire an immune suppressive profile contributing to the escape of cancer cells from the immune system surveillance, resulting in consequent cancer survival and progression[81,85]. Although breast cancer has not been characterised for being highly inflammatory, the role of inflammation in the tumour microenvironment is increasingly being recognised as an important contributor to breast cancer progression[109,110].

This present work was set to assess the role of the pro-inflammatory cytokine OSM and its signalling axis in contributing to breast cancer progression, and to determine its potential

as a new therapeutic target for breast cancer. OSM:OSMR signalling was already described to promote malignant features in breast cancer (Section 1.3.2-1.3.5), but information about the role of OSM:OSMR axis in shaping the tumour microenvironment is very scarce. The aims of this work were to determine the association of OSM:OSMR with breast cancer prognosis, to test the relevance of OSM:OSMR signalling for breast cancer progression and to check its role in the tumour microenvironment.

4.1 OSM and OSMR associate with decreased survival in breast cancer and OSMR signalling is increased in ER negative breast cancer.

In this section, the initial experiments performed in this thesis aiming to determine the association of OSM and OSMR levels with clinical prognosis are discussed.

West *et al* (2012) reported that OSMR mRNA levels correlated with shorter recurrence-free and overall survival in a cohort of 321 samples from breast cancer patients[193]. In this thesis, a more extensive bioinformatic analysis was done using publicly available data from KM plotter and Cancertool to explore further the association of the OSM:OSMR axis with disease prognosis. The findings present in Fig. 3.1.1-3 corroborated that both OSM and OSMR mRNA levels are associated with worse clinical prognosis (OS and DFS) supporting the previous report.

One of the limitations of mRNA expression data is that occasionally mRNA levels do not reflect functional protein levels due to post-transcriptional/translational modifications and it may misguide conclusions[256]. To confirm that OSM expression retained prognostic value at protein levels, a collaboration was established with a group in the University Hospital Basel that had curated a database of 141 tumours from breast cancer patients. The immunohistochemistry analysis of the tumours confirmed, for the first time, that high levels of OSM protein associated with worse OS in breast cancer patients. Moreover, the same trend was observed in ER- breast cancer (Fig. 3.1.1d) but not in ER+ (data not shown), strongly supporting the previous reports and mRNA data presented in this thesis.

Data presented in Fig. 3.1.2-3 also showed that both OSM and OSMR mRNA levels were associated with worse OS in other cancer types, including cervical cancer where our previous findings identified the OSM:OSMR axis as a possible therapeutic target for this disease[180]. These data confirmed that high levels of OSM:OSMR are associated with worse breast cancer prognosis, that this signalling axis could be contributing to breast cancer progression and that it could be exerting the same effect in other types of cancer. Of note, other groups have also reported the association of OSM and OSMR expression with worst prognosis in other types of cancer such as myeloma[257], glioblastoma[174] and gastric[170], reinforcing that the association of OSM:OSMR with disease progression could be relevant in other cancer types.

The heterogeneous nature of breast cancer urges the classification of the patients into subgroups that are more prone to respond to a specific targeted treatment. The same bioinformatic analysis mentioned previously was carried out to verify if OSM:OSMR were associated with a specific breast cancer subtype. The data in Fig. 3.1.1 indicate that high levels of OSM and OSMR are significantly associated with worse prognosis in patients with ER- tumours while this significance was not observed in ER+ tumours alone (data not shown). Interestingly, OSM downregulates ER protein levels in breast cancer cells[193]. The data presented in this thesis indicate that OSMR levels were increased in ER- breast cancer cells (Fig. 3.1.5), which suggest that OSM:OSMR signalling in those cells could be contributing to the downregulation of the ER. These data are of particular importance as ER downregulation is accompanied by development of resistance to endocrine therapy[258]. Some studies have suggested that restauration of ER expression can reverse therapy resistance[259], therefore targeting OSM:OSMR axis could help re-establish ER levels and contribute to better prognosis in this subgroup patients. Further studies would need to be done to confirm that OSM:OSMR targeting would restore sensitivity to endocrine therapy. Recently, other groups have reported the association of OSM:OSMR with clinical prognosis in the ER- subtype, which supports the clinical data presented in this thesis[233,260]. Nevertheless, OSM:OSMR axis has also been shown to be relevant for the metastatic cascade in ER+ breast cancer by regulating CD44 in ER positive cells, an important marker in stem cell phenotype and metastasis[261], highlighting the importance of understanding the OSM:OSMR role in the different breast cancer subtypes.

4.2 OSM signalling promotes breast cancer progression in multiple pre-clinical models.

Until the start of this thesis, OSM had been described to have anti-proliferative effects, to induce migratory and invasive phenotype in breast cancer cells *in vitro*[189,190], and to associate with EMT transition[194]. Although these studies strongly suggested that OSM:OSMR could be contributing to malignancy, there were no reports demonstrating that OSM:OSMR signalling was actively contributing to breast cancer progression. In this section, the relevance of OSM:OSMR axis for breast cancer progression was tested in multiple *in vitro* and *in vivo* models of BC.

One of the handicaps of studying such a complex heterogeneous disease is that *in vitro* and *in vivo* models are many times limited in several aspects and fail to reflect the whole breast cancer complexity[262]. In this study, a panel of breast cancer cell lines was characterised together with complementary *in vivo* models to try to tackle the disease complexity. The data presented in Fig. 3.1.6-8 indicated that recombinant OSM activated the OSMR pathway by inducing previously described downstream targets of OSMR in cancer such as STAT3, IL-6, VEGF and SNAIL[147,183,233]. Silencing of OSMR using siRNA technique has demonstrated that activation of these downstream targets is mediated by OSMR receptor, but nevertheless other effects mediated by OSM:LIFR cannot be discarded. Moreover, OSMR overexpression in a cell line with low basal levels of receptor (SK-BR-3 cells) increased IL-6 and FN expression (Fig. 3.1.8), factors closely associated with EMT and with worse prognosis in breast cancer patients[137,235,263,264]. The *in vitro* data confirmed that OSM:OSMR signalling activated pro-malignant factors in breast cancer cells.

One challenge of studying OSM:OSMR axis *in vivo* is the fact that human cancer cells do no secrete significant amounts of OSM and that mouse OSM has no affinity to human OSMR[236]. To circumvent this problem, MDA-MB-231 hControl and hOSM cells (over expressing OSM) were used for orthotopic injections in nude mice and the data presented in Fig. 3.1.10 revealed that OSM signalling contributed to earlier tumour onset. On the contrary, deletion of OSMR in the MMTV-PyMT mouse model delayed tumour onset (Fig 3.1.11), proving this way that OSM:OSMR axis contributes to the development of tumours in multiple breast cancer models.

With the orthotopic xenografts experiments (Fig 3.1.10) it was not possible to conclude if OSM:OSMR pathway activation was contributing to increased tumour growth as the only developed hControl tumour presented a similar size compared to hOSM tumours. In contradictory observations, the only tumour in the hOSM group that lost OSM expression presented the smallest tumour size, making it difficult to conclude if OSMR pathway activation influences tumour growth or if it only affects tumour onset. The results presented in Fig 3.1.11d revealed that deletion of OSMR signalling in the MMTV-PyMT mouse model contributed to reduced tumour growth. Intriguingly, Tawara *et al* (2018) has reported that periodical peritumoral injections of OSM in an orthotopic mouse model of BC does not affect primary tumour growth[196]. All these contradictory observations do not allow a definitive conclusion on the role of OSM:OSMR signalling in tumour growth. Further experiments would need to be done such as periodic injections of OSM, once tumours are established, in the xenografts and orthotopic models presented in this thesis, or to extend the experimental window of both hControl (Fig.3.1.10b) and MMTV-PyMT:OSMR KO (Fig. 3.1.11d) groups to compare the growth curve with hOSM and MMTV-PyMT:OSMR WT groups, respectively, to determine if OSM:OSMR signalling also contributes to tumour growth.

OSMR deletion in the MMTV-PyMT mouse model reduced the metastatic burden in the mice lungs presented in Fig. 3.1.13, suggesting that OSM:OSMR signalling was important for metastasis formation. In the orthotopic xenograft model presented in Fig. 3.1.10, none of the control animals presented lung micrometastases while around 50% of the animals injected with hOSM cells developed lung micrometastases suggesting that OSMR signalling was also contributing to the dissemination of the primary tumour. One of the questions that arose when analysing these data was if the differences seen in lung colonisation were due to different metastatic potential of MMTV-PyMT:WT and hOSM tumours, or simply because the larger tumours had more probability of generating metastasis. It would be interesting to compare the lung metastatic burden in the MMTV-PyMT mouse model from WT and KO animals with similar tumour burden to assess if OSM:OSMR influences the metastatic capacity of tumours with the same size. Surgical resection of primary tumours with the same volume in hControl and hOSM injected animals (Fig 3.1.10) could be done in future experiments to assess the rate of lung metastasis in these two groups. Another experimental setup to address this question is being performed by Andrea Abaurrea where

the lung colonisation potential of hControl and hOSM cells is being assessed by tail vein injections. Preliminary data have revealed that animals injected with hOSM cells develop higher number of metastases in the lungs (data not shown). Meanwhile, the recent work published by Tawara *et al* (2018) confirmed that OSM was increasing the number of CTCs counts and promoting lung metastasis in BC mouse models independently of tumour size[196], strongly supporting that OSM:OSMR axis plays a fundamental role in the development of breast cancer metastasis.

Mice xenografts are a valuable model to study mechanisms of disease, but one important downside of this model is that it lacks a fully functional immune system. As one of the main objectives of this thesis was to evaluate the impact of OSMR signalling, not only on tumour cells but also in the tumour microenvironment, the genetic mouse model and orthotopic injections in syngeneic mice were considered the most valuable systems to assess the contribution of OSM:OSMR signalling in breast cancer progression. The crossing of OSMR KO mice with the widely used MMTV-PyMT breast cancer model revealed that deleting OSMR signalling in the MMTV-PyMT mice delayed tumour onset, reduced tumour growth, and decreased the number of metastasis in the lungs, as mentioned previously (Fig. 3.1.11). In the Western blot analysis performed in the tumours of the MMTV-PyMT mouse model, interestingly, OSMR protein levels seemed to be identical in the tumours of MMTV-PyMT:OSMR WT and HET animals (Fig. 3.1.11f), although further analysis would need to be performed to confirm this observation as Western blot signal is saturated and becomes difficult to quantify subtle differences that might exist. Tumour onset, tumour growth, proliferation, and apoptosis (measured by ki67 and caspase 3 markers, respectively, Fig. 3.1.11c,d and Fig 3.1.12) of WT and HET groups were not greatly affected by the deletion of one OSMR allele. Nevertheless, OSMR HET animals revealed an intermediate phenotype between MMTV-PyMT:OSMR WT and KO in histopathology analysis and IHC analysis of FN, metastasis formation and myeloid cell recruitment (Fig. 3.1.12, 3.1.13 and 3.3.3). It would be important to check that, despite presenting similar levels of protein by Western blot, if all OSMR is fully functional in the MMTV-PyMT:OSMR HET animals. This intermediate phenotype suggests that a slight change in OSMR levels might not be so critical for primary tumour growth but that it can have a great impact in metastasis formation and immune remodelling.

An attempt to determine the number of CTCs in blood circulation of the MMTV-PyMT:OSMR KO and control mice was made to confirm the role of OSM:OSMR in increasing CTC counts in different animal models reported by Tawara *et al* 2018[196], but the group did not manage to setup a reliable technique that allowed reproducible results, being therefore impossible to determine if reduced lung metastasis were due to lower number of CTCs in this mouse model. Further experiments would need to be done to determine the mechanism of metastasis in the MMTV-PyMT:OSMR WT/KO animal model.

An increasing number of reports have associated extracellular vesicles (EVs) with cancer progression and metastasis. EVs transfer molecules (e.g. proteins, RNA, miRNAs) between the primary tumour and the cells in distant microenvironments, preparing the metastatic niche for metastasis seeding[265]. The potential of EVs as therapeutic targets in cancer treatment represent a new and important area of research[266]. Preliminary data generated by the group revealed that extracellular vesicles derived from MDA-MB-231 hControl and hOSM cells presented different mRNA and miRNA expression profile and that EVs derived from OSM-treated cancer cells increased the migration of breast cancer cells, potentially influencing their metastatic capability. Currently, a new line of research is being carried out by Peio Azcoaga in the laboratory to determine the role of OSM signalling in shaping extracellular vesicles content and its implication in breast cancer metastasis.

4.3 OSM:OSMR signalling in the tumour microenvironment promotes breast cancer progression.

The tumour microenvironment is fundamental in supporting tumour cells in every step of cancer progression[56,267,268]. Inflammation within the TME has been intimately linked with malignancy and responses to therapies[85,269]. The main regulators of inflammation are cytokines, secreted molecules that play central roles in mediating cell-to-cell communication[270]. Despite being a pro-inflammatory cytokine, little is known about the influence of OSM signalling in shaping the tumour microenvironment. The experimental setups presented in this section aimed to determine the effect of OSM signalling in the tumour microenvironment, to assess if OSM was conditioning the TME cells to promote

breast cancer progression and to dissect the mechanisms of communication between OSM and OSMR within the tumour.

Microarray data analysis from breast cancer tumours from GEO datasets revealed that both OSM and OSMR were induced in the stroma compartment of breast cancer (Fig. 3.2.1), indicating that this pathway could be playing a role in microenvironment signalling. To understand the mechanism of communication of OSM:OSMR axis within the tumour, scRNA-seq from MMTV-PyMT tumours and FACS sorting from tumours derived from TS1 orthotopic injections were performed (Fig. 3.2.2-3). The data revealed a clear paracrine signalling where OSM was almost exclusively expressed by myeloid cells and OSMR was mainly found in cancer cells and fibroblast. Moreover, scRNA-seq revealed that OSMR was specially highly expressed in tumour cells with basal markers and in fibroblasts expressing myofibroblasts markers (Fig. 3.2.2c). Previous reports have associated basal tumours with high expression of genes associated with EMT and stem cell like characteristics[193], both features described to be induced by OSM signalling[194,261]. Moreover, as OSM:OSMR signalling suppresses ER expression[193], a key feature of luminal epithelial differentiation in breast cancer, it is not surprising that OSMR is found highly expressed in basal cells.

Gene expression data present in TIMER and xCell datasets also revealed that OSMR levels were associated with fibroblast content within the tumour while OSM levels increased with myeloid tumour infiltration which supports the existence of paracrine signalling in human breast cancer (Fig. 3.2.4). Analysis of a breast cancer cell panel, mammary fibroblasts and the promyelocytic HL-60 cell line confirmed that this signalling pattern was also maintained *in vitro* (Fig. 3.2.5). All these results support the existence of a paracrine signalling of the OSM:OSMR pathway involving at least cancer cells, myeloid cells and fibroblasts. Of interest, OSM and OSMR expression greatly differed from the expression pattern of other members of the IL-6 family which points to a unique role of OSM:OSMR signalling in this context. This data is of particular importance as it opens an opportunity to target a cytokine with a unique pattern of expression within the IL-6 family. OSM signalling shares common downstream targets with IL-6 such as phosphorylation of STAT3, and both cytokines have reported overlapping functions in breast cancer such as EMT and metastasis-promoting functions[194,233,263]. IL-6 has been for some time now a proposed target for breast cancer treatment[271], but attempts to target IL-6:IL6R in pre-clinical and clinical models have shown some adverse effects such as susceptibility to infection, cardiovascular toxicity, and

gastrointestinal perforation[271,272]. The unique pattern of expression of OSM:OSMR opens a new therapeutic opportunity to try to reduce the toxicity associated with IL-6 targeting.

The data presented in section 3.1 indicated that OSMR signalling was contributing to breast cancer progression. To assess if OSM:OSMR signalling in breast cancer stroma was relevant for breast cancer progression, orthotopic injections of TS1 cells were carried out on OSMR WT and KO animals where TS1 cells were shown to express OSMR and respond to OSM activation (Fig. 3.2.6). Tumours that lacked OSMR signalling in the TME presented later onset and reduced tumour growth confirming, this way, that OSMR signalling was contributing to breast cancer progression in this *in vivo* model.

One of the challenges at this point was to identify which cells in the tumour stroma were taking advantage of OSM signalling to promote tumour progression. The group decided to assess the effect of OSM signalling on fibroblasts because the scRNA-seq data presented in this thesis revealed that fibroblasts express high levels of OSMR, which might indicate that they rely on OSM:OSMR signalling to accomplish cellular functions, and because CAFs have been linked with all steps of cancer progression[72,273] and represent an important target for cancer therapies[64].

Fibroblast proliferation and the ability to contract collagen are hallmarks of fibroblast activation, a process intimately linked with cancer progression[274]. Functional assays shown in Fig. 3.2.8 revealed that fibroblast treated with OSM compared to those treated with PBS (control), presented a more contractile phenotype and accelerated growth in 3D spheres, indicating that OSM was reprogramming fibroblasts into a more activated state. Intriguingly, as mentioned in the introduction in section 1.3.4, OSM was associated with anti-proliferative effects in tumour cells *in vitro*[188], which contradicts the growth promoting effects on CAFs described in Fig 3.2.8, highlighting again, that OSM effects can be extremely context dependent.

OSM was also found to induce classic activation markers described by Sahai *et al* 2020[64]. Importantly, induction of activation markers and the phenotypic effect of OSM was only observed in CAFs but not in skin or normal breast fibroblasts. Of interest, normal fibroblasts presented similar levels of OSMR expression compared to CAFs and they also induce OSMR downstream targets upon OSM treatment such as OSMR itself, although it would be interesting to further confirm OSMR pathway activation by assessing P-STAT3 levels by Western blot. These results indicate that the OSMR pathway can be activated in both CAFs

and normal fibroblasts but that it promotes differential effects. This observation suggests that, maybe, pre-events are required to "educate" CAFs and make them susceptible to OSM pro-tumoral action which might indicate that OSM is not acting from the beginning as a driver of malignancy but rather as an assistant that is potentiating the system towards breast cancer progression. This is an interesting topic to be further explored as it would allow to determine at which stage of cancer progression OSM signalling would start promoting pro-tumoral functions. Further studies such as gene expression profiling or OSMR silencing in normal and cancer associated fibroblasts would need to be performed to determine why only CAFs seem to respond to OSM reprogramming and if this effect is mediated by OSMR only or by other receptors such as LIFR in fibroblasts.

In this work, OSM was shown to induce several signatures associated with tumour promoting functions in CAFs (Fig. 3.2.10). Despite being an extremely heterogeneous population with not fully understood origin and functions, CAFs have been reported to exhibit either a matrix-producing contractile phenotype or an immunomodulating secretome, termed "myoCAFs" or "iCAFs", respectively[75,275]. Therefore, CAFs are now mainly subdivided into inflammatory or ECM remodelling CAFS, and according to Sahai *et al* (2020), there are several markers strongly associated with activation of fibroblasts that need to be taken into account depending on what population of CAFS are being studied[64]. In other types of tumours such as pancreatic cancer, myoCAFs are mainly characterised by high TGFβ-driven α-SMA expression and a contractile phenotype[276] while iCAFs express higher levels of IL-6[277]. Interestingly, despite presenting low basal levels of α-SMA determined by IHC staining[220], CAF-318 showed induction of α-SMA mRNA levels, increase of ECM modifying enzymes expression, and a more contractile phenotype with OSM treatment, which indicates that OSM could be potentiating the induction of the myoCAF profile in CAF-318. On the other hand, CAF-173 cells did not express α-SMA at mRNA and protein levels determined by RT-qPCR and IHC (data not shown and Nogueira *et al* 2020, respectively)[220], but, upon OSM treatment, they presented increased levels of IL-6 expression (Fig 3.2.9) and induction of IL-6 signature (Fig. 3.2.10), suggesting that OSM was producing an iCAF profile in these fibroblasts. Curiously, despite no expression of α-SMA, CAF-173 displayed a strong contractile capacity (Fig. 3.2.8) and induction of ECM modifying enzymes with OSM treatment (Fig 3.2.10), which again, supports the existence of very heterogeneous and plastic CAF populations where some "subgroups" can show

characteristics of other CAF profiles. It would be interesting to determine in future experiments which are the mechanisms leading to CAF-173 collagen remodelling. Sanz-Moreno *et al* (2011) have described that in melanoma, JAK1-Rho-kinase dependent signalling generates actomyosin contractility in CAFs and that this is mediated by OSM signalling[278]. Future experiments would need to be done to determine if the same molecular mechanisms were used by breast cancer associated fibroblasts. In BC, fibroblasts with high levels of FAP are correlated with Treg cell-mediated immunosuppression and a poor outcome[75]. Data presented in Fig. 3.2.9 showed that OSM was inducing FAP expression in CAF-173 which supports the idea that OSM was converting those CAFs into a more pro-malignant profile. It would be interesting to determine *in vivo* if the OSM mediated induction of FAP was contributing to Treg cell-mediated immunosuppression.

To test the relevance of OSM:OSMR signalling in CAFs for tumour progression, OSMR was knockdown by shRNA on CAF-173 and co-injected with MDA-MB-231 cancer cells (Fig. 3.2.11). The results indicated that deletion of OSMR signalling in CAF-173 contributed to delayed tumour onset and initial reduction in tumour growth, but due to possible effect of human fibroblasts replacement by murine fibroblasts it was difficult to conclude with this experimental setting if OSMR signalling abrogation in CAFs was impacting tumour growth. No further experiments were performed at the culling point to assess if human fibroblasts were replaced by murine fibroblasts so the dilution of shOSMR effect with time remains to be determined. A different strategy to answer this question was adopted, and the orthotopic MDA-MB-231 and CAF-173 co-injections data presented in Fig. 3.2.12 revealed that activation of CAF-173 with OSM contributed to tumour growth and showed a tendency towards increased micrometastases in the lungs confirming that activation of OSMR pathway in CAF-173 contributes to tumour progression. It will be interesting to perform future experiments to determine if OSM also potentiates a pro-malignant behaviour in CAF-318, CAF-220 and CAF-200 *in vivo* as it would demonstrate if OSM signalling targets CAFs in general or if there is a specific CAFs subpopulation with specific characteristics more prone to benefit from OSM signalling to promote breast cancer progression. Of note, scRNA-seq data presented in Fig. 3.2.2 revealed that myofibroblasts, ECM and inflammatory CAFs all presented similar levels of OSMR expression, which points to possible important roles in all populations.

It will also be important to determine if normal fibroblasts once in contact with tumour cells become susceptible to OSM-mediated induction of activation markers. Co-culture of cancer cells and normal fibroblasts and posterior OSM treatment of fibroblasts could be done prior to co-injections. This experiment will determine if normal fibroblasts need to be primed by tumour cells first to become susceptible to OSM pro-tumoral effect.

Despite clear evidence presented in this thesis supporting that OSM:OSMR axis in CAFs contributes to cancer progression, nevertheless, the effect of OSM on other TME cells cannot be discarded. FACs sorting data presented in Fig. 3.2.3 revealed that endothelial cells also present OSMR expression. Multiple studies have reported endothelial activation mediated by OSM signalling in other diseases[279–281]. Cytokine mediated activation of endothelial cells can trigger the expression of inflammatory markers, which can sustain or exacerbate inflammatory processes[282]. Further studies would need to be done to determine if OSM also acts on endothelial cells and if this action contributes to tumour inflammation and cancer progression.

4.4 OSM:OSMR axis shapes the immune system in the tumour microenvironment.

The last experiments of this thesis aimed to determine the effect of OSM signalling in modulating the immune system. Up to date, very few studies focused on the role of OSM:OSMR axis in shaping the tumour infiltrates. In this thesis it was shown that several factors upregulated by OSM in CAFs are associated with immune regulation such as FAP[75] and IL-6[126] which already suggested that OSM was potentially modulating the immune compartment through CAFs signalling.

Microarray data analysis (Fig. 3.3.1 and 3.3.2) revealed that OSM induced inflammatory signatures and pathways in both CAF-173 and MDA-MB-231 tumour cells. In addition, leukocyte chemotaxis was one of the enhanced pathways after OSM treatment in both cell lines which strongly suggested that OSM could be contributing to inflammation in BC. Of interest, OSM levels were also associated with inflammation in human breast cancer samples present in the TMA. Chemokine arrays revealed that OSM induces in CAFs and in cancer cells the secretion of important myeloid chemoattractants. Some of them are

fibroblast-specific (i.e. CXCL10, CXCL12 and CXCL16), others are cancer cell-specific (e.g. CXCL7), and several are induced by both cell types (e.g. VEGF, CCL2 and CXCL1), supporting activation of cell-specific transcriptional programmes by OSM[144]. OSM has previously been described to induce VEGF and CXCL1[184,283]. However, for the first time it was shown that OSM induces the neutrophil chemoattractant CXCL7 in tumour cells, previously described as a prognostic factor in clear cell renal cell carcinoma[284]. The list of OSM-induced chemokines includes CXCR2 and CCR2 ligands (i.e. CXCL1, CXCL8 and CCL2). Of interest, inhibition of recruitment of myeloid derived suppressor cells (MDSCs) by blocking CCR2 and CXCR2 activation disrupts the formation of pre-metastatic niches and inhibits metastasis[285]. This *in vitro* data strongly suggested that OSM:OSMR signalling could be involved in modulating the recruitment of myeloid cells to the tumour niche. Importantly, OSM was found to correlate with myeloid infiltration in human breast tumours (Fig. 3.2.4), which, again, indicates that myeloid chemoattractants liberated by OSM activated CAFs and tumour cells are possibly promoting the recruitment of myeloid cells to the tumour niche and establishing a feedforward loop of constant OSM secretion to the tumour.

On top of that, conditioned media assays *in vitro* (Fig. 3.3.4) showed that CM from macrophages induce OSMR in tumour cells while CM from OSM activated MDA-MB-231 cells induce further OSM release in macrophages indicating the possible existence of additional positive loops (Fig. 4.1) that would ensure constant OSM liberation into the tumour microenvironment. Similar cancer cell-induced stimulation of OSM in macrophages and neutrophils has also been described by other groups[286,287].

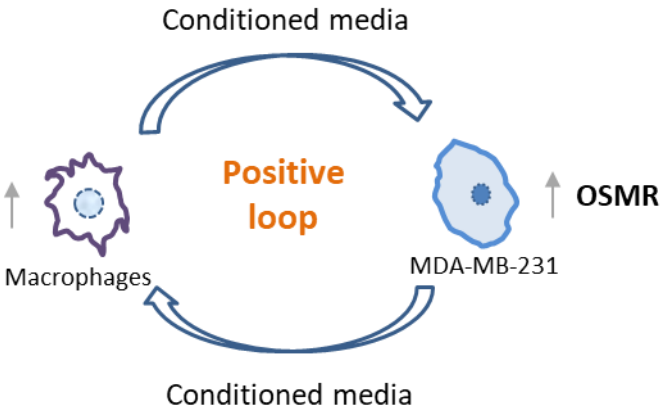

Fig. 4.1: Proposed working model of the paracrine signalling between macrophages and cancer cells resulting in activation of positive feedback loops.

Experiments to determine the effect of CM from macrophages on fibroblasts were not performed, but as it is clear now that myeloid cells express OSM and that fibroblasts present high expression of OSMR, it would be expected that CM from macrophages would activate OSMR pathway in fibroblasts and induce downstream targets.

At this point, it was important to determine functionally if OSM:OSMR axis was regulating myeloid infiltration and the MMTV-PyMT mouse model was used to answer this question. The data presented in Fig. 3.3.3 revealed that OSMR KO mice had less infiltration of Ly6G+ (neutrophils) and F4/80+ (macrophages) cells in the tumours demonstrating that OSMR signalling contributes to myeloid cell recruitment. Importantly, VEGF, CXCL1 and CXCL16, previously described as strong myeloid chemoattractants[249,288,289], were found to be downregulated in the serum of MMTV-PyMT OSMR deficient mice, indicating that OSM signalling also regulates their secretion *in vivo*. Of note, OSM and OSMR expression was found to correlate with VEGF, CXCL1 and CXCL16 in breast cancer tumours, and the three factors associate with poorer RFS in breast cancer patients. These results strongly suggest that OSM signalling promotes the recruitment of Ly6G+ and F4/80+ myeloid cells to the tumour through OSM-induced secretion of chemokines by both CAFs and cancer cells. These recruited myeloid cells will then increase the secretion of OSM within the tumour, inducing a feed-forward loop summarised in the proposed working model in Fig. 4.2. Decreased numbers of Ly6G+ neutrophils and F4/80+ macrophages may explain, at least in part, the strong anti-tumoral and anti-metastatic effect of OSMR depletion in the PyMT cancer model, as blocking neutrophil recruitment to the pre-metastatic niche with anti-Ly6G antibodies inhibits metastasis[290] and impairing recruitment of tumour-associated macrophages reduces tumour incidence and metastasis[291–293] in MMTV-PyMT mice. Ly6G is also considered a marker of granulocytic MDSCs[56], so IHC staining of LY6G+ in MMTV-PyMT tumour slides cannot exclude the presence of these cells in the samples. Of interest, MDSCs are also involved in the promotion of metastasis in the MMTV-PyMT model[294].

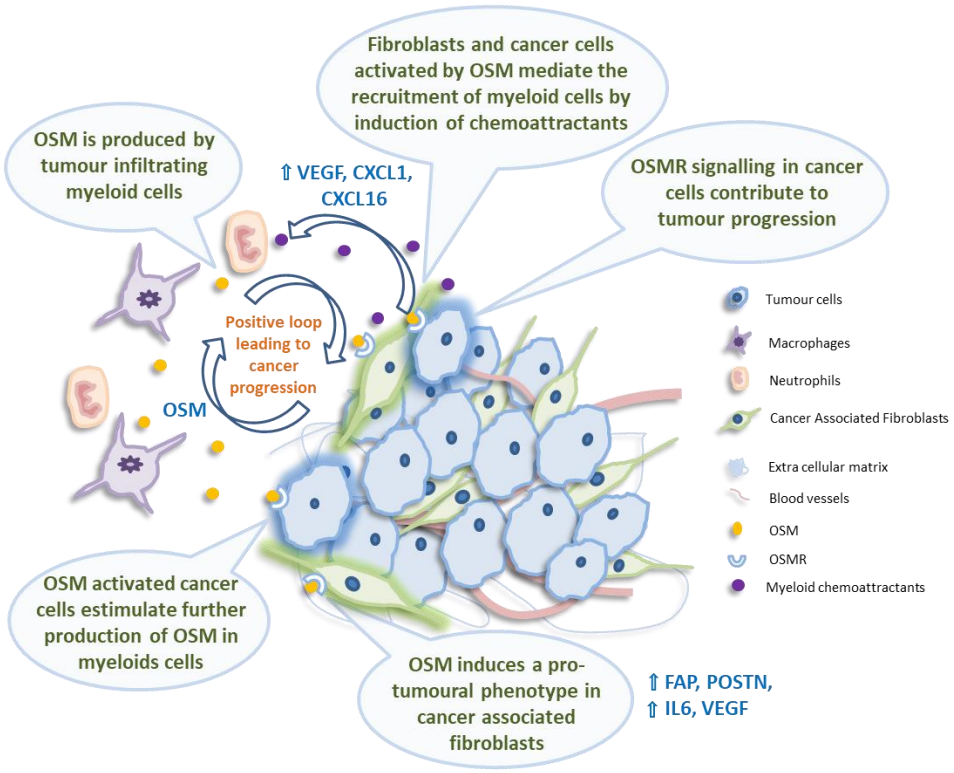

Fig. 4.2: Proposed working model for the effects of OSM signalling in breast cancer.
Myeloid cells express OSM which activates the OSMR pathway in cancer cells and cancer-associated fibroblasts (CAFs). OSM signalling in CAFs induces classical fibroblast activation markers such as FAP, POSTN, IL-6 and VEGF. This paracrine signalling induces CAFs pro-malignant phenotype by increasing their contractility and proliferation. At the same time, OSM induces myeloid chemoattractants in CAFs and cancer cells such as VEGF, CXCL1, CCXL16, CXCL12 and CCL2. This chemokine secretion results in myeloid tumour infiltration, that is further stimulated by cancer cells to induce OSM expression, creating a positive feedback loop that ensures constant secretion of OSM and sustained tumour progression. Disrupting this cancer cells-tumour microenvironment communication by blocking OSM:OSMR interactions could be a potential therapeutic strategy for breast cancer therapy.

OSM was described to induce M2 polarization in macrophages[204]. The results present in this thesis showed that immune cells and HL-60 cells differentiated to macrophages with TPA express extremely low levels of OSMR, bringing up the possibility that OSM affects macrophage polarization through other mechanisms and not by direct OSMR activation. To confirm the M2 polarization of macrophages by OSM, blood derived monocytes were extracted from healthy donors. The results (Fig. 3.3.5) showed that treatment of monocytes with recombinant OSM did not induce M2 macrophage polarization,

contradicting previous reports. Interestingly, Ayahub *et al* (2017)[295] reported that overexpression of OSM and/or IL-6 promoted myofibroblast accumulation in the lungs but that only IL-6 had the capacity to convert macrophages into a M2-like phenotype. Of note, Tripathi *et al* (2014)[204] has performed all polarization experiments under hypoxic conditions which raises the question if OSM induced polarization of macrophages is dependent on factors such as the hypoxic state of the tumour. It would be interesting to perform future experiments to answer this question.

Fig. 3.3.5 also showed that CM from MDA-MB-231 cancer cells reduced macrophage polarization towards M1 or M2-like profile while CM from CAF-173 induced M2 markers in monocytes suggesting that cancer cells could be halting monocyte differentiation into M1 or M2-like macrophages maintaining them into a more "stem" state while CAFs would drive them towards a pro-malignant M2-like phenotype, all independently from OSM signalling. This is still preliminary data that would need to be confirmed using different tumour cells and CAFs. As mentioned above, IL-6 was also reported to induce M2-like phenotype in macrophages in the lungs[295]. Despite knowing that OSM induces IL-6 in CAF-173, no significant differences were found in the effect of macrophages polarization through CM of OSM-induced CAF-173. These data lead to the conclusion that OSM was not directly impacting macrophages polarization within this experimental setting. This does not exclude the possibility that macrophages, within the tumoral context, would respond to cues induced by OSM on other types of cells that would promote their differentiation towards M2-like phenotype. Further experiments would need to be done to confirm this hypothesis.

4.5 Summary and future perspectives

In summary, the data presented in this thesis demonstrate that OSM:OSMR axis is associated with worse prognosis in breast cancer patients. OSM orchestrates a pro-tumoral crosstalk between myeloid cells, CAFs and cancer cells that has important consequences in tumour progression (Fig. 4.2). Induction of OSM:OSMR signalling in cancer cells leads to earlier tumour onset and development of lung metastasis. Constitutive genetic depletion of OSMR in the MMTV-PyMT genetic mouse model delays tumour onset, reduces tumour

growth and lung metastasis. In addition, injection of murine cancer cells in OSMR deficient mice reduced tumour burden and delayed tumour onset compared to WT mice, supporting that OSM signalling is important in both the cancer cell compartment and in the tumour microenvironment. OSM-activated CAFs were found to contribute to the tumour microenvironment influence on tumour progression. Importantly, OSMR depletion in the MMTV-PyMT breast cancer model has a profound effect in reducing metastasis, compared to its effect in tumour onset and tumour growth. In view of these results, the role of OSM:OSMR signalling in the pre-metastatic niche requires further investigation. Analysis of human breast cancer samples revealed that the results are clinically relevant, showing that OSM and its receptor OSMR are upregulated in breast cancer stroma and their transcriptional signature is associated with decreased survival. Furthermore, targeting OSM:OSMR signalling could be a new therapeutic strategy in breast cancer as targeting IL-6:IL6R in the clinic has revealed some associated toxicity [271,272]. OSM:OSMR interactions could be blocked by antibody based inhibition, a strategy that has had a major impact on cancer[296], which makes them a promising candidate for therapeutic targeting. Interestingly, anti-OSM humanized antibodies have proven to be safe and well tolerated[297] and are now in Phase 2 clinical trials for the treatment of inflammatory diseases, such as systemic sclerosis and Crohn's disease[298].

Recently, a study has been published using tofacitinib (JAK1/3 inhibitor) to treat granuloma annulare, an inflammatory disease characterised by macrophage accumulation and activation in skin. In this study, the authors have identified some JAK-STAT-dependent cytokines, including IFN-gama and OSM as possible drivers of the disease. Treatment of 5 patients with tofacitinib inhibited IFN-gama, Oncostatin M, as well as IL-15 and IL-21, activity and resulted in clinical and histologic disease remission in 3 patients and marked improvement in the other 2 without major toxicity[299]. This study has demonstrated that targeting cytokines activity can reduce inflammatory biomarkers and result in disease remission, strategy that could be applied in other diseases.

Together, the findings present in this thesis further strengthen the case for the pre-clinical investigation of OSM:OSMR blocking antibodies/inhibitors as a targeted anti-cancer therapy.

A collaboration has been established with Gerhard Müller-Newen group in Germany which has developed different receptor fusion proteins for the inhibition of murine Oncostatin M[300] (Fig. 4.3). mOSM-RFP is the one that was proved to be more effective in blocking OSM signalling *in vitro* and it will be tested *in vivo* in our breast cancer mouse models.

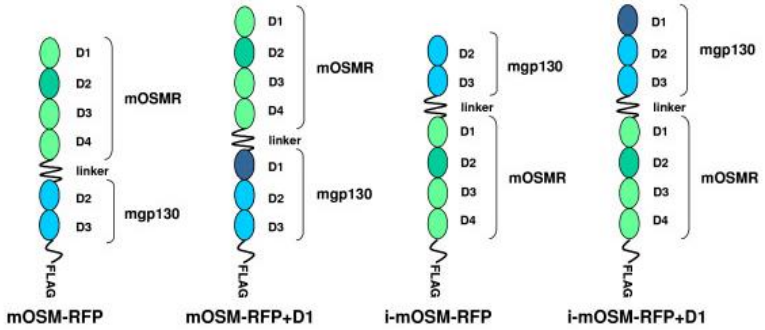

Fig. 4.3: Receptor fusion proteins designed to inhibit murine Oncostatin M. Reproduced from: Brolund *et al* (2011)[300].

To test weather inhibition of OSM:OSMR pathway *in vivo* halts tumour progression without major associated biological toxicity, we are planning to test this therapeutic strategy in the MMTV-PyMT mouse model and assess all parameters described in this thesis such as effect on tumour onset, growth, metastasis and molecular characteristics. In the future it would be interesting to test this therapeutic strategy in other models of cancer such as colon, pancreatic, ovarian, sarcoma… etc, since clinical data revealed that high OSM:OSMR levels were also associated with worse survival in those types of cancer.

Another interesting line of research would be to study the effect of OSM signalling in the liver and its contribution to liver inflammation and malignancy. In the orthotopic xenografts experiments (Fig. 3.1.10), all hOSM animals presented increased liver inflammation (data not shown) that the group hypothesised to be a secondary effect of the presence of human OSM in blood circulation of those animals that could be signalling through mouse LIFR and promote liver inflammation. Andrea Abaurrea and Peio Azcoaga are currently investigating the effect of OSM:OSMR signalling in liver hepatocarcinoma.

In this thesis, OSM:OSMR axis was demonstrated to modulate myeloid cell recruitment in the MMTV-PyMT tumours. Despite not finding direct effect on macrophage differentiation in the experiments performed, it would be interesting to explore further this topic using other models such as tumour associated macrophages instead of primary monocytes from

healthy donors. It might happen that, like fibroblasts, monocytes need to be tumour-primed before being able to respond to OSM effect on polarization. It would also be interesting to extend the analysis to other immune cell types such as Tregs since some studies have already described the role of OSM in shaping the phenotype of these cells in other diseases[301].

Preliminary data obtained at the i3S in Porto indicated that OSM upregulates PDL-1 expression in MDA-MB-231 cells (data not shown) suggesting that OSM might be involved in contributing to the escape of tumour cells from the T cells surveillance and promoting an immune suppressive TME. Currently, the effect of OSM in immune suppression and response to immunotherapy is a future line of research that the group is developing in collaboration with Prof. Maria Oliveira in i3S Porto.

Chapter 5: Conclusions

1. Oncostatin M (OSM) and Oncostatin M receptor (OSMR) are associated with poor overall survival in breast cancer, especially in the ER- tumours, and in other types of tumours.

2. OSMR pathway is over-activated in ER- breast cancer, and cancer cells do not express biological significant levels of OSM.

3. OSM signalling through OSMR receptor promotes tumorigenesis, tumour growth and metastasis in multiple mouse models of breast cancer.

4. OSM:OSMR signalling module is increased in the tumour microenvironment of breast cancer and other tumour types, and it exhibits a distinct microenvironment-restricted expression, compared to other members of IL-6 family: OSM is mostly expressed by myeloid cells while OSMR is present in tumour cells and fibroblasts.

5. OSM:OSMR signalling in the tumour microenvironment contributes to tumour progression.

6. OSM signalling induces pro-malignant features in CAFs, including proliferation and increased contractility, that have a great impact on tumorigenesis, tumour growth and metastasis.

7. OSM induces an inflammatory signature and secretion of chemoattractants in CAFs and cancer cells (e.g. VEGF, CXCL1 and CXCL16) and contributes to the remodelling of the tumour immune landscape by increasing the recruitment of myeloid cells.

8. OSM signalling in the tumour induces additional feed-forward loops, as conditioned media from macrophages induces OSMR in cancer cells while conditioned media from cancer cells induces OSM expression in macrophages.

9. OSM:OSMR axis is an attractive therapeutic target for BC as the data presented in this thesis supports that its inhibition would reduce tumour promoting inflammation and halt tumour progression.

References

1. Bray, F. *et al.* Global cancer statistics 2018: GLOBOCAN estimates of incidence and mortality worldwide for 36 cancers in 185 countries. *CA. Cancer J. Clin.* **68**, 394–424 (2018).

2. Leon-Ferre, R. A. *et al.* A contemporary review of male breast cancer: current evidence and unanswered questions. *Cancer Metastasis Rev.* **37**, 599–614 (2018).

3. Malvezzi, M. *et al.* European cancer mortality predictions for the year 2019 with focus on breast cancer. *Ann. Oncol. Off. J. Eur. Soc. Med. Oncol.* **30**, 781–787 (2019).

4. DeSantis, C. E. *et al.* Breast cancer statistics, 2019. *CA. Cancer J. Clin.* **69**, 438–451 (2019).

5. Coleman, M. P. *et al.* Cancer survival in five continents: a worldwide population-based study (CONCORD). *Lancet. Oncol.* **9**, 730–756 (2008).

6. DeSantis, C. E. *et al.* Breast cancer statistics, 2015: Convergence of incidence rates between black and white women. *CA. Cancer J. Clin.* **66**, 31–42 (2016).

7. CRUK. Breast cancer incidence (invasive) statistics. https://www.cancerresearchuk.org/health-professional/cancer-statistics/statistics-by-cancer-type/breast-cancer/incidence-invasive#heading-One (2019).

8. Hermelink, K. *et al.* Chemotherapy and Post-traumatic Stress in the Causation of Cognitive Dysfunction in Breast Cancer Patients. *J. Natl. Cancer Inst.* **109**, (2017).

9. Arrospide, A. *et al.* Cost of breast cancer treatment by clinical stage in the Basque Country, Spain. *Rev. Esp. Salud Publica* **89**, 93–97 (2015).

10. Li, C. I., Anderson, B. O., Daling, J. R. & Moe, R. E. Trends in incidence rates of invasive lobular and ductal breast carcinoma. *JAMA* **289**, 1421–1424 (2003).

11. Edge, S. B. & Compton, C. C. The American Joint Committee on Cancer: the 7th edition of the AJCC cancer staging manual and the future of TNM. *Ann. of Surg. Oncol*. **17** 1471–1474 (2010).

12. Harbeck, N. *et al.* Breast cancer. *Nat. Rev. Dis. Prim.* **5**, 66 (2019).

13. Coates, A. S. *et al.* Tailoring therapies--improving the management of early breast cancer: St Gallen International Expert Consensus on the Primary Therapy of Early Breast Cancer 2015. *Ann. Oncol. Off. J. Eur. Soc. Med. Oncol.* **26**, 1533–1546 (2015).

14. Howlader, N. *et al.* US incidence of breast cancer subtypes defined by joint hormone receptor and HER2 status. *J. Natl. Cancer Inst.* **106**, (2014).

15. Hammond, M. E. H. *et al.* American Society of Clinical Oncology/College of American Pathologists guideline recommendations for immunohistochemical testing of estrogen and progesterone receptors in breast cancer (unabridged version). *Arch. Pathol. Lab. Med.* **134**, e48-72 (2010).

16. Gao, J. J. & Swain, S. M. Luminal A Breast Cancer and Molecular Assays: A Review. *Oncologist* **23**, 556–565 (2018).

17. Voduc, K. D. *et al.* Breast Cancer Subtypes and the Risk of Local and Regional Relapse. *J.*

Clin. Oncol. Off. J. Am. Soc. Clin. Oncol. **28**, 1684–1691 (2010).

18. Bentzon, N., Düring, M., Rasmussen, B. B., Mouridsen, H. & Kroman, N. Prognostic effect of estrogen receptor status across age in primary breast cancer. *Int. J. cancer* **122**, 1089–1094 (2008).

19. James, T. A. & Vick, L. *Breast*. *Essentials of General Surgery and Surgical Specialties: Sixth Edition* (2018). doi:10.5005/jp/books/14184_23.

20. Boyle, P. Triple-negative breast cancer: epidemiological considerations and recommendations. *Ann. Oncol. Off. J. Eur. Soc. Med. Oncol.* **23 Suppl 6**, vi7-12 (2012).

21. Dent, R. *et al.* Triple-negative breast cancer: clinical features and patterns of recurrence. *Clin. cancer Res. an Off. J. Am. Assoc. Cancer Res.* **13**, 4429–4434 (2007).

22. Finnegan, T. J. & Carey, L. A. Gene-expression analysis and the basal-like breast cancer subtype. *Future Oncol.* **3**, 55–63 (2007).

23. Sørlie, T. *et al.* Gene expression patterns of breast carcinomas distinguish tumor subclasses with clinical implications. *Proc. Natl. Acad. Sci. U. S. A.* **98**, 10869–10874 (2001).

24. Perou, C. M. *et al.* Molecular portraits of human breast tumours. *Nature* **406**, 747–752 (2000).

25. Dai, X. *et al.* Breast cancer intrinsic subtype classification, clinical use and future trends. *Am. J. Cancer Res.* **5**, 2929–2943 (2015).

26. Parker, J. S. *et al.* Supervised risk predictor of breast cancer based on intrinsic subtypes. *J. Clin. Oncol. Off. J. Am. Soc. Clin. Oncol.* **27**, 1160–1167 (2009).

27. Cheang, M. C. U. *et al.* Ki67 index, HER2 status, and prognosis of patients with luminal B breast cancer. *J. Natl. Cancer Inst.* **101**, 736–750 (2009).

28. Russnes, H. G., Lingjærde, O. C., Børresen-Dale, A.-L. & Caldas, C. Breast Cancer Molecular Stratification: From Intrinsic Subtypes to Integrative Clusters. *Am. J. Pathol.* **187**, 2152–2162 (2017).

29. Toft, D. J. & Cryns, V. L. Minireview: Basal-like breast cancer: from molecular profiles to targeted therapies. *Mol. Endocrinol.* **25**, 199–211 (2011).

30. Kreike, B. *et al.* Gene expression profiling and histopathological characterization of triple-negative/basal-like breast carcinomas. *Breast Cancer Res.* **9**, R65 (2007).

31. Badve, S. *et al.* Basal-like and triple-negative breast cancers: a critical review with an emphasis on the implications for pathologists and oncologists. *Mod. Pathol.* **24**, 157–167 (2011).

32. Prat, A. *et al.* Phenotypic and molecular characterization of the claudin-low intrinsic subtype of breast cancer. *Breast Cancer Res.* **12**, R68 (2010).

33. Fougner, C., Bergholtz, H., Norum, J. H. & Sørlie, T. Re-definition of claudin-low as a breast cancer phenotype. *Nat. Commun.* **11**, 1787 (2020).

34. Cardoso, F. *et al.* Early breast cancer: ESMO Clinical Practice Guidelines for diagnosis, treatment and follow-up. *Ann. Oncol. Off. J. Eur. Soc. Med. Oncol.* **30**, 1674 (2019).

35. Darby, S. *et al.* Effect of radiotherapy after breast-conserving surgery on 10-year recurrence and 15-year breast cancer death: meta-analysis of individual patient data for

10,801 women in 17 randomised trials. *Lancet* **378**, 1707–1716 (2011).

36. Cardoso, F. *et al.* 4th ESO-ESMO International Consensus Guidelines for Advanced Breast Cancer (ABC 4)†. *Ann. Oncol. Off. J. Eur. Soc. Med. Oncol.* **29**, 1634–1657 (2018).

37. Puhalla, S., Bhattacharya, S. & Davidson, N. E. Hormonal therapy in breast cancer: a model disease for the personalization of cancer care. *Mol. Oncol.* **6**, 222–236 (2012).

38. Cobleigh, M. A. *et al.* Multinational study of the efficacy and safety of humanized anti-HER2 monoclonal antibody in women who have HER2-overexpressing metastatic breast cancer that has progressed after chemotherapy for metastatic disease. *J. Clin. Oncol. Off. J. Am. Soc. Clin. Oncol.* **17**, 2639–2648 (1999).

39. Figueroa-Magalhães, M. C., Jelovac, D., Connolly, R. & Wolff, A. C. Treatment of HER2-positive breast cancer. *Breast* **23**, 128–136 (2014).

40. Swain, S. M. *et al.* Pertuzumab, trastuzumab, and docetaxel in HER2-positive metastatic breast cancer. *N. Engl. J. Med.* **372**, 724–734 (2015).

41. van Dongen, J. A. *et al.* Long-term results of a randomized trial comparing breast-conserving therapy with mastectomy: European Organization for Research and Treatment of Cancer 10801 trial. *J. Natl. Cancer Inst.* **92**, 1143–1150 (2000).

42. Kennecke, H. *et al.* Metastatic behavior of breast cancer subtypes. *J. Clin. Oncol. Off. J. Am. Soc. Clin. Oncol.* **28**, 3271–3277 (2010).

43. Paplomata, E. & O'Regan, R. The PI3K/AKT/mTOR pathway in breast cancer: targets, trials and biomarkers. *Ther. Adv. Med. Oncol.* **6**, 154–166 (2014).

44. Baselga, J. *et al.* Everolimus in postmenopausal hormone-receptor-positive advanced breast cancer. *N. Engl. J. Med.* **366**, 520–529 (2012).

45. Sidaway, P. Survival data from PALOMA-3 reported. *Nat. Rev. Clin. Oncol.* **15**, 725 (2018).

46. Verma, S. *et al.* Trastuzumab emtansine for HER2-positive advanced breast cancer. *N. Engl. J. Med.* **367**, 1783–1791 (2012).

47. Gelmon, K. *et al.* Targeting triple-negative breast cancer: optimising therapeutic outcomes. *Ann. Oncol. Off. J. Eur. Soc. Med. Oncol.* **23**, 2223–2234 (2012).

48. Tutt, A. *et al.* Oral poly(ADP-ribose) polymerase inhibitor olaparib in patients with BRCA1 or BRCA2 mutations and advanced breast cancer: a proof-of-concept trial. *Lancet* **376**, 235–244 (2010).

49. Caulfield, S. E., Davis, C. C. & Byers, K. F. Olaparib: A Novel Therapy for Metastatic Breast Cancer in Patients With a BRCA1/2 Mutation. *J. Adv. Pract. Oncol.* **10**, 167–174 (2019).

50. Reinert, T. & Barrios, C. H. Optimal management of hormone receptor positive metastatic breast cancer in 2016. *Ther. Adv. Med. Oncol.* **7**, 304–320 (2015).

51. Lavaud, P. & Andre, F. Strategies to overcome trastuzumab resistance in HER2-overexpressing breast cancers: focus on new data from clinical trials. *BMC Med.* **12**, 132 (2014).

52. Yang, H. *et al.* Impact of molecular subtypes on metastatic behavior and overall survival in patients with metastatic breast cancer: A single-center study combined with a large cohort study based on the Surveillance, Epidemiology and End Results database. *Oncol. Lett.* **20**, 87 (2020).

53. Diaz Bessone, M. I., Gattas, M. J., Laporte, T., Tanaka, M. & Simian, M. The Tumor Microenvironment as a Regulator of Endocrine Resistance in Breast Cancer. *Front. Endocrinol.* **10**, 547 (2019).

54. Chen, F. *et al.* New horizons in tumor microenvironment biology: challenges and opportunities. *BMC Med.* **13**, 45 (2015).

55. Sun, Y. Tumor microenvironment and cancer therapy resistance. *Cancer Lett.* **380**, 205–215 (2016).

56. Quail, D. F. & Joyce, J. A. Microenvironmental regulation of tumor progression and metastasis. *Nat. Med.* **19**, 1423–1437 (2013).

57. Whiteside, T. L. The tumor microenvironment and its role in promoting tumor growth. *Oncogene* **27**, 5904–5912 (2008).

58. Roma-Rodrigues, C., Mendes, R., Baptista, P. V & Fernandes, A. R. Targeting Tumor Microenvironment for Cancer Therapy. *Int. J. Mol. Sci.* **20**, (2019).

59. Valkenburg, K. C., de Groot, A. E. & Pienta, K. J. Targeting the tumour stroma to improve cancer therapy. *Nat. Rev. Clin. Oncol.* **15**, 366–381 (2018).

60. Werb, Z. & Lu, P. The Role of Stroma in Tumor Development. *Cancer J.* **21**, 250–253 (2015).

61. Poltavets, V., Kochetkova, M., Pitson, S. M. & Samuel, M. S. The Role of the Extracellular Matrix and Its Molecular and Cellular Regulators in Cancer Cell Plasticity. *Front. Oncol.* **8**, 431 (2018).

62. Bainbridge, P. Wound healing and the role of fibroblasts. *J. Wound Care* **22**, 407-408,410-412 (2013).

63. LeBleu, V. S. & Kalluri, R. A peek into cancer-associated fibroblasts: origins, functions and translational impact. *Dis. Model. Mech.* **11**, (2018).

64. Sahai, E. *et al.* A framework for advancing our understanding of cancer-associated fibroblasts. *Nat. Rev. Cancer* **20**, 174–186 (2020).

65. Sharon, Y. *et al.* Tumor-derived osteopontin reprograms normal mammary fibroblasts to promote inflammation and tumor growth in breast cancer. *Cancer Res.* **75**, 963–973 (2015).

66. Raz, Y. *et al.* Bone marrow-derived fibroblasts are a functionally distinct stromal cell population in breast cancer. *J. Exp. Med.* **215**, 3075–3093 (2018).

67. Kidd, S. *et al.* Origins of the tumor microenvironment: quantitative assessment of adipose-derived and bone marrow-derived stroma. *PLoS One* **7**, e30563 (2012).

68. Zeisberg, E. M., Potenta, S., Xie, L., Zeisberg, M. & Kalluri, R. Discovery of endothelial to mesenchymal transition as a source for carcinoma-associated fibroblasts. *Cancer Res.* **67**, 10123–10128 (2007).

69. Monteran, L. & Erez, N. The Dark Side of Fibroblasts: Cancer-Associated Fibroblasts as Mediators of Immunosuppression in the Tumor Microenvironment. *Front. Immunol.* **10**, 1835 (2019).

70. Liu, L. *et al.* Stromal Myofibroblasts Are Associated with Poor Prognosis in Solid Cancers: A Meta-Analysis of Published Studies. *PLoS One* **11**, e0159947 (2016).

71. Kalluri, R. The biology and function of fibroblasts in cancer. *Nat. Rev. Cancer* **16**, 582–598 (2016).

72. Kalluri, R. & Zeisberg, M. Fibroblasts in cancer. *Nat. Rev. Cancer* **6**, 392–401 (2006).

73. Gascard, P. & Tlsty, T. D. Carcinoma-associated fibroblasts: orchestrating the composition of malignancy. *Genes Dev.* **30**, 1002–1019 (2016).

74. Servais, C. & Erez, N. From sentinel cells to inflammatory culprits: cancer-associated fibroblasts in tumour-related inflammation. *J. Pathol.* **229**, 198–207 (2013).

75. Costa, A. *et al.* Fibroblast Heterogeneity and Immunosuppressive Environment in Human Breast Cancer. *Cancer Cell* **33**, 463-479.e10 (2018).

76. Gabrilovich, D. I., Ostrand-Rosenberg, S. & Bronte, V. Coordinated regulation of myeloid cells by tumours. *Nat. Rev. Immunol.* **12**, 253–268 (2012).

77. Axelrod, H. & Pienta, K. J. Axl as a mediator of cellular growth and survival. *Oncotarget* **5**, 8818–8852 (2014).

78. Epelman, S., Lavine, K. J. & Randolph, G. J. Origin and functions of tissue macrophages. *Immunity* **41**, 21–35 (2014).

79. Schouppe, E., De Baetselier, P., Van Ginderachter, J. A. & Sarukhan, A. Instruction of myeloid cells by the tumor microenvironment: Open questions on the dynamics and plasticity of different tumor-associated myeloid cell populations. *Oncoimmunology* **1**, 1135–1145 (2012).

80. Haas, L. & Obenauf, A. C. Allies or Enemies-The Multifaceted Role of Myeloid Cells in the Tumor Microenvironment. *Front. Immunol.* **10**, 2746 (2019).

81. Coussens, L. M. & Werb, Z. Inflammation and cancer. *Nature* **420**, 860–867 (2002).

82. Virchow R.A. *Die Cellularpathologie in Ihrer Begründung auf Physiologische und Pathologische Gewebelehre*. (Hirschwald, 1858).

83. Dvorak, H. F. Tumors: wounds that do not heal. Similarities between tumor stroma generation and wound healing. *N. Engl. J. Med.* **315**, 1650–1659 (1986).

84. Hanahan, D. & Weinberg, R. A. Hallmarks of cancer: the next generation. *Cell* **144**, 646–674 (2011).

85. Greten, F. R. & Grivennikov, S. I. Inflammation and Cancer: Triggers, Mechanisms, and Consequences. *Immunity* **51**, 27–41 (2019).

86. Grivennikov, S. I., Greten, F. R. & Karin, M. Immunity, inflammation, and cancer. *Cell* **140**, 883–899 (2010).

87. Osuský, R., Malik, P. & Ryan, S. J. Retinal pigment epithelium cells promote the maturation of monocytes to macrophages in vitro. *Ophthalmic Res.* **29**, 31–36 (1997).

88. Wynn, T. A. & Barron, L. Macrophages: master regulators of inflammation and fibrosis. *Semin. Liver Dis.* **30**, 245–257 (2010).

89. Moustakas, A., Pardali, K., Gaal, A. & Heldin, C. H. Mechanisms of TGF-beta signaling in regulation of cell growth and differentiation. *Immunol. Lett.* **82**, 85–91 (2002).

90. Multhoff, G., Molls, M. & Radons, J. Chronic inflammation in cancer development. *Front. Immunol.* **2**, 98 (2012).

91. Maeda, H. & Akaike, T. Nitric oxide and oxygen radicals in infection, inflammation, and cancer. *Biochemistry.* **63**, 854–865 (1998).

92. Mantovani, A., Allavena, P., Sica, A. & Balkwill, F. Cancer-related inflammation. *Nature* **454**, 436–444 (2008).

93. Binnewies, M. *et al.* Understanding the tumor immune microenvironment (TIME) for effective therapy. *Nat. Med.* **24**, 541–550 (2018).

94. Liao, W. *et al.* KRAS-IRF2 Axis Drives Immune Suppression and Immune Therapy Resistance in Colorectal Cancer. *Cancer Cell* **35**, 559-572.e7 (2019).

95. Dmitrieva-Posocco, O. *et al.* Cell-Type-Specific Responses to Interleukin-1 Control Microbial Invasion and Tumor-Elicited Inflammation in Colorectal Cancer. *Immunity* **50**, 166-180.e7 (2019).

96. Grivennikov, S. *et al.* IL-6 and Stat3 are required for survival of intestinal epithelial cells and development of colitis-associated cancer. *Cancer Cell* **15**, 103–113 (2009).

97. Karin, M. & Greten, F. R. NF-kappaB: linking inflammation and immunity to cancer development and progression. *Nat. Rev. Immunol.* **5**, 749–759 (2005).

98. Vakkila, J. & Lotze, M. T. Inflammation and necrosis promote tumour growth. *Nature reviews. Immunology* **4**, 641–648 (2004).

99. Huang, F.-P. Autoimmuno-Anti-Tumor Immunity - Understanding the Immune Responses against 'self' and 'Altered-Self'. *Front. Immunol.* **5**, 582 (2014).

100. Melero, I., Rouzaut, A., Motz, G. T. & Coukos, G. T-cell and NK-cell infiltration into solid tumors: a key limiting factor for efficacious cancer immunotherapy. *Cancer Discov.* **4**, 522–526 (2014).

101. Munn, D. H. & Bronte, V. Immune suppressive mechanisms in the tumor microenvironment. *Curr. Opin. Immunol.* **39**, 1–6 (2016).

102. Garrido, F., Aptsiauri, N., Doorduijn, E. M., Garcia Lora, A. M. & van Hall, T. The urgent need to recover MHC class I in cancers for effective immunotherapy. *Curr. Opin. Immunol.* **39**, 44–51 (2016).

103. Awad, R. M., De Vlaeminck, Y., Maebe, J., Goyvaerts, C. & Breckpot, K. Turn Back the TIMe: Targeting Tumor Infiltrating Myeloid Cells to Revert Cancer Progression. *Front. Immunol.* **9**, 1977 (2018).

104. Kortylewski, M. & Yu, H. Role of Stat3 in suppressing anti-tumor immunity. *Curr. Opin. Immunol.* **20**, 228–233 (2008).

105. Dufait, I. *et al.* Signal transducer and activator of transcription 3 in myeloid-derived suppressor cells: an opportunity for cancer therapy. *Oncotarget* **7**, 42698–42715 (2016).

106. Burkholder, B. *et al.* Tumor-induced perturbations of cytokines and immune cell networks. *Biochim. Biophys. Acta* **1845**, 182–201 (2014).

107. Barroso-Sousa, R. *et al.* Prevalence and mutational determinants of high tumor mutation burden in breast cancer. *Ann. Oncol. Off. J. Eur. Soc. Med. Oncol.* **31**, 387–394 (2020).

108. Gatti-Mays, M. E. *et al.* If we build it they will come: targeting the immune response to breast cancer. *NPJ breast cancer* **5**, 37 (2019).

109. Tower, H., Ruppert, M. & Britt, K. The Immune Microenvironment of Breast Cancer

Progression. *Cancers* **11**, (2019).

110. Taniguchi, K. & Karin, M. IL-6 and related cytokines as the critical lynchpins between inflammation and cancer. *Semin. Immunol.* **26**, 54–74 (2014).

111. Denkert, C. *et al.* Tumor-associated lymphocytes as an independent predictor of response to neoadjuvant chemotherapy in breast cancer. *J. Clin. Oncol. Off. J. Am. Soc. Clin. Oncol.* **28**, 105–113 (2010).

112. Denkert, C. *et al.* Tumour-infiltrating lymphocytes and prognosis in different subtypes of breast cancer: a pooled analysis of 3771 patients treated with neoadjuvant therapy. *Lancet. Oncol.* **19**, 40–50 (2018).

113. Loi, S. *et al.* Tumor-Infiltrating Lymphocytes and Prognosis: A Pooled Individual Patient Analysis of Early-Stage Triple-Negative Breast Cancers. *J. Clin. Oncol. Off. J. Am. Soc. Clin. Oncol.* **37**, 559–569 (2019).

114. Toor, S. M. *et al.* Myeloid cells in circulation and tumor microenvironment of breast cancer patients. *Cancer Immunol. Immunother.* **66**, 753–764 (2017).

115. Veglia, F., Perego, M. & Gabrilovich, D. Myeloid-derived suppressor cells coming of age. *Nat. Immunol.* **19**, 108–119 (2018).

116. Lin, L. *et al.* CCL18 from tumor-associated macrophages promotes angiogenesis in breast cancer. *Oncotarget* **6**, 34758–34773 (2015).

117. Kuan, E. L. & Ziegler, S. F. A tumor-myeloid cell axis, mediated via the cytokines IL-1α and TSLP, promotes the progression of breast cancer. *Nat. Immunol.* **19**, 366–374 (2018).

118. Esquivel-Velázquez, M. *et al.* The role of cytokines in breast cancer development and progression. *J. Interferon Cytokine Res.* **35**, 1–16 (2015).

119. Nicolini, A., Carpi, A. & Rossi, G. Cytokines in breast cancer. *Cytokine Growth Factor Rev.* **17**, 325–337 (2006).

120. Kawaguchi, K. *et al.* Alteration of specific cytokine expression patterns in patients with breast cancer. *Sci. Rep.* **9**, 2924 (2019).

121. Qian, B.-Z. *et al.* CCL2 recruits inflammatory monocytes to facilitate breast-tumour metastasis. *Nature* **475**, 222–225 (2011).

122. Dominguez, C., McCampbell, K. K., David, J. M. & Palena, C. Neutralization of IL-8 decreases tumor PMN-MDSCs and reduces mesenchymalization of claudin-low triple-negative breast cancer. *JCI insight* **2**, (2017).

123. Conlon, K. C., Miljkovic, M. D. & Waldmann, T. A. Cytokines in the Treatment of Cancer. *J. Interferon Cytokine Res.* **39**, 6–21 (2019).

124. Zarogoulidis, P. *et al.* Interleukin-6 cytokine: a multifunctional glycoprotein for cancer. *Immunome Res.* **9**, 16535 (2013).

125. Guo, Y., Xu, F., Lu, T., Duan, Z. & Zhang, Z. Interleukin-6 signaling pathway in targeted therapy for cancer. *Cancer Treat. Rev.* **38**, 904–910 (2012).

126. Tanaka, T., Narazaki, M. & Kishimoto, T. IL-6 in inflammation, immunity, and disease. *Cold Spring Harb. Perspect. Biol.* **6**, a016295 (2014).

127. Rose-John, S. Interleukin-6 Family Cytokines. *Cold Spring Harb. Perspect. Biol.* **10**, a028415 (2018).

128. Jones, S. A. & Jenkins, B. J. Recent insights into targeting the IL-6 cytokine family in inflammatory diseases and cancer. *Nat. Rev. Immunol.* **18**, 773–789 (2018).

129. McGonagle, D., Sharif, K., O'Regan, A. & Bridgewood, C. The Role of Cytokines including Interleukin-6 in COVID-19 induced Pneumonia and Macrophage Activation Syndrome-Like Disease. *Autoimmun. Rev.* **19**, 102537 (2020).

130. West, N. R. Coordination of Immune-Stroma Crosstalk by IL-6 Family Cytokines. *Front. Immunol.* **10**, 1093 (2019).

131. Harrison, D. A. The Jak/STAT pathway. *Cold Spring Harb. Perspect. Biol.* **4**, (2012).

132. Liau, N. P. D. *et al.* The molecular basis of JAK/STAT inhibition by SOCS1. *Nat. Commun.* **9**, 1558 (2018).

133. Carow, B. & Rottenberg, M. E. SOCS3, a Major Regulator of Infection and Inflammation. *Front. Immunol.* **5**, 58 (2014).

134. Schmitz, J. *et al.* The cytoplasmic tyrosine motifs in full-length glycoprotein 130 have different roles in IL-6 signal transduction. *J. Immunol.* **164**, 848–854 (2000).

135. Sasser, A. K. *et al.* Interleukin-6 is a potent growth factor for ER-alpha-positive human breast cancer. *FASEB J. Off. Publ. Fed. Am. Soc. Exp. Biol.* **21**, 3763–3770 (2007).

136. Bharti, R., Dey, G., Das, A. K. & Mandal, M. Differential expression of IL-6/IL-6R and MAO-A regulates invasion/angiogenesis in breast cancer. *Br. J. Cancer* **118**, 1442–1452 (2018).

137. Salgado, R. *et al.* Circulating interleukin-6 predicts survival in patients with metastatic breast cancer. *Int. J. cancer* **103**, 642–646 (2003).

138. Weng, Y.-S. *et al.* MCT-1/miR-34a/IL-6/IL-6R signaling axis promotes EMT progression, cancer stemness and M2 macrophage polarization in triple-negative breast cancer. *Mol. Cancer* **18**, 42 (2019).

139. Gyamfi, J., Lee, Y.-H., Eom, M. & Choi, J. Interleukin-6/STAT3 signalling regulates adipocyte induced epithelial-mesenchymal transition in breast cancer cells. *Sci. Rep.* **8**, 8859 (2018).

140. Ma, Y. *et al.* IL-6, IL-8 and TNF-α levels correlate with disease stage in breast cancer patients. *Adv. Clin. Exp. Med. Off. organ Wroclaw Med. Univ.* **26**, 421–426 (2017).

141. Fisher, D. T., Appenheimer, M. M. & Evans, S. S. The two faces of IL-6 in the tumor microenvironment. *Semin. Immunol.* **26**, 38–47 (2014).

142. Linsley, P. S., Kallestad, J., Ochs, V. & Neubauer, M. Cleavage of a hydrophilic C-terminal domain increases growth-inhibitory activity of oncostatin M. *Mol. Cell. Biol.* **10**, 1882–1890 (1990).

143. Tanaka, M. & Miyajima, A. Oncostatin M, a multifunctional cytokine. *Rev. Physiol. Biochem. Pharmacol.* **149**, 39–52 (2003).

144. Richards, C. D. The enigmatic cytokine oncostatin m and roles in disease. *ISRN Inflamm.* **2013**, 512103 (2013).

145. Zarling, J. M. *et al.* Oncostatin M: a growth regulator produced by differentiated histiocytic lymphoma cells. *Proc. Natl. Acad. Sci. U. S. A.* **83**, 9739–9743 (1986).

146. Mosley, B. *et al.* Dual oncostatin M (OSM) receptors. Cloning and characterization of an alternative signaling subunit conferring OSM-specific receptor activation. *J. Biol. Chem.* **271**, 32635–32643 (1996).

147. West, N. R., Owens, B. M. J. & Hegazy, A. N. The oncostatin M-stromal cell axis in health and disease. *Scand. J. Immunol.* **88**, e12694 (2018).

148. Sims, N. A. & Quinn, J. M. W. Osteoimmunology: oncostatin M as a pleiotropic regulator of bone formation and resorption in health and disease. *Bonekey Rep.* **3**, 527 (2014).

149. Hermanns, H. M. Oncostatin M and interleukin-31: Cytokines, receptors, signal transduction and physiology. *Cytokine Growth Factor Rev.* **26**, 545–558 (2015).

150. Hintzen, C. *et al.* Box 2 region of the oncostatin M receptor determines specificity for recruitment of Janus kinases and STAT5 activation. *J. Biol. Chem.* **283**, 19465–19477 (2008).

151. Dillon, S. R. *et al.* Interleukin 31, a cytokine produced by activated T cells, induces dermatitis in mice. *Nat. Immunol.* **5**, 752–760 (2004).

152. Blanchard, F. *et al.* Oncostatin M regulates the synthesis and turnover of gp130, leukemia inhibitory factor receptor alpha, and oncostatin M receptor beta by distinct mechanisms. *J. Biol. Chem.* **276**, 47038–47045 (2001).

153. Heinrich, P. C. *et al.* Principles of interleukin (IL)-6-type cytokine signalling and its regulation. *Biochem. J.* **374**, 1–20 (2003).

154. Nakamura, K., Nonaka, H., Saito, H., Tanaka, M. & Miyajima, A. Hepatocyte proliferation and tissue remodeling is impaired after liver injury in oncostatin M receptor knockout mice. *Hepatology* **39**, 635–644 (2004).

155. Tanaka, M. *et al.* Targeted disruption of oncostatin M receptor results in altered hematopoiesis. *Blood* **102**, 3154–3162 (2003).

156. Guo, S. *et al.* Oncostatin M Confers Neuroprotection against Ischemic Stroke. *J. Neurosci.* **35**, 12047–12062 (2015).

157. Li, C., Ahlborn, T. E., Kraemer, F. B. & Liu, J. Oncostatin M-induced growth inhibition and morphological changes of MDA-MB231 breast cancer cells are abolished by blocking the MEK/ERK signaling pathway. *Breast Cancer Res. Treat.* **66**, 111–121 (2001).

158. Friedrich, M. *et al.* Complete inhibition of in vivo glioma growth by oncostatin M. *J. Neurochem.* **76**, 1589–1592 (2001).

159. Kong, N. *et al.* Inhibition of growth and induction of differentiation of SMMC-7721 human hepatocellular carcinoma cells by Oncostatin M. *Asian Pac. J. Cancer Prev.* **14**, 747–752 (2013).

160. Kim, M. S. *et al.* Promoter DNA methylation of oncostatin m receptor-beta as a novel diagnostic and therapeutic marker in colon cancer. *PLoS One* **4**, e6555–e6555 (2009).

161. Pan, C.-M., Wang, M.-L., Chiou, S.-H., Chen, H.-Y. & Wu, C.-W. Oncostatin M suppresses metastasis of lung adenocarcinoma by inhibiting SLUG expression through coordination of STATs and PIASs signalings. *Oncotarget* **7**, 60395–60406 (2016).

162. David, E. *et al.* Direct anti-cancer effect of oncostatin M on chondrosarcoma. *Int. J. cancer* **128**, 1822–1835 (2011).

163. Amaral, M. C., Miles, S., Kumar, G. & Nel, A. E. Oncostatin-M stimulates tyrosine protein phosphorylation in parallel with the activation of p42MAPK/ERK-2 in Kaposi's cells. Evidence that this pathway is important in Kaposi cell growth. *J. Clin. Invest.* **92**, 848–857 (1993).

164. Li, Q. *et al.* Oncostatin M promotes proliferation of ovarian cancer cells through signal transducer and activator of transcription 3. *Int. J. Mol. Med.* **28**, 101–108 (2011).

165. David, E. *et al.* Oncostatin M is a growth factor for Ewing sarcoma. *Am. J. Pathol.* **181**, 1782–1795 (2012).

166. Godoy-Tundidor, S. *et al.* Interleukin-6 and oncostatin M stimulation of proliferation of prostate cancer 22Rv1 cells through the signaling pathways of p38 mitogen-activated protein kinase and phosphatidylinositol 3-kinase. *Prostate* **64**, 209–216 (2005).

167. Smith, D. A., Kiba, A., Zong, Y. & Witte, O. N. Interleukin-6 and oncostatin-M synergize with the PI3K/AKT pathway to promote aggressive prostate malignancy in mouse and human tissues. *Mol. Cancer Res.* **11**, 1159–1165 (2013).

168. Lacreusette, A. *et al.* Loss of oncostatin M receptor beta in metastatic melanoma cells. *Oncogene* **26**, 881–892 (2007).

169. Fossey, S. L., Bear, M. D., Kisseberth, W. C., Pennell, M. & London, C. A. Oncostatin M promotes STAT3 activation, VEGF production, and invasion in osteosarcoma cell lines. *BMC Cancer* **11**, 125 (2011).

170. Yu, Z. *et al.* Oncostatin M receptor, positively regulated by SP1, promotes gastric cancer growth and metastasis upon treatment with Oncostatin M. *Gastric cancer Off. J. Int. Gastric Cancer Assoc. Japanese Gastric Cancer Assoc.* **22**, 955–966 (2019).

171. Lamouille, S., Xu, J. & Derynck, R. Molecular mechanisms of epithelial-mesenchymal transition. *Nat. Rev. Mol. Cell Biol.* **15**, 178–196 (2014).

172. Argast, G. M. *et al.* Cooperative signaling between oncostatin M, hepatocyte growth factor and transforming growth factor-β enhances epithelial to mesenchymal transition in lung and pancreatic tumor models. *Cells. Tissues. Organs* **193**, 114–132 (2011).

173. Natesh, K. *et al.* Oncostatin-M differentially regulates mesenchymal and proneural signature genes in gliomas via STAT3 signaling. *Neoplasia* **17**, 225–237 (2015).

174. Jahani-Asl, A. *et al.* Control of glioblastoma tumorigenesis by feed-forward cytokine signaling. *Nat. Neurosci.* **19**, 798–806 (2016).

175. Chen, D. *et al.* Expression of short-form oncostatin M receptor as a decoy receptor in lung adenocarcinomas. *J. Pathol.* **215**, 290–299 (2008).

176. Diveu, C. *et al.* Molecular and functional characterization of a soluble form of oncostatin M/interleukin-31 shared receptor. *J. Biol. Chem.* **281**, 36673–36682 (2006).

177. Kausar, T. *et al.* Overexpression of a splice variant of oncostatin M receptor beta in human esophageal squamous carcinoma. *Cell. Oncol.* **34**, 177–187 (2011).

178. Deng, G. *et al.* Unique methylation pattern of oncostatin m receptor gene in cancers of colorectum and other digestive organs. *Clin. cancer Res. an Off. J. Am. Assoc. Cancer Res.* **15**, 1519–1526 (2009).

179. Ng, G. *et al.* Gain and overexpression of the oncostatin M receptor occur frequently in cervical squamous cell carcinoma and are associated with adverse clinical outcome. *J. Pathol.* **212**, 325–334 (2007).

180. Caffarel, M. M. & Coleman, N. Oncostatin M receptor is a novel therapeutic target in cervical squamous cell carcinoma. *J. Pathol.* **232**, 386–390 (2014).

181. Winder, D. M. *et al.* Overexpression of the oncostatin M receptor in cervical squamous cell carcinoma cells is associated with a pro-angiogenic phenotype and increased cell motility and invasiveness. *J. Pathol.* **225**, 448–462 (2011).

182. Caffarel, M. M. *et al.* Tissue transglutaminase mediates the pro-malignant effects of oncostatin M receptor over-expression in cervical squamous cell carcinoma. *J. Pathol.* **231**, 168–179 (2013).

183. Kucia-Tran, J. A. *et al.* Overexpression of the oncostatin-M receptor in cervical squamous cell carcinoma is associated with epithelial-mesenchymal transition and poor overall survival. *Br. J. Cancer* **115**, 212–222 (2016).

184. Kucia-Tran, J. A. *et al.* Anti-oncostatin M antibody inhibits the pro-malignant effects of oncostatin M receptor overexpression in squamous cell carcinoma. *J. Pathol.* **244**, 283–295 (2018).

185. Katt, M. E., Placone, A. L., Wong, A. D., Xu, Z. S. & Searson, P. C. In Vitro Tumor Models: Advantages, Disadvantages, Variables, and Selecting the Right Platform. *Front. Bioeng. Biotechnol.* **4**, 12 (2016).

186. Place, A. E., Jin Huh, S. & Polyak, K. The microenvironment in breast cancer progression: biology and implications for treatment. *Breast Cancer Res.* **13**, 227 (2011).

187. Bahcecioglu, G., Basara, G., Ellis, B. W., Ren, X. & Zorlutuna, P. Breast cancer models: Engineering the tumor microenvironment. *Acta Biomater.* **106**, 1–21 (2020).

188. Douglas, A. M. *et al.* Oncostatin M induces the differentiation of breast cancer cells. *Int. J. cancer* **75**, 64–73 (1998).

189. Holzer, R. G., Ryan, R. E., Tommack, M., Schlekeway, E. & Jorcyk, C. L. Oncostatin M stimulates the detachment of a reservoir of invasive mammary carcinoma cells: role of cyclooxygenase-2. *Clin. Exp. Metastasis* **21**, 167–176 (2004).

190. Jorcyk, C. L., Holzer, R. G. & Ryan, R. E. Oncostatin M induces cell detachment and enhances the metastatic capacity of T-47D human breast carcinoma cells. *Cytokine* **33**, 323–336 (2006).

191. Kan, C. E., Cipriano, R. & Jackson, M. W. c-MYC functions as a molecular switch to alter the response of human mammary epithelial cells to oncostatin M. *Cancer Res.* **71**, 6930–6939 (2011).

192. García-Tuñón, I. *et al.* OSM, LIF, its receptors, and its relationship with the malignance in human breast carcinoma (in situ and in infiltrative). *Cancer Invest.* **26**, 222–229 (2008).

193. West, N. R., Murphy, L. C. & Watson, P. H. Oncostatin M suppresses oestrogen receptor-α expression and is associated with poor outcome in human breast cancer. *Endocr. Relat. Cancer* **19**, 181–195 (2012).

194. West, N. R., Murray, J. I. & Watson, P. H. Oncostatin-M promotes phenotypic changes associated with mesenchymal and stem cell-like differentiation in breast cancer. *Oncogene* **33**, 1485–1494 (2014).

195. Guo, L. *et al.* Stat3-coordinated Lin-28-let-7-HMGA2 and miR-200-ZEB1 circuits initiate and maintain oncostatin M-driven epithelial-mesenchymal transition. *Oncogene* **32**, 5272–5282 (2013).

196. Tawara, K. *et al.* OSM potentiates preintravasation events, increases CTC counts, and promotes breast cancer metastasis to the lung. *Breast Cancer Res.* **20**, 53 (2018).

197. Hinshaw, D. C. & Shevde, L. A. The Tumor Microenvironment Innately Modulates Cancer Progression. *Cancer Res.* **79**, 4557–4566 (2019).

198. Hu, M. *et al.* Distinct epigenetic changes in the stromal cells of breast cancers. *Nat. Genet.* **37**, 899–905 (2005).

199. Finak, G. *et al.* Stromal gene expression predicts clinical outcome in breast cancer. *Nat. Med.* **14**, 518–527 (2008).

200. Farmer, P. *et al.* A stroma-related gene signature predicts resistance to neoadjuvant chemotherapy in breast cancer. *Nat. Med.* **15**, 68—74 (2009).

201. Kramer, C. J. H. *et al.* The prognostic value of tumour–stroma ratio in primary breast cancer with special attention to triple-negative tumours: a review. *Breast Cancer Res. Treat.* **173**, 55–64 (2019).

202. Soysal, S. D., Tzankov, A. & Muenst, S. E. Role of the Tumor Microenvironment in Breast Cancer. *Pathobiology* **82**, 142–152 (2015).

203. Segovia-Mendoza, M. & Morales-Montor, J. Immune Tumor Microenvironment in Breast Cancer and the Participation of Estrogen and Its Receptors in Cancer Physiopathology. *Front. Immunol.* **10**, 348 (2019).

204. Tripathi, C. *et al.* Macrophages are recruited to hypoxic tumor areas and acquire a pro-angiogenic M2-polarized phenotype via hypoxic cancer cell derived cytokines Oncostatin M and Eotaxin. *Oncotarget* **5**, 5350–5368 (2014).

205. Ishibashi, H. *et al.* Sex steroid hormone receptors in human thymoma. *J. Clin. Endocrinol. Metab.* **88**, 2309–2317 (2003).

206. Curtis, C. *et al.* The genomic and transcriptomic architecture of 2,000 breast tumours reveals novel subgroups. *Nature* **486**, 346–352 (2012).

207. Cortazar, A. R. *et al.* Cancertool: A visualization and representation interface to exploit cancer datasets. *Cancer Res.* **78**, 6320–6328 (2018).

208. Wang, Y. *et al.* Gene-expression profiles to predict distant metastasis of lymph-node-negative primary breast cancer. *Lancet* **365**, 671–679 (2005).

209. Győrffy, B. *et al.* An online survival analysis tool to rapidly assess the effect of 22,277 genes on breast cancer prognosis using microarray data of 1,809 patients. *Breast Cancer Res. Treat.* **123**, 725–731 (2010).

210. Casey, T. *et al.* Molecular signatures suggest a major role for stromal cells in development of invasive breast cancer. *Breast Cancer Res. Treat.* **114**, 47—62 (2009).

211. Yeung, T.-L. *et al.* TGF-β modulates ovarian cancer invasion by upregulating CAF-derived versican in the tumor microenvironment. *Cancer Res.* **73**, 5016–5028 (2013).

212. Nishida, N. *et al.* Microarray analysis of colorectal cancer stromal tissue reveals upregulation of two oncogenic miRNA clusters. *Clin. Cancer Res. an Off. J. Am. Assoc. Cancer Res.* **18**, 3054–3070 (2012).

213. Uhlén, M. *et al.* Proteomics. Tissue-based map of the human proteome. *Science* **347**, 1260419 (2015).

214. Koboldt, D. C. *et al.* Comprehensive molecular portraits of human breast tumours. *Nature* **490**, 61–70 (2012).

215. Li, T. *et al.* TIMER2.0 for analysis of tumor-infiltrating immune cells. *Nucleic Acids Res.* **48**, W509–W514 (2020).

216. Aran, D., Hu, Z. & Butte, A. J. xCell: digitally portraying the tissue cellular heterogeneity landscape. *Genome Biol.* **18**, 220 (2017).

217. Cerami, E. *et al.* The cBio cancer genomics portal: an open platform for exploring multidimensional cancer genomics data. *Cancer Discov.* **2**, 401–404 (2012).

218. Neve, R. M. *et al.* A collection of breast cancer cell lines for the study of functionally distinct cancer subtypes. *Cancer Cell* **10**, 515–527 (2006).

219. Shree, T. *et al.* Macrophages and cathepsin proteases blunt chemotherapeutic response in breast cancer. *Genes Dev.* **25**, 2465–2479 (2011).

220. Fernández-Nogueira, P. *et al.* Tumor-Associated Fibroblasts Promote HER2-Targeted Therapy Resistance through FGFR2 Activation. *Clin. cancer Res. an Off. J. Am. Assoc. Cancer Res.* **26**, 1432–1448 (2020).

221. Zheng, X. *et al.* Gene expression of TPA induced differentiation in HL-60 cells by DNA microarray analysis. *Nucleic Acids Res.* **30**, 4489–4499 (2002).

222. Zijlstra, A. *et al.* A quantitative analysis of rate-limiting steps in the metastatic cascade using human-specific real-time polymerase chain reaction. *Cancer Res.* **62**, 7083–7092 (2002).

223. Schneider, T., Osl, F., Friess, T., Stockinger, H. & Scheuer, W. V. Quantification of human Alu sequences by real-time PCR--an improved method to measure therapeutic efficacy of anti-metastatic drugs in human xenotransplants. *Clin. Exp. Metastasis* **19**, 571–582 (2002).

224. Pfaffl, M. W. A new mathematical model for relative quantification in real-time RT-PCR. *Nucleic Acids Res.* **29**, e45–e45 (2001).

225. Subramanian, A. *et al.* Gene set enrichment analysis: A knowledge-based approach for interpreting genome-wide expression profiles. *Proc. Natl. Acad. Sci.* **102**, 15545 LP – 15550 (2005).

226. Macosko, E. Z. *et al.* Highly Parallel Genome-wide Expression Profiling of Individual Cells Using Nanoliter Droplets. *Cell* **161**, 1202–1214 (2015).

227. Valdes-Mora, F. *et al.* Single cell transcriptomics reveals involution mimicry during the specification of the basal breast cancer subtype. *bioRxiv* 624890 (2020) doi:10.1101/624890.

228. Butler, A., Hoffman, P., Smibert, P., Papalexi, E. & Satija, R. Integrating single-cell transcriptomic data across different conditions, technologies, and species. *Nat. Biotechnol.* **36**, 411–420 (2018).

229. McInnes, L., Healy, J. & Melville, J. UMAP: Uniform Manifold Approximation and Projection for Dimension Reduction. *bioRxiv* 877522 (2018). doi:10.1101/2019.12.19.877522.

230. Caffarel, M. M. *et al.* Cannabinoids reduce ErbB2-driven breast cancer progression through Akt inhibition. *Mol. Cancer* **9**, 196 (2010).

231. Guy, C. T., Cardiff, R. D. & Muller, W. J. Induction of mammary tumors by expression of polyomavirus middle T oncogene: a transgenic mouse model for metastatic disease. *Mol. Cell. Biol.* **12**, 954–961 (1992).

232. Stross, C. *et al.* Oncostatin M receptor-mediated signal transduction is negatively regulated by SOCS3 through a receptor tyrosine-independent mechanism. *J. Biol. Chem.* **281**, 8458–8468 (2006).

233. Tawara, K. *et al.* HIGH expression of OSM and IL-6 are associated with decreased breast cancer survival: synergistic induction of IL-6 secretion by OSM and IL-1β. *Oncotarget* **10**, 2068–2085 (2019).

234. Bonnans, C., Chou, J. & Werb, Z. Remodelling the extracellular matrix in development and disease. *Nat. Rev. Mol. Cell Biol.* **15**, 786–801 (2014).

235. Park, J. & Schwarzbauer, J. E. Mammary epithelial cell interactions with fibronectin stimulate epithelial-mesenchymal transition. *Oncogene* **33**, 1649–1657 (2014).

236. Adrian-Segarra, J. M. *et al.* The AB loop of oncostatin M (OSM) determines species-specific signaling in humans and mice. *J. Biol. Chem.* **293**, 20181–20199 (2018).

237. Price, J. E., Polyzos, A., Zhang, R. D. & Daniels, L. M. Tumorigenicity and metastasis of human breast carcinoma cell lines in nude mice. *Cancer Res.* **50**, 717–721 (1990).

238. Lin, E. Y. *et al.* Progression to Malignancy in the Polyoma Middle T Oncoprotein Mouse Breast Cancer Model Provides a Reliable Model for Human Diseases. *Am. J. Pathol.* **163**, 2113–2126 (2003).

239. Li, C.-L. *et al.* Fibronectin induces epithelial-mesenchymal transition in human breast cancer MCF-7 cells via activation of calpain. *Oncol. Lett.* **13**, 3889–3895 (2017).

240. Serini, G. *et al.* The fibronectin domain ED-A is crucial for myofibroblastic phenotype induction by transforming growth factor-beta1. *J. Cell Biol.* **142**, 873–881 (1998).

241. Shree, T. *et al.* Macrophages and cathepsin proteases blunt chemotherapeutic response in breast cancer. *Genes Dev.* **25**, 2465–2479 (2011).

242. Ferrari, N. *et al.* Dickkopf-3 links HSF1 and YAP/TAZ signalling to control aggressive behaviours in cancer-associated fibroblasts. *Nat. Commun.* **10**, (2019).

243. Erdogan, B. & Webb, D. J. Cancer-associated fibroblasts modulate growth factor signaling and extracellular matrix remodeling to regulate tumor metastasis. *Biochem. Soc. Trans.* **45**, 229–236 (2017).

244. Bell, E., Ivarsson, B. & Merrill, C. Production of a tissue-like structure by contraction of collagen lattices by human fibroblasts of different proliferative potential in vitro. *Proc. Natl. Acad. Sci. U. S. A.* **76**, 1274–1278 (1979).

245. Zhang, T. *et al.* Investigating Fibroblast-Induced Collagen Gel Contraction Using a Dynamic Microscale Platform. *Front. Bioeng. Biotechnol.* **7**, 196 (2019).

246. Zanconato, F., Cordenonsi, M. & Piccolo, S. YAP/TAZ at the Roots of Cancer. *Cancer Cell* **29**, 783–803 (2016).

247. Maykel, J. *et al.* NOD-scidIl2rg (tm1Wjl) and NOD-Rag1 (null) Il2rg (tm1Wjl) : a model for stromal cell-tumor cell interaction for human colon cancer. *Dig. Dis. Sci.* **59**, 1169–1179 (2014).

248. Mollinedo, F. Neutrophil Degranulation, Plasticity, and Cancer Metastasis. *Trends Immunol.* **40**, 228–242 (2019).

249. Allaoui, R. *et al.* Cancer-associated fibroblast-secreted CXCL16 attracts monocytes to

promote stroma activation in triple-negative breast cancers. *Nat. Commun.* **7**, 13050 (2016).

250. Ceci, C., Atzori, M. G., Lacal, P. M. & Graziani, G. Role of VEGFs/VEGFR-1 Signaling and its Inhibition in Modulating Tumor Invasion: Experimental Evidence in Different Metastatic Cancer Models. *Int. J. Mol. Sci.* **21**, (2020).

251. Gschwandtner, M., Derler, R. & Midwood, K. S. More Than Just Attractive: How CCL2 Influences Myeloid Cell Behavior Beyond Chemotaxis. *Front. Immunol.* **10**, 2759 (2019).

252. Howlader N, Noone AM, Krapcho M, Miller D, Brest A, Yu M, Ruhl J, Tatalovich Z, Mariotto A, Lewis DR, Chen HS, Feuer EJ, C. K. SEER Cancer Statistics Review. *MD: National Cancer Institute.* https://seer.cancer.gov/csr/1975_2017/ (2019).

253. World Health Organization. Cancer. https://www.who.int/news-room/fact-sheets/detail/cancer (2018).

254. Nahta, R. & Esteva, F. J. Trastuzumab: triumphs and tribulations. *Oncogene* **26**, 3637–3643 (2007).

255. Witz, I. P. The tumor microenvironment: the making of a paradigm. *Cancer Microenviron. Off. J. Int. Cancer Microenviron. Soc.* **2 Suppl 1**, 9–17 (2009).

256. Vogel, C. & Marcotte, E. M. Insights into the regulation of protein abundance from proteomic and transcriptomic analyses. *Nat. Rev. Genet.* **13**, 227–232 (2012).

257. Koskela, K., Pelliniemi, T. T., Remes, K., Rajamäki, A. & Pulkki, K. Serum oncostatin M in multiple myeloma: association with prognostic factors. *Br. J. Haematol.* **96**, 158–160 (1997).

258. Musgrove, E. A. & Sutherland, R. L. Biological determinants of endocrine resistance in breast cancer. *Nat. Rev. Cancer* **9**, 631–643 (2009).

259. Brinkman, J. A. & El-Ashry, D. ER re-expression and re-sensitization to endocrine therapies in ER-negative breast cancers. *J. Mammary Gland Biol. Neoplasia* **14**, 67–78 (2009).

260. Parashar, D. *et al.* miRNA551b-3p Activates an Oncostatin Signaling Module for the Progression of Triple-Negative Breast Cancer. *Cell Rep.* **29**, 4389-4406.e10 (2019).

261. Covert, H. *et al.* OSM-induced CD44 contributes to breast cancer metastatic potential through cell detachment but not epithelial-mesenchymal transition. *Cancer Manag. Res.* **11**, 7721–7737 (2019).

262. Holen, I., Speirs, V., Morrissey, B. & Blyth, K. In vivo models in breast cancer research: progress, challenges and future directions. *Dis. Model. Mech.* **10**, 359–371 (2017).

263. Sullivan, N. J. *et al.* Interleukin-6 induces an epithelial-mesenchymal transition phenotype in human breast cancer cells. *Oncogene* **28**, 2940–2947 (2009).

264. Fernandez-Garcia, B. *et al.* Expression and prognostic significance of fibronectin and matrix metalloproteases in breast cancer metastasis. *Histopathology* **64**, 512–522 (2014).

265. Becker, A. *et al.* Extracellular Vesicles in Cancer: Cell-to-Cell Mediators of Metastasis. *Cancer Cell* **30**, 836–848 (2016).

266. Kogure, A., Yoshioka, Y. & Ochiya, T. Extracellular Vesicles in Cancer Metastasis: Potential as Therapeutic Targets and Materials. *Int. J. Mol. Sci.* **21**, (2020).

267. Balkwill, F. R., Capasso, M. & Hagemann, T. The tumor microenvironment at a glance. *J.*

Cell Sci. **125**, 5591–5596 (2012).

268. Hanahan, D. & Coussens, L. M. Accessories to the Crime: Functions of Cells Recruited to the Tumor Microenvironment. *Cancer Cell* **21**, 309–322 (2012).

269. Gonzalez, H., Hagerling, C. & Werb, Z. Roles of the immune system in cancer: from tumor initiation to metastatic progression. *Genes Dev.* **32**, 1267–1284 (2018).

270. García Morán GA, Parra-Medina R, Cardona AG, et al. Cytokines, chemokines and growth factors. In: Anaya JM, Shoenfeld Y, Rojas-Villarraga A, et al. Cytokines, chemokines and growth factors. in *Autoimmunity: From Bench to Bedside* (2013).

271. Heo, T.-H., Wahler, J. & Suh, N. Potential therapeutic implications of IL-6/IL-6R/gp130-targeting agents in breast cancer. *Oncotarget* **7**, 15460–15473 (2016).

272. Calabrese, L. H. & Rose-John, S. IL-6 biology: implications for clinical targeting in rheumatic disease. *Nat. Rev. Rheumatol.* **10**, 720–727 (2014).

273. Ostman, A. & Augsten, M. Cancer-associated fibroblasts and tumor growth--bystanders turning into key players. *Curr. Opin. Genet. Dev.* **19**, 67–73 (2009).

274. Xing, F., Saidou, J. & Watabe, K. Cancer associated fibroblasts (CAFs) in tumor microenvironment. *Front. Biosci.* **15**, 166–179 (2010).

275. Mhaidly, R. & Mechta-Grigoriou, F. Fibroblast heterogeneity in tumor micro-environment: Role in immunosuppression and new therapies. *Semin. Immunol.* **48**, 101417 (2020).

276. Öhlund, D. *et al.* Distinct populations of inflammatory fibroblasts and myofibroblasts in pancreatic cancer. *J. Exp. Med.* **214**, 579–596 (2017).

277. Biffi, G. *et al.* IL1-Induced JAK/STAT Signaling Is Antagonized by TGFβ to Shape CAF Heterogeneity in Pancreatic Ductal Adenocarcinoma. *Cancer Discov.* **9**, 282–301 (2019).

278. Sanz-Moreno, V. *et al.* ROCK and JAK1 signaling cooperate to control actomyosin contractility in tumor cells and stroma. *Cancer Cell* **20**, 229–245 (2011).

279. Marden, G. *et al.* The role of the oncostatin M/OSM receptor β axis in activating dermal microvascular endothelial cells in systemic sclerosis. *Arthritis Res. Ther.* **22**, 179 (2020).

280. Ruprecht, K. *et al.* Effects of oncostatin M on human cerebral endothelial cells and expression in inflammatory brain lesions. *J. Neuropathol. Exp. Neurol.* **60**, 1087–1098 (2001).

281. van Keulen, D. *et al.* Inflammatory cytokine oncostatin M induces endothelial activation in macro- and microvascular endothelial cells and in APOE*3Leiden.CETP mice. *PLoS One* **13**, e0204911 (2018).

282. Hsu, T., Nguyen-Tran, H.-H. & Trojanowska, M. Active roles of dysfunctional vascular endothelium in fibrosis and cancer. *J. Biomed. Sci.* **26**, 86 (2019).

283. Bierie, B. *et al.* Abrogation of TGF-beta signaling enhances chemokine production and correlates with prognosis in human breast cancer. *J. Clin. Invest.* **119**, 1571–1582 (2009).

284. Grépin, R. *et al.* The CXCL7/CXCR1/2 axis is a key driver in the growth of clear cell renal cell carcinoma. *Cancer Res.* **74**, 873–883 (2014).

285. Lu, Z. *et al.* Epigenetic therapy inhibits metastases by disrupting premetastatic niches. *Nature* **579**, 284–290 (2020).

286. Queen, M. M., Ryan, R. E., Holzer, R. G., Keller-Peck, C. R. & Jorcyk, C. L. Breast cancer cells stimulate neutrophils to produce oncostatin M: potential implications for tumor progression. *Cancer Res.* **65**, 8896–8904 (2005).

287. Vlaicu, P. *et al.* Monocytes/macrophages support mammary tumor invasivity by co-secreting lineage-specific EGFR ligands and a STAT3 activator. *BMC Cancer* **13**, 197 (2013).

288. Yang, J., Yan, J. & Liu, B. Targeting VEGF/VEGFR to modulate antitumor immunity. *Front. Immunol.* **9**, 1–9 (2018).

289. Acharyya, S. *et al.* A CXCL1 paracrine network links cancer chemoresistance and metastasis. *Cell* **150**, 165–178 (2012).

290. Swierczak, A., Mouchemore, K. A., Hamilton, J. A. & Anderson, R. L. Neutrophils: important contributors to tumor progression and metastasis. *Cancer Metastasis Rev.* **34**, 735–751 (2015).

291. Lin, E. Y., Nguyen, A. V., Russell, R. G. & Pollard, J. W. Colony-stimulating factor 1 promotes progression of mammary tumors to malignancy. *J. Exp. Med.* **193**, 727–739 (2001).

292. Strachan, D. C. *et al.* CSF1R inhibition delays cervical and mammary tumor growth in murine models by attenuating the turnover of tumor-associated macrophages and enhancing infiltration by CD8+ T cells. *Oncoimmunology* **2**, 1–12 (2013).

293. Boyle, S. T., Faulkner, J. W., McColl, S. R. & Kochetkova, M. The chemokine receptor CCR6 facilitates the onset of mammary neoplasia in the MMTV-PyMT mouse model via recruitment of tumor-promoting macrophages. *Mol. Cancer* **14**, 1–14 (2015).

294. Gallego-Ortega, D. *et al.* ELF5 Drives Lung Metastasis in Luminal Breast Cancer through Recruitment of Gr1+ CD11b+ Myeloid-Derived Suppressor Cells. *PLoS Biol.* **13**, e1002330 (2015).

295. Ayaub, E. A. *et al.* Overexpression of OSM and IL-6 impacts the polarization of pro-fibrotic macrophages and the development of bleomycin-induced lung fibrosis. *Sci. Rep.* **7**, 13281 (2017).

296. Weiner, G. J. Building better monoclonal antibody-based therapeutics. *Nat. Rev. Cancer* **15**, 361–370 (2015).

297. Reid, J. *et al.* In vivo affinity and target engagement in skin and blood in a first-time-in-human study of an anti-oncostatin M monoclonal antibody. *Br. J. Clin. Pharmacol.* **84**, 2280—2291 (2018).

298. ClinicalTrials.gov. Study to Evaluate Safety, Tolerability and Efficacy of GSK2330811 in Crohn's Disease (COSMIS). https://clinicaltrials.gov/ct2/show/NCT04151225 (2019).

299. Wang, A. *et al.* Treatment of granuloma annulare and suppression of proinflammatory cytokine activity with tofacitinib. *J. Allergy Clin. Immunol.* (2020) doi:10.1016/j.jaci.2020.10.012.

300. Brolund, L., Küster, A., Korr, S., Vogt, M. & Müller-Newen, G. A receptor fusion protein for the inhibition of murine oncostatin M. *BMC Biotechnol.* **11**, 3 (2011).

301. Son, H.-J. *et al.* Oncostatin M Suppresses Activation of IL-17/Th17 via SOCS3 Regulation in CD4+ T Cells. *J. Immunol.* **198**, 1484–1491 (2017).

Supplementary information

Supplementary Table 1: Gene list for the fibroblast activation markers signature, manually curated from Sahai *et al* (2020)[64], used in Fig. 3.2.9.

Fibroblast/ fibroblast subtype/ activation markers	**Molecules produced by activated fibroblasts/ CAFs**
PDGFRa	TGFb
Vimentin	VEGFA
aSMA	CCN1 (CYR61)
FAP	CCN2 (CTGF)
Col1a2	Tenascin
Col5a1	Periostin
Downregulation of CD36	LIF
GPR77	GAS6
CD10	FGF5
FSP1 (S100A4)	GDF15
	HGF
	IL6
	CXCL9
	CXCL12
	FAK